YGS Open File 2025-7

Summary of geothermal indicators in the Yukon

Sarah Sternbergh[1] and Maurice Colpron[2]

[1] Tetra Tech (formerly with Yukon Geological Survey)
[2] Yukon Geological Survey

YGS Open File
2025-7

Summary of geothermal indicators in the Yukon

Sarah Sternbergh[1] and Maurice Colpron[2]

[1] Tetra Tech (formerly with Yukon Geological Survey)
[2] Yukon Geological Survey

Published under the authority of the Department of Energy, Mines and Resources, Government of Yukon https://yukon.ca/en/department-energy-mines-resources.

Publié avec l'autorisation du Ministères de l'Énergie, des Mines et des Ressources du gouvernement du Yukon, https://yukon.ca/en/department-energy-mines-resources.

This, and other Yukon Geological Survey publications, may be obtained from:

Yukon Geological Survey
102-300 Main Street
Box 2703 (K-102)
Whitehorse, Yukon, Canada Y1A 2C6

email geology@yukon.ca

Visit the Yukon Geological Survey website at https://yukon.ca/en/science-and-natural-resources/geology.

In referring to this publication, please use the following citation:

Sternbergh, S. and Colpron, M., 2025. Summary of geothermal indicators in the Yukon. Government of Yukon, Yukon Geological Survey, Open File 2025-7, 92 p. plus appendices.

Front cover: Aerial view of tufa mound at the Coal River thermal spring, southeastern Yukon. Photo credit: Lee Pigage, Yukon Geological Survey

Table of Contents

Abstract . . . 1

Plain language summary . . . 1

Introduction . . . 1

Geothermal research by the Yukon Geological Survey . . . 6

Structure of this report, data and methods . . . 9

- Geothermometer calculations . . . 9
- Noble gas analysis . . . 15
- Borehole temperature measurements . . . 17
- Radiogenic heat production . . . 17

North Yukon . . . 19

Central Yukon . . . 21

- Mayo warm water boreholes . . . 22
- Nash Creek hot springs . . . 22
- Mactung hot spring . . . 24
- Cantung, McPherson Lake and Caesar Lake thermal springs . . . 26

Southeast Yukon . . . 28

- Pool Creek and Larsen Creek hot springs . . . 29
- Canyon Creek warm springs . . . 32
- Crow River warm springs . . . 32
- Thorpe Creek warm springs . . . 33
- Coal River warm springs . . . 34

Tintina Trench . . . 37

- Partridge Creek warm spring . . . 38
- McArthur hot springs . . . 39
- Ross River area . . . 41
- Watson Lake area . . . 44

Pelly–Cassiar Mountains . . . 47

- Teslin area . . . 48
- Swift River area . . . 49

Yukon Plateaus . . . 52

- Whitehorse area . . . 53
  - *Takhini hot spring* . . . 53
  - *Vista Mountain warm springs* . . . 55
  - *City of Whitehorse* . . . 57
- Volcano Mountain (Nelruna) . . . 60
- Carmacks area . . . 61

Southwest Yukon . . . 66

- Haines Junction (Dakwăkăda) area . . . 68
- Jarvis River warm springs . . . 69
- Burwash Landing area . . . 72

Summary and conclusions . . . 76
- Geothermal gradients . . . 76
- Thermal springs . . . 78
- Geothermometers . . . 78
- Helium isotopes . . . 79
- Geological modelling . . . 80
- Regional geophysical studies . . . 80
- Geothermal opportunities in the Yukon . . . 81

Acknowledgments . . . 82

References . . . 83

Appendix A – Metadata for geothermal data compilations . . . 93

Appendix B – Groundwater noble isotope data collected by the Yukon Geological Survey [digital only] . . . 104

Appendix C – Temperature profile data collected by the Yukon Geological Survey (2017–2023) [digital only] . . . 105

Appendix D – Carmacks EY22-01 drill log . . . 106

Appendix E – Duke River borehole: Phase 1 completion report . . . 110

Abstract

Evidence suggests that crustal heat flow in the Yukon is higher than in the southern Canadian Cordillera and much higher than the average continental crustal heat flow. The occurrence of numerous thermal springs combined with local exposures of Neogene to Recent volcanic rocks in the northern Canadian Cordillera suggests there may be potential for geothermal resources in the Yukon and adjacent regions. This report summarizes the current state of knowledge for geothermal indicators in the Yukon. It is anchored on the compilation of geothermal datasets and summarizes previously unpublished, contracted geothermal studies, as well as research conducted by the Yukon Geological Survey between 2016 and 2024. More than 20 thermal springs are described and water chemistry for these springs and selected boreholes are presented. The compilation datasets include regional estimation of Curie point depths, potential radiogenic heat production of granitoid plutons, observations from open-water surveys, and temperature data from boreholes. The main observations from eight focused studies, including geophysical surveys in five communities, are summarized, and recommendations for future geothermal exploration are proposed.

Known geothermal indicators in the Yukon suggest that higher heat flow is more likely in southwestern Yukon, but measured geothermal gradients indicate limited opportunities for electricity generation using conventional technologies, which require temperatures greater than 120°C within approximately 2 km of the surface; however, a range of direct-use geothermal opportunities are possible for some Yukon communities where subsurface temperatures range from 20 to 80°C. The common association of thermal springs with radiogenic granites invites further exploration near granitic plutons, particularly where they occur near communities (e.g., Whitehorse, Mayo). Thermal springs in southeast and southwest Yukon have elevated $^3He/^4He$ ratios that suggest deep circulation, enhanced permeability, and high fluid flux near major lithospheric-scale faults (e.g., Denali fault, Liard line). The development of 3D geological models for Yukon communities provides constraints to guide future exploration.

Plain language summary

It has been suggested that more heat is generated from the Earth's crust in the Yukon compared to other parts of Canada. Tapping into the Earth's heat could provide renewable energy to offset the use of hydrocarbons in the Yukon. This report summarizes a range of technical studies intended to identify potential shallow (within 2 km of surface) heat sources in the Yukon, particularly near communities. Findings from this report indicate that there are opportunities to harness heat for direct use in southern Yukon, and that a wide range of applications may be possible. There is, however, little evidence that sufficient heat is available at shallow depths for electrical power generation using conventional technologies. Further studies are proposed to better define the geothermal potential of the Yukon.

Introduction

The Yukon is located in the northern part of the North American Cordillera, the mountain belt that formed as a result of the convergence of the North American and Pacific plates, which began during the Mesozoic (ca. 200 Ma) and continues today (Colpron and Nelson, 2021). The Pacific Ocean is bounded the 'Pacific Ring of Fire' (Fig. 1), a collection of subduction zones and associated magmatic arcs that are prospective regions for geothermal energy. The current tectonic regime for the Pacific-North American plate interaction has the Pacific Plate subducting to the northwest beneath the Aleutian Trench at rates of 5.1 to 7.9 cm/year, and much of the western edge of the North American Plate is defined by transform faults (Queen Charlotte and San Andreas faults; Fig. 1).

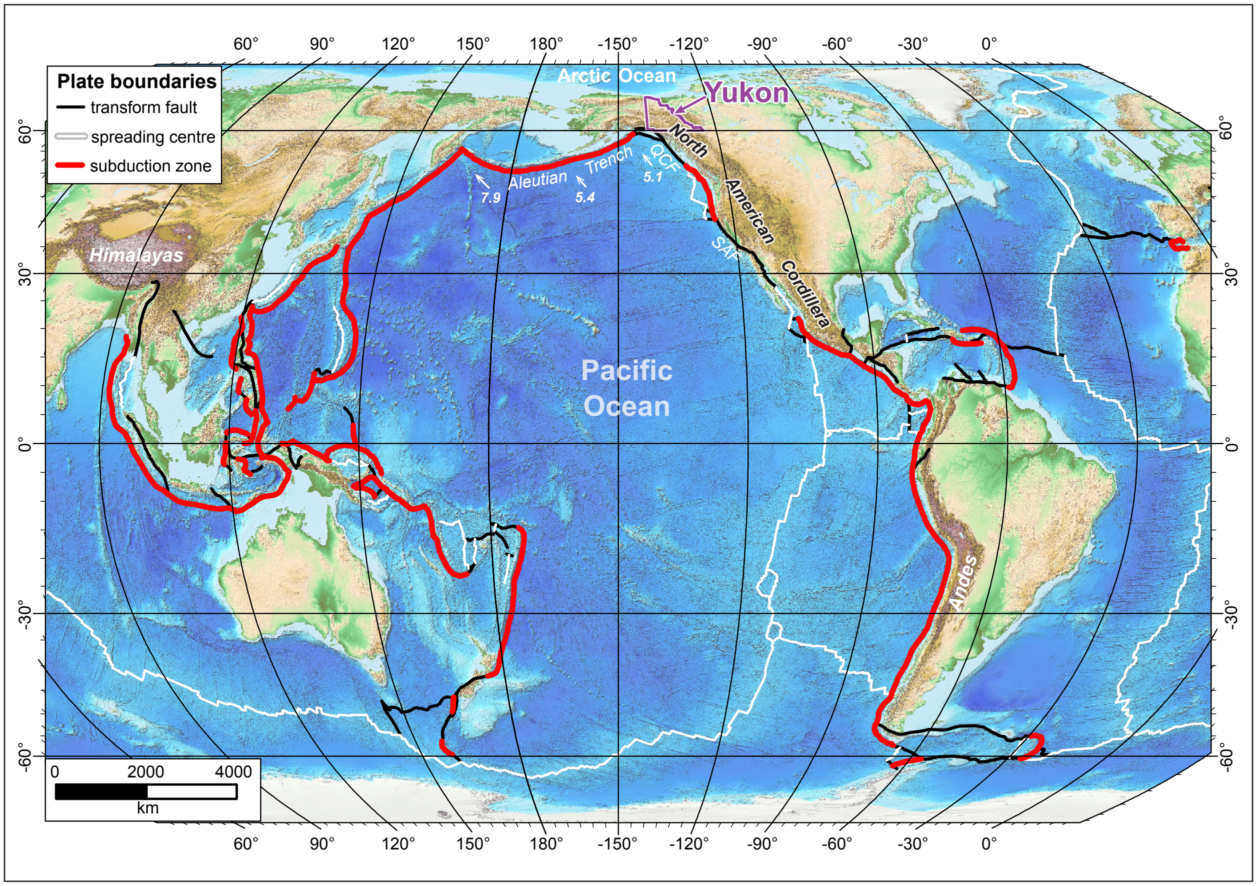

Figure 1. *The Pacific Ring of Fire. The Pacific Ocean is rimmed by subduction zones and associated magmatic arcs that are prospective regions for geothermal energy. The Yukon lies near the northeastern edge of the Pacific Plate, at the northern end of the North American Cordillera. Movement of the northern Pacific Plate is shown as GPS velocity (cm/yr; white arrows). Plate boundaries are from the compilation of Hasterok et al. (2022). Global relief model (ETOPO1) from Amante and Eakins (2009). Equal Earth projection (centred on 150°W), datum WGS84. QCF: Queen Charlotte fault; SAF: San Andreas fault.*

The North American Cordillera is generally characterized by higher heat flow compared to the continental interior and global crustal average, which is approximately 64 mW/m^2 (Fig. 2; Global Heat Flow Assessment Group, 2024). Although heat flow measurements are relatively sparse in the northern Cordillera, Lewis et al. (2003) suggested that average heat flow is higher in the Yukon (105 ± 22 mW/m^2) than in British Columbia (BC) to the south (73 ± 11 mW/m^2; Fig. 3). The higher heat flow estimated for the Yukon is comparable to the approximately 100 mW/m^2 documented in part of the Great Basin of the western United States (DeAngelo et al., 2022, 2023), where geothermal systems are actively exploited. The recognition of this potentially higher heat flow in the north, the occurrence of numerous thermal springs, and the presence locally of Neogene to Recent volcanic rocks (<20 Ma; Fig. 4) have spurred interest in evaluating the geothermal potential of the Yukon and adjacent regions.

Initial efforts were focused on studies of thermal springs and young volcanic centres (Crandall and Sadlier-Brown, 1978). Water chemistry and geothermometry were determined for 42 thermal springs in the Yukon, Northwest Territories (NWT) and northern BC. These initial studies benefitted from funding from the Government of Canada's Geothermal Energy Program (1976–1986). Subsequent studies capitalized on petroleum and mineral exploration boreholes to collect temperature profiles and thermal conductivity data, and determine temperature gradients, heat flow and depth-temperature maps (Burgess et al., 1982; Geotech Ltd., 1984; Jessop et al., 1984, 2005; Majorowicz and Dietrich, 1989; Majorowicz and Morrow, 1998;

Majorowicz and Grasby, 2014). Lewis et al. (2003) built on these earlier studies and provided additional temperature data from mineral exploration boreholes to inform their assessment of heat flow in the northern Canadian Cordillera (Fig. 3). Although these studies provided critical insights into the regional geothermal potential in the Yukon, most of these data were collected in remote areas, far from population centres, and varied in the depth and quality of the temperature measurements. For the most part, only boreholes drilled for petroleum exploration in remote sedimentary basins penetrated to sufficient depths (≥300 m) to collect reliable crustal temperature data. Additionally, in most cases only the bottom-hole temperature was recorded, and it is unknown whether all measurements were acquired after a re-equilibration period. Temperature data collected from mineral exploration boreholes are commonly of better quality (e.g., they include temperature profiles rather than single temperature measurements and were measured after a re-equilibration period) but are generally from shallower depths (<300 m).

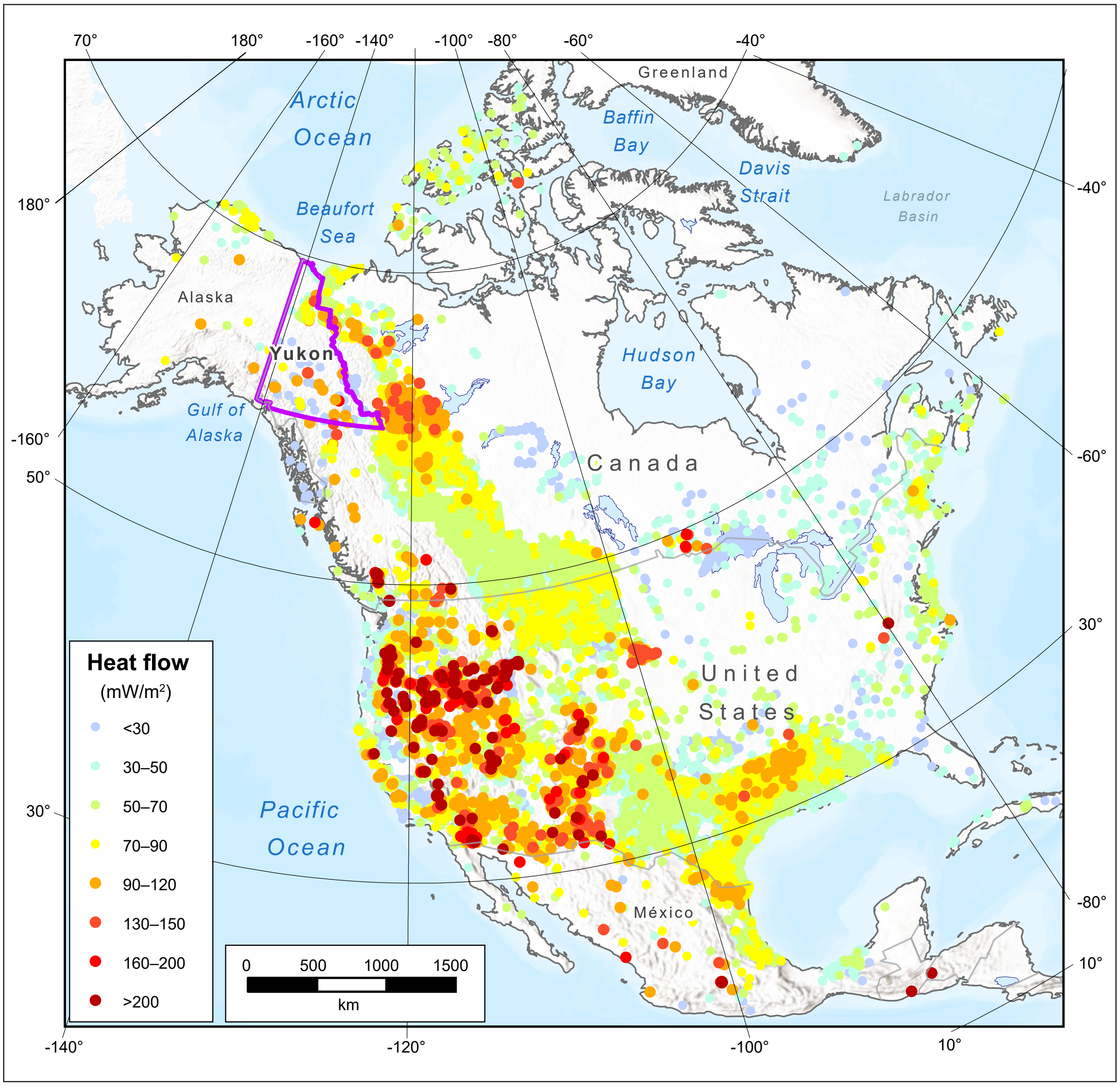

Figure 2. Heat flow map of North America. Data from International Heat Flow Commission (2016) with additional data for the northern Cordillera from Lewis et al. (2003).

Grasby et al. (2000) published water chemistry and geothermometry data for thermal springs in western Canada, including Takhini Hot Springs near the City of Whitehorse. Between 2008 and 2013, Yukon Energy commissioned several studies to further evaluate the geothermal potential of thermal springs in the Yukon. These studies were previously unpublished and are summarized for the first time in this report. Most of these earlier studies were mainly focused on identifying geothermal resources for electricity generation (temperatures ≥120°C within drilling depths of ≤2 km). Based on these studies, KGS Group (2016) performed an economic resource analysis and concluded that geothermal resources in the Yukon are modest, with inferred temperatures of less than 150°C and potential development requiring a binary geothermal power plant. They noted, however, that the assessment was based on limited geological information and a general lack of subsurface data from temperature gradient boreholes near potential development sites.

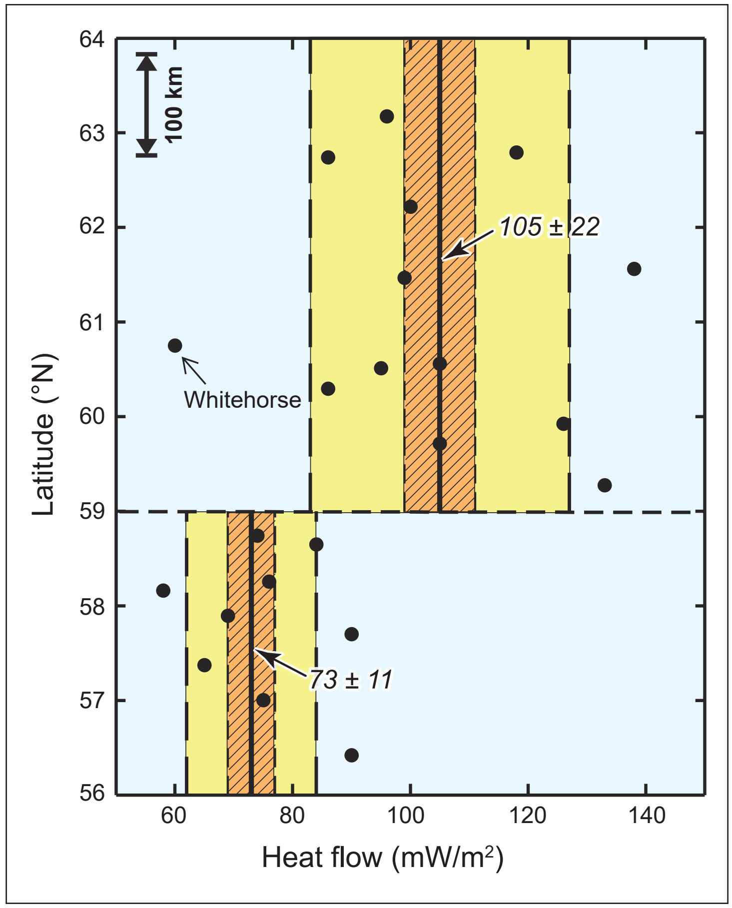

Figure 3. *Heat flow as a function of latitude for the northern Cordillera (modified from Lewis et al., 2003). The average heat flow in the Yukon (north of 60°N) is generally higher (105 ± 22 mW/m^2) than in British Columbia (south of 59°N; 73 ± 11 mW/m^2). The overall standard deviation is shown in yellow and the standard error of the mean in orange. Black dots show individual data points.*

A few studies evaluated potential geothermal resources near Yukon communities, not only for power generation but also for possible direct-use applications. In 2012, the Kluane First Nation commissioned a 387 m-deep borehole to determine the potential for heat exchange applications (Tetra Tech EBA Inc., 2015a). Results from this borehole, including additional evaluation by the Yukon Geological Survey (YGS) are discussed in this report. In 2014, the Dena Nizziddi Development Corporation of the Ross River Dena Council commissioned a study of geothermal potential within the Tintina Trench near the community of Ross River. This study was the first in the Yukon to integrate field mapping with a range of geophysical techniques to construct a 3D geological model of the area and propose potential sites for drilling temperature gradient boreholes (Mira Geoscience, 2017).

More recent interest in geothermal resources in the Yukon was in part spurred by a geothermal favourability study conducted by the Canadian Geothermal Energy Association (CanGEA; Canadian Geothermal Energy Association, 2016) based on existing qualitative and quantitative information. The CanGEA report, along with increasing government priorities toward transition to cleaner energy sources, and the potential for higher heat flow in Yukon reported by Lewis et al. (2003), provided the impetus for geothermal research by the YGS.

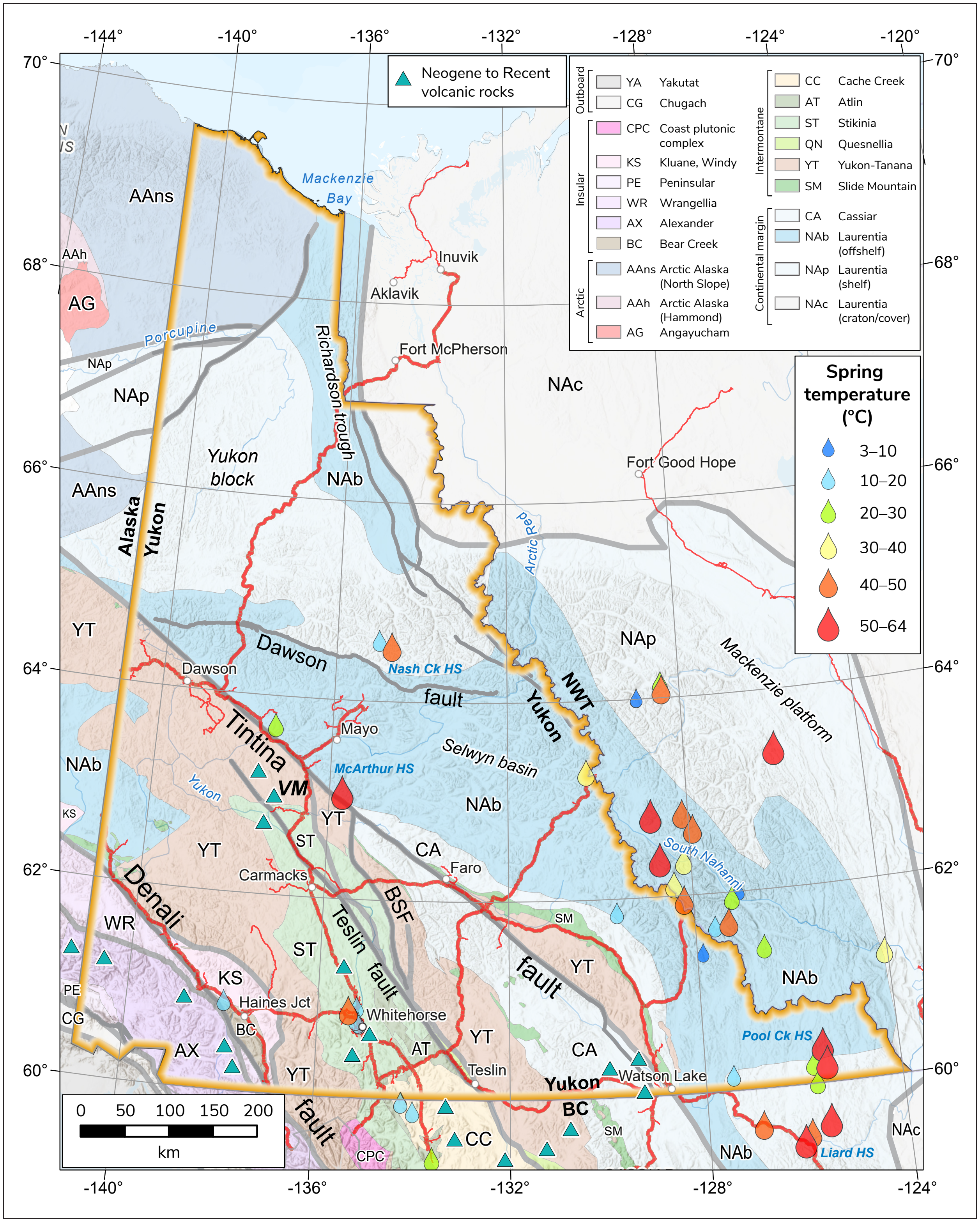

Figure 4. Occurrences of thermal springs and Neogene to recent volcanic rocks in the Yukon. Only selected hot springs are labeled on this map. Terrane map and major faults (dark grey black lines) are shown in background (Yukon Geological Survey, 2020). BC: British Columbia; BSF: Big Salmon fault; NWT: Northwest Territories; VM: Volcano Mountain (Nelruna).

Geothermal research by the Yukon Geological Survey

In 2016, the YGS initiated a geothermal research program to address some of the gaps identified in previous studies and improve understanding of geothermal potential near communities where heat resources could be used to offset reliance on hydrocarbons for heating and power generation. Initial studies focused on desktop compilation and identification of favourable geological settings for geothermal exploration. A regional estimate of crustal temperatures in the Yukon was derived by mapping the Curie point depth (CPD) using regional aeromagnetic data (Fig. 5; Li et al., 2017; Witter and Miller, 2017; Witter et al., 2018). The Curie point is the temperature at which certain materials lose their permanent magnetic properties. For magnetite, the most common magnetic mineral, the Curie point is 580°C; therefore, the CPD is taken as the depth at which a temperature of approximately 580°C is encountered in the Earth's crust. The map in Figure 5 shows the depth to the 580°C isotherm and can be used as a proxy for the estimated average geothermal gradient. Southern Yukon is generally characterized by relatively shallow CPDs ranging from 12 to 24 km; therefore, higher temperature gradients and heat flow may be present in this region. The CPD map can be used as a first-order estimate to guide further geothermal exploration. Various assumptions and uncertainties limit this approach for more focused exploration (cf. Witter and Miller, 2017 and Witter et al., 2018).

Whole-rock lithogeochemical data compiled by the YGS (Yukon Geological Survey, 2023a) was also used to calculate the potential radiogenic heat production (**A**) from granitoid plutons in the Yukon (Fig. 6; Friend and Colpron, 2017; Colpron, 2019). The calculations for Yukon granitoids show that approximately 28% of samples (~1760 in total) have **A** values above the global average of 2.5 to 2.8 μW/m^3 for granites (Rybach, 1981; Hasterok and Webb, 2017). In particular, Cretaceous granitoid plutons have anomalously elevated **A** values, commonly greater than 4 μW/m^3 and locally greater than 10 μW/m^3 (Fig. 6; Colpron, 2019). Anomalously elevated **A** values also occur in Devonian granitoids from North Yukon.

More focused studies conducted by the YGS include drilling of temperature gradient boreholes near Takhini Hot Springs, Ross River and Burwash Landing (Fraser et al., 2019; this study). Since 2018, a systematic approach to develop 3D geological models near target communities has been the foundation of geothermal research by the YGS. These models are developed using geological mapping and a range of geophysical methods aimed at characterizing the subsurface geology of focused areas, generally approximately 100 km^2, near select Yukon communities. Geophysical methods include ground gravity, aeromagnetic, and passive electromagnetic and seismic methods. The 3D geological models are used to identify potential targets that could be tested by drilling temperature gradient boreholes. The basic approach used for these targeted studies was built on the model adopted by Mira Geoscience (2017) for generating drill targets in the Tintina Trench near Ross River.

From 2020 to 2024, funding from Natural Resources Canada's Emerging Renewal Power Program and the Government of Yukon's Our Clean Future initiative was used by the YGS to assess the geothermal potential of major fault zones in southern Yukon (Fig. 4). This phase of research produced initial assessments and 3D geological models for Burwash Landing (Denali fault; Witter, 2020), Watson Lake (Tintina fault; Witter, 2022), the Village of Teslin (Teslin fault; Witter, 2023), and the Village of Haines Junction (Dakwǻkǻda; Witter, 2024). At the time of completion of this report, new data had been acquired in Haines Junction (Dakwǻkǻda) and the northern part of Whitehorse to build similar 3D models to inform future geothermal exploration.

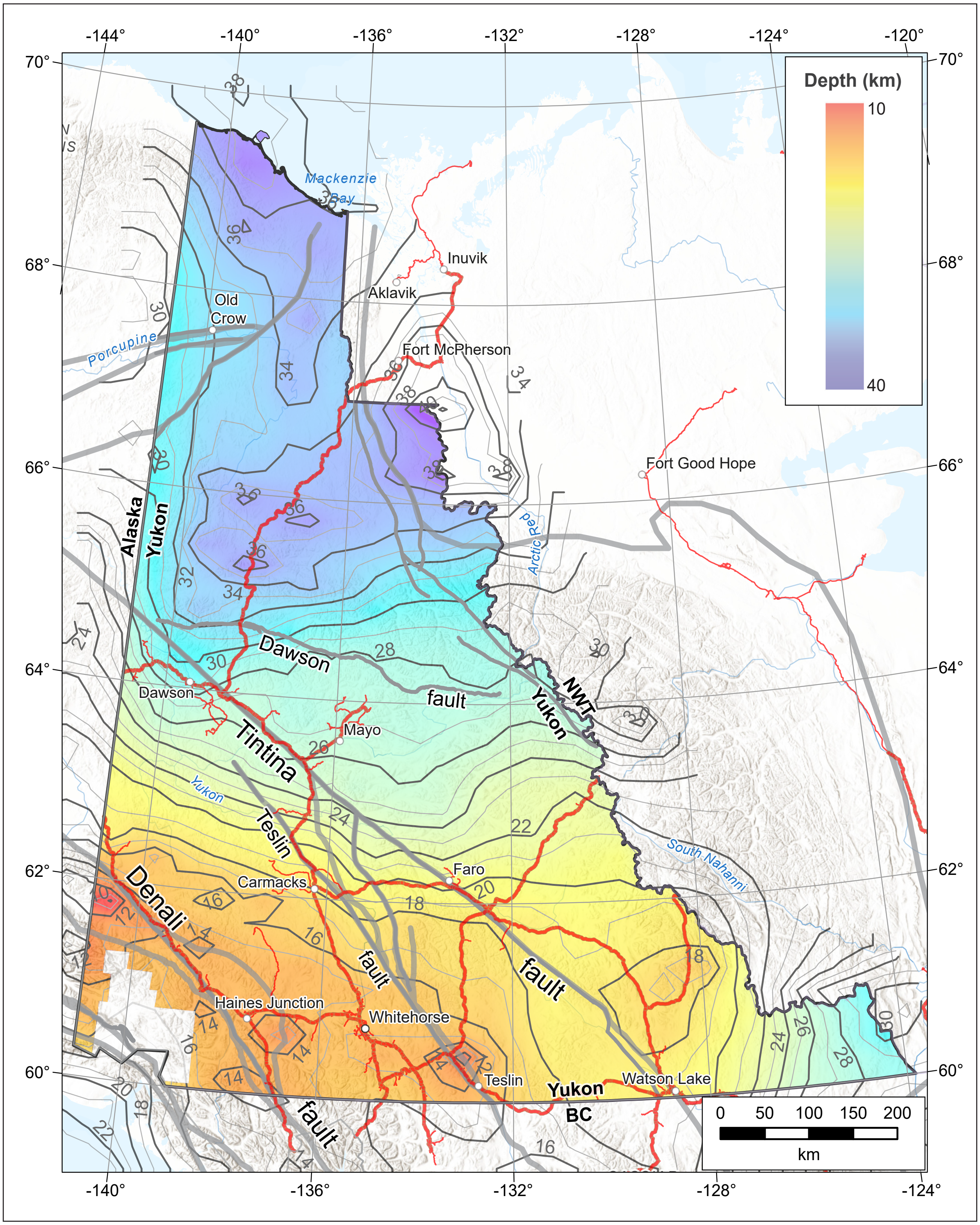

Figure 5. Curie point depth map for the Yukon, generated using data from Li et al. (2017). BC: British Columbia, NWT: Northwest Territories.

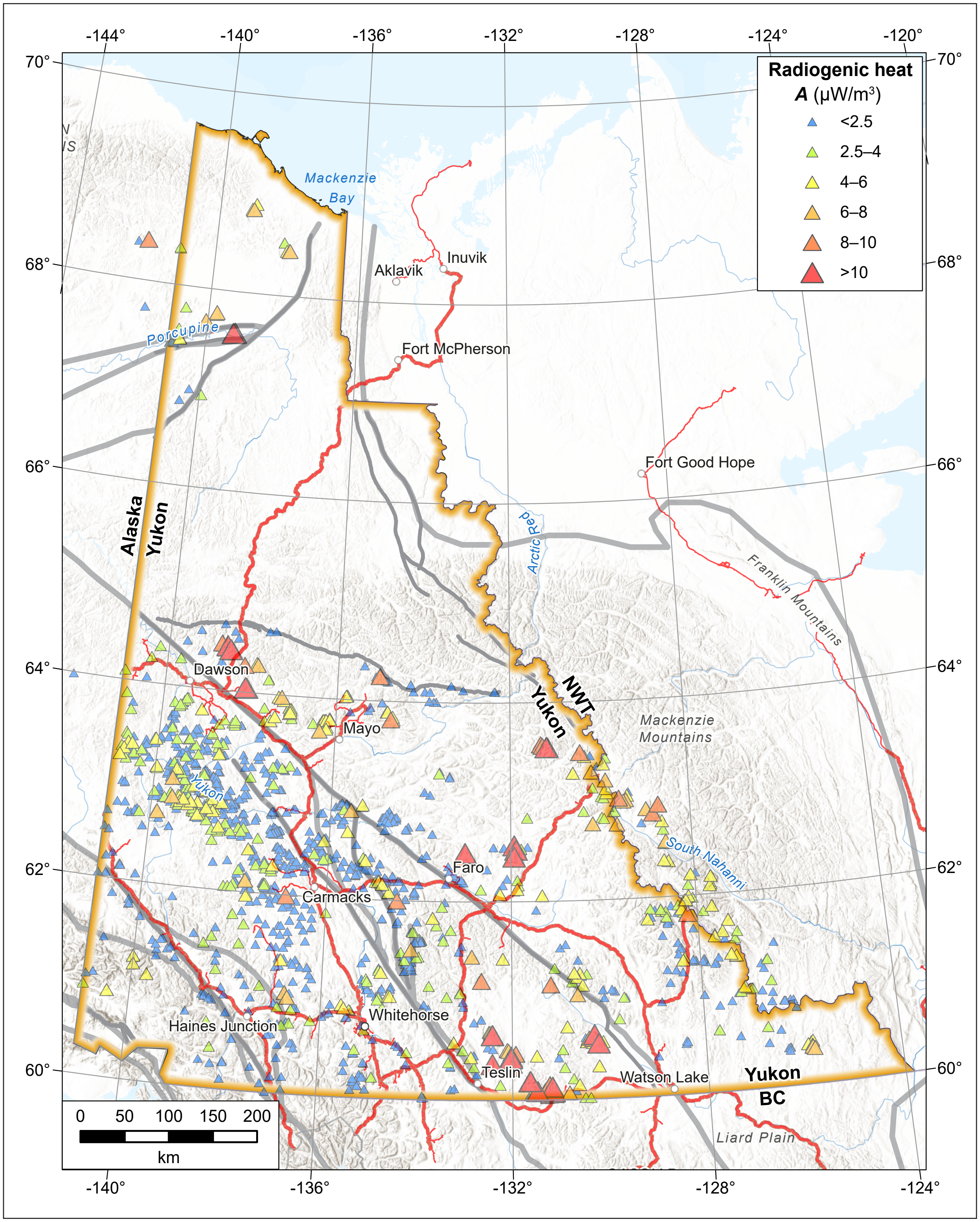

Figure 6. *Potential radiogenic heat production (*A*) from granitoid plutons in the Yukon (after Colpron, 2019, using data from Yukon Geological Survey, 2024). Solid grey lines delineate major crustal faults. BC: British Columbia, NWT: Northwest Territories.*

Structure of this report, data and methods

This report presents a summary of known geothermal indicators and data for the Yukon. It is anchored on compilations of geothermal datasets available from the YGS website (Yukon Geological Survey, 2024) and includes

- data from thermal springs (Fig. 4), including water temperature, chemistry, geothermometry and isotopic composition (where available).
- data from boreholes for which temperature data (temperature gradient, thermal conductivity and heat flow) were collected (Fig. 7). Water chemistry is also compiled for boreholes where data are available.
- results of radiogenic heat production calculations for granitoid plutons in the Yukon (Fig. 6; updated from Colpron, 2019).
- locations where open water has been observed in winter (Fig. 8). Information for this dataset is relatively sparse and mostly derived from open-water surveys commissioned by Yukon Energy (EBA Engineering Consultants Ltd., 2009a) and anecdotal information.
- a Curie point depth map of the Yukon (Fig. 5; generated using data from Li et al. [2017]).

Appendix A describes the metadata parameters of the various geothermal compilation datasets available from the YGS website.

This report is largely derived from previously unpublished reports submitted to Yukon Energy, First Nations, and community governments. We present summaries of observations derived from these reports for each study site and in some cases draw on material from several reports. The original reports are available from the YGS website (Table 1).

When describing thermal springs in this report, we use the term ‘hot spring’ when the water temperature is greater than 30°C, ‘warm spring’ the water temperature is between 10 and 30°C and ‘cold spring’ when the water temperature is less than 10°C. Throughout this report, the geological setting of the locations studied for geothermal potential is illustrated using geological maps extracted from the Yukon bedrock geology compilation (Yukon Geological Survey, 2022). For brevity, only key map units are identified in the text and most of these maps have no accompanying lithological legend. The reader can refer to the Yukon bedrock geology compilation or Colpron (2022) for full descriptions of geological map units.

The summary of geothermal indicators presented in this report is organized by region as shown in Figure 9. The indicators include a mix of direct observations and measurements (e.g., temperature profiles) and modelled values (e.g., geothermometer calculations, radiogenic heat production and Curie point depth).

Geothermometer calculations

Geothermometers can be used to provide an indication of potential geothermal source temperatures based on the concentrations of various elements in groundwater (Ferguson et al., 2009). A basic assumption for geothermometers is that elemental concentrations in groundwater are in equilibrium with the bedrock at depth. Silica geothermometers assume that silica concentration in groundwater reflects the temperature of the host rock, but both residence time and water pH can affect silica concentrations (Khan et al., 2015). Geothermometers also assume that the groundwater is representative of a given thermal reservoir or aquifer and does not account for mixing of shallow groundwater or surface water into the sample, the effects of depressurization and precipitation during transport, or interaction with the atmosphere. Geothermometers used

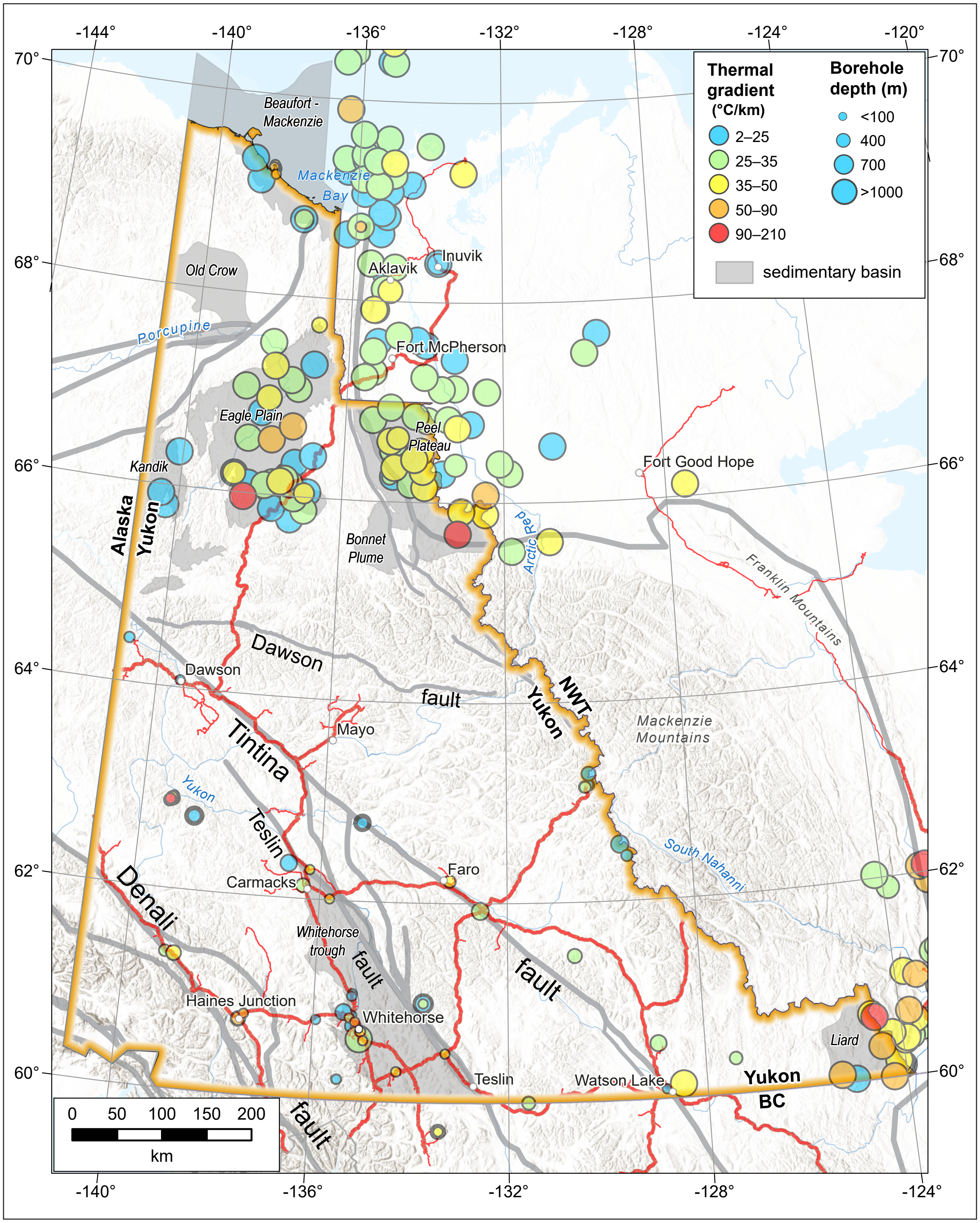

Figure 7. Compilation of temperature gradients for boreholes in the Yukon and surrounding regions (data from Yukon Geological Survey, 2024). Grey shaded areas indicate the extent of successor sedimentary basins where deep drilling associated with oil and gas exploration has been concentrated. Solid grey lines delineate major crustal faults. BC: British Columbia, NWT: Northwest Territories.

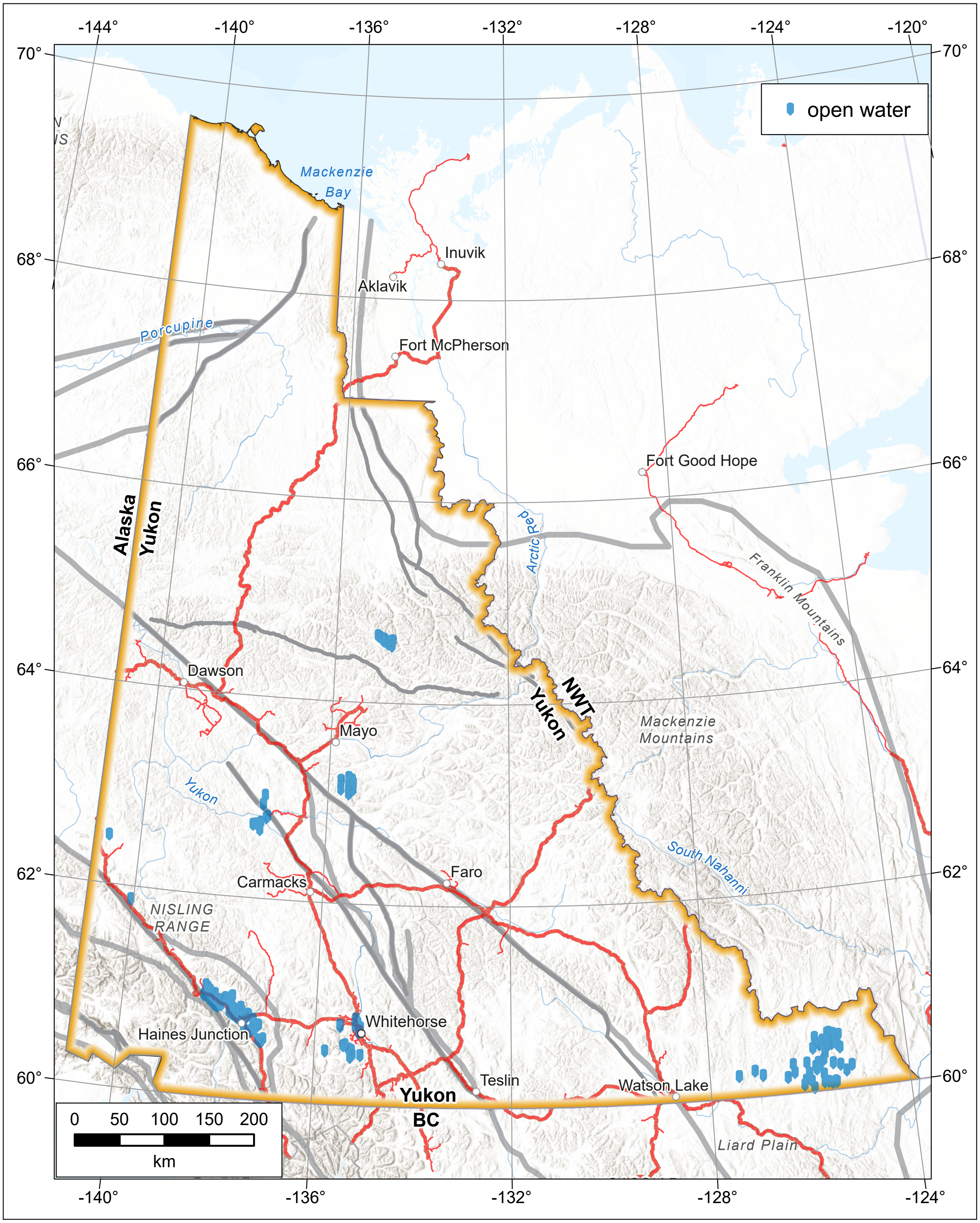

Figure 8. *Locations of open water observed in the Yukon during winter (data from Yukon Geological Survey, 2024). Solid grey lines delineate major crustal faults. BC: British Columbia, NWT: Northwest Territories.*

Table 1. *Previously unpublished reports available from the Yukon Geological Survey.*

Area	Author	Year	Title	Public URL
Beaver River	EBA Engineering Consultants Ltd.	2009b	Larsen Creek/Beaver River Open Water Survey	https://data.geology.gov.yk.ca/Reference/95996
Beaver River	EBA Engineering Consultants Ltd.	2010a	Ground-Based Geothermal Reconnaissance - Larsen Creek/Beaver River Area, Southeast Yukon	https://data.geology.gov.yk.ca/Reference/96011
Burwash Landing	EBA Engineering Consultants Ltd.	2007	Aquifer and Wellhead Protection Plan - Kluane First Nation Community Wells Burwash Landing, YT	https://data.geology.gov.yk.ca/Reference/95989
Burwash Landing	EBA, A Tetra Tech Company	2012a	Completion Report for Warm Water Well KFN-L Burwash Landing, Yukon	https://data.geology.gov.yk.ca/Reference/95990
Burwash Landing	EBA, A Tetra Tech Company	2013a	Guidance Document for Development of Cold and Warm Water Well System, Burwash Landing, Yukon	https://data.geology.gov.yk.ca/Reference/95991
Burwash Landing	Tetra Tech EBA Inc.	2015a	GeoExchange Feasibility, Burwash Landing, Yukon	https://data.geology.gov.yk.ca/Reference/95988
Burwash Landing	Tetra Tech EBA Inc.	2015b	2015 Hydrogeological Assessement Program - Burwash Landing, Yukon	https://data.geology.gov.yk.ca/Reference/95987
Haines Junction	Stanley Associates Engineering Ltd.	1980	Warm Water Well #2 Haines Junction, Yukon Territory	https://data.geology.gov.yk.ca/Reference/96021
Haines Junction	Gartner Lee Ltd.	2002	Haines Junction Well No. 5 Completion Report	https://data.geology.gov.yk.ca/Reference/96020
Haines Junction	EBA, A Tetra Tech Company	2013b	Well No.5 Gas Sampling and Analysis, Haines Junction, Yukon	https://data.geology.gov.yk.ca/Reference/96022
Jarvis River	EBA Engineering Consultants Ltd.	2009c	Discovery of Artesian Aquifer 30 km North of Haines Junction During the Geothermal Exploration Drill Program	https://data.geology.gov.yk.ca/Reference/95992
Jarvis River	EBA Engineering Consultants Ltd.	2009d	Gas Sampling, Jarvis River Warm Springs, Yukon	https://data.geology.gov.yk.ca/Reference/95993
Jarvis River	EBA Engineering Consultants Ltd.	2010b	Exploration of Geothermal Potential at Jarvis River Warm Springs - 2009 Electromagnetic Geophysics Survey Program	https://data.geology.gov.yk.ca/Reference/96006
Jarvis River	EBA Engineering Consultants Ltd.	2010c	Exploration of Geothermal Potential at Jarvis River Warm Springs - 2009 Detailed Geology Mapping Program	https://data.geology.gov.yk.ca/Reference/96000
Jarvis River	EBA Engineering Consultants Ltd.	2010e	Exploration of Geothermal Potential at Jarvis River Warm Springs - 2009 Diamond Drill Program	https://data.geology.gov.yk.ca/Reference/96005
Jarvis River	EBA Engineering Consultants Ltd.	2010f	Advanced Geochemistry, Jarvis River Warm Springs and Shakwak Valley Area, Southwest Yukon	https://data.geology.gov.yk.ca/Reference/96002
Jarvis River	EBA Engineering Consultants Ltd.	2010*	2009 Air Photograph Acquisition - Jarvis River Area, Yukon	https://data.geology.gov.yk.ca/Reference/96007
Mayo	Hydrogeological Consultants Ltd.	2011	1990 Warm Water Supply Well (PW2) Field Program Results, Yukon Territory	https://data.geology.gov.yk.ca/Reference/96024
Mayo	Hydrogeological Consultants Ltd.	2012	Recompletion of the 1975 Mayo Warm Water Supply Well (PW1) Yukon Territory	https://data.geology.gov.yk.ca/Reference/96023
Nash Creek	EBA Engineering Consultants Ltd.	2010g	Ground-based geothermal reconnaissance, Nash Creek hot springs, Wernecke Mountains, central Yukon	https://data.geology.gov.yk.ca/Reference/96001

Table 1 (continued). *Previously unpublished reports available from the Yukon Geological Survey.*

Area	Author	Year	Title	Public URL
Partridge Creek	Aurora Geosciences	2013	Partridge Creek ELF 3D Inversion	https://data.geology.gov.yk.ca/Reference/96019
Partridge Creek	EBA, A Tetra Tech Company	2011a	Preliminary Geothermal Assessment, Partridge Creek Warm Spring, North of Stewart Crossing, Yukon	https://data.geology.gov.yk.ca/Reference/96012
Partridge Creek	EBA, A Tetra Tech Company	2012b	Geological Mapping and Geochemistry, Partridge Creek Warm Spring, Yukon	https://data.geology.gov.yk.ca/Reference/96017
Partridge Creek	EBA, A Tetra Tech Company	2012c	Summary of Result: Geophysics Survey of the Partridge Creek Warm Spring, Yukon	https://data.geology.gov.yk.ca/Reference/96016
Swift River	EBA Engineering Consultants Ltd.	2010h	Desktop Study - Geothermal Potential in the Swift River Area, Yukon and British Columbia	https://data.geology.gov.yk.ca/Reference/96010
Tagish	EBA, A Tetra Tech Company	2018	Summary of Water Temperature and Groundwater Level Results at Tagish Community Centre Test Wells, Tagish, Yukon	https://data.geology.gov.yk.ca/Reference/96025
Various	EBA Engineering Consultants Ltd.	2009a	Yukon Geothermal Exploration Program - Open Water Survey	https://data.geology.gov.yk.ca/Reference/95997
Various	EBA Engineering Consultants Ltd.	2009e	Ground-based geothermal reconnaissance program, multiple areas, Yukon	https://data.geology.gov.yk.ca/Reference/95994
Various	EBA Engineering Consultants Ltd.	2009f	Yukon Geothermal Project - Results of Thermal Infrared Imagery Analysis	https://data.geology.gov.yk.ca/Reference/95999
Various	EBA Engineering Consultants Ltd.	2009g	Yukon Geothermal Project - Results of Satellite Imagery Analysis	https://data.geology.gov.yk.ca/Reference/95998
Various	EBA Engineering Consultants Ltd.	2010i	Noble Gas Data from Multiple Warm and Hot Springs in Southern and Central Yukon	https://data.geology.gov.yk.ca/Reference/96003
Various	EBA Engineering Consultants Ltd.	2010j	Summary Report - 2009 Geothermal Exploration Program - Multiple Areas, Yukon	https://data.geology.gov.yk.ca/Reference/96008
Various	EBA Engineering Consultants Ltd.	2010k	Yukon Geothermal Study - Structural Interpretation of Regional Aeromagnetic Mapping	https://data.geology.gov.yk.ca/Reference/96004
Various	EBA, A Tetra Tech Company	2011b	Subsurface Temperature Data from Borehole Measurements In Yukon	https://data.geology.gov.yk.ca/Reference/96013
Volcano Mountain	EBA Engineering Consultants Ltd.	2010l	Exploration of Geothermal Potential at Volcano Mountain - 2009 Geophysics Survey Program	https://data.geology.gov.yk.ca/Reference/96009
Whitehorse	EBA Engineering Consultants Ltd.	2009h	Integrated Geothermal Assessment Takhini Hot Springs, Yukon	https://data.geology.gov.yk.ca/Reference/96026
Whitehorse	EBA Engineering Consultants Ltd.	2009i	Hydrogeochemistry and isotope signature of Stinky Lake and Versluce Warm Springs in Whitehorse, Yukon	https://data.geology.gov.yk.ca/Reference/95995
Whitehorse	EBA, A Tetra Tech Company	2011c	Geology and Hydrogeochemistry of the Stinky Lake Warm Spring, Whitehorse, Yukon	https://data.geology.gov.yk.ca/Reference/96014
Whitehorse	EBA, A Tetra Tech Company	2011c	Geophysical Survey at Stinky Lake, Whitehorse	https://data.geology.gov.yk.ca/Reference/96015
Whitehorse	EBA, A Tetra Tech Company	2012d	Preliminary geothermal assessment, Vista Mountain warm springs, north of Whitehorse, Yukon	https://data.geology.gov.yk.ca/Reference/96018

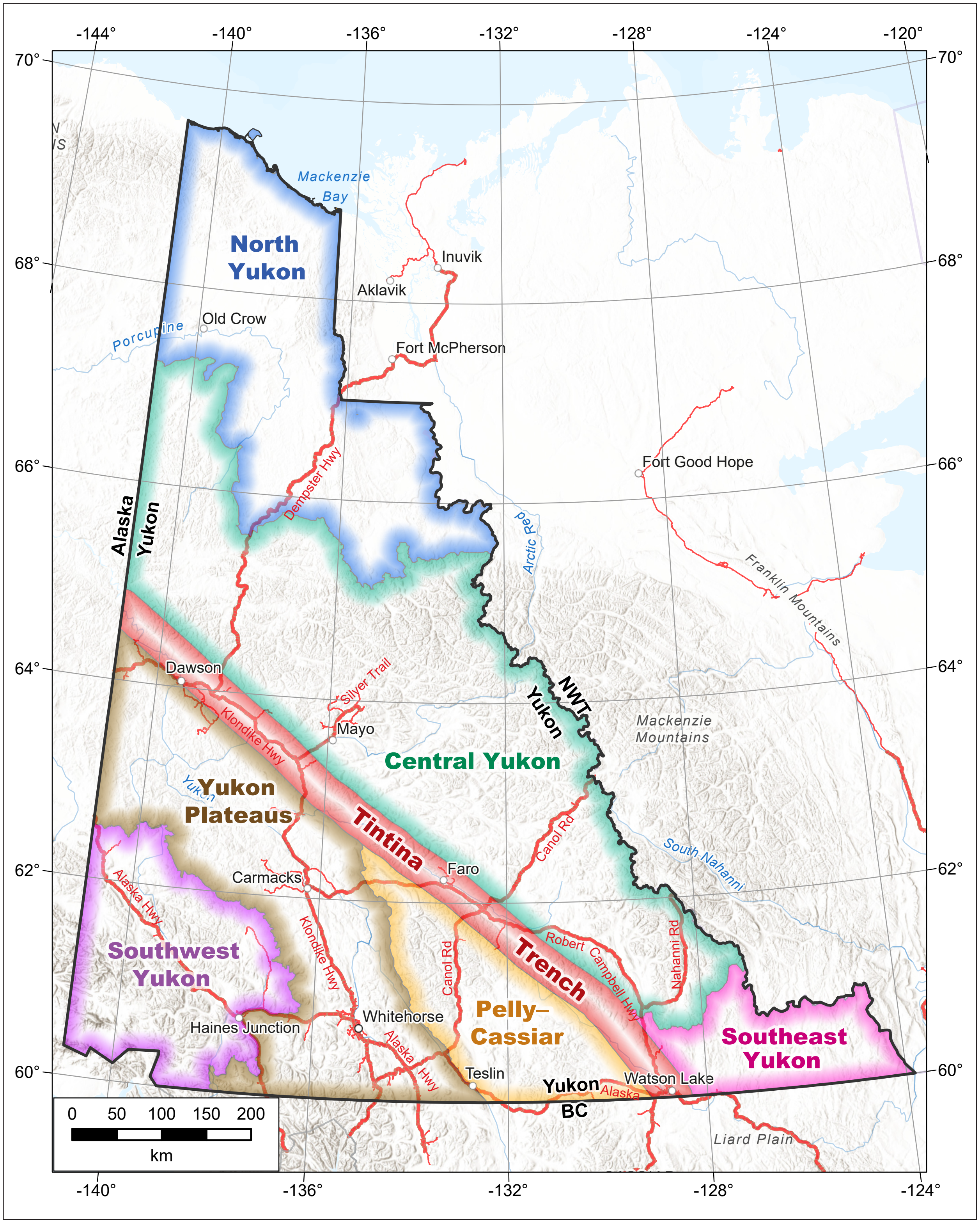

Figure 9. *Geothermal regions used in this report. BC: British Columbia, NWT: Northwest Territories.*

in this compilation include silica and alkali geothermometers reported in the summarized reports (Table 2; Khan et al., 2015).

Verma and Santoyo (1995, 1997) developed a silica geothermometer based on the regression of experimental silica solubility temperature data and refined it based on outlier rejection to create two equations: one applicable for reservoir temperatures between 20 and 210°C (equation 1) and a second for reservoir temperatures between 210 and 330°C. The second equation is not used in this compilation because reservoir temperatures above 210°C are not indicated in the dataset. Silica concentration is expressed in mg/kg or mg/L, where the fluid density is less than 1 kg/L.

$$T°C = -44.119 + 0.24469 \times [SiO_2] + 79.305 \log_{10}[SiO_2] \tag{1}$$

Fournier and Truesdell (1973) developed an alkali geothermometer to estimate the temperature of the last water–rock interaction of a given sample based on the concentrations of Na, K and Ca in groundwater. The geothermometer was developed to account for thermal waters where Na-K geothermometers underestimated temperatures because Ca concentration was not considered. Fournier and Truesdell's equation (equation 2) is applicable for a wide range of reservoir temperatures. The value of β is defined as the temperature one third below the boiling point of water (100°C). The concentrations of Na, K and Ca in equation 2 are expressed in mg/kg or mg/L, where water density is less than 1 kg/L.

$$T°C = \frac{1647}{\log\left(\frac{Na}{K}\right) + \beta \log\left(\sqrt{\left(\frac{Ca}{Na}\right) + 2.06}\right) + 2.47} - 273.15 \tag{2}$$

Fournier (1979) developed a revised Na-K geothermometer designed for reservoir temperatures ranging from 150 to 200°C. It is likely to give anomalously high temperatures in environments where temperatures are less than 100°C. In this compilation, Na-K geothermometer results are not considered for samples with anomalously high calculated temperature compared to those calculated using the Na-K-Ca and silica geothermometers. Fournier's (1979) Na-K geothermometer uses equation 3, where Na and K concentrations are expressed in mg/kg, or mg/L when calculated for liquid water.

$$T°C = \frac{1217}{\log\left(\frac{Na}{K}\right) + 1.483} - 273.15 \tag{3}$$

Noble gas analysis

Isotopes of noble gases Ar, He and Ne can be used as tracers for groundwater history, including residence time and crustal or mantle rock interactions. In particular, He isotopes are useful in determining contributions of primordial $^3He/^4He$ degassing from the mantle (characterized by elevated ^3He concentrations) versus crustal ratios, which are affected by increased ^4He produced by radiogenic decay of U and Th in the crust (Kennedy and van Soest, 2007). Helium isotopic composition ($^3He/^4He$) is generally expressed as R/Ra, the ratio of $^3He/^4He$ in the water sample (R) to $^3He/^4He$ in the atmosphere (Ra = 1.4×10^{-6}) and reported as a multiple of Ra (Kennedy and van Soest, 2007; Timmerman et al., 2019). The continental crust is characterized by low $^3He/^4He$ ratios of approximately 0.02 Ra, whereas mantle ratios are typically greater than 6 Ra. The degassing of He from the mantle is thought to occur primarily through active magmatism or actively deforming lithospheric-scale fault zones.

The He isotopic composition of water samples collected at thermal springs in the Yukon (EBA Engineering Consultants Ltd., 2010i) are summarized in this report along with results from

Table 2. *Summary of water geochemistry and geothermometry for thermal springs and select groundwater wells in Yukon. Complete analyses are provided in source reports. HS: Hot Spring, WS: Warm Spring.*

Springs	Latitude	Longitude	Temp. (°C)	Discharge (L/s)	Silica GT[1] (°C)	Alkali GT[1] (°C)	pH	Conductivity (µS/cm)	Hardness (mg/L)	^{18}O (‰)	^{2}H (deuterium; ‰)	^{3}H (tritium; TU[2])	$^{3}He/^{4}He$ (measured)	R/Ra[3]	Source(s)
Caesar Lake	61.410	–127.88	3	40	82	–	7.4	–	–	–	–	–	–	–	Crandall and Sadlier-Brown, 1978
Canyon Creek WS	60.276	–125.648	15	–	43–58	178	7.3	423	225	–22.9	–175	6.3	–	–	EBA Engineering Consultants Ltd., 2010a
Coal River WS	60.152	–127.436	13.2	45	15	167–172	6.6	531	285	–22.6	–172.2	4.7	6.97×10^{-7}	0.50	EBA Engineering Consultants Ltd., 2010a
Crestview SLC1 WS	60.789	–135.203	15.8	–	–	–	7.8	360	213	–20.8	–166.8	9.8	–	–	EBA Engineering Consultants Ltd., 2009i
Crestview SLC2 WS	60.789	–135.201	12	1	39	163	7.7	404	162	–19.5	–161.6	7.9	–	–	EBA Engineering Consultants Ltd., 2009i
Crow River WS	60.199	–125.790	29.2	–	53–65	232	6.9	367	254	–22.7	–174.4	<0.8	–	–	EBA Engineering Consultants Ltd., 2010a
Jarvis River WS	60.901	–137.970	17.7	5	73–111	62–100	8.1	660	79	–25.6	–198	<0.8	7.01×10^{-7}	0.50	EBA Engineering Consultants Ltd., 2009d, 2010b
Larsen North HS	60.199	–125.513	53	40	83-92	220	7	554	284	–23	–176	<0.8	3.79×10^{-7}	0.27	EBA Engineering Consultants Ltd., 2010a
Larsen South HS	60.198	–125.524	43	30	77–99	216–219	6.8	538	282	–22.8	–175.2	<0.8	4.07×10^{-7}	0.29	EBA Engineering Consultants Ltd., 2010a
McArthur HS	63.068	–135.712	54.5	30	150–164	117–129	7.2	268	4	–21.9	–169.3	–	–	–	EBA Engineering Consultants Ltd., 2009e
McPherson Lake WS	61.861	–129.669	16	20	85	–	7.3	–	–	–	–	–	–	–	Crandall and Sadlier-Brown, 1978
Nash Creek HS	64.551	–134.710	45.6	3	76–83	49–50	7.3	390	170	–21.8	–173.6	3.7	1.40×10^{-7}	0.10	EBA Engineering Consultants Ltd., 2010e
Nash Creek WS (N09S-10)	64.609	–135.009	10.2	–	28	–	8.2	207	106	–22.7	–172.7	–	2.39×10^{-7}	0.17	EBA Engineering Consultants Ltd., 2010e
North Cantung HS	62.115	–128.405	32	40	66	–	–	–	–	–	–	–	–	–	Crandall and Sadlier-Brown, 1978
Partridge Creek WS	63.705	–137.311	25.1	–	112–116	95–122	8.8	441	17	–21.5	–172.2	<0.8	–	–	EBA, A Tetra Tech Company, 2011a, 2012b
Pool Creek HS	60.381	–125.569	54.5	3	74–99	203	6.4	667	345	–23	–177.9	<0.8	7.85×10^{-7}	0.56	EBA Engineering Consultants Ltd., 2010a
Stinky Lake WS	60.752	–135.128	18.5	1	83–87	160	7.6	347	190	–21.3	–169.8	5.9	3.50×10^{-6}	2.50	EBA Engineering Consultants Ltd., 2009i; EBA, A Tetra Tech Company, 2011c
Takhini HS	60.879	–135.360	47	6.5	94–136	–	6.6	2905	–	–	–	–	–	–	van Everdingen, 1973a; Crandall and Sadlier-Brown, 1978; Grasby et al., 2000; this study
Thorpe Creek WS	60.010	–125.747	25.3	5	35–60	180–183	6.9	488	256	–21.5	–172.6	1.2	2.26×10^{-7}	0.16	EBA Engineering Consultants Ltd., 2010a
Versluce WS	60.761	–135.146	12.7	1	54–97	164	7.6	336	182	–20.6	–167.1	11.3	–	–	Crandall and Sadlier-Brown, 1978; EBA Engineering Consultants Ltd., 2009i; this study
Vista Mountain WS	60.916	–135.189	13.7	4	110	108	10.07	624	14	–22.42	–177.25	<0.8	–	–	EBA, A Tetra Tech Company, 2012d
West Cantung HS	61.955	–128.206	41	30	109	–	–	–	–	–	–	–	–	–	Crandall and Sadlier-Brown, 1978
Wells															
TH02-01 Miles Canyon Aquifer	60.7	–135.017	8.81	–	–	–	8.51	819	113	–21.55	–174.99	–	–	–	EBA Engineering Consultants Ltd., 2008b
Haines Junction Well No.5	60.757	–137.529	20	13	73–110	26–65.5	8.7	345	9	–23.07	–176	–	1.34×10^{-6}	0.96	Gartner Lee Ltd., 2002; EBA Engineering Consultants Ltd., 2003, 2009e; Tetra Tech, 2017
Burwash Landing (KFN-L)	61.354	–138.978	15.9	0.3	–	–	7.84	1060	406	–	–	–	8.14×10^{-7}	0.58	EBA, A Tetra Tech Company, 2012a; Tetra Tech EBA, 2015b

Notes:

1. The range of geothermometer (GT) calculations are shown here. Consult the cited report(s) for details. A number of geothermometers were recalculated for this study using updated equations listed in the Methods section of this report.
2. TU: Tritium Units (1 TU = 0.1181 Becquerels/L; 1 TU equals 1 ^{3}H atom in 10^{18} ^{1}H atoms).
3. Ratio of $^{3}He/^{4}He_{measured}$ (R) to $^{3}He/^{4}He_{air}$ (1.4×10^{-6}; Ra).

two water samples collected for this study from deep (>300 m) boreholes at Haines Junction (Dakwǎkǎda) and Burwash Landing (Table 2; Appendix B).

Noble gas samples were collected using dedicated noble gas sampling equipment. In Haines Junction (Dakwǎkǎda), Well No. 5 was sampled at the wellhead using silicone between the sample port and sample containers. The water sample was collected in triplicate in copper tubing sealed by clamping each end following standard methods: Water was allowed to flow through each sample tube for a minimum of 5 minutes, the sample tube was tapped to dislodge any air bubbles, then the flow was restricted and the clamps closed at the downstream end followed by the upstream end to prevent any atmospheric air exchange or degassing.

In Burwash Landing, noble gas was collected from the KFN-L borehole by placing a submersible gas diffusion sampler downhole into the screened section of the borehole and allowing the sampler to equilibrate in the borehole over a 24-hour period. The diffusion sampler consists of a gas-permeable tube attached to copper tubing. Three gas samples were clamped in the copper tubing following retrieval from the borehole.

All gas samples were extracted and analyzed at the Noble Gas Tritium Laboratory at the University of Ottawa using a Helix SFT noble gas mass spectrometer (Appendix B).

Borehole temperature measurements

The borehole data compilation includes geothermal gradients and downhole temperatures measured in a range of settings and depths throughout the Yukon. The data are presented as a guide to future exploration but must be used with caution because not all temperature data in the compilation are of equal quality. Borehole temperature measurements were collected at various times after drilling using several different methods, including: thermistor cables with one or more nodes, vibrating wire piezometers, temperature probes collecting continuous profiles, and distributed temperature sensor (DTS) fibre optic cables. The reliability of downhole temperature measurements collected immediately after borehole completion as part of a logging suite, such as those collected in oil exploration boreholes, should be evaluated carefully. Drilling activities affect thermal regimes by adding heat to the system (through friction on the drill bit, rods and equipment) and removing heat from the system (through circulation of cool drilling fluid). For many boreholes, only a bottom-of-hole temperature was reported. A qualitative confidence estimate of temperature gradient is provided in the attribute table (Appendix A; Fig. 10) as an indicator of the reliability of the data in the borehole data compilation.

Radiogenic heat production

The decay of radioactive elements converts mass into radiation energy, which is in turn converted to heat. Though all naturally radioactive isotopes generate some heat, significant heat generation only occurs during the decay of ^{238}U, ^{235}U, ^{232}Th and ^{40}K; therefore, potential heat production is governed by the concentrations of U, Th and K in the rock (Rybach, 1981). In igneous rocks, radiogenic heat production is dependent on the bulk chemistry of the rock and decreases from acidic (e.g., granite) through basic to ultrabasic rock types (Rybach, 1981).

A method for calculating potential radiogenic heat production (**A**) from plutonic rocks is given by equation 4:

$$\mathbf{A}\ (\mu W/m^3) = 10^{-5}\ \boldsymbol{\rho}\ (9.52\mathbf{c}_U + 3.48\mathbf{c}_{Th} + 2.56\mathbf{c}_K), \qquad (4)$$

where c is the concentration of radioactive elements U (in ppm), Th (in ppm), and K (in %), and $\boldsymbol{\rho}$ is the rock density (in kg/m^3). The heat production constants of the natural radioactive elements U, Th and K are 9.525×10^{-5}, 2.561×10^{-5} and 3.477×10^{-9} W/kg, respectively (Rybach, 1981).

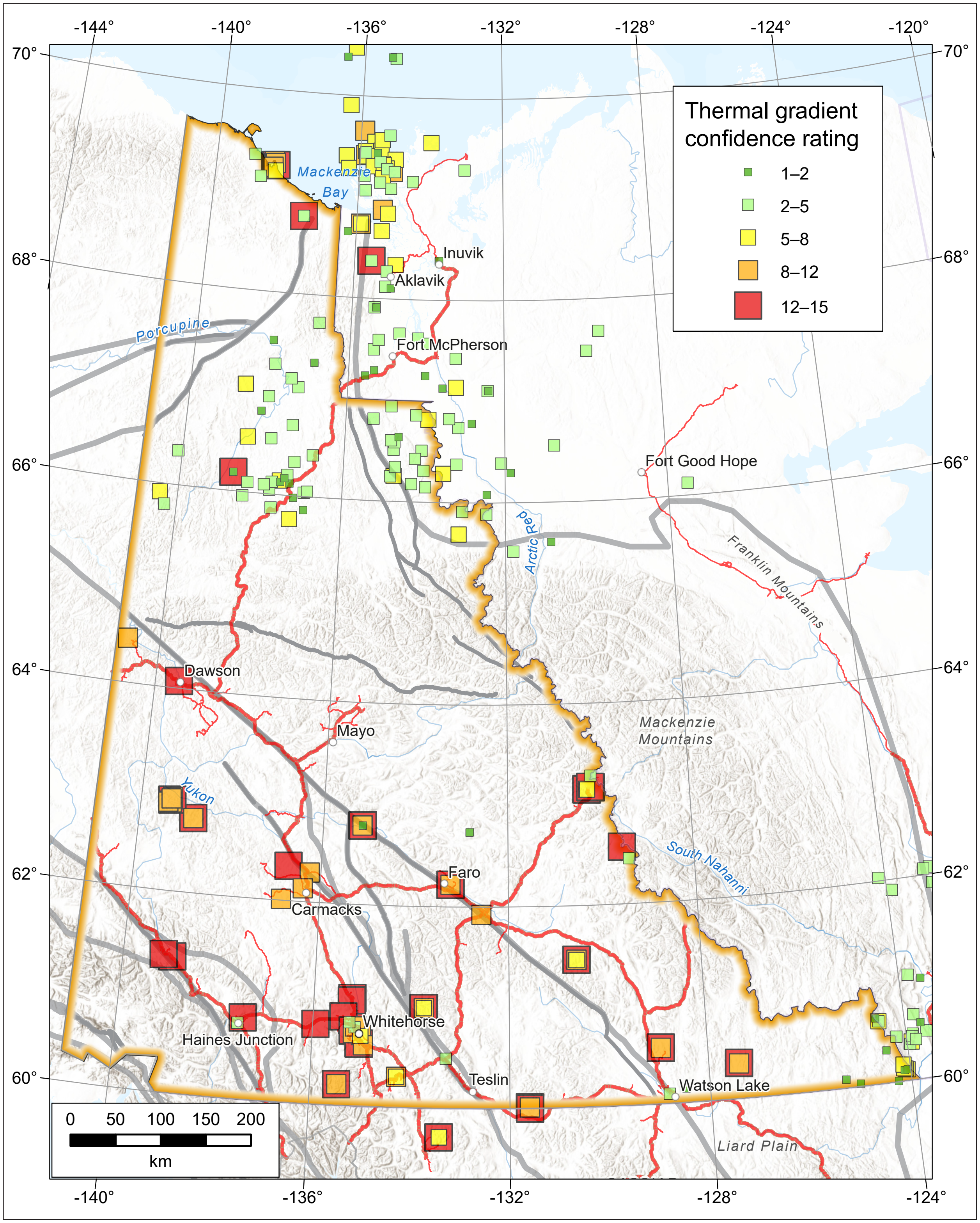

Figure 10. Confidence rating for thermal gradients included in the borehole compilation (Fig. 7), based on the criteria listed in Appendix A. Higher values indicate greater confidence.

North Yukon

The North Yukon region comprises the area north of the northern Ogilvie and Mackenzie mountain ranges (Fig. 9). Old Crow is the only community in this region. The Dempster Highway (Yukon Highway 5) bisects the region and there is one service area at Eagle Plains (Fig. 11). South of Old Crow, the area is underlain by Proterozoic to Cretaceous sedimentary rocks of the Yukon block, including Paleozoic strata of the Ogilvie platform and Richardson trough (Fig. 4; Yukon Geological Survey, 2022). The eastern part of the area is dissected by the seismically active Richardson fault array, including the Knorr and Trevor faults (Fig. 11). North of the Porcupine and Yukon faults, the region is characterized by Neoproterozoic to Devonian sedimentary rocks of the North Slope subterrane (part of Arctic Alaska terrane) intruded by a suite of Devonian plutons and overlapped by Carboniferous to Cenozoic sedimentary strata (Yukon Geological Survey, 2022). The Porcupine fault zone is a lithospheric-scale structure associated with apparent offset of the Mohorovičić discontinuity (Miller and Moresi, 2018).

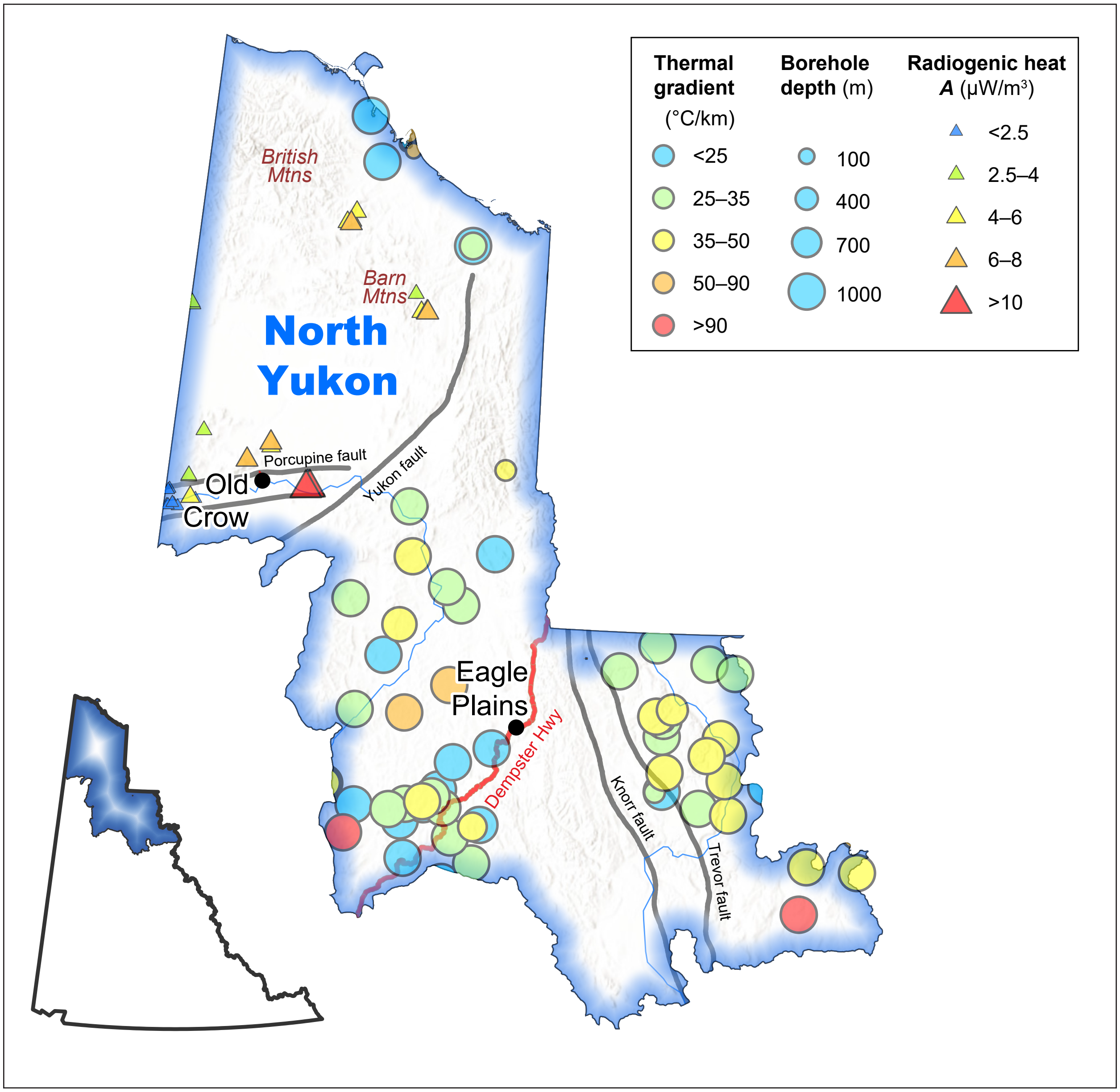

Figure 11. *Geothermal indicators in the North Yukon region.*

Geophysical modelling indicates that North Yukon is mainly underlain by thick and cold lithosphere (Amaru, 2007; Estève et al., 2020a). This is consistent with CPD modelling that shows depths of greater than 32 km for much of the region (Fig. 5), an estimated geothermal gradient of less than or equal to 18°C/km (lower than crustal average), and low heat flow (~50 mW/m^2; Witter et al., 2018). North Yukon and the adjacent NWT have been targeted for petroleum exploration with drilling of more than 140 deep boreholes. Majorowicz and Morrow (1998) provided geothermal gradient estimates for many of these boreholes. Most have low to moderate geothermal gradients (<40°C/km; Fig. 7) and a low confidence rating (Fig. 10) because the measurements were taken during drilling operations. A few boreholes have anomalously high thermal gradients (>50°C/km) but are located far (>40 km) from Old Crow and Eagle Plains (Fig. 11).

Devonian granitoid plutons of the Old Crow suite intrude the North Slope subterrane of Arctic Alaska near Old Crow and the British and Barn mountains to the north (Yukon Geological Survey, 2022). Radiogenic heat production values (A) calculated from samples of the Old Crow plutonic suite range from 1.5 to 14.7 µW/m^3, and plutons closest to Old Crow generally yielded **A** values in excess of 5 µW/m^3 (Figs. 6 and 11). The combination of heat-producing plutons and deep crustal faults in the vicinity of Old Crow represents the best opportunity for further investigation of geothermal potential in the North Yukon region.

Central Yukon

The Central Yukon region comprises the area northeast of the Tintina Trench, north of the Southeast Yukon region, and south of the North Yukon region (Fig. 9). The main communities in Central Yukon are the Village of Mayo and Keno City, both accessed via the Silver Trail (Yukon Highway 11; Fig. 12). The Dempster Highway (Yukon Highway 5), Robert Campbell Highway (Yukon Highway 4), North Canol Road (Yukon Highway 6) and Nahanni Range Road (Yukon Highway 10) provide additional access to the region. The region encompasses the southern Ogilvie and Wernecke mountains in the north, the Stewart Plateau near Mayo, and parts of the Selwyn and Mackenzie mountains southeast of Mayo.

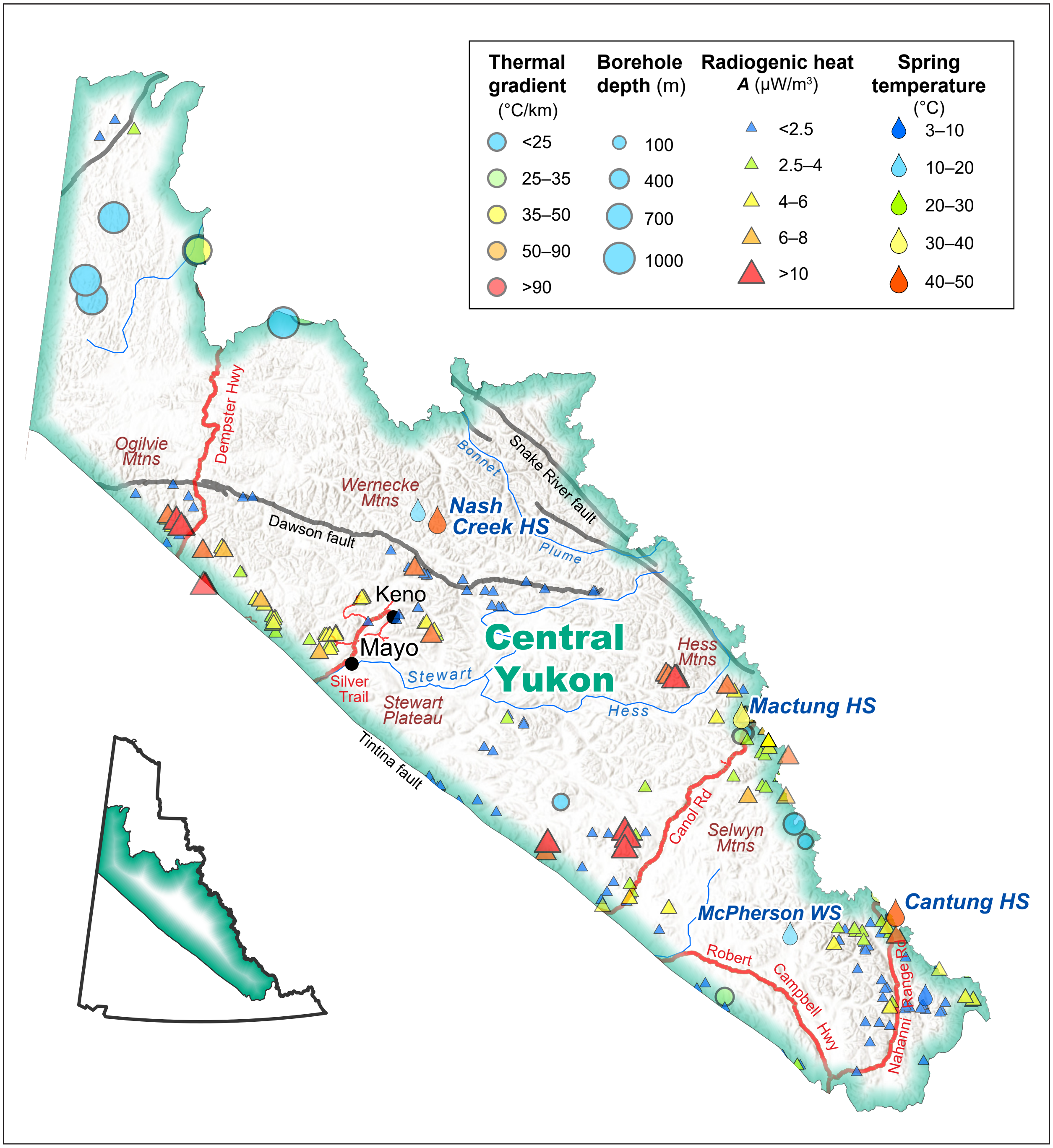

Figure 12. Geothermal indicators in the Central Yukon region. HS: hot spring, WS: warm spring.

The northern part of the Central Yukon region is underlain by Paleoproterozoic to late Paleozoic sedimentary rocks of the Yukon block north of the Dawson fault (Yukon Geological Survey, 2022). South of the Dawson fault, the region comprises mainly Neoproterozoic to Triassic sedimentary rocks of the Selwyn basin, including local occurrences of Cambrian to Devonian volcanic rocks. Rocks of the Selwyn basin are intruded by Cretaceous plutons, some of which yielded anomalously high values of radiogenic heat production (**A** >4 μW/m^3), including clusters of radiogenic plutons occurring between the City of Dawson and Mayo, east of Faro, and along the Yukon-NWT border (Fig. 6).

Curie point depths in the Central Yukon region range from deep (>30 km) in the north to moderate (16–30 km) in the southeast. The shallowest CPD (16 km) occurs beneath the Nahanni Range Road (Fig. 5). Central Yukon is host to thermal springs, some of which may be related to the numerous springs found in the Mackenzie Mountains, NWT (Fig. 4). There is limited subsurface temperature data from boreholes in the Central Yukon region. Deep boreholes for petroleum exploration were drilled in the northern part of the region (Fig. 12). The data are of moderate to low confidence and generally have thermal gradients below the crustal average (~25°C/km). In the southern part of the region, temperatures were measured in shallower mineral exploration boreholes at a few localities. Thermal gradients from these boreholes are generally less than 30°C/km (Figs. 7 and 12). Warm water has also been encountered in municipal boreholes in Mayo.

Mayo warm water boreholes

Warm water occurs in Mayo in six municipal boreholes ranging in depth from 95.5 to 268.8 m. Two of the warm water boreholes are owned by the Village of Mayo, produce approximately 15°C water, and have been used as a heat source for the municipal water supply for more than 50 years. Another four boreholes were advanced into a shallower aquifer at the First Nation of Na-Cho Nyäk Dun administration building and produce water at 6.5 to 7.5°C that is used as a potable water supply.

The geology of Mayo comprises a Quaternary alluvial terrace unit underlain by bedrock of the Hyland Group, which was encountered at depths of 262.5 and 268.8 m in the Mayo municipal boreholes (Kennedy, 2011). These municipal boreholes are artesian and have pressures of 165 to 490 kPa, which correspond to static water levels 17 to 50 m above ground surface (MLM Ground-Water Engineering Ltd., 1986; Tetra Tech, 2017). The First Nation of Na-Cho Nyäk Dun boreholes were installed in a sand and gravel aquifer encountered at depths of 90.2 to 109.0 m and have static water levels approximately 43 m below ground surface (Tetra Tech, 2017). Both municipal boreholes produce sodium-calcium-bicarbonate–type water with basic pH (7.74–8.25), and elevated sulphate (73.7–86.0 mg/L) and magnesium (21.0–21.6 mg/L; Hydrogeological Consultants Ltd., 2011, 2012) concentrations. The First Nation of Na-Cho Nyäk Dun warm water boreholes produce calcium-bicarbonate–type water with neutral to basic pH (6.95–8.16) and elevated sulphate (86.0–97.4 mg/L) and magnesium (35.8–57.6 mg/L; Tetra Tech, 2017) concentrations. A geothermal gradient of 48°C/km was measured to a depth of 104.8 m in one of the First Nation of Na-Cho Nyäk Dun boreholes (EBA, A Tetra Tech Company, 2011e). Radiogenic granites approximately 20 km northwest of Mayo have **A** values of 3.1–6.2 μW/m^3 (Figs. 6, 12) that could provide a local heat source in the region.

Nash Creek hot springs

The Nash Creek hot springs are located approximately 110 km northeast of Mayo in the Wernecke Mountains (Fig. 12). Nash Creek is a tributary of the Wind River, and the springs are situated along its south bank, approximately 10 km upstream of the confluence with the Wind River (Fig. 13). The springs occur within a Category A Settlement Land parcel of the First Nation of Na-Cho

Nyäk Dun (block NND R-11A). The Nash Creek hot springs are hosted in carbonate rocks of the Cambrian to Devonian Bouvette Formation (CDB on Fig. 13; Yukon Geological Survey, 2022).

A total of 27 thermal spring features emanate from a single linear structure striking 075° and extending approximately 350 m, and many of the springs vent from joints in the limestone (EBA Engineering Consultants Ltd., 2010g, j). The springs produce clear, odourless water and form a small, hot stream that flows into Nash Creek (Fig. 14; Woodsworth, 2009). The highest temperature measured was 46°C (EBA Engineering Consultants Ltd., 2010g). An aerial open-water and infrared survey identified numerous thermal anomalies in the region and a warm spring approximately 15 km west-northwest of the Nash Creek hot springs (Figs. 8, 13). The warm spring has moderate flow and measures 10.8°C (EBA Engineering Consultants Ltd., 2010g).

The Nash Creek hot springs have calcium-magnesium-sodium-bicarbonate-chloride–type water chemistry characterized by relatively high sodium concentrations (EBA Engineering Consultants Ltd., 2010g). Water from the warm springs to the west-northwest is calcium-magnesium-bicarbonate type. All thermal waters in this region appear to be sourced from local groundwater with enrichment in sodium and chloride in the hot springs. Stable isotopes and noble gas concentrations in the Nash Creek hot springs suggest the thermal water is from local meteoric water sources with residence times of less than 60 years (EBA Engineering Consultants Ltd., 2010i; Terzer-Wassmuth et al., 2022).

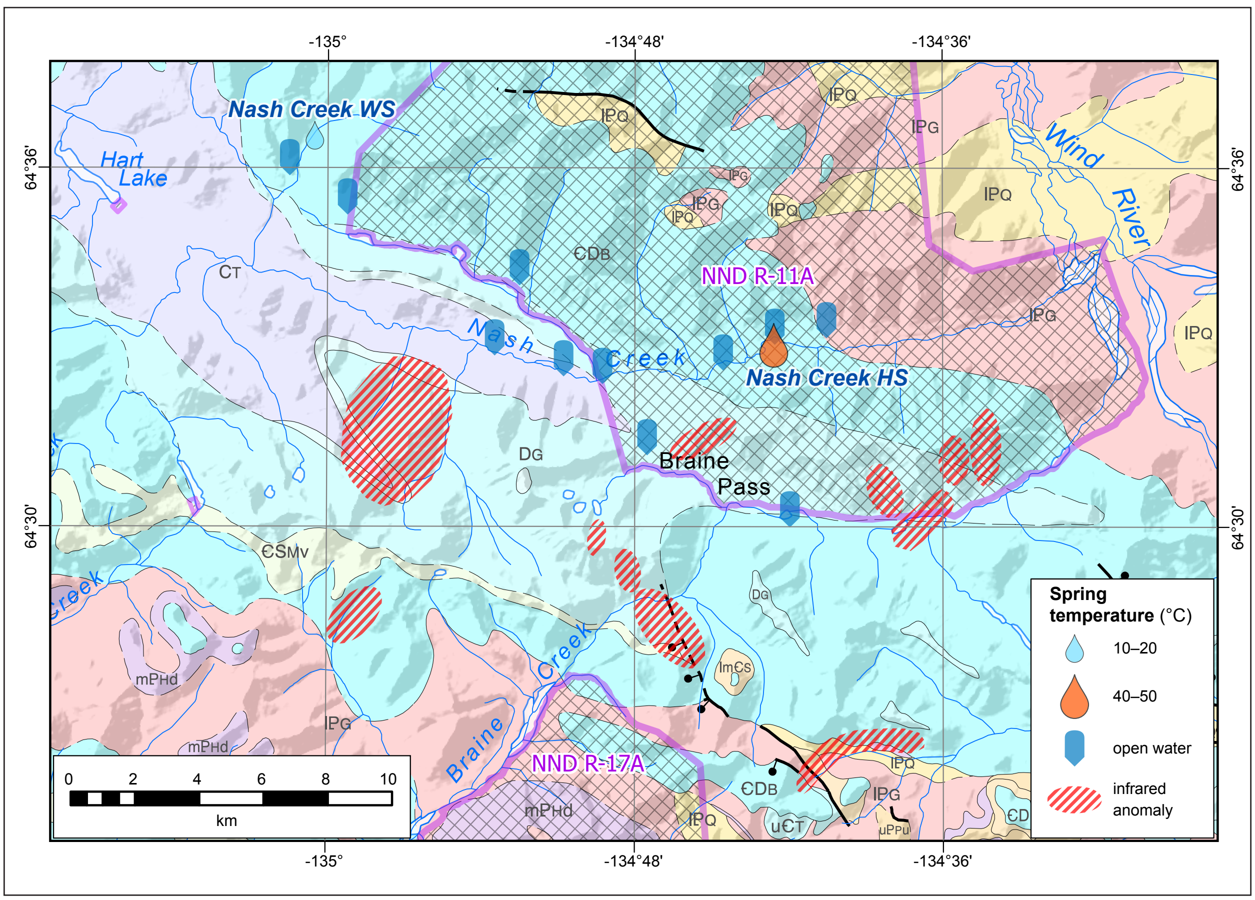

Figure 13. *Geology of the Nash Creek area with location of hot (HS) and warm springs (WS), and thermal anomalies identified from infrared satellite analysis and open water surveys (EBA Engineering Consultants Ltd., 2010j). Geology from Yukon Geological Survey (2022). Cross hatched areas indicate Category A Settlement Lands of the First Nation of Na-Cho Nyäk Dun.*

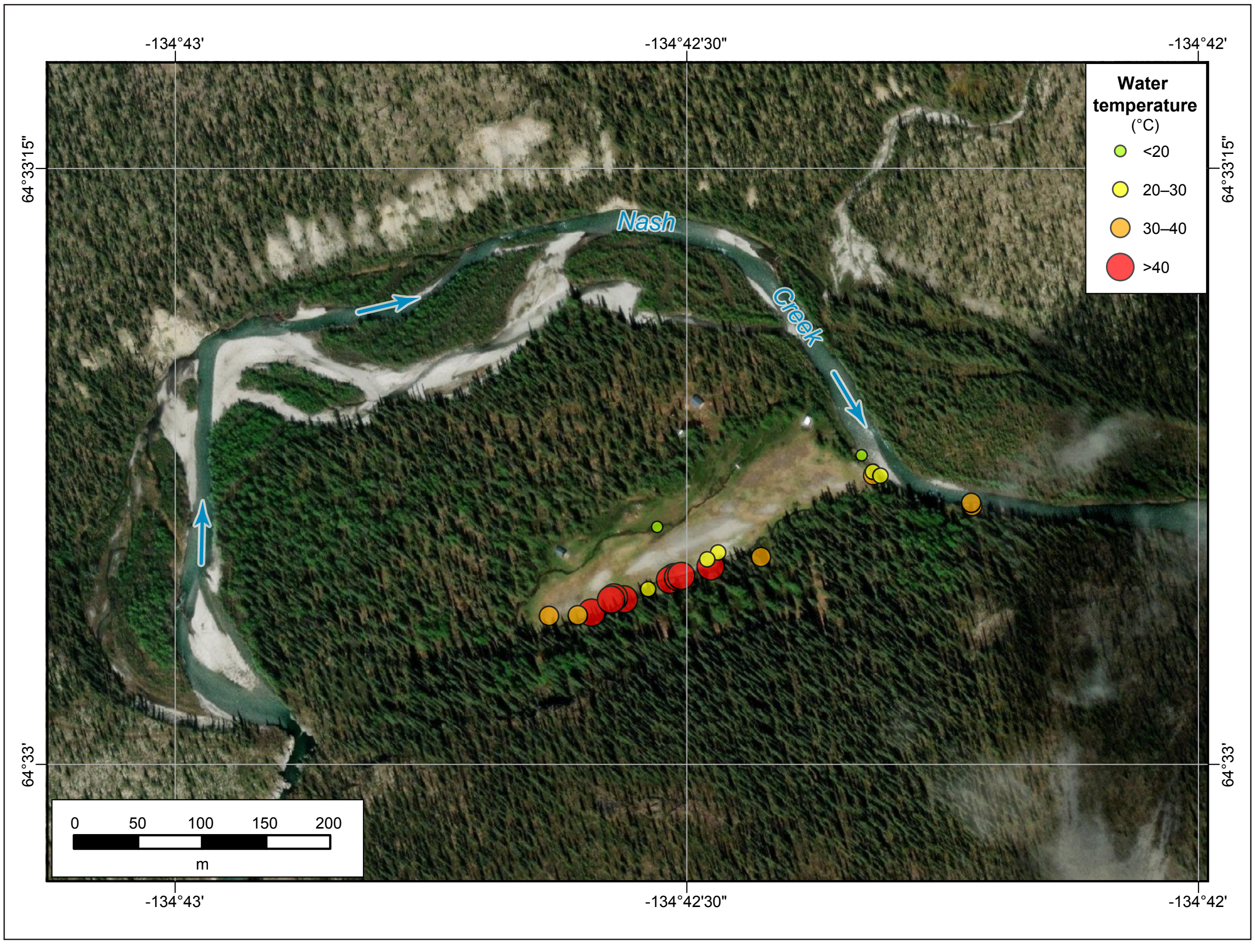

Figure 14. *High-resolution satellite image of the Nash Creek hot springs showing surface water temperature measurements collected along a linear structural feature (EBA Engineering Consultants Ltd., 2010g). Satellite image from ESRI World Imagery (ESRI, 2015).*

The silica geothermometer results from diluted and filtered samples collected at the Nash Creek hot springs indicate source temperatures of 76 to 83°C, which likely underestimates the hydrothermal resource (Table 2; EBA Engineering Consultants Ltd., 2010j). The alkali geothermometer yielded even lower temperatures of 49 to 50°C, which is similar to the hottest surface temperature readings collected in the area (41–46°C; Fig. 14).

Mactung hot spring

The Mactung hot spring is in the Hess Mountains near the Yukon-NWT border, approximately 11 km west-northwest of Macmillan Pass (Figs. 12, 15). The thermal spring is approximately 4 km west of the Mactung deposit, a scheelite skarn occurrence developed in limestone in the contact aureole of the mid-Cretaceous (ca. 96 Ma) Mactung pluton. The small flow of water emanating from the spring measures 32.9°C (EBA Engineering Consultants Ltd., 2008a). The Mactung pluton is radiogenic with elevated **A** values of 4.7 to 7.9 μW/m^3 and may contribute to the source of the thermal spring (Fig. 15; Colpron, 2019).

Water samples collected at the Mactung hot spring have sodium-sulphate-carbonate–type chemistry and high pH (~9.7; EBA Engineering Consultants Ltd., 2008a). The pH, carbonate, chloride, sodium, boron and silicon concentrations are elevated but calcium and magnesium concentrations are lower when compared to samples of other groundwater sources and a cold water (1.2°C) spring in the area (EBA Engineering Consultants Ltd., 2008a).

The geothermal gradient measured in a 339 m deep hole at the Mactung deposit is only 14°C/km (EBA Engineering Consultants Ltd., 2008a). Measurements between 14 and 29°C/km from other mineral exploration boreholes south of Macmillan Pass indicate a heat flow of 96 mW/m^2 for the region (Fig. 7; Lewis et al., 2003). The YGS measured a continuous temperature profile down to 585 m in a borehole drilled in shale of the Earn Group at the Tom deposit south of Macmillan Pass (Figs. 15, 16; Appendix C). The measured temperature profile shows three linear segments with geothermal gradients of 22.3°C/km (215–400 m), 52.9°C/km (400–440 m) and 27.2°C/km (440–585 m). The higher gradient of 52.9°C/km is likely due to a more porous and permeable zone between 400 and 440 m that facilitates advective heat transfer. On average, the geothermal gradient calculated from the other two segments is approximately 25°C/km.

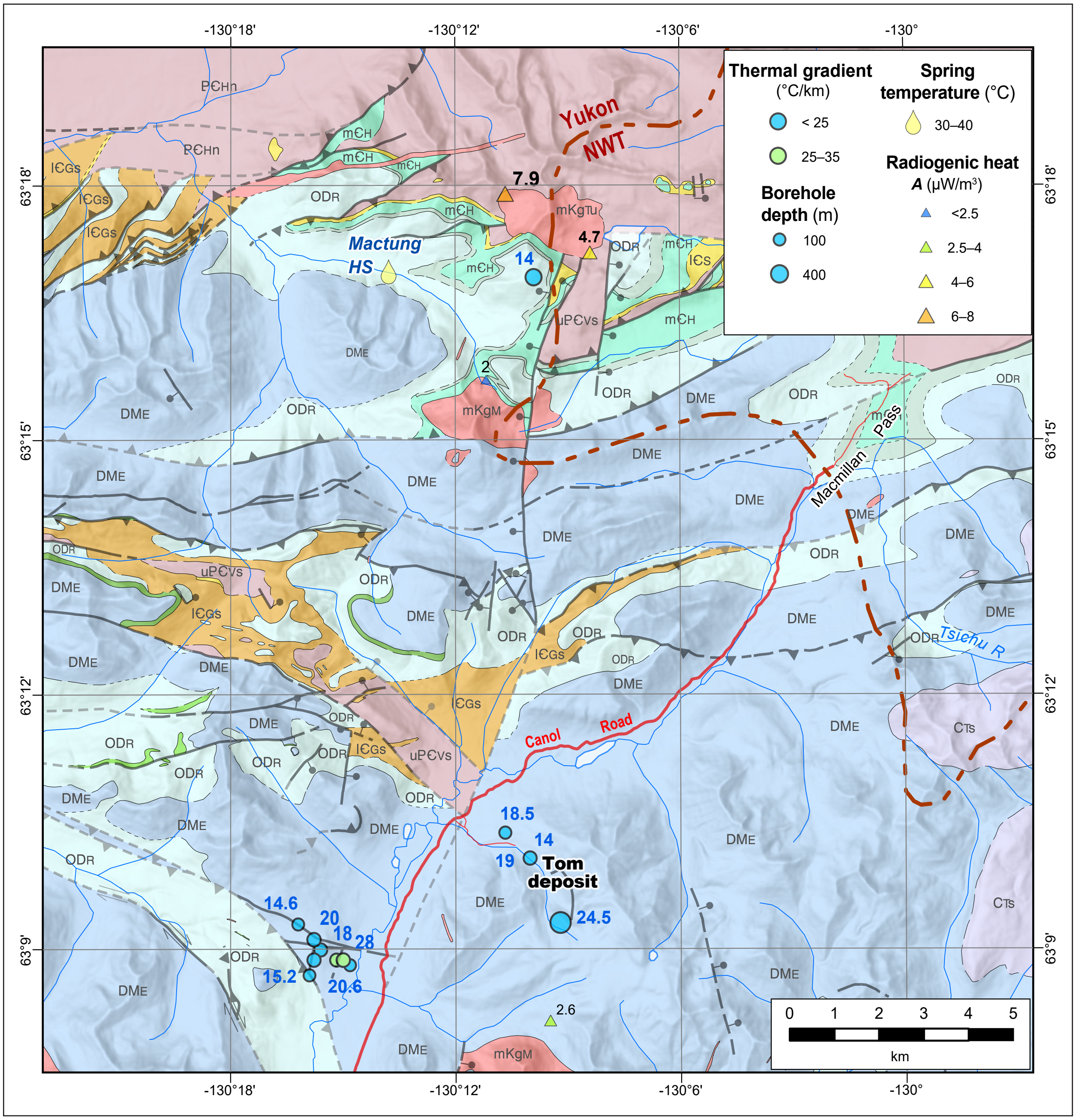

Figure 15. *Geology map of the Macmillan Pass area showing spring temperatures, radiogenic heat production, and thermal gradient values in the vicinity of the Mactung hot spring (HS; Yukon Geological Survey, 2022). NWT: Northwest Territories.*

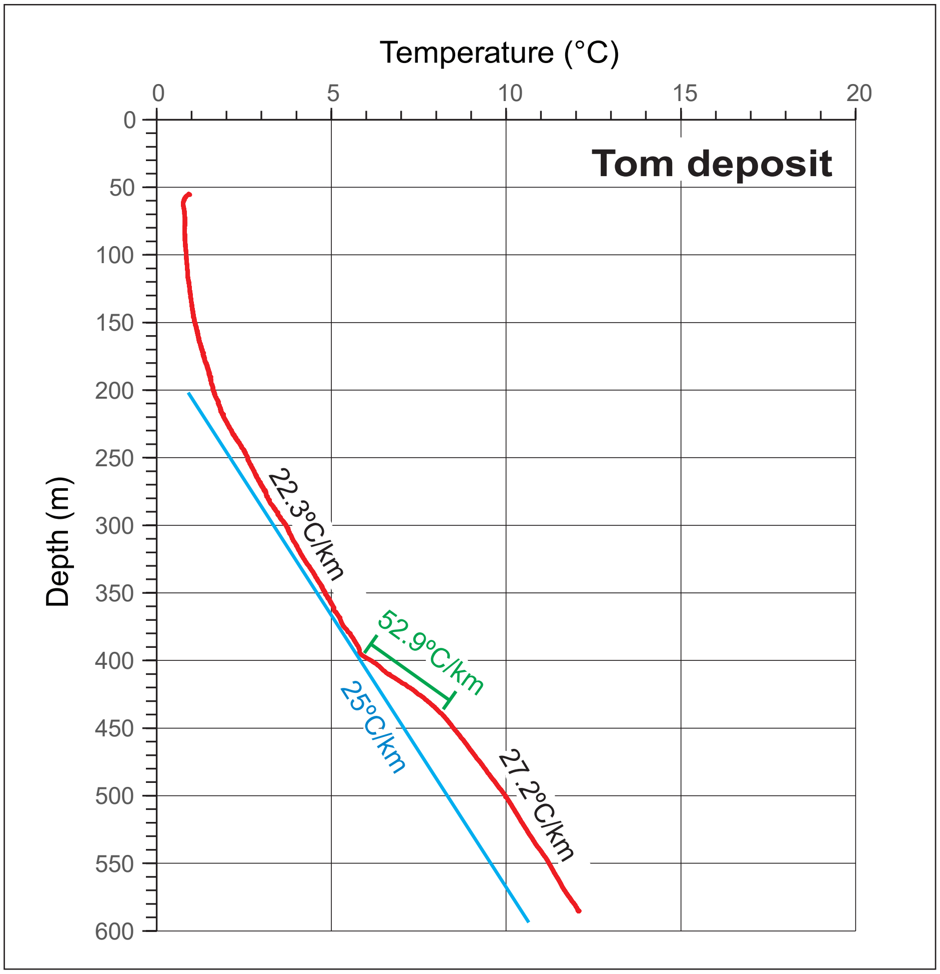

Figure 16. *Temperature profile measured at the Tom deposit near Macmillan Pass. The blue line indicates the average geothermal gradient of 25°C/km. The red curve shows the measured temperature profile, divided into three segments with geothermal gradients of 22.3°C/km, 52.9°C/km and 27.2°C/km. Data in Appendix C.*

Cantung, McPherson Lake and Caesar Lake thermal springs

A cluster of thermal springs straddles the Yukon-NWT border near the headwater of the South Nahanni River, more than 200 km north of Watson Lake (Fig. 4). The springs all occur east of the border in the NWT and include the Cantung thermal springs, which are summarized below. Only two thermal springs in the cluster are located in the Yukon: one near McPherson Lake and another near Caesar Lake (Fig. 17). Additional thermal springs in NWT are described in Crandall and Sadlier-Brown (1978) and Caron et al. (2008).

Cantung is the site of a past-producing tungsten mine and is accessed via the Nahanni Range Road (Yukon Highway 10). Thermal springs were identified at three locations near Cantung. The East and West Cantung springs are close together and emerge from the bottom of a steep bank west of the Flat River near the Cantung airstrip. The North Cantung spring is approximately 20 km north of the East and West Cantung springs, and approximately 3 km north of Flat Lakes (Fig. 17). The East and West Cantung thermal springs emanate from the mid-Cretaceous (ca. 98 Ma) Cantung pluton, whereas the North Cantung warm spring emerges from carbonate and sandstone of the lower Cambrian Sekwi Formation (Yukon Geological Survey, 2022). The West Cantung spring has a water temperature of 41°C and was developed for bathing during mining operations. The East Cantung spring is cooler at 29°C, has a faint sulphurous odour,

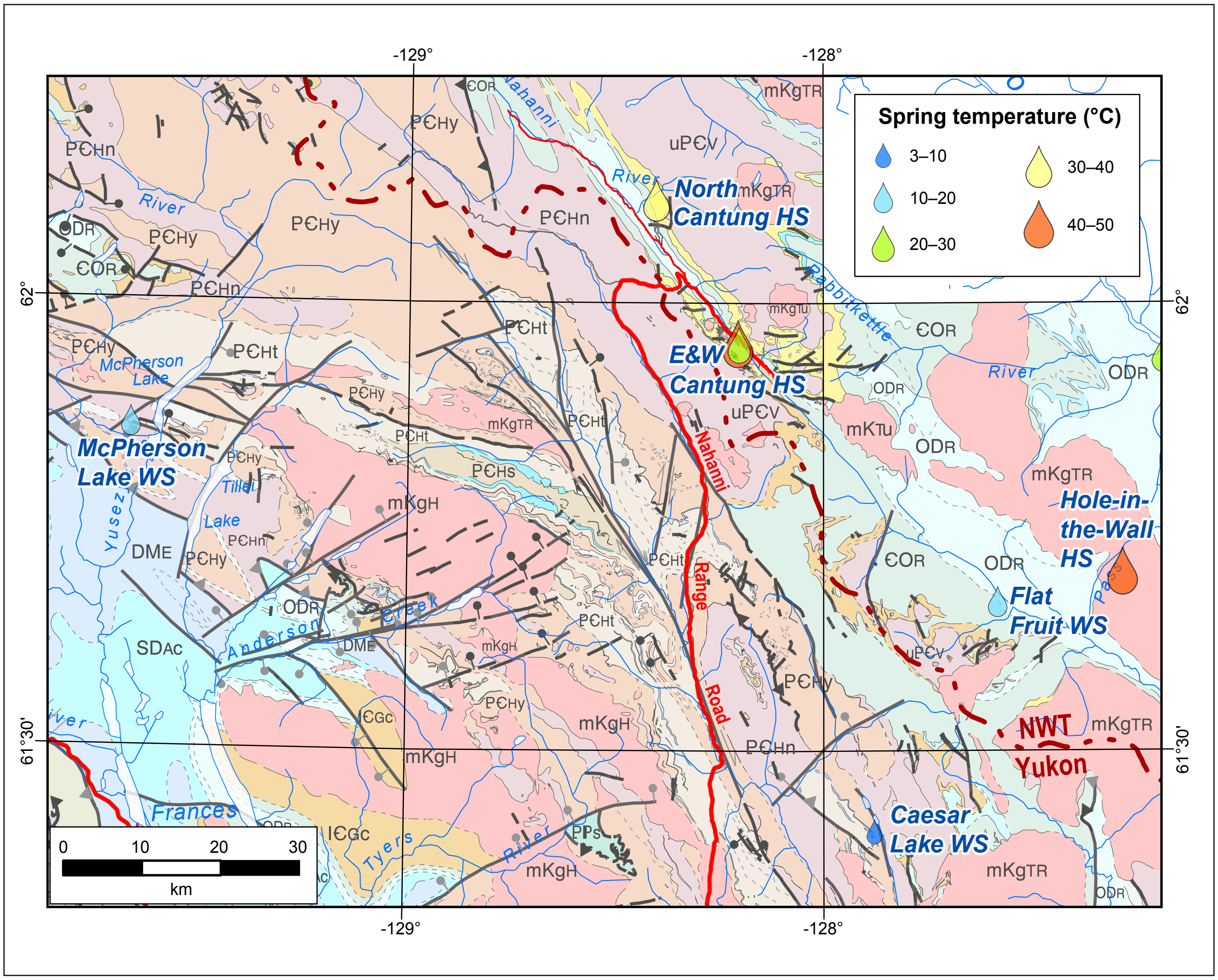

Figure 17. Geology map of the Cantung area showing the location and temperature of hot (HS) and warm springs (WS) in the region (Yukon Geological Survey, 2022). NWT: Northwest Territories.

and supports algal growth (Woodsworth, 2009). The North Cantung springs occur as several small seeps over an area approximately 200 m in diameter. The water is clear and odourless, and temperatures range from 12 to 32°C. Orange algae grow at this site and boulders are covered in white sinter deposits (Woodsworth, 2009).

Mid-Cretaceous felsic plutons in the Cantung area have **A** values greater than 4 $\mu W/m^3$ (Fig. 6) and may be the heat source for the thermal springs in the area. The West and East Cantung springs have sodium-bicarbonate–type water with a pH of 8.2 to 8.9. The North Cantung warm springs have magnesium-bicarbonate–type water and a pH of 7.4 (Crandall and Sadlier-Brown, 1978). Silica geothermometer determinations for West and North Cantung springs suggest source temperatures of 109 and 66°C, respectively (Table 2).

The McPherson Lake warm spring is located approximately 77 km west of Cantung and has a temperature of 16°C. The Caesar Lake spring is approximately 63 km south of Cantung and has cooler water, measuring 3.3°C (Fig. 17). Both springs form extensive sinter deposits and occur in proximity to faults cutting rocks of the Hyland Group (Yukon Geological Survey, 2022). They have calcium-bicarbonate–type water with pH values of 7.3 to 7.4 (Crandall and Sadlier-Brown, 1978). Geothermometer determinations calculated from silica (SiO_2) concentrations in the McPherson Lake and Caesar Lake springs indicate source temperatures of 85 and 82°C, respectively (Table 2).

Southeast Yukon

Southeast Yukon comprises the region east of Watson Lake (Figs. 9, 18). It is characterized by a cluster of thermal springs that extends north from BC, including the Liard Hot Springs (Fig. 4). In the Yukon, the main cluster includes the Pool Creek and Larsen Creek hot springs and the Canyon Creek, Crow River and Thorpe Creek warm springs. A pair of warm springs have also been identified along the Coal River more than 100 km east of the main cluster (Fig. 19). Open-water surveys in Southeast Yukon identified numerous thermal anomalies (Figs. 8, 19; EBA Engineering Consultants Ltd., 2010a). The geology in the area west of the main cluster of springs is dominated mainly by lower Paleozoic carbonate and clastic rocks; to the east, upper Paleozoic to Mesozoic sandstone and shale are more common. Small mid-Cretaceous (ca. 98 Ma) granitoid plutons occur sporadically in the western part of the region and superposed Neoproterozoic and Eocene alkaline intrusions are mapped near Pool Creek (Fig. 19; Pigage and Mortensen, 2004; Pigage, 2009; Yukon Geological Survey, 2022).

The CPDs in Southeast Yukon range from approximately 18 km in the west to approximately 30 km along the Yukon-NWT border (Fig. 5). Temperature gradients measured during mineral and petroleum exploration borehole drilling in this region primarily range from 25 to 55°C/km, but most of these have low confidence ratings (Fig. 10; Burgess et al., 1982; Majorowicz and Morrow, 1998; Lewis et al., 2003; Jessop et al., 2005). Calculated heat flow ranges from 43 to 105 mW/m^2.

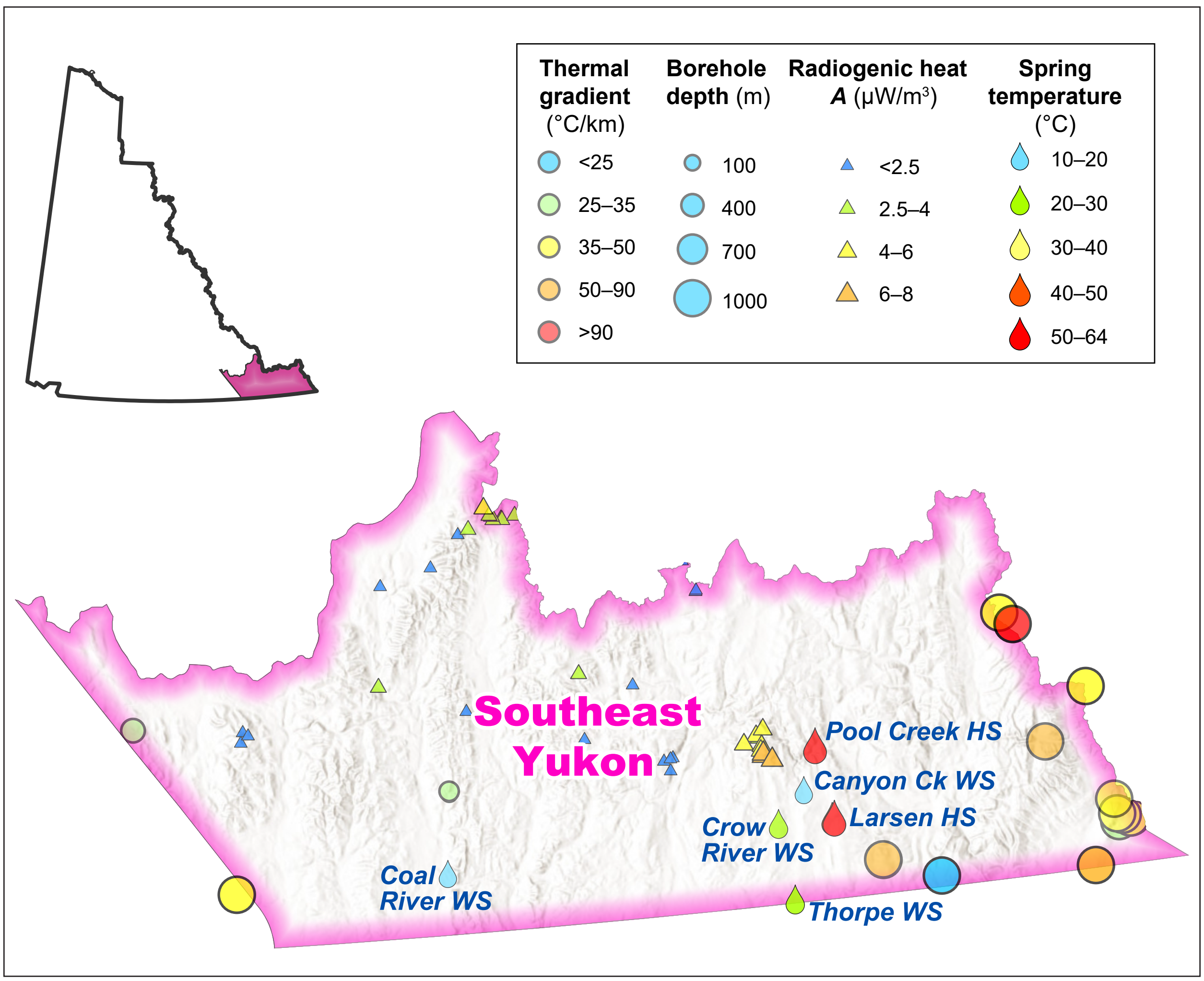

Figure 18. *Geothermal indicators in the Southeast Yukon region. HS: hot spring, WS: warm spring.*

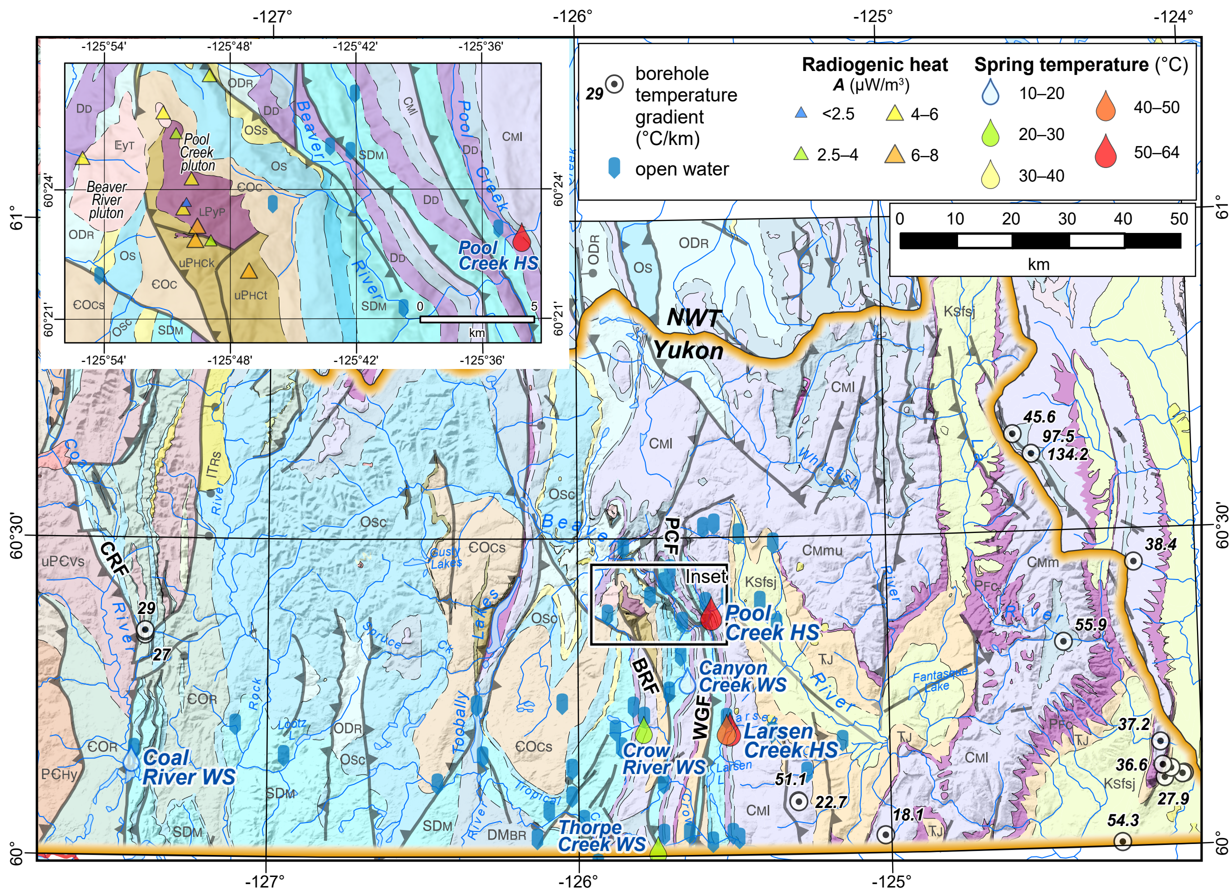

Figure 19. *Geology of part of the southeast Yukon region showing the locations of thermal springs, measurements of radiogenic heat production, and petroleum exploration boreholes from which temperature gradients have been estimated. Geology from Yukon Geological Survey (2022). BRF: Beaver River fault, CRF: Coal River fault, HS: hot spring, NWT: Northwest Territories, PCF: Pool Creek fault, WGF: West Grayling fault, WS: warm spring.*

Pool Creek and Larsen Creek hot springs

The Pool Creek hot springs occur along the Beaver River floodplain downstream of Pool Creek and are characterized by four large, open meadows with dense ground vegetation (Figs. 19, 20). More than 30 springs were identified over a distance of 1150 m along the Beaver River floodplain (Fig. 20; EBA Engineering Consultants Ltd., 2010a; Grasby et al., 2016). The thermal waters are clear and odourless, and have a maximum temperature of 53.2°C.

The Larsen Creek hot springs are located approximately 20 km south of Pool Creek and occur in two areas approximately 600 m apart (Fig. 21). The springs have water temperatures up to 51°C (EBA Engineering Consultants Ltd., 2010a). The northern Larsen Creek area comprises a series of small springs forming a linear array approximately 500 m long along a small tributary of Larsen Creek. The main spring emanates with high flow and high temperature from a limestone outcrop. The southern Larsen Creek area consists of a main circular pool, 7 m in diameter, situated atop a tufa dome, and four smaller springs along Larsen Creek (Figs. 21, 22; EBA Engineering Consultants Ltd., 2010a). The Pool Creek and Larsen Creek hot springs occur in proximity to the north-striking West Grayling and Pool Creek faults (Fig. 19). Alkaline intrusive complexes approximately 15 km west of Pool Creek hot spring—Neoproterozoic Pool Creek syenite and Eocene Beaver River pluton—have anomalous heat production values (**A**) of 4.8 to 7.8 μW/m³

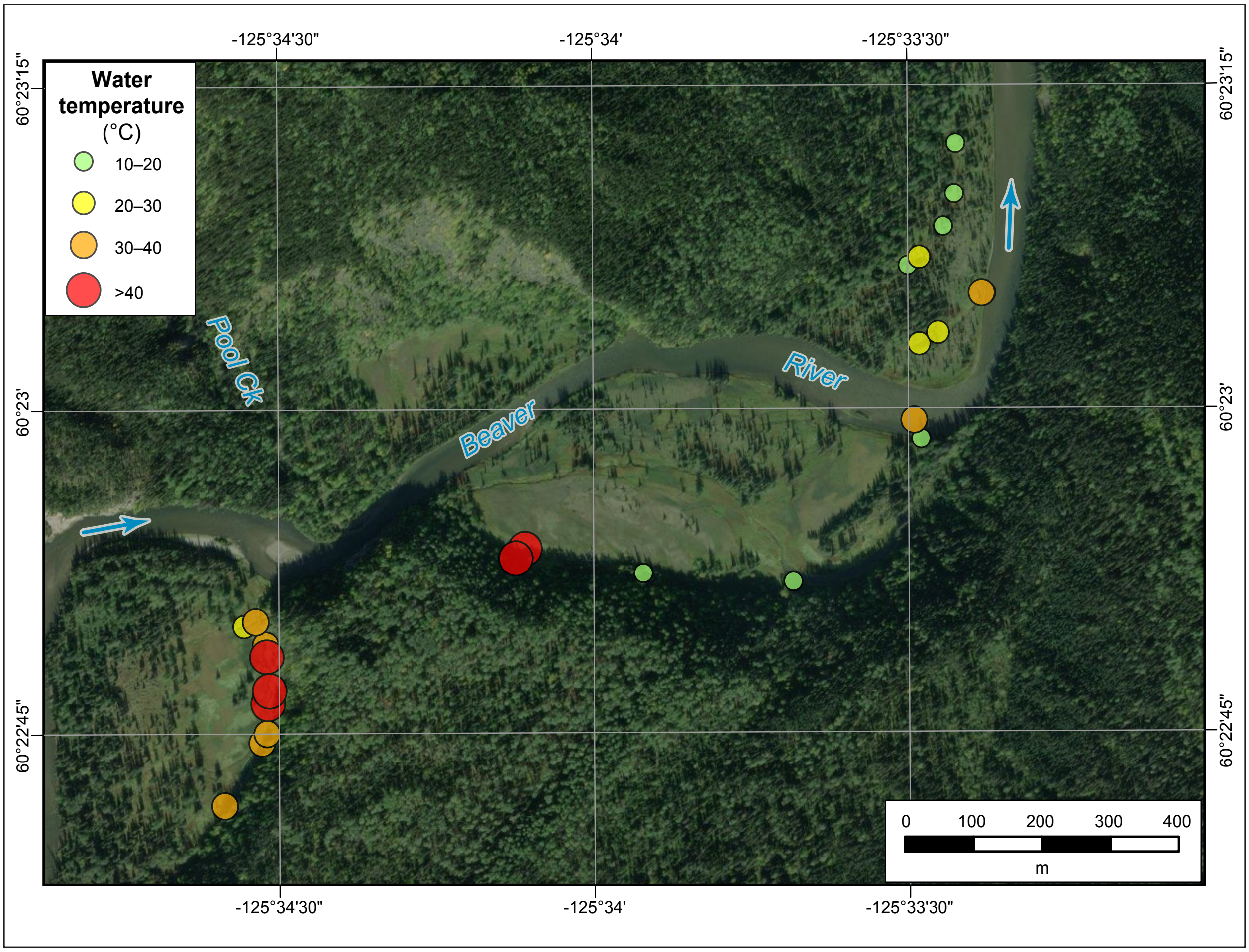

Figure 20. *Satellite image of the Pool Creek hot springs showing open meadows and measured water temperatures from springs along the Beaver River floodplain. Satellite image from ESRI World Imagery (ESRI, 2019).*

and are potential heat sources for thermal springs in the Beaver River area (Fig. 19 inset; Pigage and Mortensen, 2004; Pigage, 2009).

The Pool Creek and Larsen Creek hot springs are characterized by calcium-magnesium-bicarbonate-sulphate–type water (EBA Engineering Consultants Ltd., 2010a). The hottest spring at Pool Creek (53.2°C) has a pH of 6.4 and slightly elevated total dissolved solids (TDS; 428 mg/L), whereas at Larsen Creek the pH is 7.01 and TDS are relatively low (273 mg/L). Tritium (^3H) concentrations at both springs are below detection limit (<0.8 TU), suggesting the thermal waters are not mixed with modern meteoric waters and that residence time is greater than 70 years (Terzer-Wassmuth et al., 2022). Samples from the highest temperature hot springs at Pool Creek and Larsen Creek were collected for stable isotope analyses, including helium isotopes (EBA Engineering Consultants Ltd., 2010i). Ratios of $^3He/^4He$ at Pool Creek hot springs (0.56 Ra) and Larsen Creek hot springs (0.27–0.29 Ra) suggest some admixture of mantle helium and, therefore, enhanced permeability in the crust (Table 2; Kennedy and van Soest, 2007). Silica geothermometer results indicate thermal source temperatures between 74 and 99°C at Pool Creek and Larsen Creek hot springs, whereas the alkali geothermometer results suggest higher temperatures in the range of 203 to 219°C (Table 2; EBA Engineering Consultants Ltd., 2010a). The silica geothermometer provides a conservative thermal source temperature of approximately 99°C for both systems (EBA Engineering Consultants Ltd., 2010a).

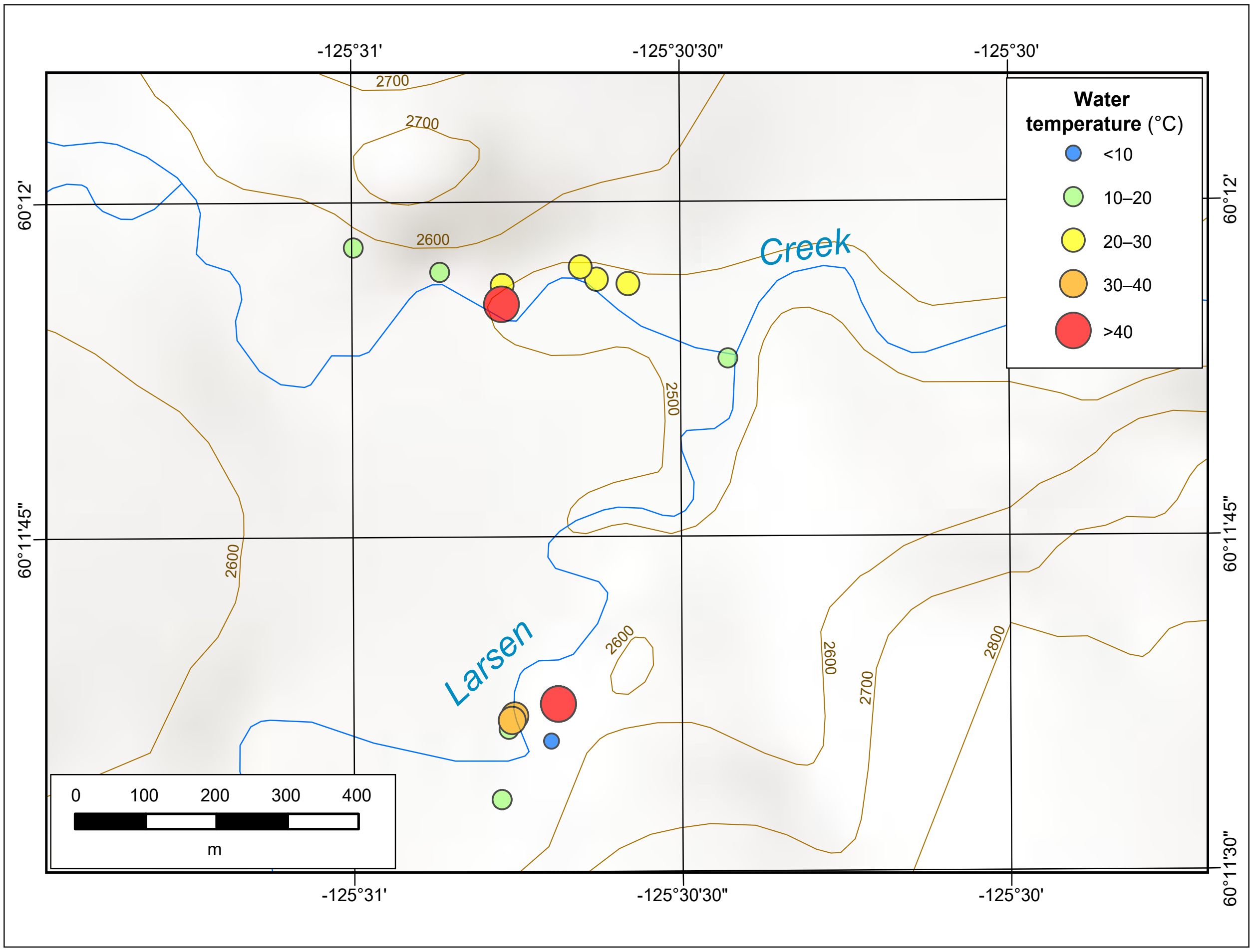

Figure 21. *Distribution and measured water temperatures of hot springs located along Larsen Creek and a small tributary.*

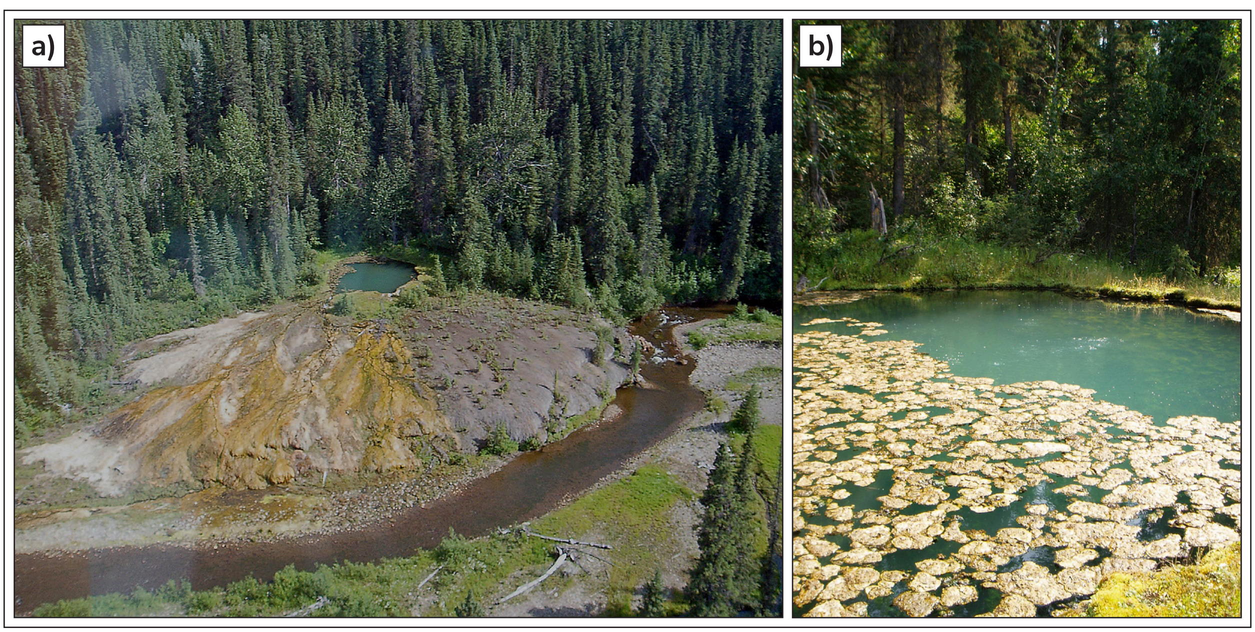

Figure 22. ***a)*** *Aerial view of the southern Larsen Creek hot springs;* ***b)*** *sinter deposits are present in the main pool, which is situated on top of a tufa dome.*

Canyon Creek warm springs

The Canyon Creek warm springs were discovered during an open-water survey of the Beaver River and Larsen Creek area (Fig. 19; EBA Engineering Consultants Ltd., 2009b). The warm springs are approximately 12 km south of Pool Creek, at the headwaters of Canyon Creek, a tributary of the Beaver River. The warm springs are clearly identified by a mat of bright green moss near a high-volume spring that emerges from a limestone canyon (Fig. 23). Two thermal vents were identified; the larger of the two is a high-flow spring measuring 15.1°C and occurs upstream from a smaller, 14.9°C spring (EBA Engineering Consultants Ltd., 2010a). The Canyon Creek warm springs emanate from limestone in a deep, north-south canyon that parallels bedding in the area. The water has calcium-magnesium-bicarbonate–type chemistry, low TDS (179 mg/L) and a pH of 7.27. Stable isotopes indicate a local meteoric source and little to no fractionation in the subsurface (EBA Engineering Consultants Ltd., 2010a). An ^{3}H concentration of 6.3 TU at Canyon Creek suggests admixture of surface water and a groundwater residence time of less than 60 years (Terzer-Wassmuth et al., 2022). Silica and alkali geothermometers yielded temperatures of 58 and 178°C, respectively (Table 2).

Crow River warm springs

The Crow River warm springs are located approximately 15 km west of the Larsen Creek hot springs (Fig. 19). They form a northwest-trending array, approximately 650 m long, consisting of more than 25 closely spaced thermal vents that produce clear, odourless water with temperatures ranging from 11.3 to 29.2°C (Fig. 24). The springs occur in meadows within a forest and form two large thermal pools that remain open in winter (EBA Engineering Consultants Ltd., 2009b, 2010a).

Figure 23. *Green moss at the Canyon Creek warm spring. Photo from EBA Engineering Consultants Ltd. (2010a).*

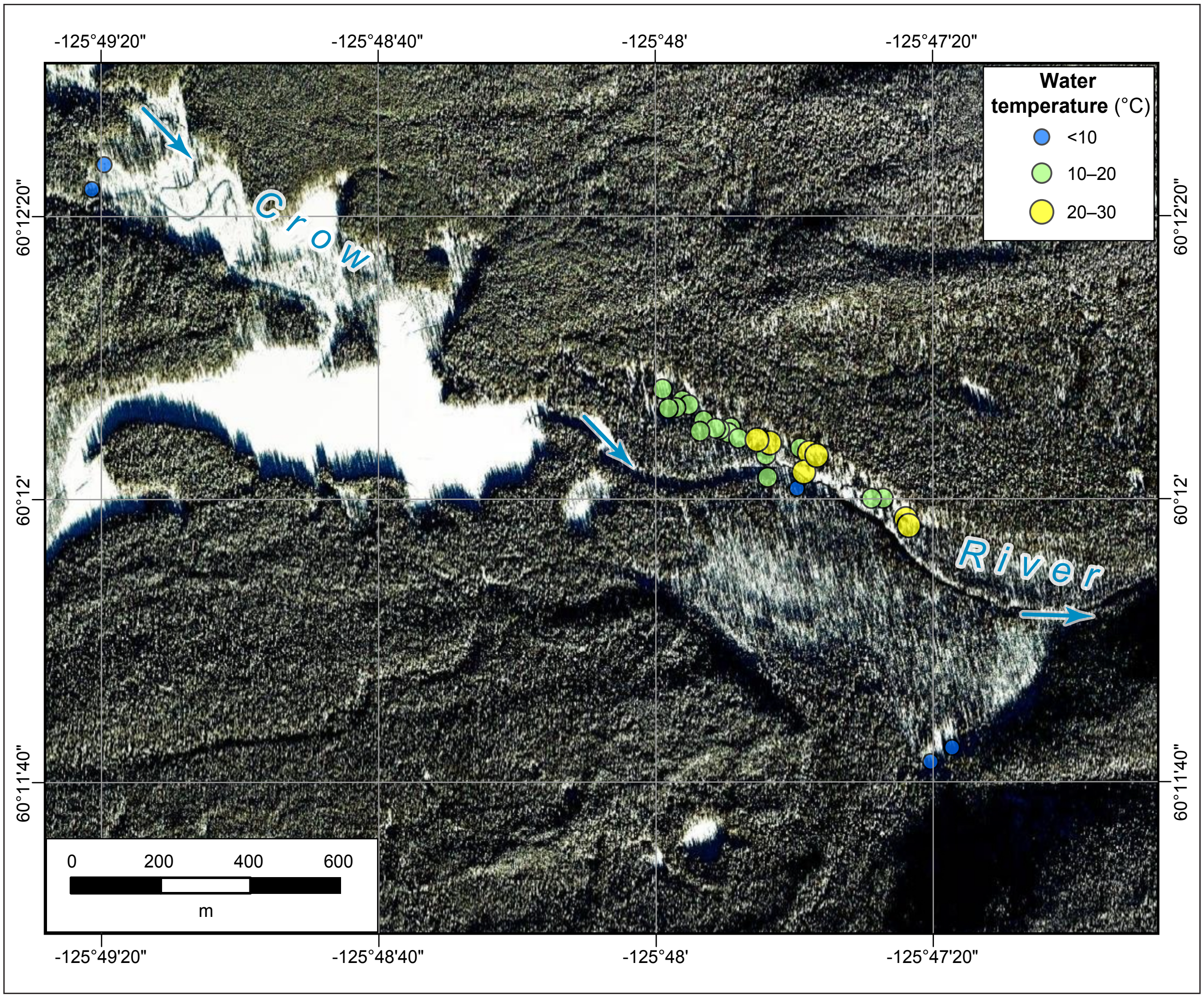

__Figure 24.__ Satellite image of the Crow River area showing distribution of warm springs and thermal anomalies. The flow of the Crow River is marked with blue arrows. Satellite image from ESRI World Imagery (ESRI, 2021).

The water is calcium-magnesium-bicarbonate type with a pH of 6.8 and relatively low TDS (188 mg/L; EBA Engineering Consultants Ltd., 2010a). Stable isotopes (^{18}O, ^{2}H) indicate a local meteoric source and ^{3}H concentrations below detection limit suggest a residence time of greater than 70 years (Terzer-Wassmuth et al., 2022). Silica geothermometer results suggest source temperatures of 53 to 65°C, whereas alkali geothermometer calculations indicates a thermal source temperature of 232°C (Table 2; EBA Engineering Consultants Ltd., 2010a).

Thorpe Creek warm springs

The Thorpe Creek warm springs were identified during an open-water survey in spring 2009 (Fig. 19; EBA Engineering Consultants Ltd., 2009b). They occur along the Yukon-BC border, approximately 24 km southwest of the Larsen Creek hot springs (Fig. 19). Two distinct springs occur approximately 1 km apart. The east spring comprises four vents emerging from the base of a limestone outcrop to form a thermal pool 2.5 m in diameter that discharges into Thorpe Creek. The west spring emerges from a forested area into a small wetland feeding a small tributary of Thorpe Creek. Temperatures up to 25.3°C were measured in the west spring (Table 2; EBA Engineering Consultants Ltd., 2010a). The Thorpe Creek springs have calcium-magnesium-bicarbonate–type water chemistry with a pH of 6.9 and a hardness of 256 mg/L. Stable isotopes

(^{18}O, ^{2}H) are characteristic of local meteoric sources and the ^{3}H concentration (1.2 TU) suggests a residence time of less than 60 years (Terzer-Wassmuth et al., 2022). The $^{3}He/^{4}He$ ratio of 0.16 Ra at Thorpe Creek suggests some admixture of mantle and/or atmospheric helium in the groundwater (Table 2; EBA Engineering Consultants Ltd., 2010i).

Coal River warm springs

The Coal River warm springs are located within the Coal River Territorial Park, approximately 70 km east of Watson Lake and approximately 105 km west of Larsen Creek (Fig. 19). The thermal springs occur in two distinct areas along an abandoned channel east of Coal River (Fig. 25; EBA Engineering Consultants Ltd., 2010a). The south spring area is characterized by a deposit of benched tufa, approximately 15 m high, 65 m long and 15 m wide, holding turquoise-coloured, elongate pools (Fig. 26). The spring forms one larger pool approximately 75 m long, 20 m wide, and up to 5 m deep. Gas bubbles were observed at the centre of this pool and the water temperature is 13.2°C (EBA Engineering Consultants Ltd., 2010a). The source of this spring is dense spruce forest approximately 90 m to the east, upslope from the tufa mound (Fig. 25), where it emerges from limestone in proximity to the south-striking Coal River thrust fault (Fig. 19; Pigage et al., 2015).

The north spring forms an elongated pool of clear water atop a long shallow unforested tufa, more than 600 m to the north of the south spring (Fig. 25). Its source is in a forested area approximately 25 m west of the pool. The water at the source of the north spring is 11.7°C, slightly cooler than the south spring (EBA Engineering Consultants Ltd., 2010a).

The Coal River warm springs have calcium-magnesium-bicarbonate–type chemistry, with a pH of 7.26 to 7.33 and relatively low TDS (216–275 mg/L; EBA Engineering Consultants Ltd., 2010a). Concentrations of deuterium (^{2}H), ^{3}H and ^{18}O suggest local meteoric waters with a groundwater residence time of less than 60 years (Table 2; Terzer-Wassmuth et al., 2022). The Coal River springs have a $^{3}He/^{4}He$ ratio of 0.5 Ra, which suggests admixture of mantle helium in the groundwater and possible enhanced deep permeability in the crust (Kennedy and van Soest, 2007; EBA Engineering Consultants Ltd., 2010i). The silica geothermometer result was calculated for an undiluted water sample and indicates a low temperature of 15°C. The alkali geothermometer yielded much higher source temperatures of 167 to 172°C (Table 2; EBA Engineering Consultants Ltd., 2010a).

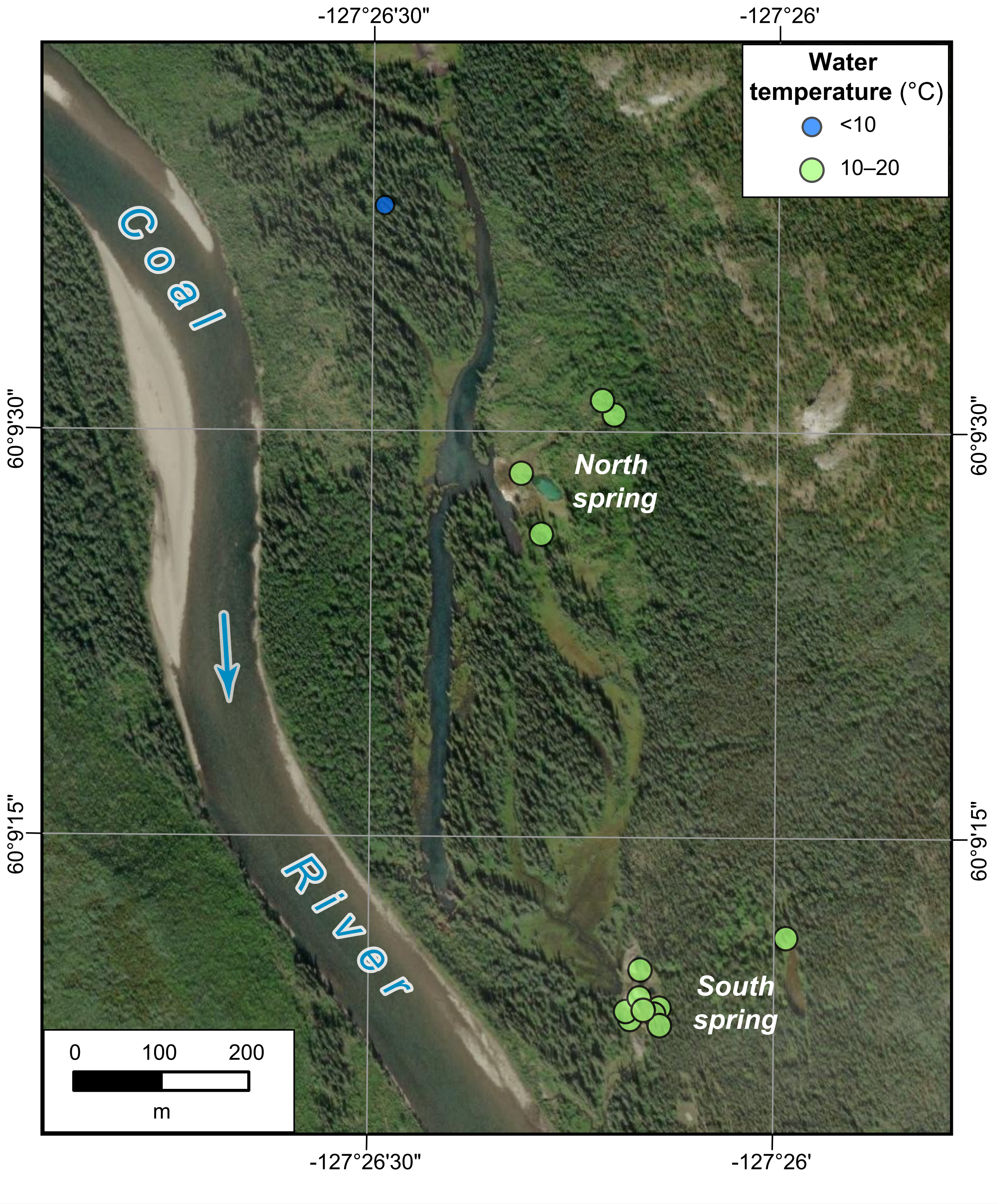

***Figure 25.** Satellite image of the Coal River area showing the distribution of springs and thermal anomalies. Satellite image from ESRI World Imagery (ESRI, 2012).*

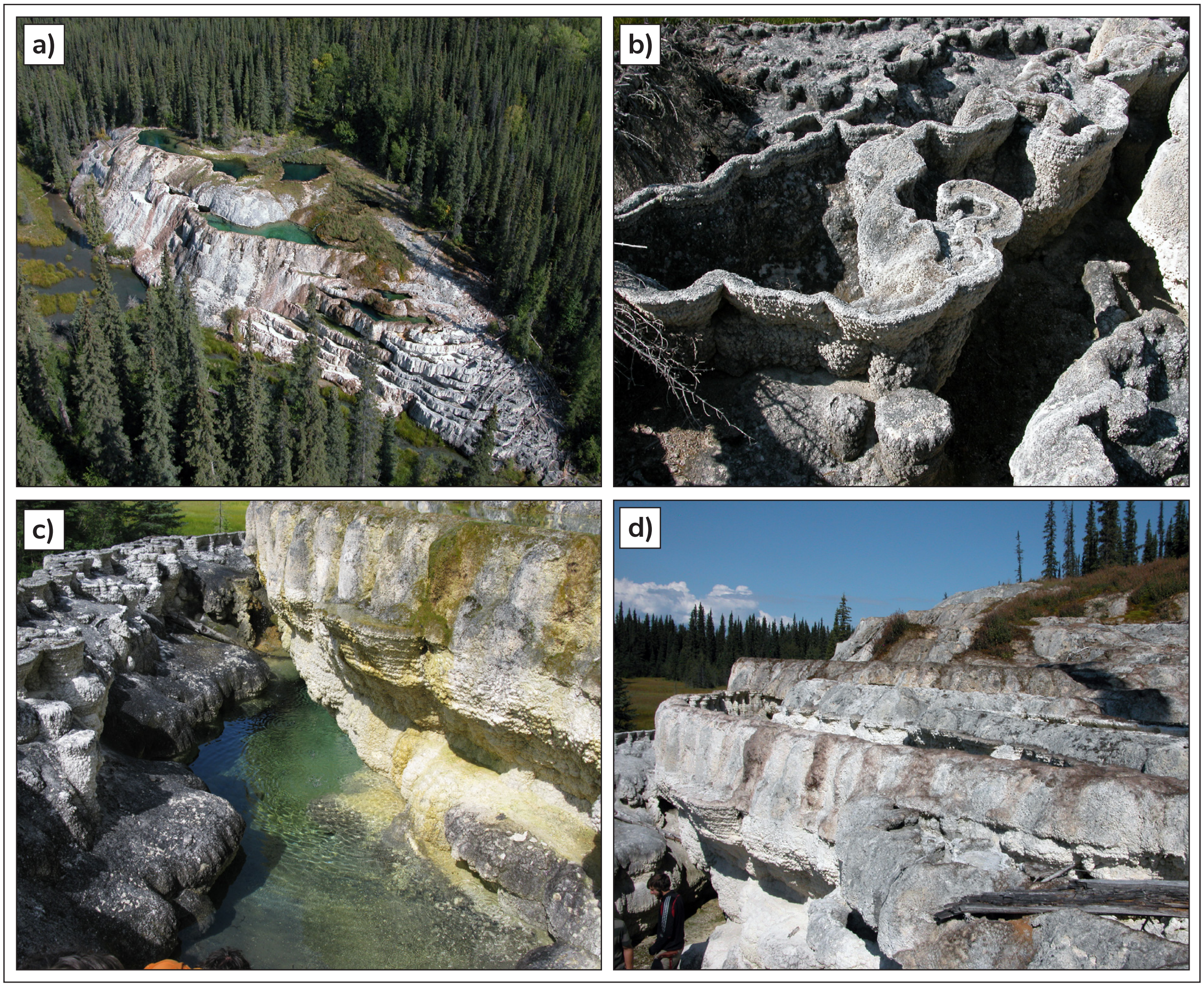

Figure 26. *Photographs of tufa mounds and thermal pools at the Coal River warm spring:* ***a)*** *aerial view of the main tufa mound at the southern spring;* ***b)*** *close-up of mineral growth structure in the tufa;* ***c)*** *one of the thermal pools; and* ***d)*** *surface view of the tufa mound.*

Tintina Trench

The Tintina Trench is a major northwest-trending physiographic feature that transects the Yukon (Fig. 9) and extends southeast into the northern Rocky Mountain Trench in BC. The Tintina Trench is underlain by a major dextral strike-slip fault—the Tintina fault—with displacement of 430 to 490 km (Fig. 4; Roddick, 1967; Gabrielse, 1985; Gabrielse et al., 2006). Seismic data reveal that the Tintina fault zone extends into the upper mantle (e.g., Cook et al., 2004; Estève et al., 2020b). It experiences rare, low-magnitude earthquakes and its current deformation rate is estimated at approximately 0.5 mm/yr (Leonard et al., 2008).

Here, we consider geothermal indicators within a 40 km-wide swath centred on the Tintina fault (Fig. 27). This region is home to the communities of Dawson, Stewart Crossing, Faro, Ross River and Watson Lake, and is accessed by the North Klondike and Robert Campbell highways (Yukon Highways 2 and 4, respectively). The Tintina Trench hosts two thermal springs—Partridge Creek warm spring and McArthur hot spring—and was the target of two studies focused on evaluating fault-controlled geothermal potential near Ross River and Watson Lake (Mira Geoscience, 2017; Witter, 2022). The CPD varies from approximately 30 km near Dawson

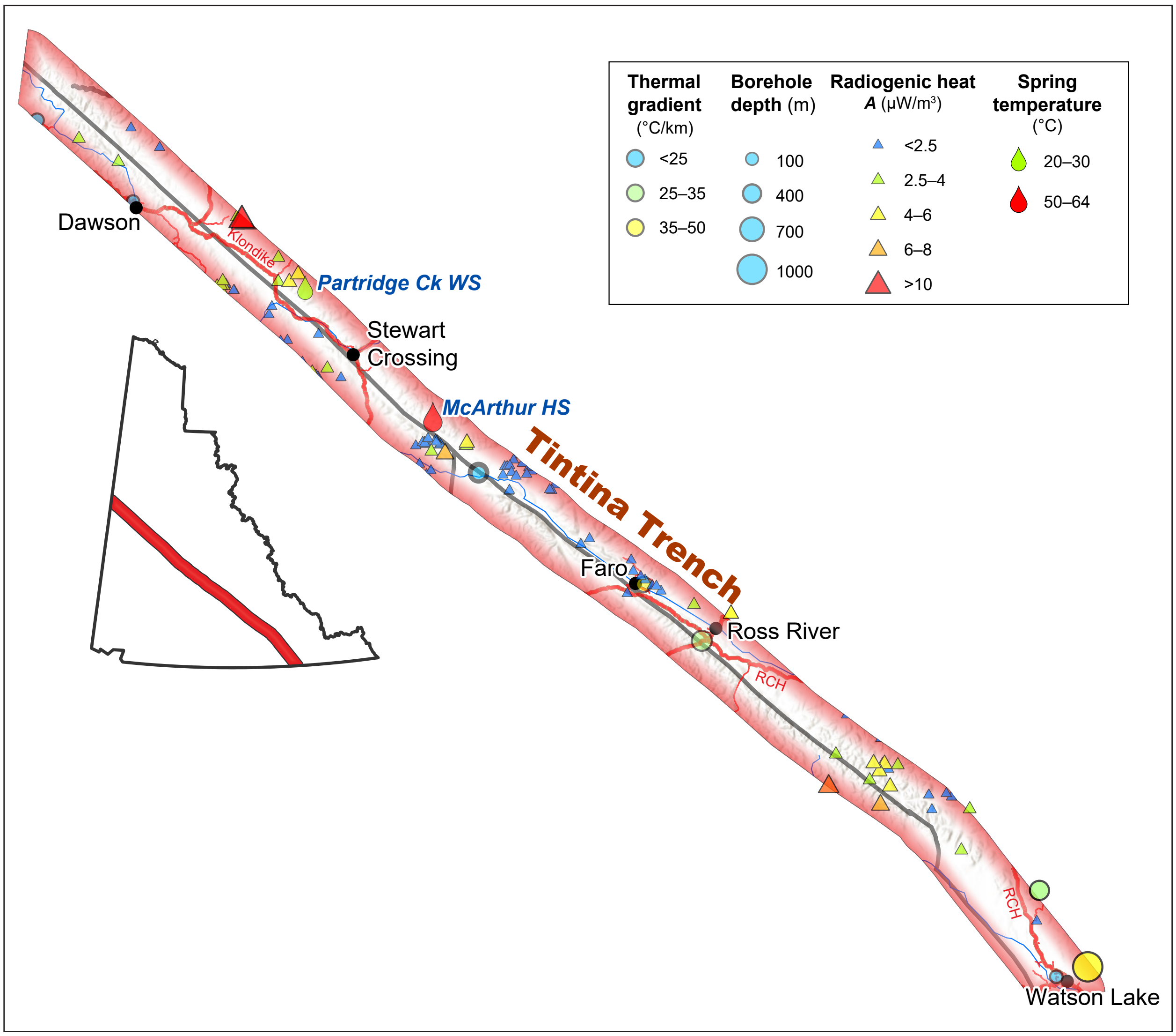

Figure 27. *Geothermal indicators in the Tintina Trench region. HS: hot spring, RCH: Robert Campbell Highway, WS: warm spring.*

to approximately 18 km near Watson Lake (Fig. 5). Limited drilling for mineral and petroleum exploration indicates modest to low thermal gradients along the Tintina Trench (Fig. 7).

Partridge Creek warm spring

A warm spring is present near the headwaters of Partridge Creek, approximately 15 km northeast of the Klondike Highway between Stewart Crossing and Dawson (Figs. 27, 28). Several small vents discharge 13.2 to 25.1°C water at low flow rates into a shallow, natural pool (EBA, A Tetra Tech Company, 2011a). Sinter deposits of opaline silica are developed on boulders within the pool (Fig. 29). The warm spring occurs along a fault juxtaposing the Late Cretaceous (ca. 64 Ma) granite of the Two Sisters pluton (part of the McQuesten plutonic suite; Colpron et al., 2016a) against Neoproterozoic–Cambrian sandstone and phyllite of the Hyland Group (Fig. 28; EBA, A Tetra Tech Company, 2012b). The Two Sisters pluton is radiogenic, with **A** values of 3.0 to 5.4 μW/m^3 (Fig. 28). A geophysical survey (extremely low frequency electromagnetic [ELF-EM] and magnetic) in the vicinity of Partridge Creek identified a shallow, weak, east-northeast–trending

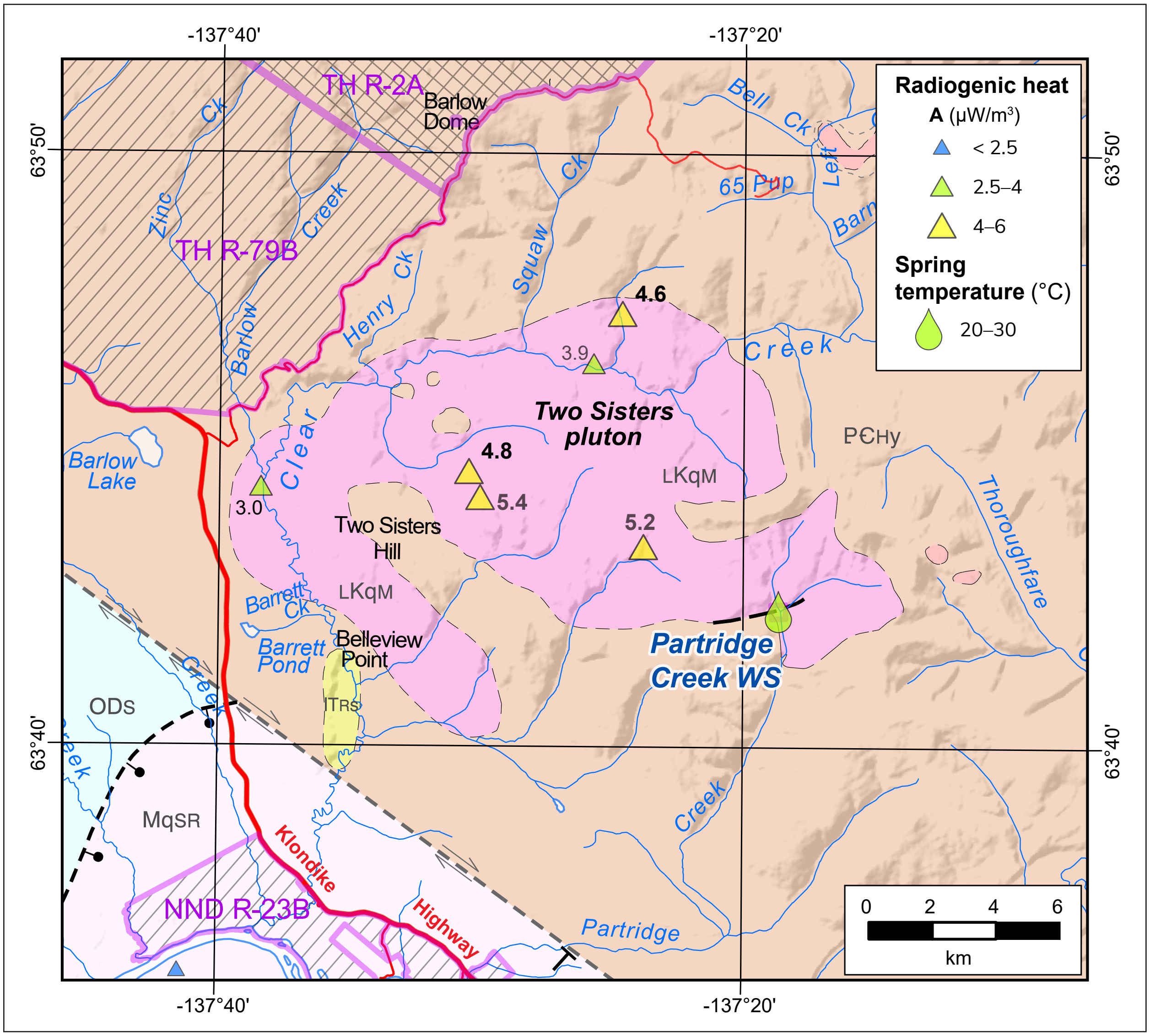

Figure 28. Geology and geothermal characteristics in the vicinity of the Partridge Creek warm spring (WS). Geology after Yukon Geological Survey (2022). Hatched areas indicate First Nations Settlement Lands: cross hatch: Category A, simple hatch: Category B.

Figure 29. *Photograph of the Partridge Creek warm spring (from EBA, A Tetra Tech Company, 2012b).*

conductor following the fault across Partridge Creek and extending beneath the warm spring (EBA, A Tetra Tech Company, 2012c).

The Partridge Creek warm spring has sodium-bicarbonate-sulphate–type water with low hardness (16–17 mg/L) and high fluoride (9.11–9.37 mg/L), which suggest interaction with granitoid rocks (EBA Engineering Consultants Ltd., 2011a). Deuterium (^{2}H) and ^{18}O concentrations indicate local meteoric sources for the groundwater. The lack of ^{3}H (below detection limit of 0.8 TU) in the Partridge Creek water suggests a residence time of greater than 70 years (EBA, A Tetra Tech Company, 2011a, 2012b; Terzer-Wassmuth et al., 2022). Radiocarbon (^{14}C) analysis of a water sample suggests that the groundwater source is more than 18 000 years old. Source temperatures of 95 to 122°C were calculated using alkali and silica geothermometers (Table 2; EBA, A Tetra Tech Company, 2012b).

McArthur hot springs

The McArthur hot springs occur along the central part of the Tintina Trench, approximately 50 km southeast of Stewart Crossing (Fig. 27). The hot springs are located within the Ddhaw Ghro Habitat Protection Area on Category A Settlement Land of the Selkirk First Nation (Fig. 30). Temperatures ranging from 12.5 to 54.0°C have been measured from 18 distinct vents and seeps over a 150 m^2 area along Hotspring Creek (Fig. 31; Brandon, 1965; van Everdingen, 1973b; EBA Engineering Consultants Ltd., 2009c). A faint hydrogen sulphide (H_2S) smell was noticed at the hottest vent. A white precipitate deposited on rocks at the McArthur hot springs is composed primarily of opal with approximately 5% calcite and 2% quartz (Fig. 32; van Everdingen, 1973b). The hot springs occur in sedimentary rocks of the Hyland Group, approximately 1.2 km southwest of their contact with the mid-Cretaceous (ca. 95 Ma) McArthur batholith (Fig. 30). The McArthur batholith is composed of granodiorite and granite and yielded local radiogenic heat production

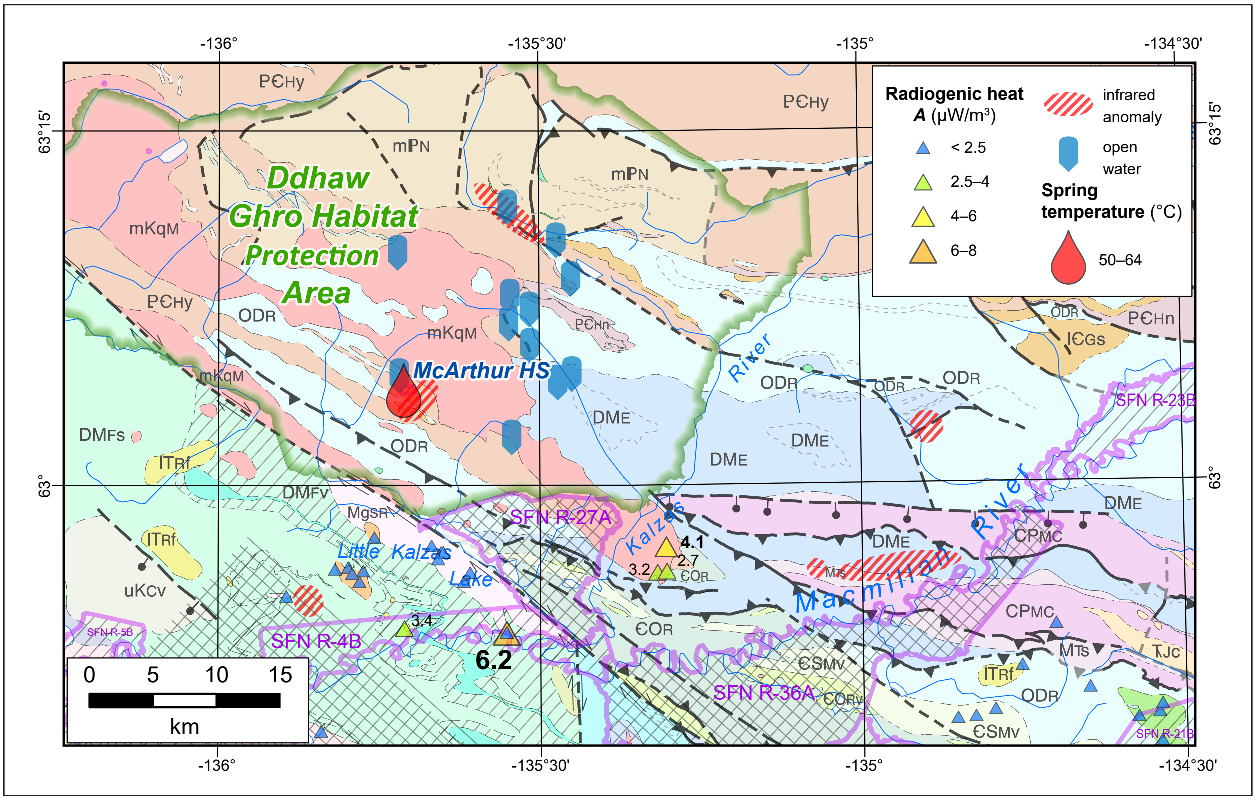

Figure 30. *Geology and geothermal characteristics of the McArthur hot spring area, within the Ddhaw Ghro Habitat Protection area (green border). Geology after Yukon Geological Survey (2022). Hatched areas indicate First Nations Settlement Lands: cross hatch: Category A, simple hatch: Category B.*

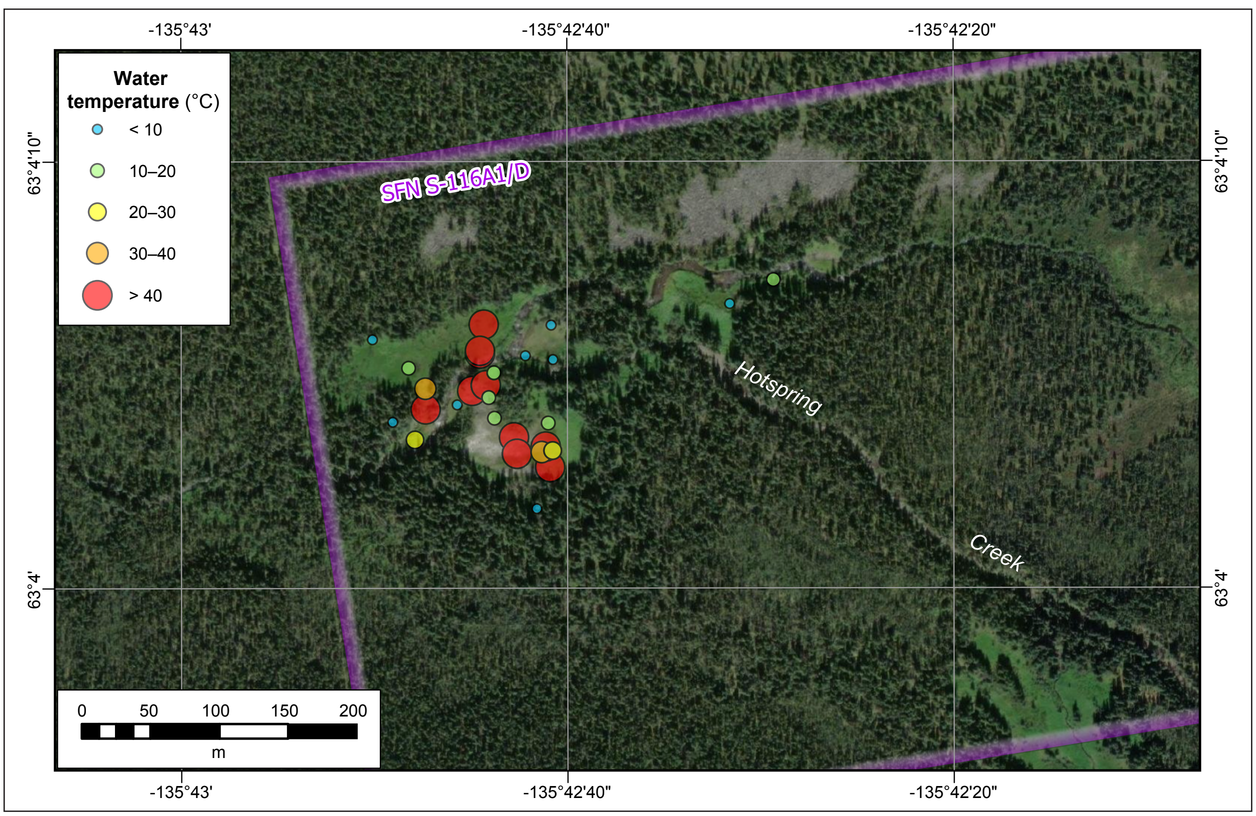

Figure 31. *Satellite imagery of the McArthur hot springs showing temperatures measured at various vents along Hotspring Creek. Satellite image from ESRI World Imagery (ESRI, 2014).*

values (**A**) between 2.7 and 4.1 μW/m^3 from samples collected approximately 25 km southeast of the springs. Analysis of satellite thermal imagery followed by helicopter infrared and open-water surveys identified numerous thermal anomalies in the vicinity of McArthur hot springs (Fig. 30; EBA Engineering Consultants Ltd., 2009a, f, g).

The McArthur hot springs have soft (hardness <14 mg/L), sodium-bicarbonate–type water with a pH of 7.13 to 9.50 (Brandon, 1965; van Everdingen, 1973b; EBA Engineering Consultants Ltd., 2009e). The water is high in fluoride (7.30–7.61 mg/L), low in chloride (<1 mg/L), and has low electrical conductivity (149–298 μS/cm; EBA Engineering Consultants Ltd., 2009e). Deuterium and ^{18}O concentrations indicate a local meteoric source for the groundwater. Geothermometer calculations indicate source temperatures of 117 to 129°C using the alkali geothermometer and 150 to 164°C with the silica geothermometer (Table 2; EBA Engineering Consultants Ltd., 2009e).

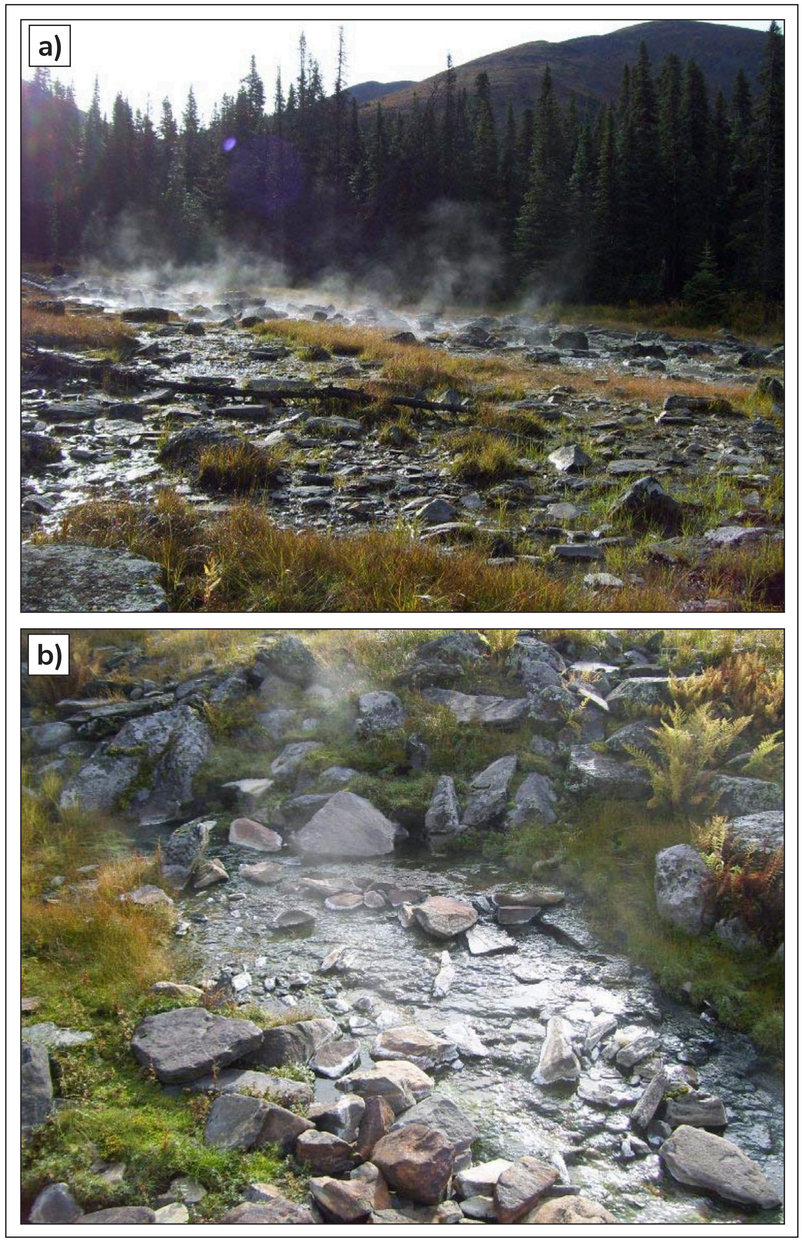

Figure 32. *Photographs of the McArthur hot springs:* ***a)*** *general view of the McArthur hot springs;* ***b)*** *white opal precipitate on boulders at the McArthur hot springs. Photos from EBA Engineering Consultants Ltd. (2009e).*

Ross River area

An assessment of the geothermal potential of the Tintina Trench near Ross River was commissioned by the Dena Nezziddi Development Corporation of the Ross River Dena Council (Mira Geoscience, 2017). This study integrated field-based structural analysis and mapping with acquisition and modelling of aeromagnetic and magnetotelluric (MT) geophysical data. In this area, the dextral strike-slip Tintina fault zone is approximately 3.5 km wide and comprises multiple strands, including a series of north-south–striking extension faults bound by strike-slip faults (Fig. 33). The fault zone comprises predominantly Paleogene volcanic (rhyolite and basalt; units ITRv and ITRf) and sedimentary rocks (shale, siltstone, sandstone, conglomerate and coal; unit ITRs) interleaved with upper Paleozoic shale (unit CKs). Paleozoic sedimentary strata

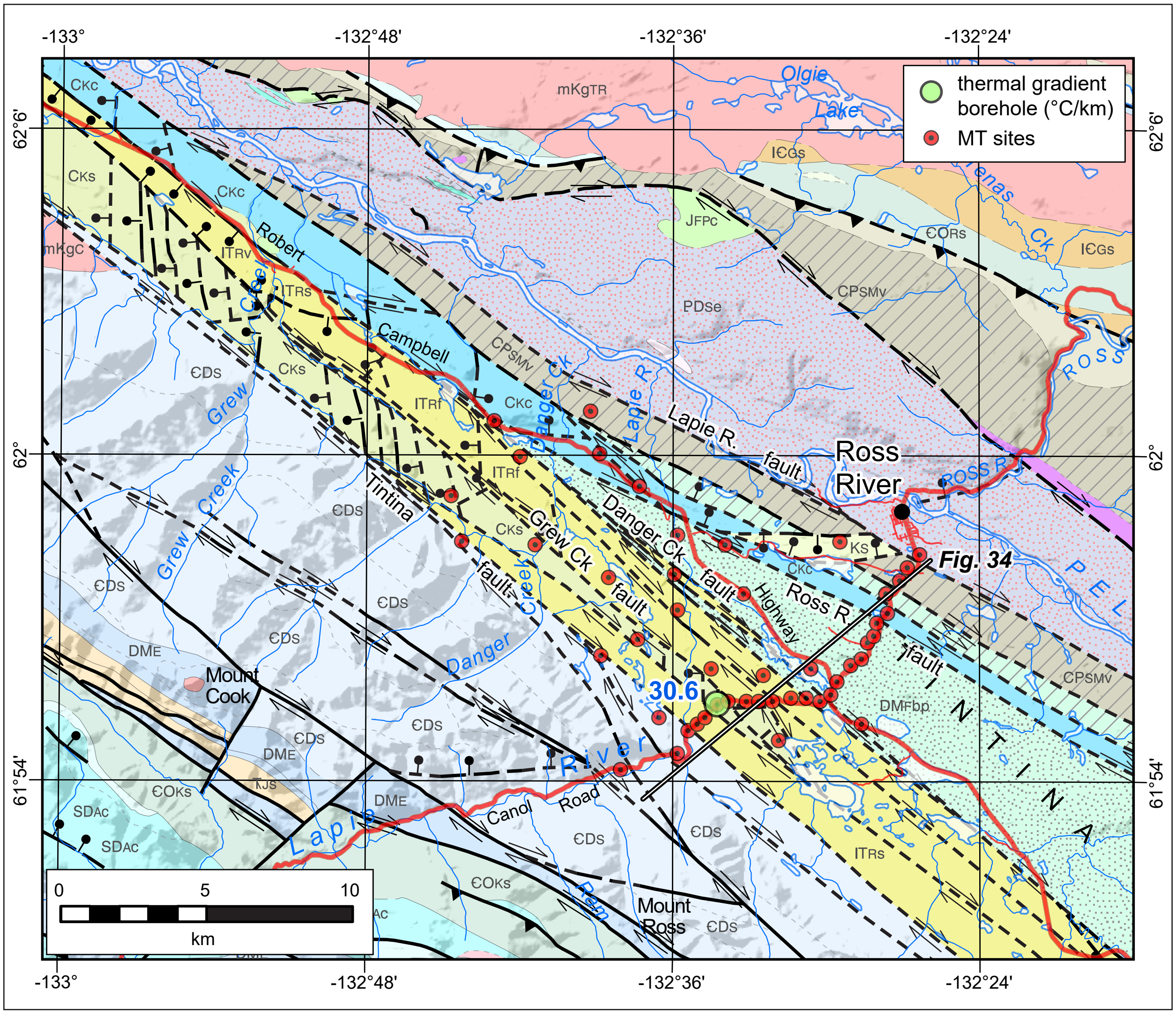

Figure 33. Geology and geothermal characteristics of the Tintina Trench near Ross River (geology after Yukon Geological Survey, 2022). The locations of a thermal gradient borehole measuring 30.6°C/km and magnetotelluric (MT) sites in the area are shown. The approximate line of section for the MT resistivity model shown in Figure 34 is also indicated.

assigned to the Cassiar terrane occur southwest of the Tintina fault, whereas mid-Paleozoic metasedimentary and metavolcanic rocks of the Yukon-Tanana terrane bound the fault zone to the northeast.

Modelling of magnetic data highlights the structural style within the Tintina fault zone and suggests possible fluid pathways at intersections of extension and strike-slip faults. Three-dimensional MT data modelling suggests that the western portion of the fault zone may be underlain by a granitoid pluton (A4, Fig. 34; Mira Geoscience, 2017).

A 480 m deep temperature gradient borehole was drilled along the Canol Road, southwest of Ross River, to further investigate the potential of a fault-controlled geothermal system (Fraser et al., 2019). The borehole encountered approximately 205 m of glaciofluvial, glaciolacustrine and till deposits overlying interbedded mudstone, sandstone and pebble to cobble conglomerate (Paleogene); several intervals of fault gouge and breccia were also encountered (Langevin et al., 2020). The temperature profile measured in this borehole is characterized by a near-surface temperature inversion and permafrost depth of 38.4 m, followed by a linear geothermal gradient of 30.6°C/km (Fig. 35, Appendix C; Fraser et al., 2019).

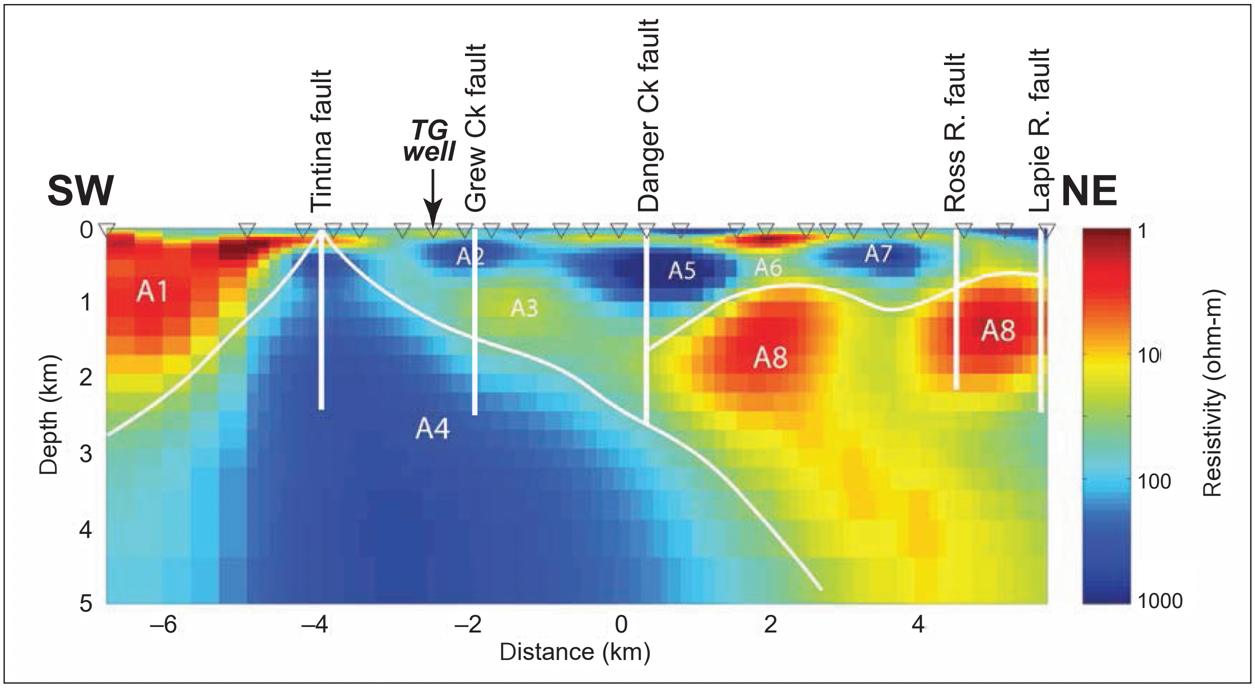

Figure 34. *Section through the 3D resistivity model derived from MT data collected by Mira Geoscience (2017). The approximate line of the section is indicated on Figure 33. The strong resistivity of feature A4 suggests the presence of crystalline rocks (granitoid?) at depth northeast of the Tintina fault. Conductive features A1 and A8 likely indicate presence of graphitic rocks, though A8 could also be due in part to aqueous fluids.*

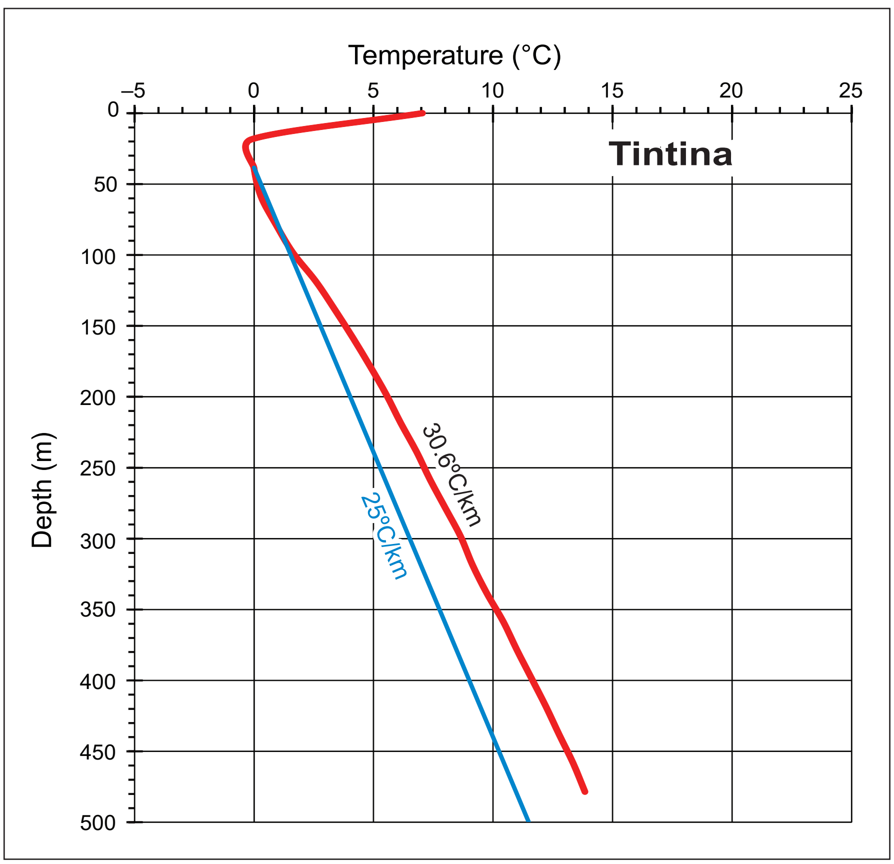

Figure 35. *Temperature profile measured at the borehole in the Tintina Trench region near Ross River (after Fraser et al., 2019). The blue line indicates the average geothermal gradient of 25°C/km. The red curve shows the measured temperature profile, which has a geothermal gradient of 30.6°C/km. Data in Appendix C.*

Watson Lake area

The geothermal potential of the Tintina Trench was also evaluated in the Watson Lake area (Witter, 2022). This project was a collaboration between the YGS and Liard First Nation and involved acquisition of new gravity and MT data in an area centred on the Alaska Highway between Watson Lake and Junction 37 (Fig. 36). In this area, the Tintina Trench is approximately 17 km wide and filled with Cenozoic clastic sedimentary rocks (siltstone, shale, coal, conglomerate). The Tintina fault zone is bounded to the southwest by lower Paleozoic shale and carbonate of the Cassiar terrane. Northeast of the fault zone, mid to late-Paleozoic shale, carbonate, conglomerate and volcanic rocks are part of the Yukon-Tanana and Slide Mountain terranes, and the western Laurentian continental margin (Figs. 4, 36; Yukon Geological Survey, 2022). Sporadic occurrences of Pleistocene basalt (765–232 Kyr) across the trench suggest recently elevated heat flow through the region. The CPD near Watson Lake is 18 to 19 km, suggesting a thermal gradient of approximately 30°C/km; a single bottom-hole temperature measurement from a petroleum exploration borehole approximately 15 km northeast of Watson Lake indicates a possible gradient of up to 49°C/km in the region (Figs. 7, 36).

Geophysical and geological modelling of the Tintina Trench near Watson Lake was designed to evaluate the potential for fault-controlled geothermal systems. The new geophysical data provides new constraints on fault locations and the extent of Cenozoic strata in the poorly exposed Liard Plateau (Figs. 37 and 38). Modelling of the gravity and MT data indicates that Cenozoic sedimentary rocks are up to 1 km thick near the centre of the basin (Fig. 39) and that the western strand of the Tintina fault zone occurs farther west, near Junction 37, compared to

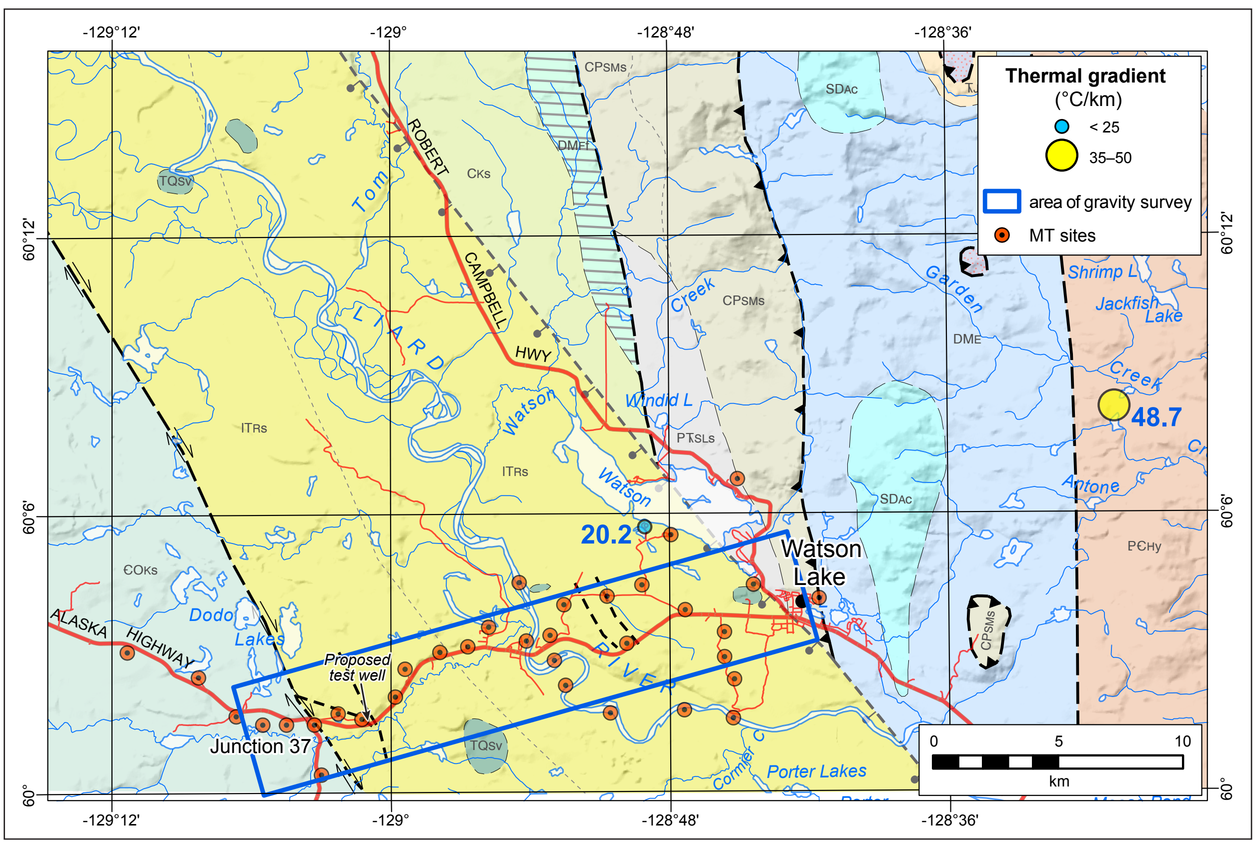

__Figure 36.__ Geology and geothermal characteristics of the Tintina Trench near Watson Lake (geology after Yukon Geological Survey, 2022). Area of gravity survey (Fig. 37a) indicated by blue rectangle; orange dots show locations of magnetotelluric (MT) sites. Thermal gradient measurements for the area are also shown.

previous interpretations (e.g., Colpron et al., 2016b). Three-dimensional inversion of the residual total field magnetic data suggests the presence of a strongly magnetic plutonic body at depths of greater than 4 km (Fig. 37b). This inferred pluton may be related to Pleistocene mafic volcanic rocks sporadically exposed in the area or could be a buried equivalent to highly radiogenic Late Cretaceous and Eocene plutons exposed 100 to 140 km northwest of Watson Lake (Fig. 6; Colpron, 2019). The Cenozoic pull-apart basin within the Tintina Trench is floored by a strong conductor (C1 in Fig. 38) that extends approximately 15 km across the fault zone at depths greater than 1 km. This conductor could result from extensive clay alteration, the presence of graphite, and/or salty brines at depth. Because shales are important components of Paleozoic rock units of the Cassiar terrane, Slide Mountain terrane and western Laurentian continental margin strata on either side of the Tintina fault zone, the presence at depth of clay and/or graphite-rich lithology seems the most likely interpretation for conductor C1 (Fig. 38). Witter (2022) proposed the location of a scientific borehole to test various aspects of the model and provide a direct measurement of the thermal gradient in the Tintina Trench near Watson Lake (Figs. 36, 39).

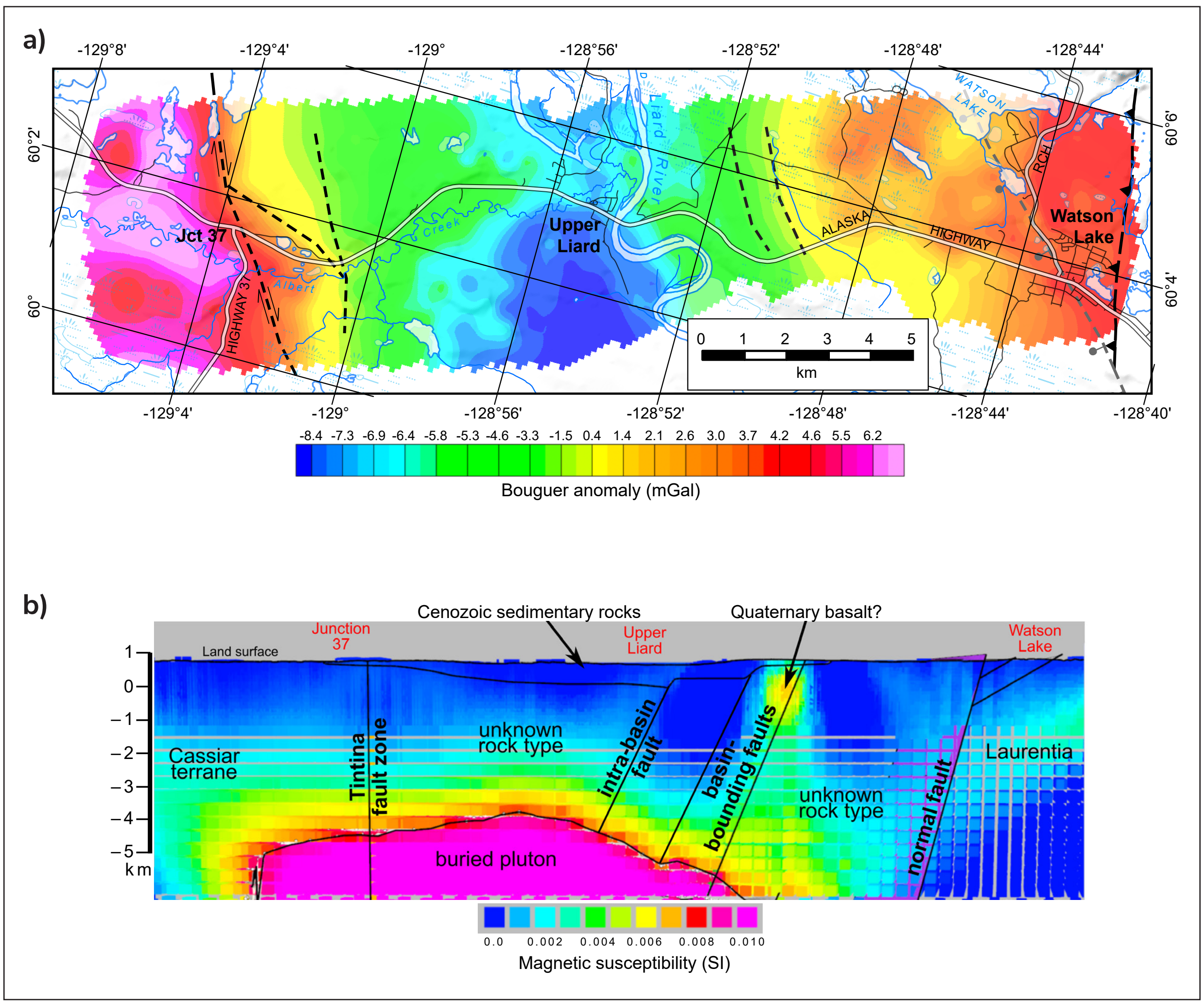

Figure 37. a) *Bouguer gravity anomaly map for density of 2.67 g/cm³ with upward continued 2500 m trend removed (Aurora Geosciences, adapted from Witter, 2022). RCH: Robert Campbell Highway.* ***b)*** *Section through 3D magnetic inversion model along the Alaska Highway corridor near Watson Lake (modified from Witter, 2022). A strong magnetic anomaly straddling the western part of the Tintina fault zone is modelled to represent a possible pluton at depth of >4 km below sea level.*

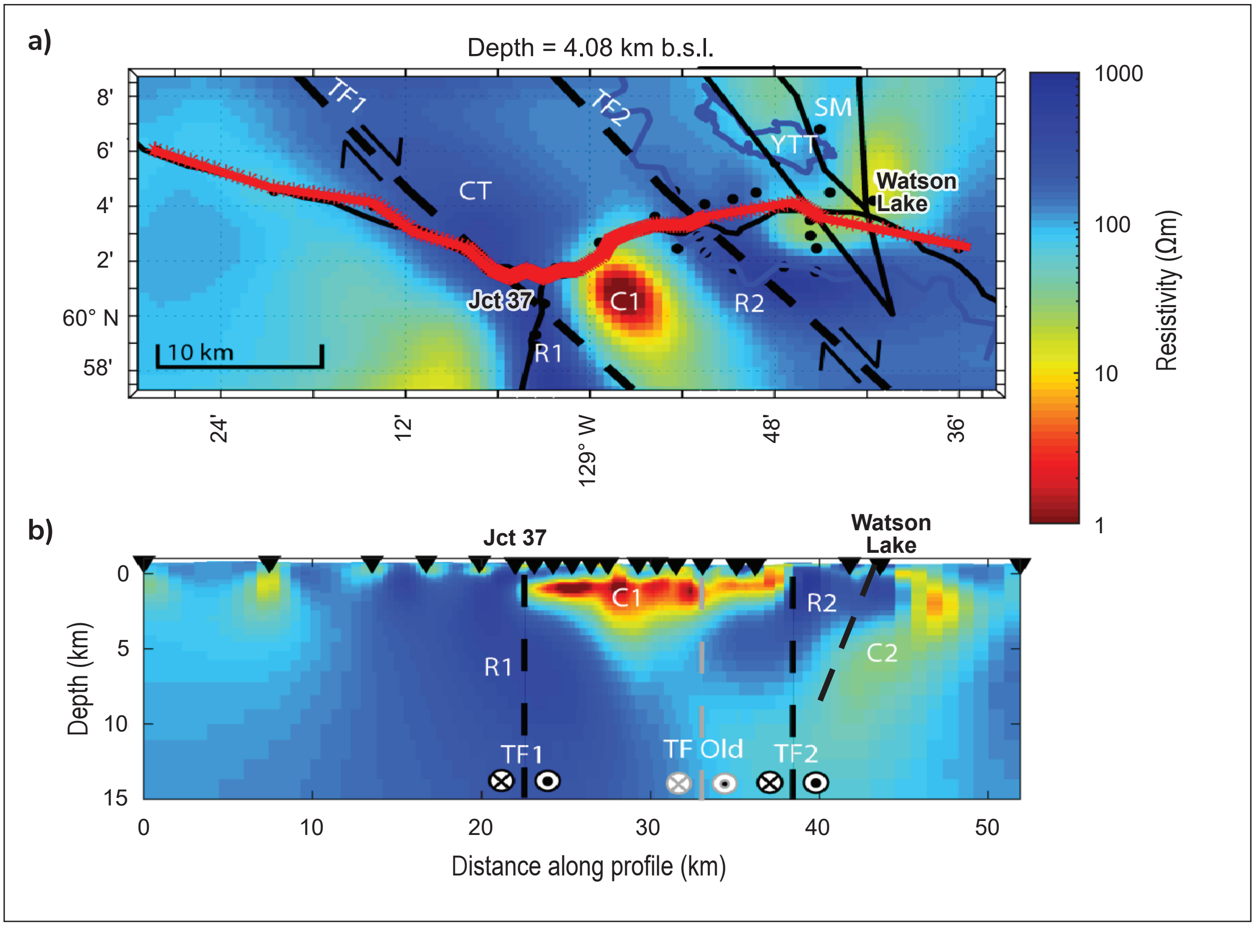

Figure 38. *Images of a 3D inversion model of the resistivity across the Tintina fault zone, based on magnetotelluric data (after Slobodian, 2023).* ***a)*** *Plan view through the model at a depth of 4.08 km below sea level.* ***b)*** *Vertical section through the model along the Alaska Highway (red line in a). TF1 and TF2 are the two main strands of the Tintina fault zone bounding conductive layer C1. 'TF Old' is the previously mapped location of the Tintina fault inferred from regional aeromagnetic data (Colpron et al., 2016b). C1 and C2 are conductors; R1 and R2 are resistors. CT: Cassiar terrane, SM: Slide Mountain terrane, YTT: Yukon-Tanana terrane.*

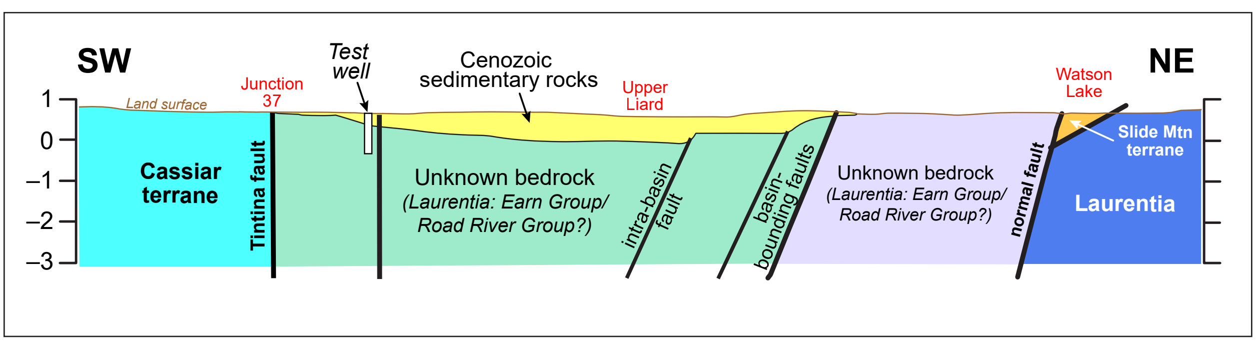

Figure 39. *Cross section of the geological model constructed using geophysical and geological data from across the Tintina Trench near Watson Lake, Yukon (modified from Witter, 2022).*

Pelly–Cassiar Mountains

This region encompasses the Pelly and Cassiar mountain ranges southwest of Tintina Trench and northeast of the Teslin fault (Figs. 4, 9). The region is traversed by the South Canol Road (Yukon Highway 6) and is bounded by the Alaska Highway (Yukon Highway 1) to the south and the Robert Campbell Highway (Yukon Highway 4) to the north.

There are a few interesting geothermal indicators in the Pelly–Cassiar Mountains (Fig. 40). The few mineral exploration boreholes measured in the area have temperature gradients ranging from 19 to 29°C/km (Fig. 7; Jessop et al., 2005) and heat flow estimates of 95 to 126 mW/m^2 were calculated by Lewis et al. (2003). The CPD varies from approximately 19 km near the Tintina fault to approximately 12 km north of Teslin (Fig. 5). The region contains some of the most highly radiogenic plutons in the Yukon, particularly in granites of the Seagull plutonic suite (Fig. 6). Targeted geothermal studies were conducted near Teslin and the Seagull batholith near Swift River (Fig. 40).

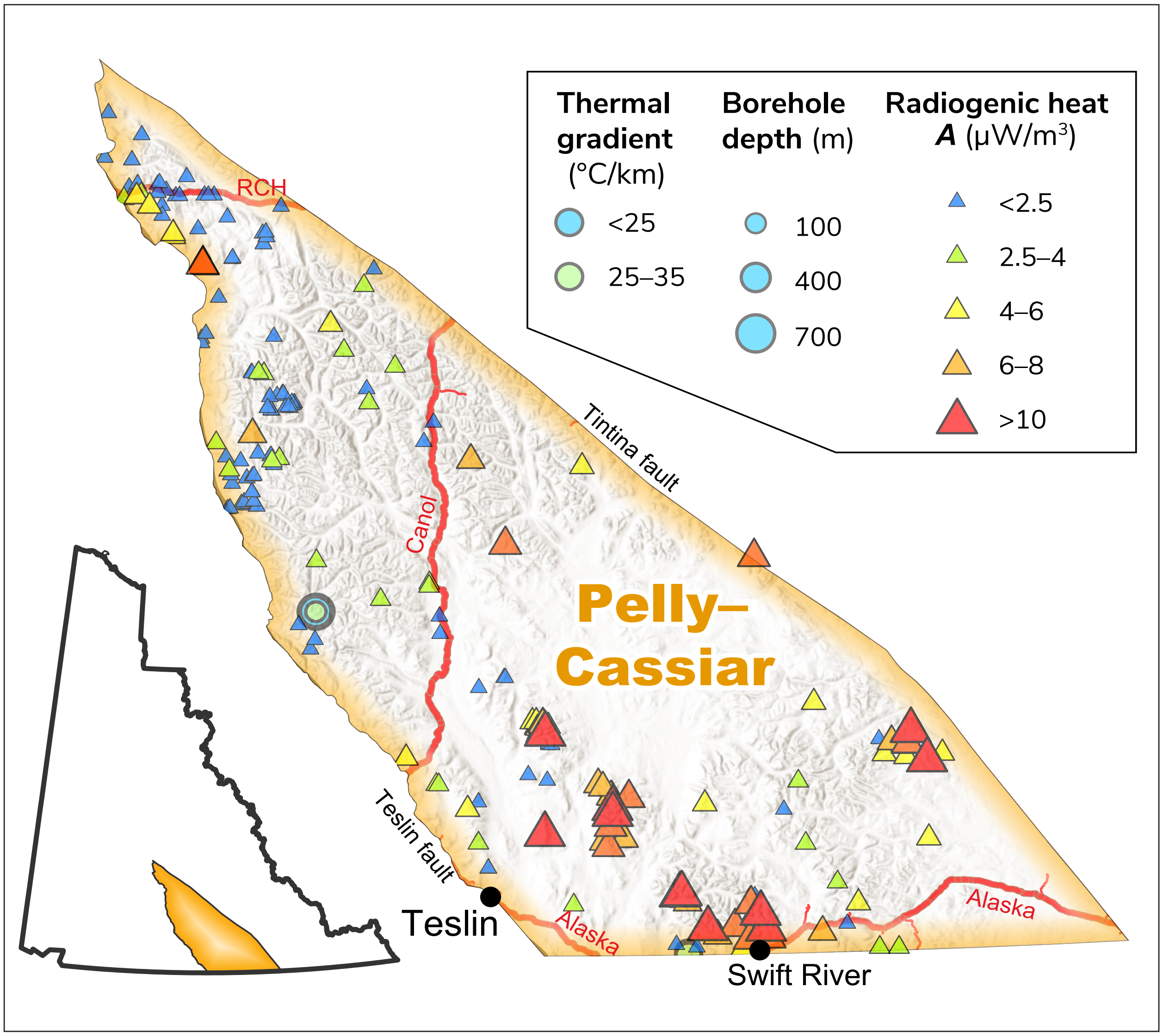

Figure 40. *Geothermal indicators in the Pelly-Cassiar region. RCH: Robert Campbell Highway.*

Teslin area

The Teslin area was the subject of a detailed investigation as part of the YGS' fault-controlled geothermal research program. The area was targeted because of the shallow CPD (12–14 km) and the location of the Village of Teslin near a bifurcation within the Teslin fault zone (Fig. 41). The main Teslin fault is beneath Teslin Lake and separates rocks of the Cache Creek (unit mTJC) and Atlin (unit PTNv) terranes to the southwest from those of Quesnellia (unit uTJSs) northeast of the lake. The eastern Teslin fault has a more northerly strike and juxtaposes metamorphic rocks of the Yukon-Tanana terrane (units PDSs and DMFv) to the east of Teslin against those of Quesnellia to the west. Early Cretaceous (ca. 120–110 Ma) granodiorite of the Deadman Creek batholith (unit EKgT) intrudes the Yukon-Tanana terrane east of Teslin.

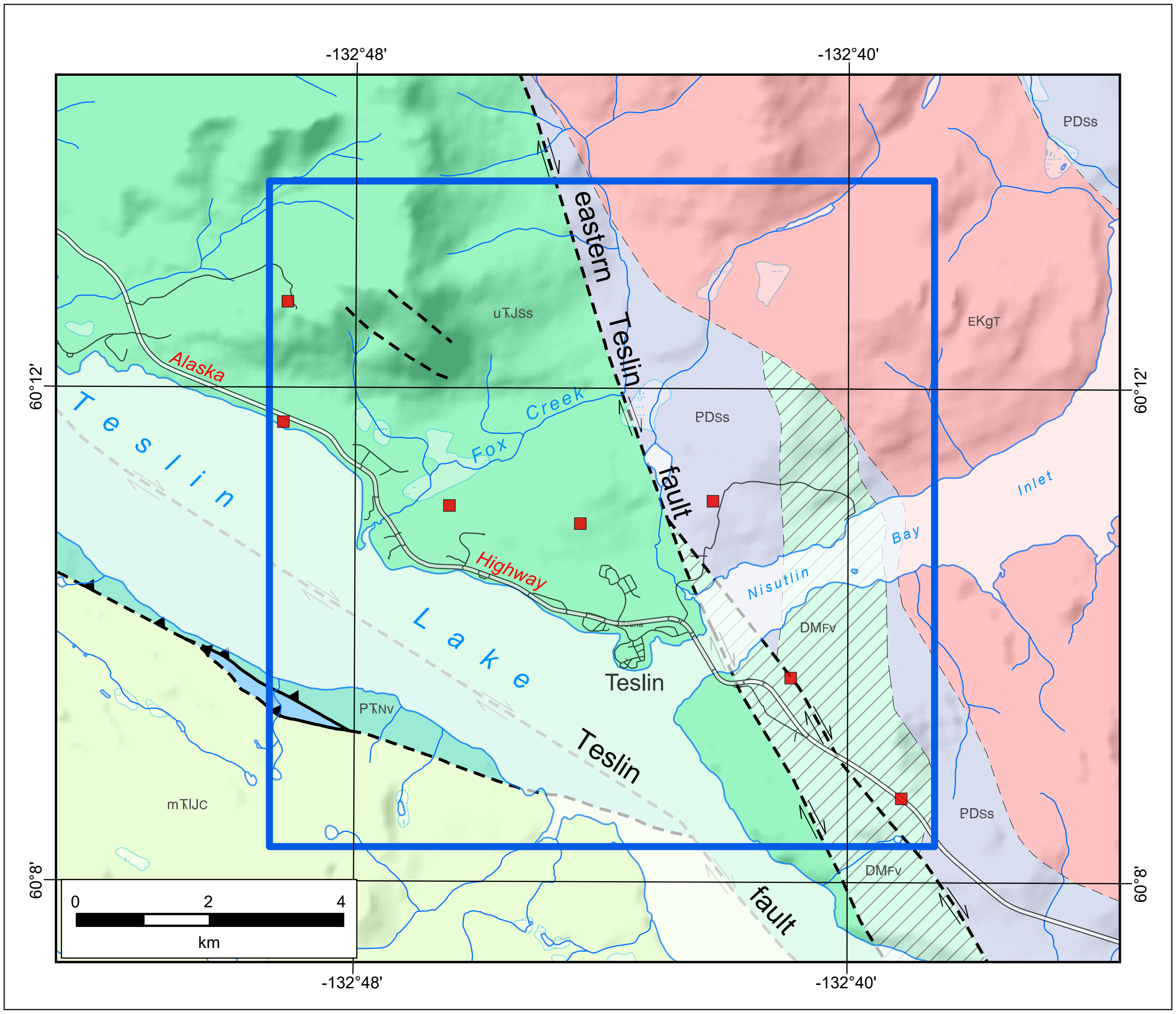

Figure 41. *Geology of the Teslin area (geology after Yukon Geological Survey, 2022). The Village of Teslin is situated between two strands of the Teslin fault (dashed lines). The area of the gravity survey shown in Figure 42 is indicated by the blue rectangle; the locations of audiomagnetotelluric sites are shown with red squares.*

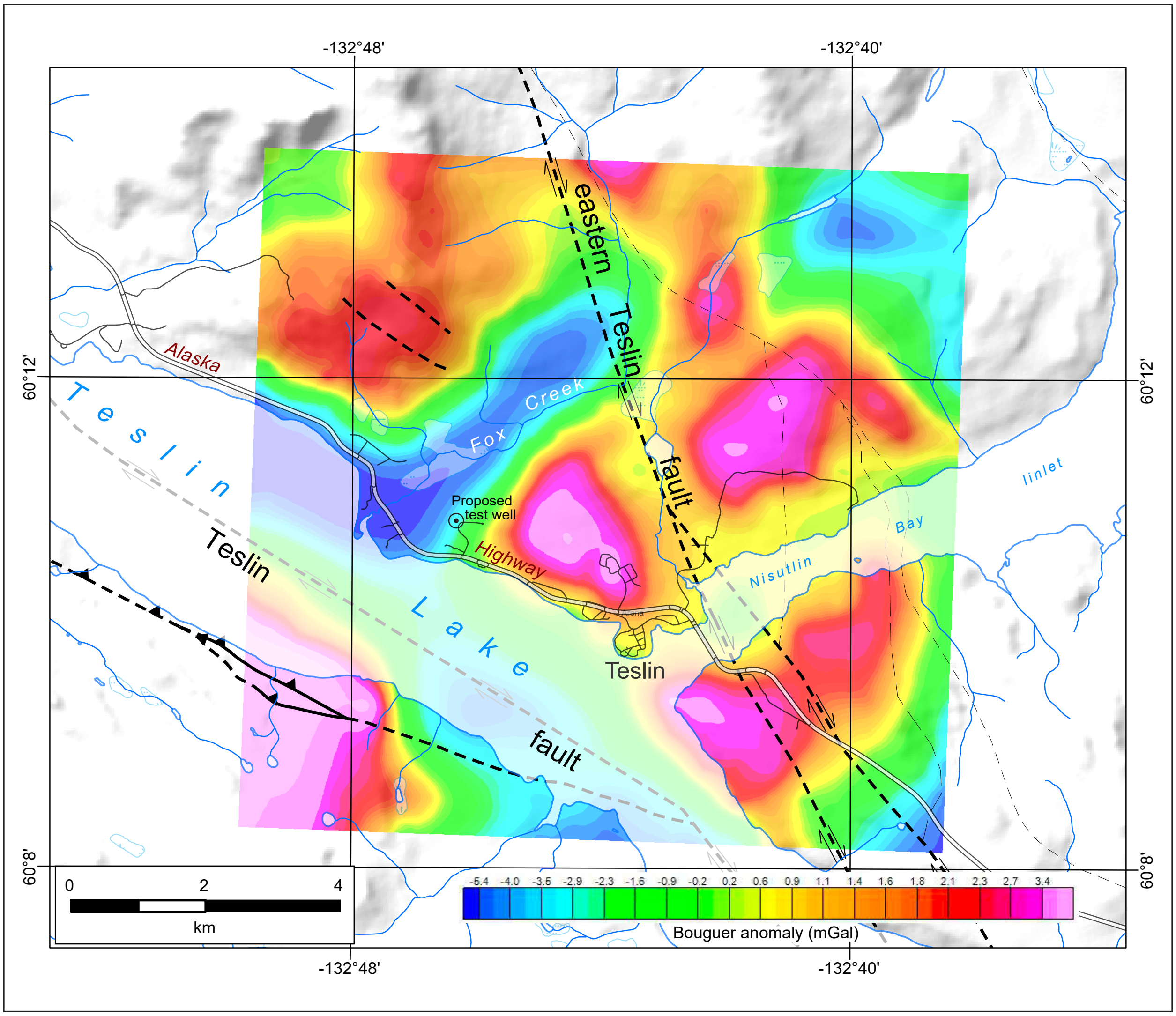

Figure 42. *Bouguer gravity anomaly map of the Teslin area for a density of 2.67 g/cm*^{3} *with second order trend removed (Aurora Geosciences, adapted from Witter, 2023). The location of a proposed temperature gradient borehole near Fox Creek is indicated.*

Investigation of the Teslin area integrated regional aeromagnetic data with newly acquired gravity and audiomagnetotelluric (AMT) data (Figs. 41, 42; Witter, 2023). The detailed gravity survey of the Teslin area shows a prominent, northeast-trending gravity low along the Fox Creek valley that could represent a zone of extension between the two strands of the Teslin fault (Fig. 42). The low-density material is inferred to reflect thicker sediment fill in Fox Creek (Witter, 2023). The extensional regime along Fox Creek could be conducive to groundwater circulation in this area. Passive seismic and airborne electromagnetic data acquired in 2023 will further constrain the geological model for the Teslin area. Witter (2023) proposed a borehole location along the southern edge of the Fox Creek anomaly to test the preliminary geological model and measure the local geothermal gradient (Fig. 42).

Swift River area

East of Teslin, granite of the mid-Cretaceous (103–101 Ma) Seagull plutonic suite intrudes the Yukon-Tanana terrane along a northwest-trending belt north of Swift River (Fig. 43). Plutons of the Seagull suite are some of the most radiogenic granites in the Yukon (Fig. 6; Colpron, 2019),

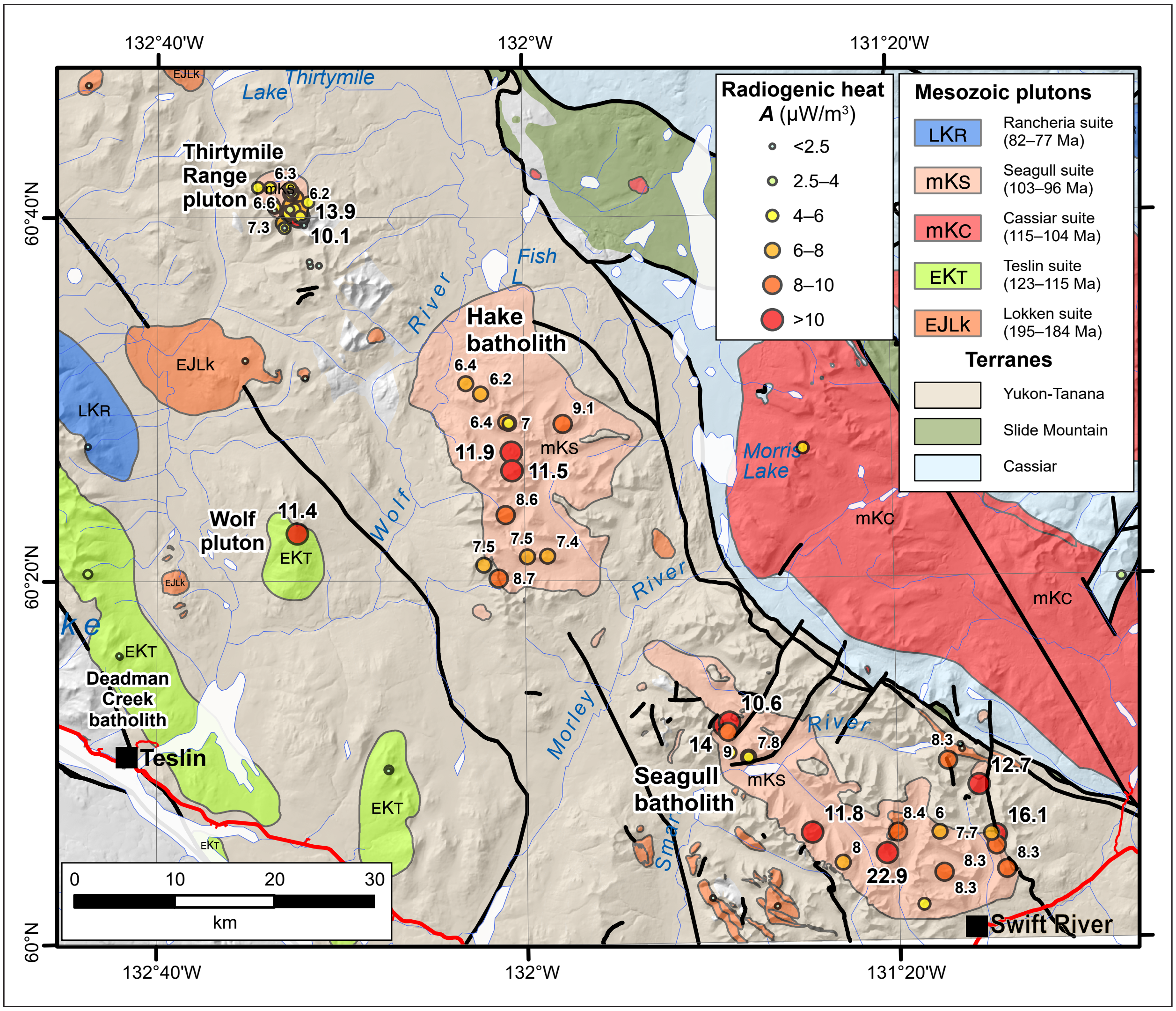

Figure 43. *Geology and radiogenic heat potential (***A***) of the Seagull plutonic suite in the Swift River area (modified from Colpron et al., 2021).*

with approximately 50% of samples analyzed yielding **A** values greater than 6 μW/m³ (Colpron et al., 2021). The Seagull batholith, the pluton closest to Swift River and the Alaska Highway, was studied in more detail than other plutons of this suite due to the availability of regional gravity data and an airborne radiometric survey, which were acquired during previous mineral exploration (Fig. 44; Kalkowski et al., 2015; Colpron et al., 2021). The radiometric survey shows that the southern part of the Seagull batholith is more highly radiogenic and that north-striking faults cutting the pluton could provide conduits for geothermal fluids, as suggested by Th and U anomalies extending along the faults. These preliminary results provide potential targets for further geothermal exploration near Swift River.

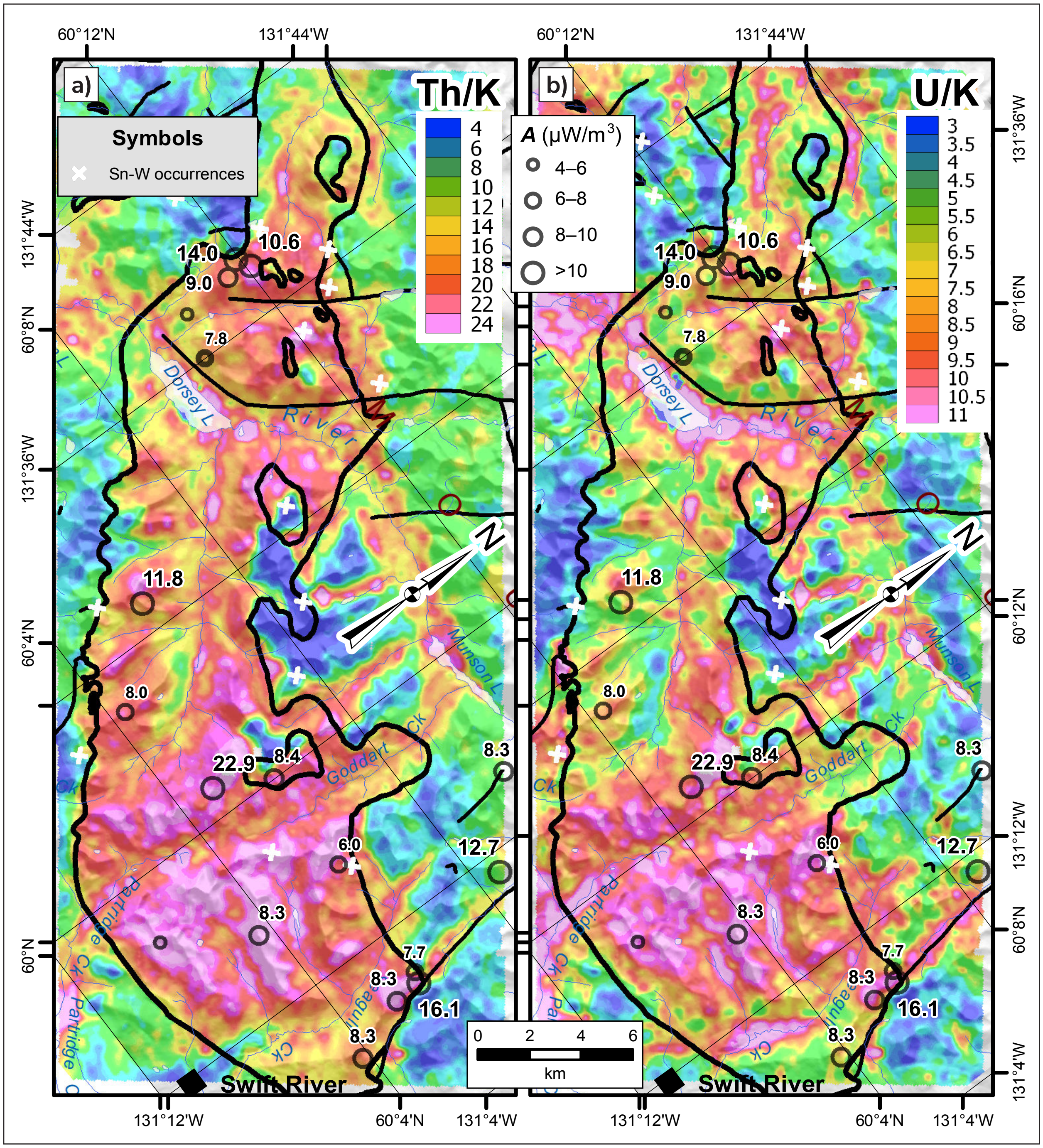

Figure 44. *Airborne radiometric survey results for the Seagull batholith (after Kalkowski et al., 2015; Colpron et al., 2021):* **a)** *Th/K map;* **b)** *U/K map. Radiogenic heat production values (***A***) from Figure 43 are shown; all measurements of* **A** *within the Seagull batholith are >4 μW/m³. Note that the geographic frame is rotated clockwise, with North pointing to the upper right.*

Yukon Plateaus

The Yukon Plateaus region comprises the area southwest of the Tintina Trench, west of the Pelly–Cassiar Mountains, and northeast of the Ruby Ranges (Fig. 9). The region includes Whitehorse; the communities of Carmacks, Pelly Crossing, Carcross and Tagish; and numerous rural subdivisions, connected via the Alaska, Klondike and Robert Campbell highways (Yukon Highways 1, 2 and 4, respectively) and the Atlin and Tagish roads (Yukon Highways 7 and 8, respectively; Fig. 45). The western part of the region comprises the Dawson Range, an area of intermittent mineral exploration and development.

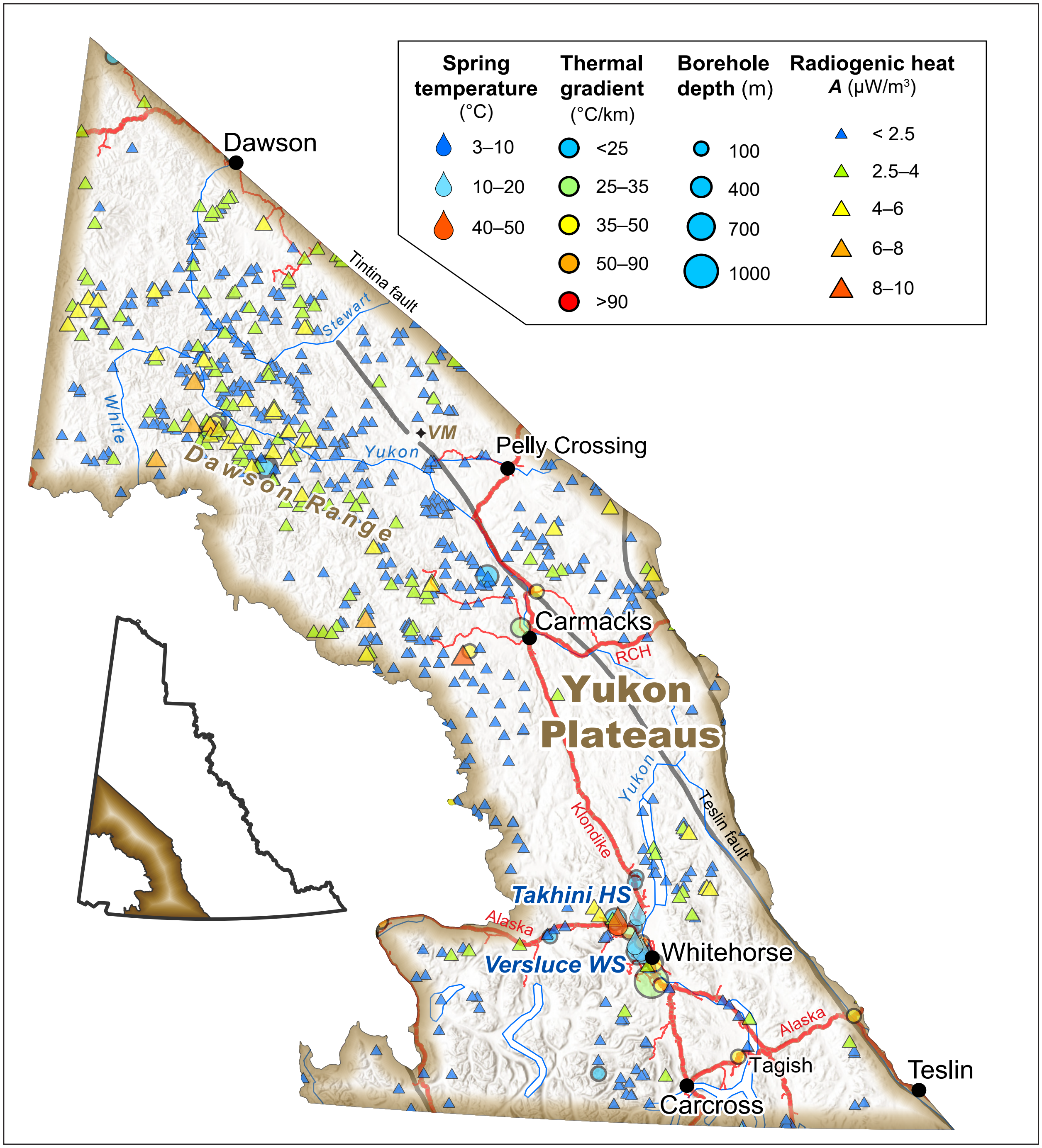

Figure 45. *Geothermal indicators in the Yukon Plateaus region. HS: hot spring, RCH: Robert Campbell Highway, WS: warm spring.*

The Yukon Plateaus are underlain by the Intermontane terranes, comprising sedimentary and volcanic rocks of the Yukon-Tanana, Stikine, Atlin, and Cache Creek terranes, and the overlying Whitehorse trough, intruded by numerous Jurassic to Eocene granitoid plutons (Yukon Geological Survey, 2022). Geothermal indicators in this region include a few thermal springs, including the Takhini hot spring near Whitehorse, and sporadic occurrences of Neogene–Recent (<10 Ma) volcanic rocks that suggest recent elevated heat flow in this part of Yukon (Fig. 4). The CPD varies from approximately 30 km near Dawson to approximately 15 km near Whitehorse (Fig. 5). In the Dawson Range northwest of Carmacks, and in the Whitehorse area, Cretaceous and Eocene plutons locally have anomalous radiogenic heat production values (**A** >4 μW/m^3; Fig. 6). Data from limited mineral exploration boreholes and shallow water boreholes generally show average to low temperature gradients (<30°C/km; Fig. 7).

Whitehorse area

The Whitehorse area is the most densely populated region of the Yukon and contains several geothermal indicators including thermal springs, areas of open water during winter, and satellite infrared anomalies near Alligator Lake, south of the city (Fig. 46; EBA Engineering Consultants Ltd., 2009a, f). Areas of open water occur in two distinct regions: along the edge of the Whitehorse batholith near the city and along the trace of the Ibex thrust and near Alligator Lake, southwest of the city. Warm water was also encountered in a few shallow water boreholes in the region. Thermal springs occur along the western edge of the Whitehorse trough (filled by sedimentary rocks of the Laberge Group) and include Takhini hot spring and Vista Mountain warm springs north of Whitehorse, and Versluce, Stinky Lake and Crestview warm springs within city limits (Fig. 46).

Takhini hot spring

The Takhini hot spring is located north of the Takhini River, approximately 25 km northwest of Whitehorse (Fig. 46). The spring occurs in Upper Triassic sandstone interbedded with limestone of the Aksala Formation (units uTAh, uTAm and uTAc, Fig. 47; Yukon Geological Survey, 2022). It is located approximately 2.3 km east of an Eocene (ca. 54 Ma) granite pluton (Flat Creek pluton, Fig. 46) that yielded radiogenic heat values of 3.2 to 5.8 μW/m^3 (Fig. 6). The spring emerges from a single seep with a water temperature of 46.5°C and flow rate of approximately 6.5 L/s (EBA Engineering Consultants Ltd., 2009h). An airborne thermal infrared survey identified five anomalies in the vicinity of the hot spring (EBA Engineering Consultants Ltd., 2009h). The Takhini hot spring is operated as a commercial spa under the name Eclipse Nordic Hot Springs.

The Takhini hot spring is a calcium-sulphate–type thermal spring with a hardness of 1854 mg/L $CaCO_3$, a neutral pH (6.6–7.4), and electrical conductivity of 2676 to 2905 μS/cm (van Everdingen, 1973a; Crandall and Sadlier-Brown, 1978; EBA Engineering Consultants Ltd., 2009h). The spring water has elevated fluoride (3.2–4.4 mg/L), which suggests interaction with a granitoid body. Water boreholes near the Takhini hot spring have water temperatures between 5 and 19°C. Dissolved silica concentrations at Takhini hot spring range from 41 to 98 mg/L, resulting in geothermometer temperatures of 94 to 136°C (Table 2; van Everdingen, 1973a; Crandall and Sadlier-Brown, 1978; Grasby et al., 2000; EBA Engineering Consultants Ltd., 2009h). Tritium concentrations of approximately 0.8 TU indicate a groundwater residence time of more than 70 years (Terzer-Wassmuth et al., 2022).

A 500 m deep temperature gradient borehole was drilled approximately 1.5 km west of Takhini hot spring (Fig. 47; Fraser et al., 2019). The borehole encountered mostly sandstone, shale and volcaniclastic rocks of the Lower to Middle Jurassic Laberge Group (Whitehorse trough). Below a

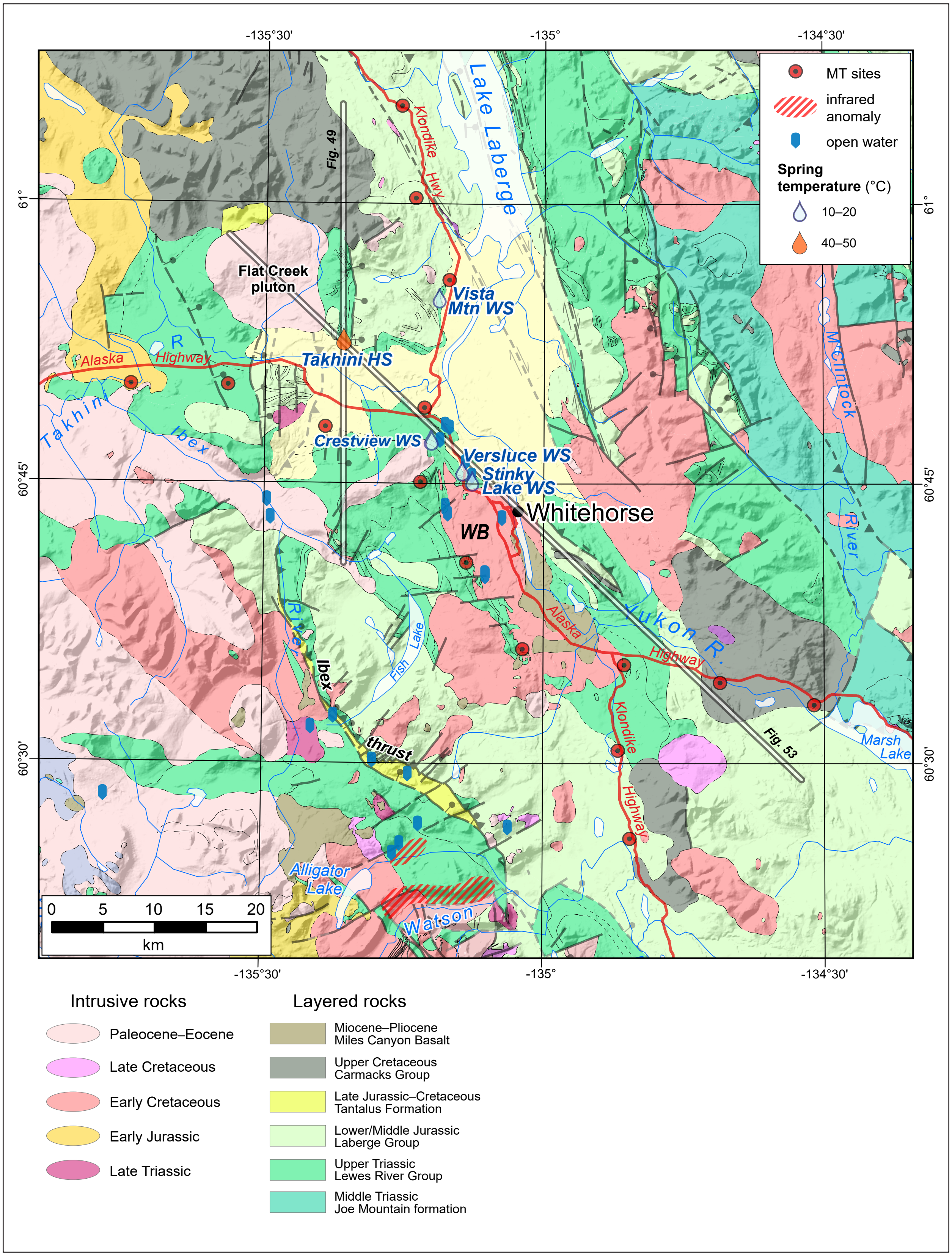

Figure 46. *Geology of the Whitehorse area (after Yukon Geological Survey, 2022). The locations of thermal springs, open water and infrared anomalies are indicated. Broadband magnetotelluric (BBMT) sites are shown as red dots. Section lines for the 3D resistivity models shown in Figures 49 and 53 are indicated. HS: hot spring, WB: Whitehorse batholith, WS: warm spring.*

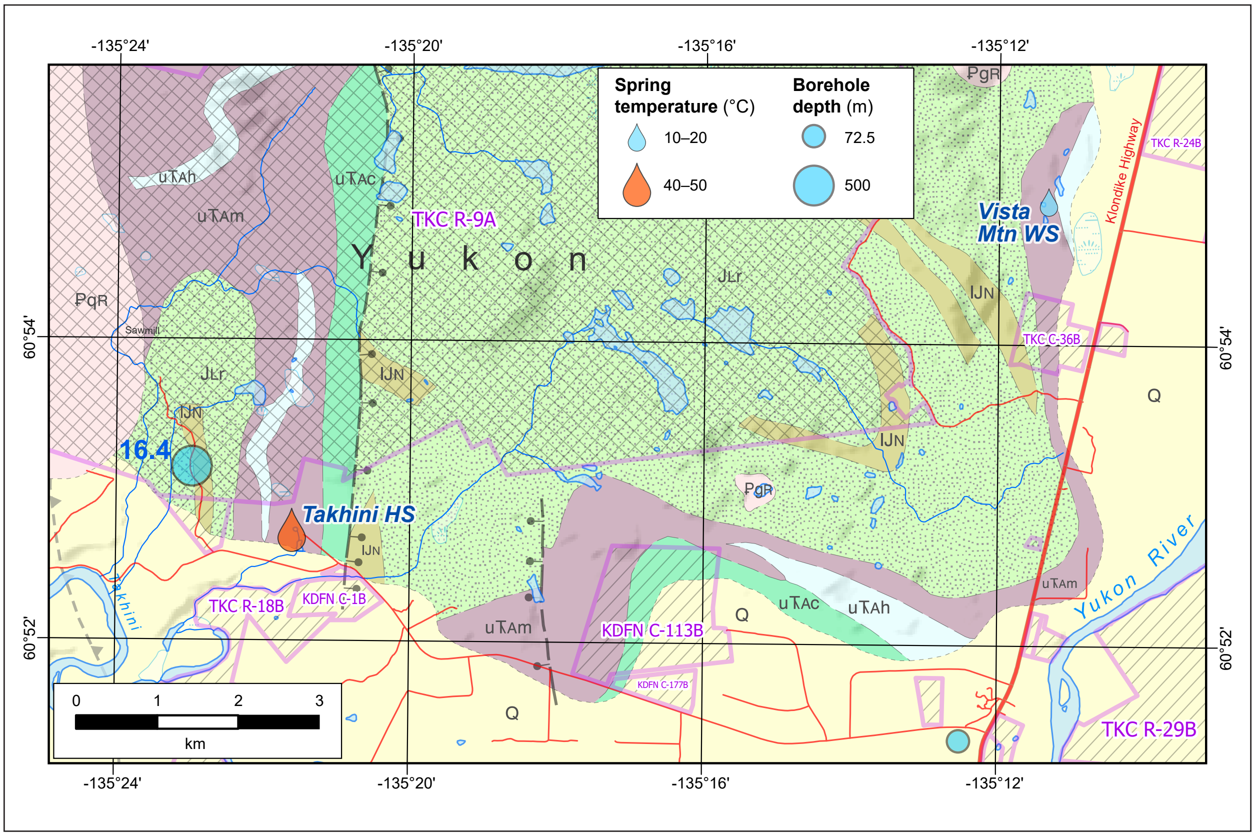

Figure 47. Geology of the Takhini hot spring area (after Yukon Geological Survey, 2022) with location of thermal springs and temperature gradient boreholes. First Nations Settlement Lands are indicated by cross hatched (Category A) and simple hatched (Category B) areas with pink borders.

near-surface subtle inversion, the temperature profile shows a relatively constant increase with a gradient of 16.5°C/km to a depth of 450 m, followed by a sharp increase to a gradient of approximately 250°C/km in the lower 50 m of the borehole (Fig. 48, Appendix C; Fraser et al., 2019). These results suggest conductive heat transfer in the upper part of the borehole and the presence of a fault or fractured rocks with convective heat transfer below 450 m (Langevin et al., 2020). A numerical model of groundwater flow and heat transfer for the Takhini hot spring area shows that geothermal fluids were probably heated by the nearby radiogenic granite and infiltrated along inclined, permeable, sedimentary strata to surface at the hot spring (Léveillée-Dallaire and Raymond, 2024). A broadband magnetotelluric (BBMT) survey of the Whitehorse area (Fig. 46) imaged a strong, south-dipping resistivity contrast that surfaces at the Takhini hot spring and may indicate a deep crustal influence on the hot spring (Fig. 49; C. Hanneson, pers. comm., 2024).

Vista Mountain warm springs

The Vista Mountain warm springs are located west of the Klondike Highway, approximately 10 km northeast of the Takhini hot spring (Figs. 46, 47). The warm springs comprise four distinct seeps over approximately 60 m along a south-striking limestone–sandstone contact. The water temperature is 10.5 to 13.7°C and flow rates are 1 to 2 L/s (EBA, A Tetra Tech Company, 2012d). Gas bubbles and a slight H_2S odour were noted at one of the seeps.

The Vista Mountain warm springs is characterized by sodium-sulphate–type water chemistry with pH of 10.02 and a measured TDS concentration of 381 ppm (EBA, A Tetra Tech Company, 2012d). The fluoride concentration is 9.85 to 10.00 mg/L, suggesting interaction of the

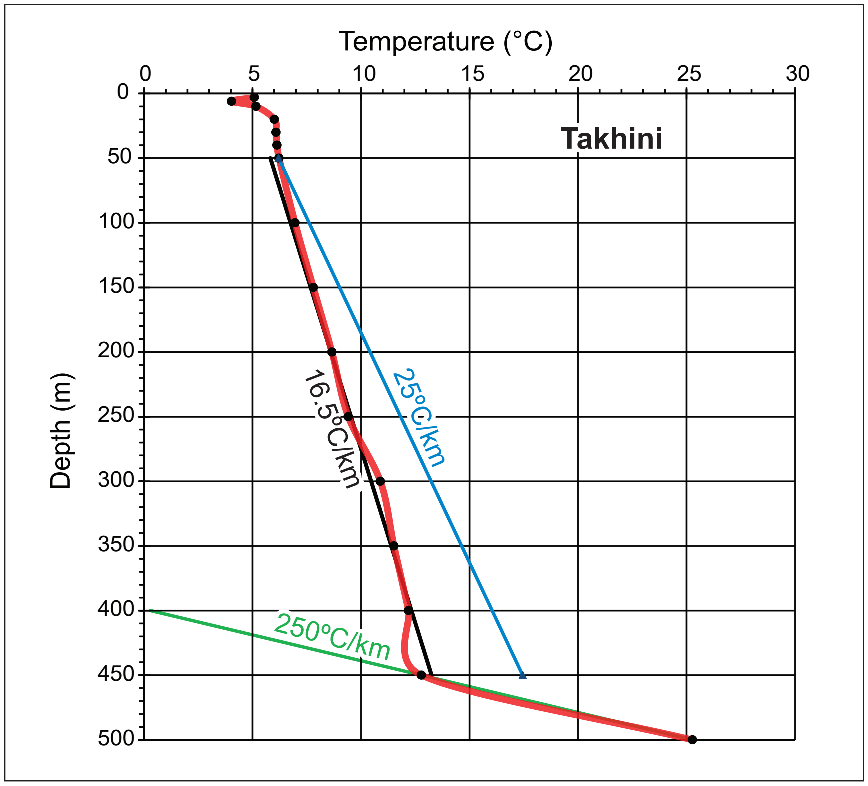

Figure 48. *Temperature profile measured in a borehole in the Takhini area (modified from Fraser et al., 2019). The blue line indicates the average geothermal gradient (25°C/km; the red curve shows the measured temperature profile, with a geothermal gradient of 16.5°C/km (black line) to 450 m depth; and the green line shows the elevated geothermal gradient (250°C/km) measured in the bottom 50 m of the borehole. Data in Appendix C.*

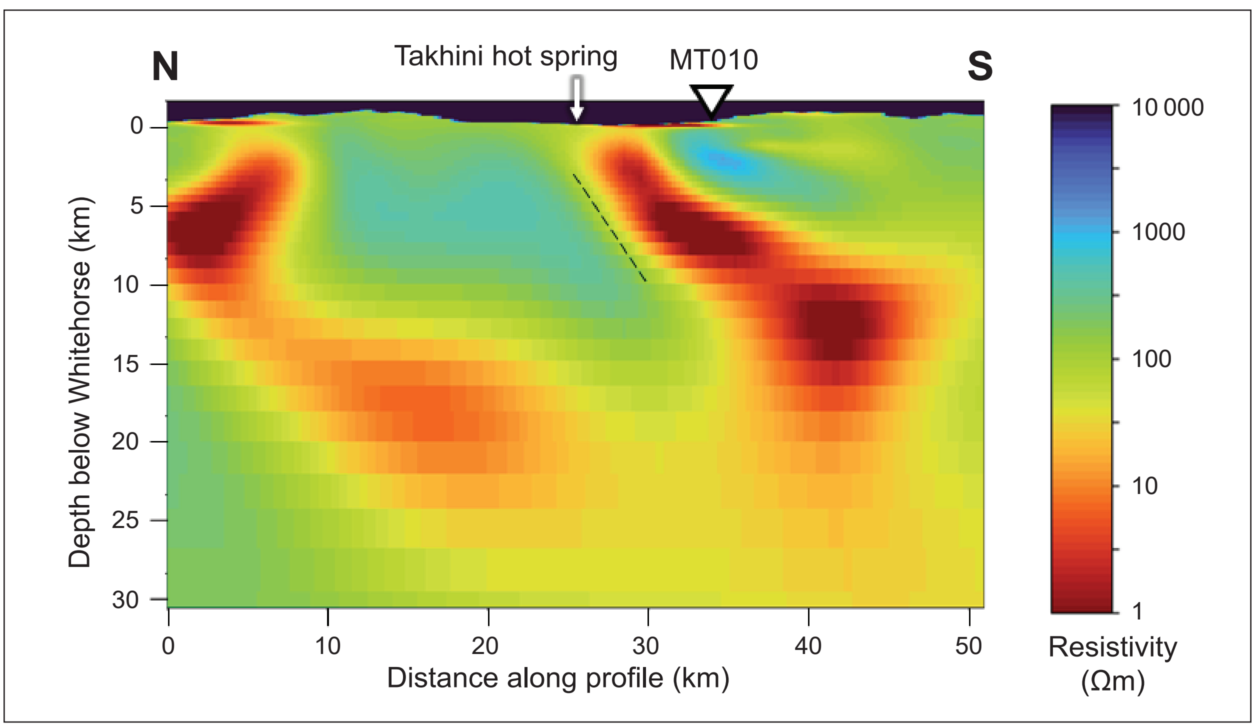

Figure 49. *Section through a 3D resistivity model from broadband magnetotelluric data highlighting a strong resistivity contrast beneath Takhini hot spring, Yukon (C. Hanneson, pers. comm., 2024). The location of this section is shown in Figure 46.*

groundwater with granitoid rocks (EBA, A Tetra Tech Company, 2012d). Environmental ^2H and ^{18}O concentrations show that the groundwater is derived from local meteoric water. Tritium isotopes at the detection limit of 0.8 ± 0.3 TU indicate a groundwater residence time of more than 70 years (Terzer-Wassmuth et al., 2022). The silica and alkali geothermometers suggest source reservoir temperatures in the range of 104 to 110°C (Table 2; EBA, A Tetra Tech Company, 2012d).

City of Whitehorse

The City of Whitehorse is mainly underlain by the mid-Cretaceous (113–109 Ma) Whitehorse batholith (units mKgW and mKqW), which intrudes Upper Triassic limestone, sandstone and conglomerate of the Aksala formation (Lewes River Group; units uTAc, uTAh and uTAm, Fig. 50). In the southern part of the city, subaerial flows of the Miocene (ca. 8.4 Ma) Miles Canyon basalt (unit MPMC) cover large parts of the area. The Whitehorse batholith consists mainly of granodiorite and diorite that generally have low heat production values (**A** <2.9 μW/m^3; Fig. 50). In the northern part of the city, Upper Triassic sedimentary rocks are intruded by a Paleogene granite (Haeckel pluton, unit PqR) that is part of the same intrusive suite as the radiogenic Flat Creek pluton west of the Takhini hot spring. The Haeckel pluton has anomalous radiogenic heat production values (**A**) that range from 2.9 to 5.0 μW/m^3 (Fig. 50).

Warm springs in the vicinity of the Porter Creek and Crestview neighbourhoods in the northern part of the city occur along the contact between limestone (unit uTAh) and sandstone of the Upper Triassic Aksala formation (Lewes River Group, unit uTAm; Fig. 50). The springs all occur along the edges of a strong gravity high (Fig. 51).

The Versluce warm spring is located on private property in the Porter Creek neighbourhood and produces clear, odourless, 12.5 to 12.7°C water (Crandall and Sadlier-Brown, 1978; EBA Engineering Consultants Ltd., 2009i). It flows at a rate of a few litres per second and produces small gas bubbles. The Versluce warm spring has calcium-magnesium-bicarbonate–type water chemistry with a pH of 7.6, 181 ppm TDS and 0.35 mg/L fluoride (Crandall and Sadlier-Brown, 1978; EBA Engineering Consultants Ltd., 2009g). Environmental ^2H and ^{18}O concentrations show that the groundwater is derived from local meteoric water. The ^3H concentration (11.3 ± 1.1 TU) is within the expected range for modern meteoric water in this part of North America (~10 TU; Terzer-Wassmuth et al., 2022). The silica geothermometer suggests a source temperature greater than 54°C for the Versluce warm spring (Table 2; EBA Engineering Consultants Ltd., 2009i).

The Stinky Lake warm spring emerges from a slope above Stinky Lake, south of the Porter Creek neighbourhood (Figs. 50, 51; EBA Engineering Consultants Ltd., 2009i). The spring water is clear with a faint H_2S odour, flows at approximately 1 L/s, and has a temperature of 18.5°C. Geological mapping and a detailed magnetic survey show that the Stinky Lake warm spring occurs within the contact aureole of the Whitehorse batholith (EBA, A Tetra Tech Company, 2011c, d). The Stinky Lake warm spring has calcium-magnesium-bicarbonate–type water with a pH of 7.56, 176 ppm TDS, and 0.5 mg/L fluoride (EBA, A Tetra Tech Company, 2011c, d). Environmental ^2H and ^{18}O concentrations show that the groundwater is derived from local meteoric water. The ^3H concentration (5.9 ± 0.8 TU) is close to expected values for modern meteoric water (Terzer-Wassmuth et al., 2022). These results indicate a residence time of less than 60 years for the groundwater. The $^3He/^4He$ ratio of 2.5 Ra suggests a significant contribution of mantle helium to groundwater and possible deep permeability in the northern part of Whitehorse (EBA Engineering Consultants Ltd., 2010a). Temperature estimates using the silica geothermometer suggest a source temperature greater than 85°C (Table 2; EBA, A Tetra Tech Company, 2011c).

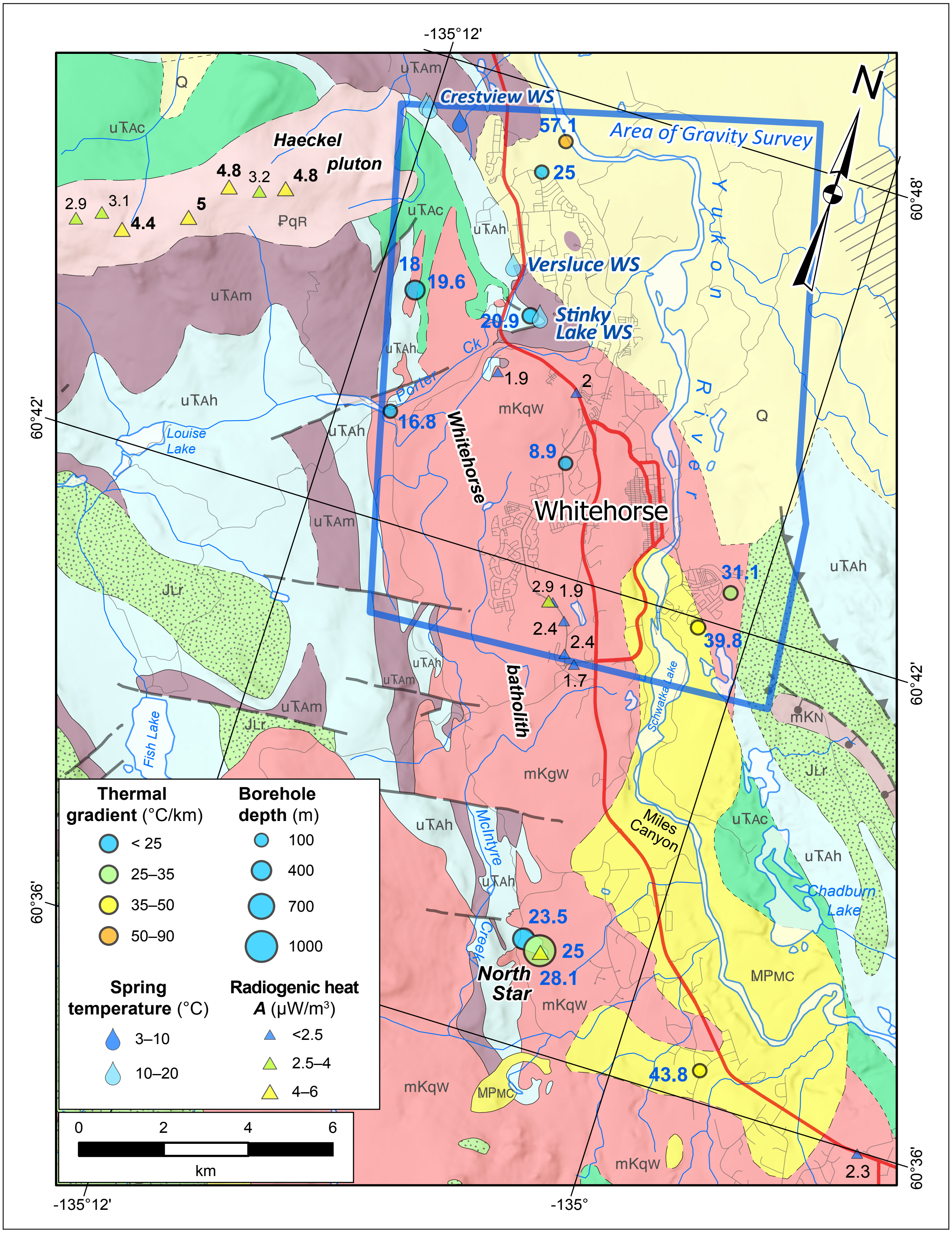

Figure 50. Geology of the City of Whitehorse (Yukon Geological Survey, 2022). The Stinky Lake, Versluce, and Crestview warm springs (WS) occur in the northern part of the city along a limestone-sandstone contact.

The Crestview warm springs are upwellings in a small wetland west of the Crestview subdivision (Figs. 50, 51). One of the springs has clear, odourless water with a temperature of 12.0°C and a flow rate of less than 1 L/s (EBA Engineering Consultants Ltd., 2009i). The water has calcium-magnesium-bicarbonate–type chemistry with a pH of 7.67, 206 ppm TDS, and 0.32 mg/L fluoride (EBA Engineering Consultants Ltd., 2009i). Environmental ^{2}H and ^{18}O concentrations show that the groundwater is derived from local meteoric water, and the ^{3}H concentration (7.9 ± 0.9 TU) is consistent with values for modern meteoric water (Terzer-Wassmuth et al., 2022). The silica

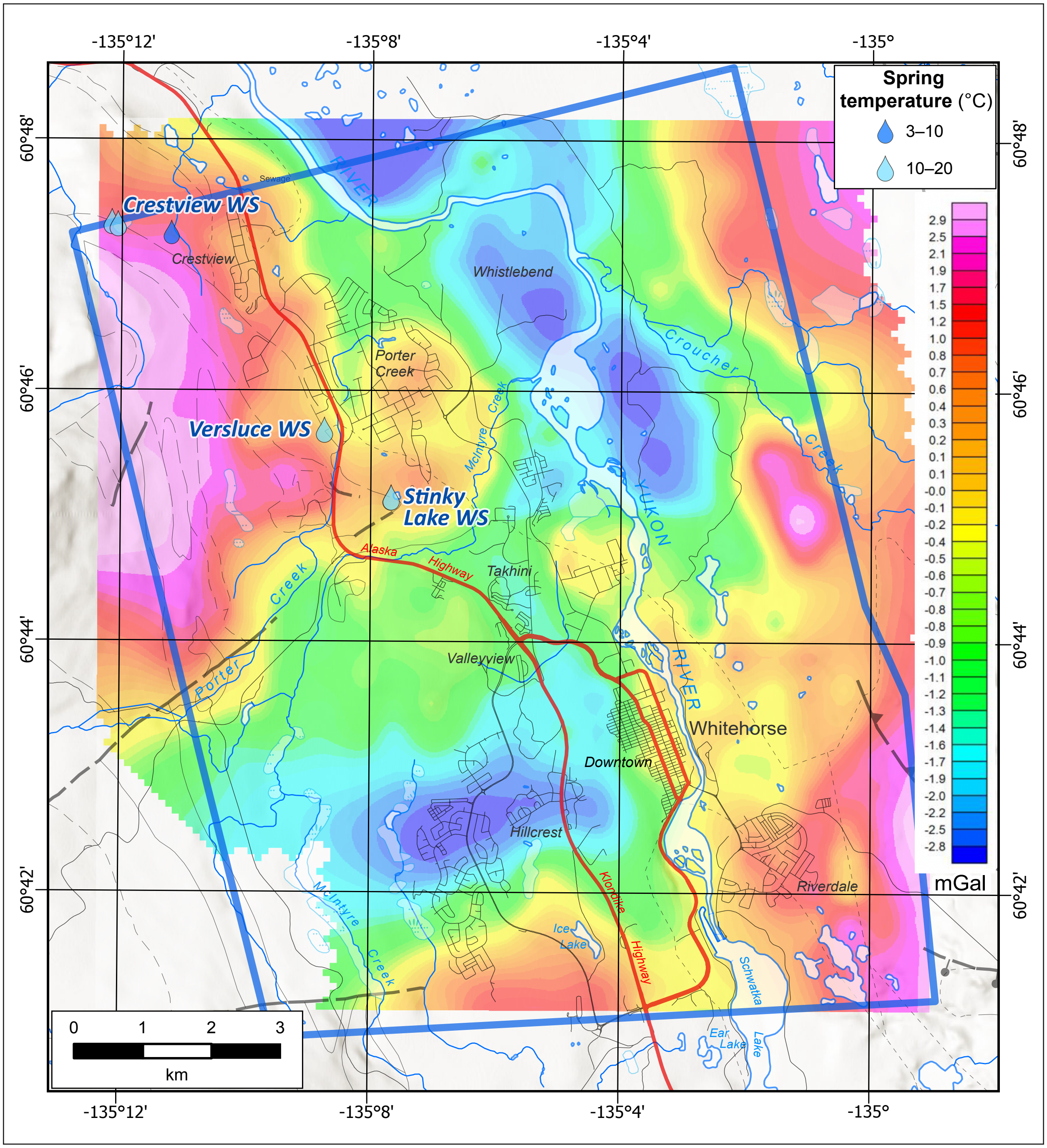

Figure 51. *Bouguer gravity anomaly map of northern Whitehorse for a density of 2.67 g/cm³ with upward continued 2500 m trend removed (Yukon Geological Survey, unpublished preliminary data, 2024). Warm springs (WS) near the subdivisions of Porter Creek and Crestview occur near the edge of a prominent gravity high. There is a sharp gravity gradient between the neighbourhoods of Porter Creek and Whistlebend.*

geothermometer suggests a relatively low source temperature of 39°C for the Crestview springs (Table 2; EBA Engineering Consultants Ltd., 2009i).

Temperature profiles measured from mineral exploration boreholes in the Whitehorse batholith, with depths ranging from 200 to 2000 m, yielded generally low gradients of 18 to 28°C/km (Fig. 50). A continuous temperature profile measured to 670 m in a deep borehole at the North Star prospect in the Whitehorse Copper Belt yielded a geothermal gradient of only 25°C/km (Figs. 50, 52; Appendix C). Shallow boreholes (<145 m) drilled through the Miles Canyon basalt encountered water with temperatures of 3.4 to 8.8°C that could indicate elevated thermal gradients of approximately 40°C/km (Fig. 50; Gartner Lee Limited, 2003; EBA Engineering Consultants Ltd., 2008b). These boreholes produce magnesium-sodium-bicarbonate–type water. Environmental isotope concentrations in these boreholes indicate that the groundwater is derived from local precipitation.

A BBMT survey shows strong conductors in the upper crust beneath Whitehorse (Fig. 53; C. Hanneson, pers. comm., 2024). These features are comparable to the resistivity contrast observed at the Takhini hot spring (Fig. 49) and may suggest potential for additional thermal springs in the area. Note that warm springs in the northern part of Whitehorse (Versluce, Stinky Lake and Crestview) are associated with a shallow conductor (Fig. 53).

Volcano Mountain (Nelruna)

The Fort Selkirk area is the site of some of the most recent volcanic activity in the Yukon, including extensive basalt flows, breccias, hyaloclastite and tuff along Wolverine Creek and the Yukon River and a well-preserved cinder cone and flows at Volcano Mountain (Nelruna; Figs. 54, 55a).

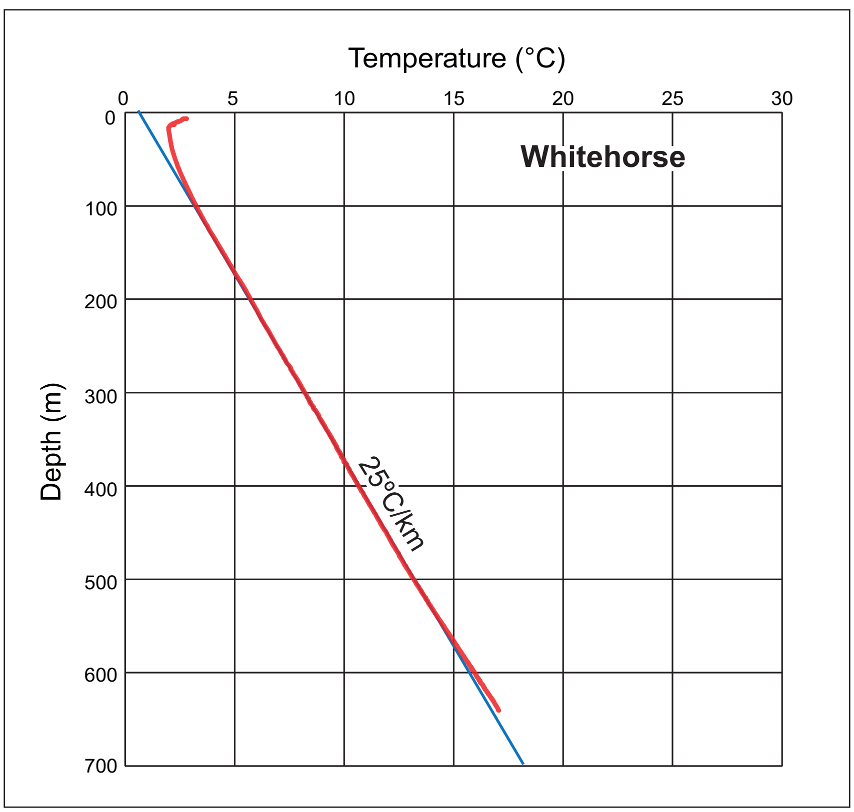

Figure 52. *Continuous temperature profile measured to 670 m in a deep borehole at the North Star prospect, within the Whitehorse Copper Belt. The blue line indicates average geothermal gradient of 25°C/km; the red curve shows the measured temperature profile, which has a geothermal gradient of 25°C/km. Data in Appendix C.*

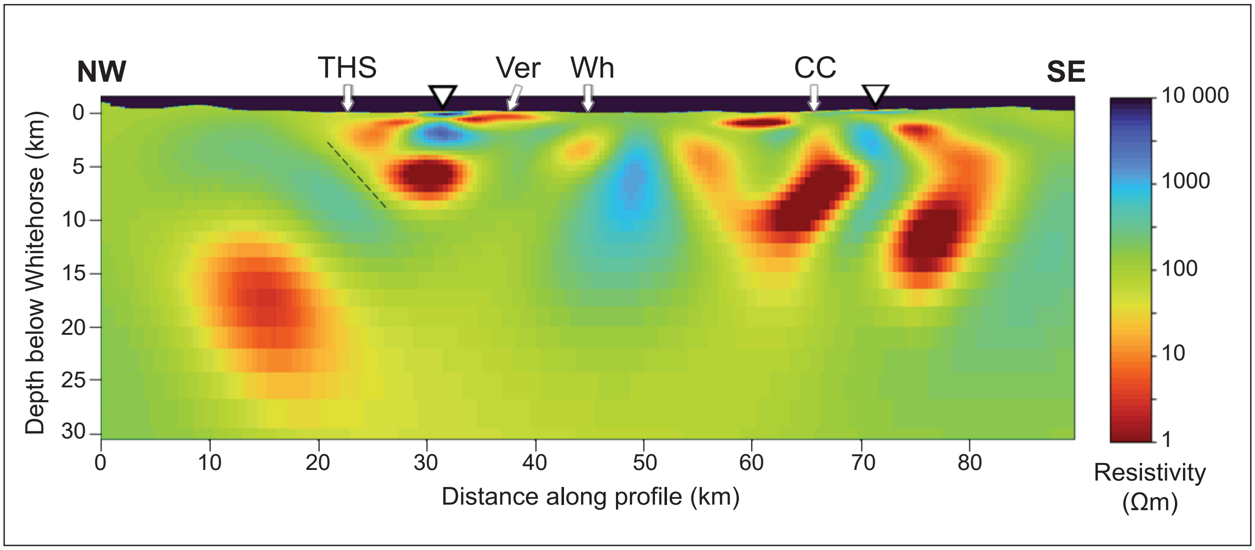

Figure 53. *Section through a 3D resistivity model from broadband magnetotelluric data highlighting the presence of several conductive zones in the upper crust beneath the City of Whitehorse (C. Hanneson, pers. comm., 2024). The location of the section is shown in Figure 46. CC: Carcross Cutoff (junction of Alaska and Klondike highways south of the city), THS: Takhini hot spring, Ver: Versluce/Stinky Lake warm springs, Wh: Whitehorse.*

The Selkirk Volcanic Group is part of the Northern Cordilleran Volcanic Province, which includes more than 100 Pleistocene–Holocene volcanic centres across northwestern BC (north of 55°N), the Yukon and east-central Alaska, USA (Russell et al., 2023). Volcanism near Fort Selkirk began in the mid-Pliocene ($^{40}Ar/^{39}Ar$ date of ca. 4.34 Ma) and occurred intermittently until the Holocene eruptions at Volcano Mountain (Fig. 54; Jackson and Huscroft, 2023). Radiocarbon (^{14}C) dating of organic sediments in small lakes overlying lava flows at Volcano Mountain indicates that the youngest flows in the area are older than 7300 years. Local occurrences of pillow breccia, hyaloclastite and radiating columns suggest that some flows erupted below the Yukon River or beneath a glacial ice cover (Fig. 55b; Jackson and Huscroft, 2023).

The assessment of the geothermal potential of Volcano Mountain included field reconnaissance, open-water surveys, infrared imagery analysis and geophysical investigations (Crandall and Sadlier-Brown, 1978; EBA Engineering Consultants Ltd., 2009a, e, f, g, 2010l). Field studies failed to identify thermal springs in the vicinity of Volcano Mountain, but thermal anomalies were delineated near Fort Selkirk and Volcano Mountain by an open-water survey and infrared imagery analysis (Fig. 54). A water sample collected near Volcano Mountain has sodium-bicarbonate–type chemistry with moderate chloride (4.33 mg/L) and elevated silicon (18.7 mg/L; EBA Engineering Consultants Ltd., 2009e). An electromagnetic survey southwest of Volcano Mountain defined a linear anomaly trending 60°N that delineates the edge of the oldest lava flow in the area (EBA Engineering Consultants Ltd., 2010l; Jackson and Huscroft, 2023).

Carmacks area

The Village of Carmacks lies near the north end of the Whitehorse trough, a Jurassic sedimentary basin filled with sandstone, shale and conglomerate of the Laberge Group (unit JLt; Fig. 56). The Laberge Group is overlain by sandstone, conglomerate and coal of the Upper Jurassic to Lower Cretaceous Tantalus Formation, and basalt of the Upper Cretaceous Carmacks Group (Yukon Geological Survey, 2022). Previous temperature measurements from shallow boreholes (<50 m) in the northern Whitehorse trough suggested that the geothermal gradient could be as much

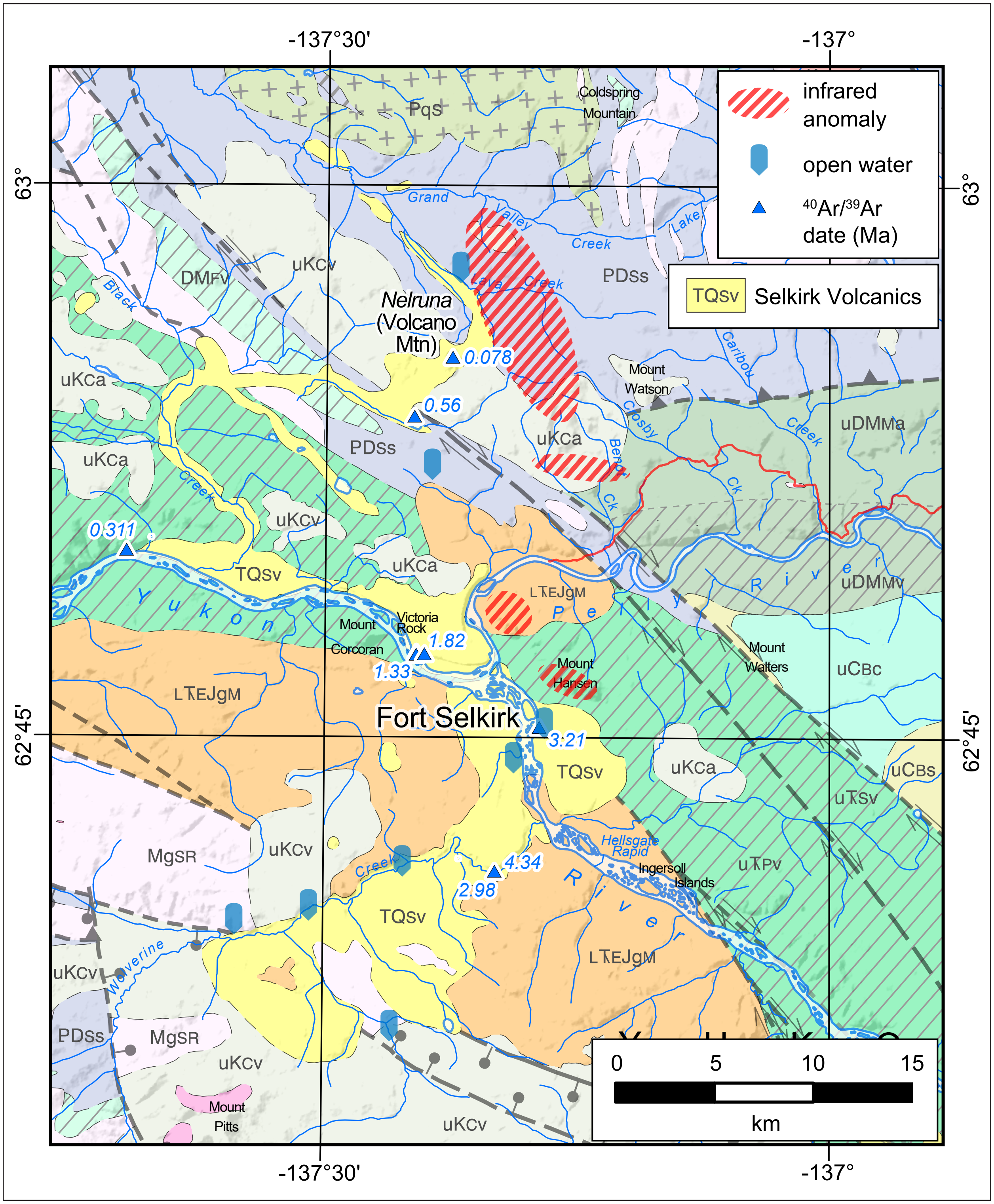

Figure 54. Geology of the Fort Selkirk area showing distribution of Pliocene–Holocene flows of the Selkirk Volcanic Group (Yukon Geological Survey, 2022). The results of open-water surveys and satellite infrared analysis are also shown. The blue triangles show the locations of flows for which radiometric dates (blue numbers) have been determined (K/Ar and $^{40}Ar/^{39}Ar$ dates from Yukon Geological Survey, 2023b).

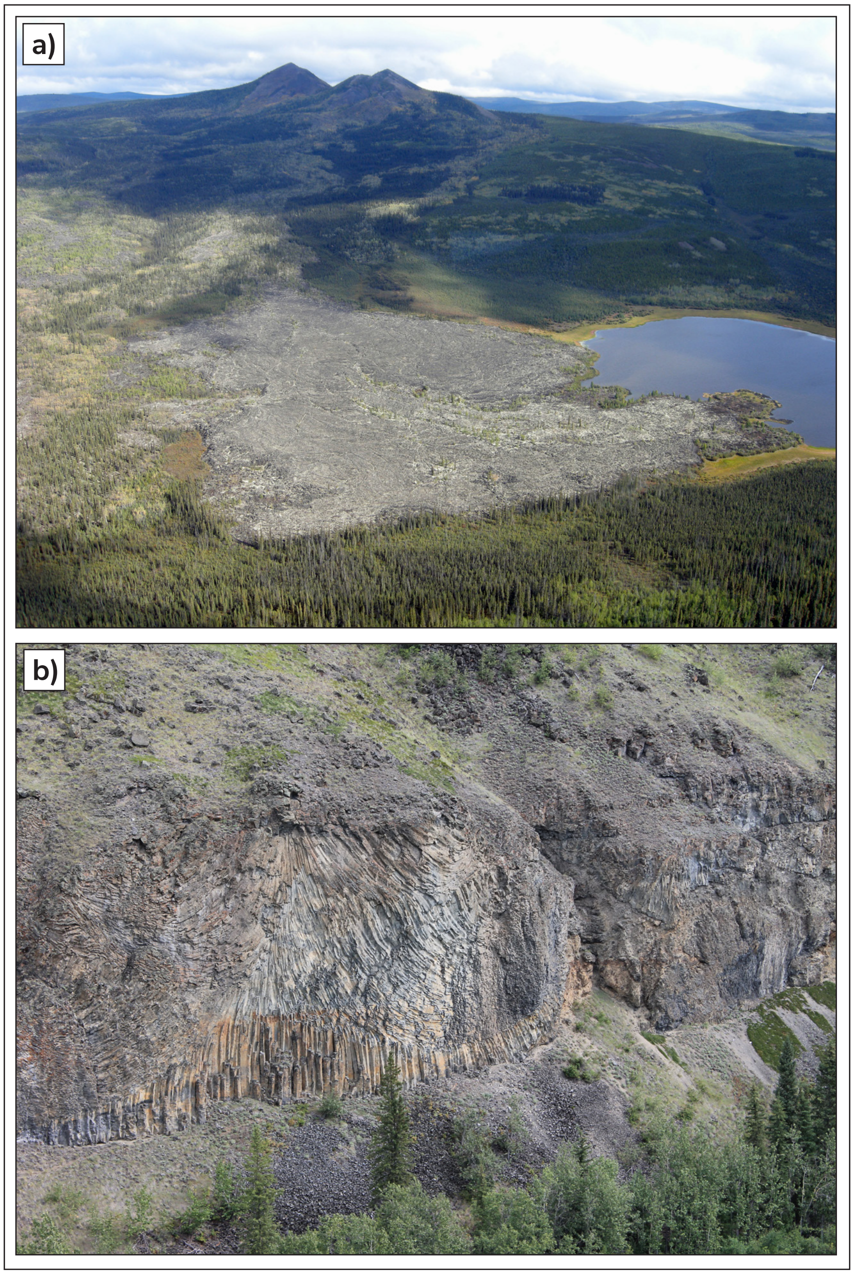

Figure 55. a) *Cinder cone and lava flow at Volcano Mountain (Nelruna).* ***b)*** *Columnar-jointed lava flows at "The Mushroom", located along the Yukon River near Fort Selkirk, Yukon.*

as 48°C/km (Burgess et al., 1982). To test this hypothesis, temperature profiles were measured in two deep boreholes in the Carmacks area (Figs. 56, 57). In 2022, Eavor Technologies Inc. drilled a 720 m thermal gradient borehole with funding from the Government of Yukon. The borehole is located in a gravel pit along the Freegold Road, approximately 6.5 km northwest of Carmacks, and encountered mainly sandstone, shale, conglomerate and coal of the Tantalus Formation and Laberge Group, and numerous clay-altered felsic dikes (Appendix D). A continuous temperature profile was measured down to 410 m before an obstruction was encountered in the borehole. The measured profile indicates a geothermal gradient of 30°C/km (Fig. 57a; Appendix C). Another temperature profile was measured down to 468 m in an existing mineral exploration borehole at the Carmacks Copper project, approximately 35 km northwest of Carmacks (Fig. 56). The Carmacks Copper borehole was drilled in granodiorite of the Granite Mountain batholith (Late Triassic–Early Jurassic Minto suite; ca. 205–195 Ma). The temperature gradient from that borehole is only 23.3°C/km (Fig. 57b, Appendix C). Samples from granitoid plutons in the Carmacks area generally yielded low radiogenic heat production values (**A** <2.5 μW/m^3) except for a single sample from a Mississippian augen granite more than 30 km west of Carmacks, which yielded an anomalous **A** value of 8.8 μW/m^3 (Fig. 56; Colpron, 2019).

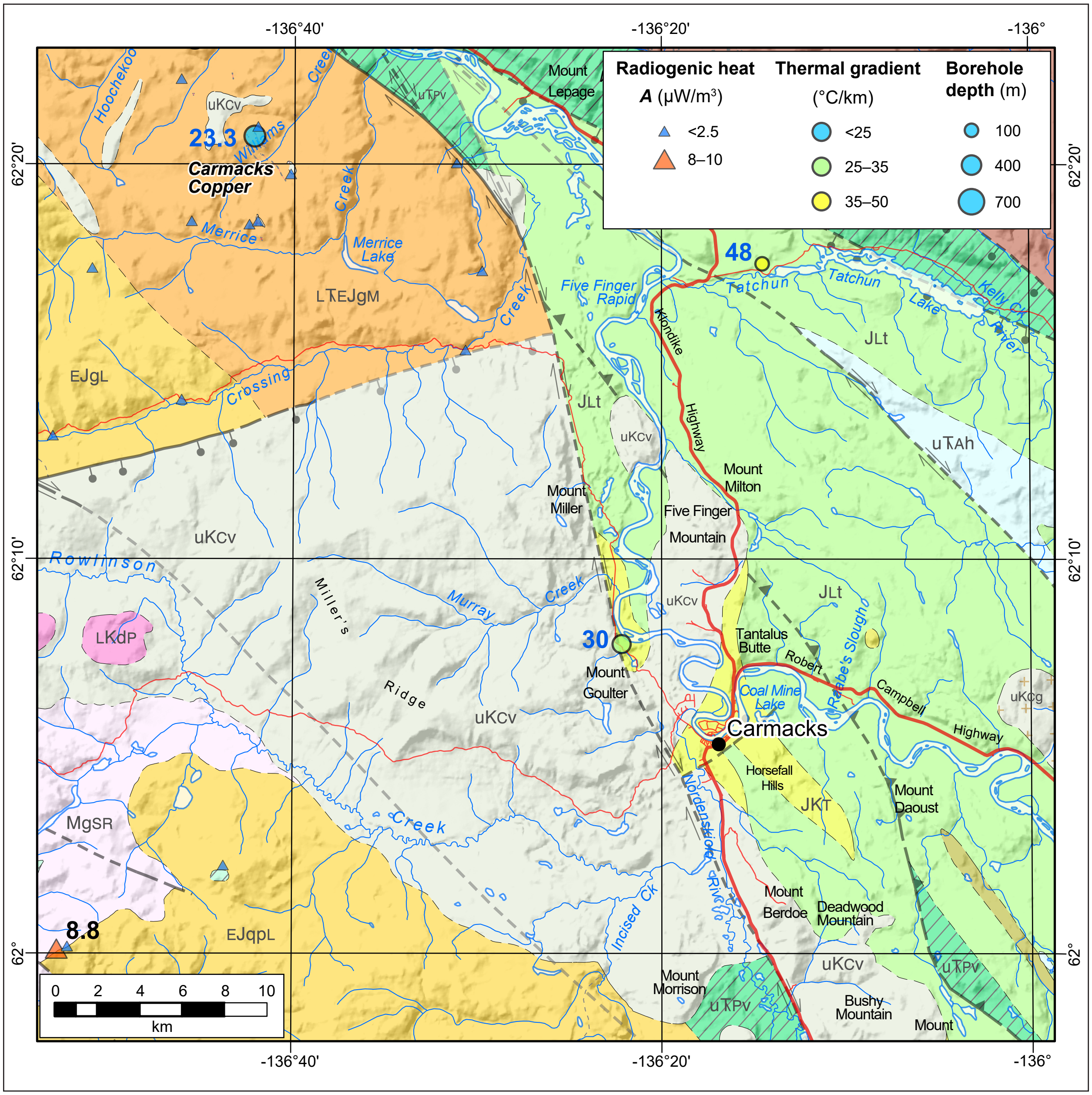

Figure 56. *Geology of the Carmacks area (Yukon Geological Survey, 2022) showing radiogenic heat values and the locations of the few boreholes in the area with temperature profiles. Thermal gradient values are shown in blue.*

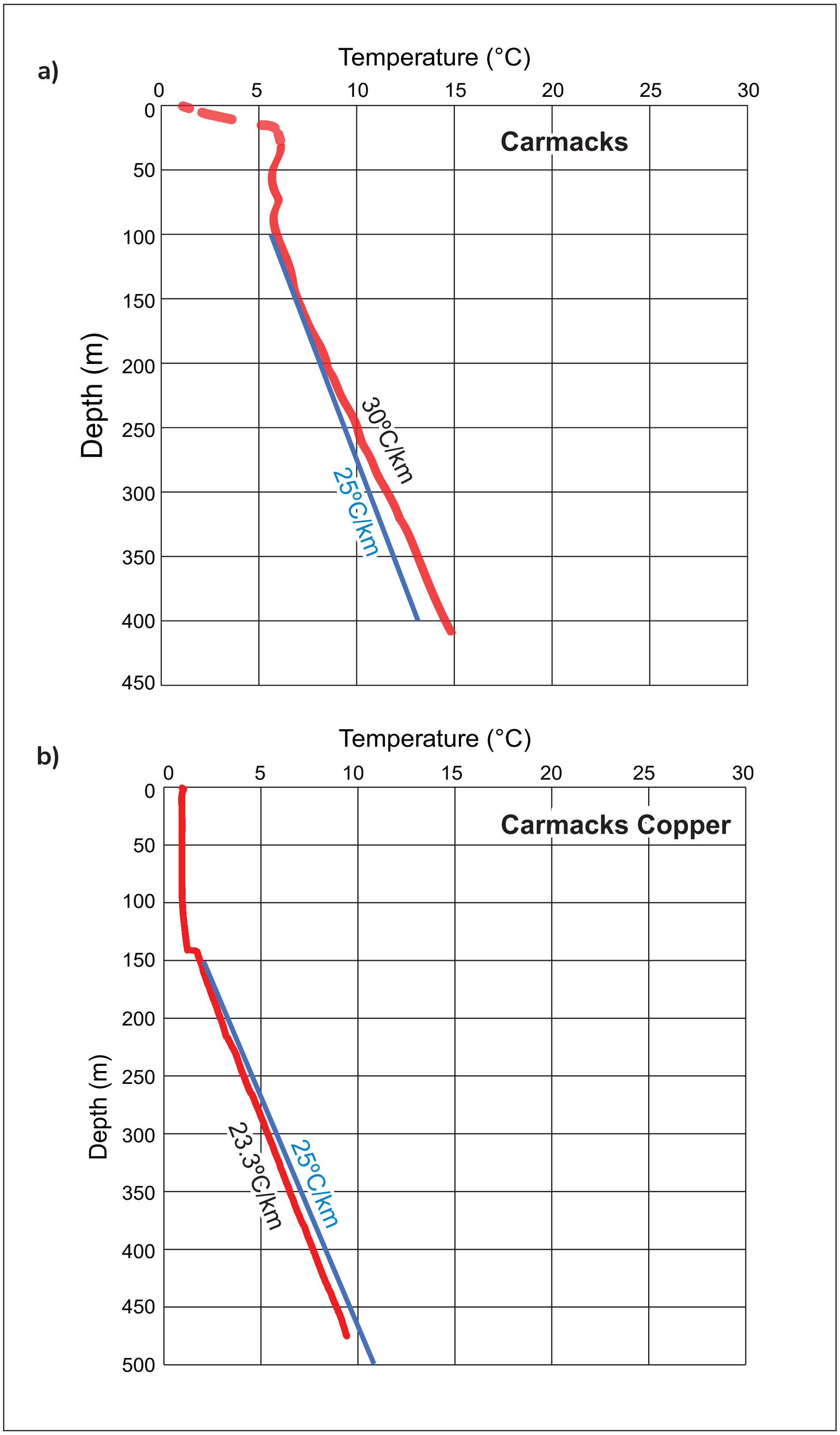

Figure 57. *Temperature profiles measured in the Carmacks area:* **a)** *Eavor Yukon borehole near Carmacks;* **b)** *Mineral exploration borehole at the Carmacks Copper project, approximately 35 km northwest of Carmacks. The blue line indicates the average geothermal gradient of 25°C/km; the red curve shows the measured temperature profile, with geothermal gradient presented in black. Data in Appendix C.*

Southwest Yukon

The Southwest Yukon region comprises the Nisling and Ruby ranges northeast of the Shakwak Trench, and the St. Elias Mountains—including the Kluane and Icefield ranges—to the southwest (Figs. 9, 58). The St. Elias Mountains host the largest non-polar icefield in the world and the highest peak in Canada, Mount Logan (5959 m elevation). The most prominent geological feature in southwest Yukon is the Denali fault, which follows the Shakwak Trench from the Alaska border to the south end of Kluane Lake (Łù'àn Mān̈), where it continues into the Kluane Ranges (Fig. 58). The Denali and related faults are the locus of seismic activity in Southwest Yukon (e.g., Colpron and Nelson, 2021; Drooff and Freymueller, 2023) and have been the focus of recent studies evaluating the geothermal potential for fault-controlled geothermal systems in the region (e.g., Witter, 2020; Tschirhart et al., 2022a). The Denali fault separates the Insular terranes (Alexander and Wrangellia) to the southwest from the Intermontane terranes (Yukon-Tanana, Kluane and Bear Creek) to the northeast (Fig. 4), and records approximately 370 to 480 km of dextral strike-slip displacement (e.g., Lowey, 1998; Waldien et al., 2021).

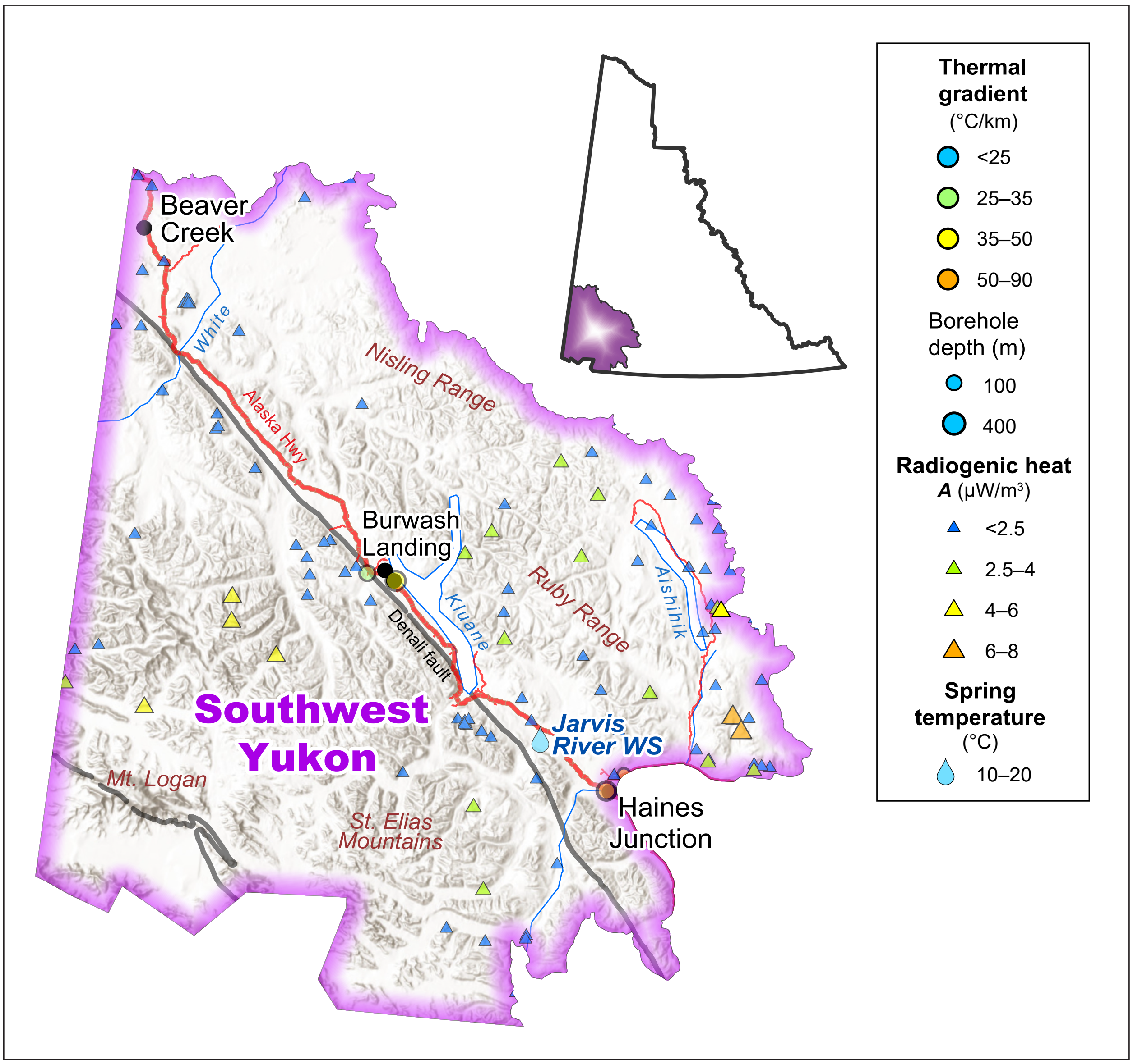

Figure 58. *Geothermal indicators in the Southwest Yukon region. WS: warm spring.*

The Southwest Yukon region includes the communities of Haines Junction (Dakwăkăda), Destruction Bay, Burwash Landing and Beaver Creek, connected by the Alaska Highway (Yukon Highway 1), which follows the Shakwak Trench from Kluane Lake (Łù'àn Mā̈n) to the White River (Fig. 58). Most of the area southwest of the Shakwak Trench is within Kluane National Park and Reserve.

The Jarvis River warm spring is the only thermal spring documented in southwest Yukon, but there are extensive areas of open water in winter and warm water has been encountered in municipal boreholes in Haines Junction (Dakwăkăda) and Burwash Landing (Figs. 4, 8, 59; EBA Engineering Consultants Ltd., 2009a). Infrared anomalies have also been identified along the Kaskawulsh and Alsek Rivers, and south of Kathleen Lakes (Mät'àtäna Mā̈n; EBA Engineering Consultants Ltd., 2009f). Southwest Yukon is characterized by relatively shallow CPDs (10–16 km), with the shallowest depths occurring near the Denali fault (Fig. 5).

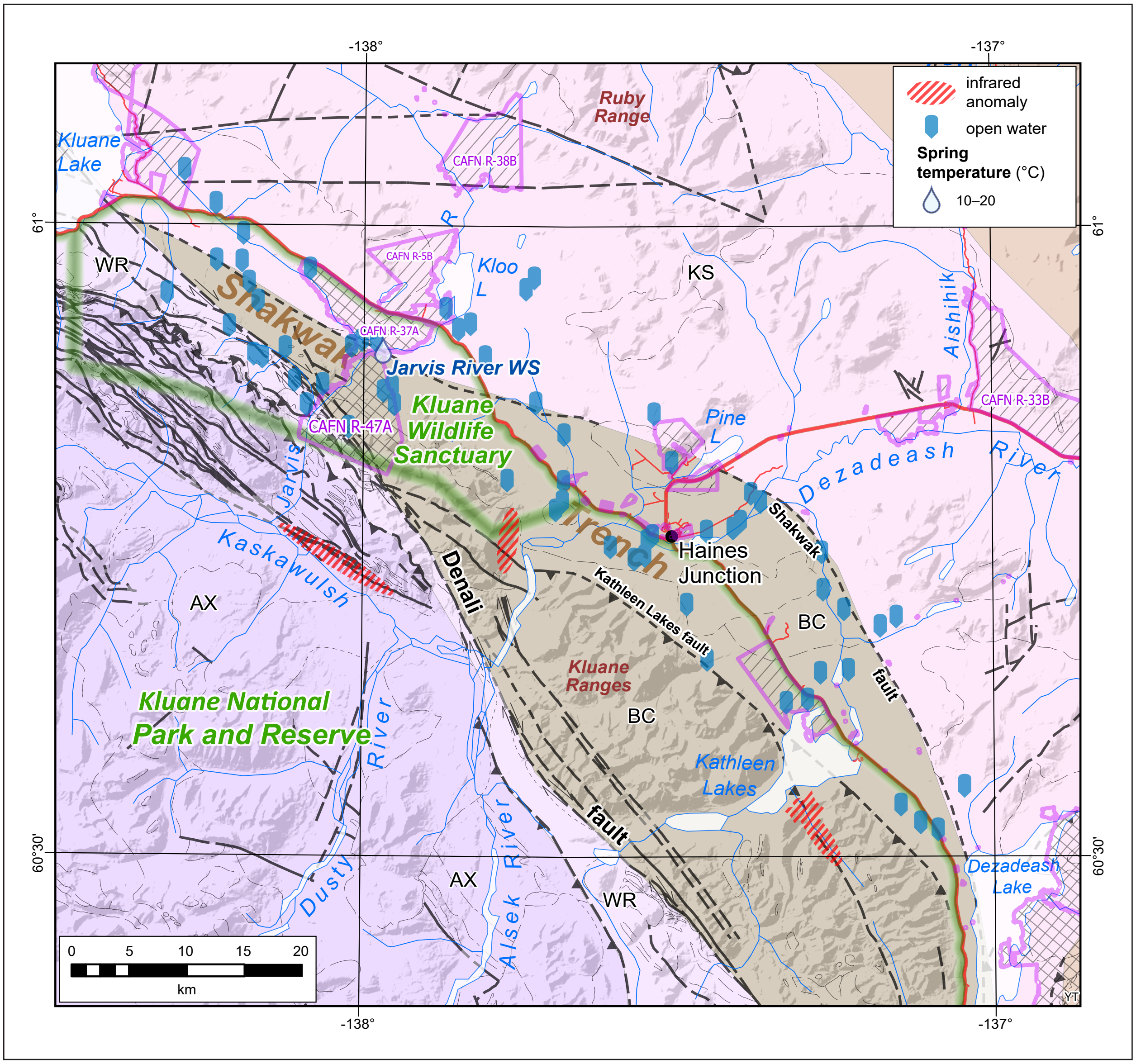

Figure 59. Simplified terrane map of the Haines Junction area showing the locations of the Jarvis River warm spring, open water areas, and infrared anomalies. Terrane map after Yukon Geological Survey (2020). First Nations Settlement Lands are indicated by cross hatched (Category A) and simple hatched areas (Category B).

Haines Junction (Dakwäkäda) area

Haines Junction (Dakwäkäda) is in the Shakwak Trench, a broad valley filled with Quaternary sediments between the Kluane Ranges to the southwest and the Ruby Range to the northeast (Figs. 58 and 59). The community is underlain by variable thicknesses of lacustrine, alluvial and fluvial sediments deposited in Glacial Lake Champagne and Neoglacial Lake Alsek (Clague and Rampton, 1982; Rampton and Paradis, 1982; Gartner Lee Limited, 2002). The bedrock geology beneath Haines Junction (Dakwäkäda) is primarily composed of greenstone and phyllite of the Upper Triassic Bear Creek assemblage (unit uTBv), gabbro and pyroxenite of the Early Cretaceous Pyroxenite Creek suite (ca. 125–113 Ma, unit EKP) to the south, and diorite of the Eocene Hayden Lake suite (ca. 48–45 Ma, unit EH, Paint Mountain pluton) to the north (Fig. 60; Yukon Geological Survey, 2022). The Bear Creek assemblage is bounded by the Denali fault to the southwest and the Shakwak fault to the northeast (Fig. 59), and locally overlain by sandstone and shale of the Upper Jurassic to Lower Cretaceous Dezadeash Formation (unit JKD, Fig. 60). The Cretaceous Kluane Schist occurs northeast of the Shakwak fault.

Geothermal indicators in the Haines Junction (Dakwäkäda) area include a relatively shallow CPD (~14 km; Fig. 5), numerous thermal anomalies (open water or infrared anomalies; Figs. 8, 58), and the occurrence of warm water in artesian boreholes in Haines Junction (Dakwäkäda; Gartner Lee Limited, 2002; EBA Engineering Consultants Ltd., 2003).

Haines Junction (Dakwäkäda) community water supply Well No. 5 is a 382 m deep, artesian borehole that produces water of approximately 16 to 20°C (Gartner Lee Limited, 2002; EBA Engineering Consultants Ltd., 2003). A temperature profile measured in the bottom 82 m of Well No. 5 showed variable geothermal gradients of approximately 40°C/km between 305 and 330 m deep and approximately 15°C/km in the lower 52 m of the borehole (Gartner Lee Limited, 2002). The Haines Junction (Dakwäkäda) boreholes have sodium-bicarbonate–type groundwater chemistry with hardness ranging from 9 to 47 mg/L (Tetra Tech, 2017). Concentrations of ^{2}H and ^{18}O indicate that the water is meteoric and the ^{3}H concentration (0.8 TU) suggests a residence time of more than 70 years (EBA Engineering Consultants Ltd., 2003, 2009a; Terzer-Wassmuth et al., 2022). Dissolved gasses are present in the deep confined aquifer of Well No. 5 and contain 97.16% N, 2.81% O and 0.03% CO_2, although the oxygen is likely from atmospheric contamination during sampling (EBA Engineering Consultants Ltd., 2013b). Temperature calculations using the silica geothermometer for undiluted water samples from Well No. 5 indicate source temperatures of 69 to 73°C (Gartner Lee Limited, 2002; Tetra Tech, 2017), whereas results for a diluted sample yielded 110.4°C (Table 2; EBA Engineering Consultants Ltd., 2009e). Calculations using the alkali geothermometers (Na-K or Na-K-Ca) yielded temperatures of 26.0 to 65.5°C (EBA Engineering Consultants Ltd., 2003, 2009e). Analysis of helium and neon isotopes from water in Well No. 5 yielded a $^{3}He/^{4}He$ ratio of 0.96 Ra and Ne/He ratio of 0.54, suggesting a long residence time and mantle helium contributions to the groundwater (Table 2, Appendix B).

To further evaluate the geothermal potential of the Haines Junction (Dakwäkäda) area, the YGS acquired gravity and MT data to support development of a 3D geological model (Fig. 60; Witter, 2024). Results of the gravity survey show that Haines Junction (Dakwäkäda) is underlain by a gravity low, suggesting that the greatest thickness of glaciolacustrine sediments occurs in this area (Fig. 61). Preliminary 3D inversion of MT data further constrains the subsurface geology beneath Haines Junction (Dakwäkäda; Fig. 62; C. Hanneson, pers. comm., 2024). Diorite of the Paint Mountain pluton (Eocene Hayden Lake suite) is strongly resistive, and the thick Quaternary sediment cover corresponds to a strong, shallow conductor in the resistivity section. Using these data, geological modelling suggests that Quaternary sediments are equal to or more than 1200 m

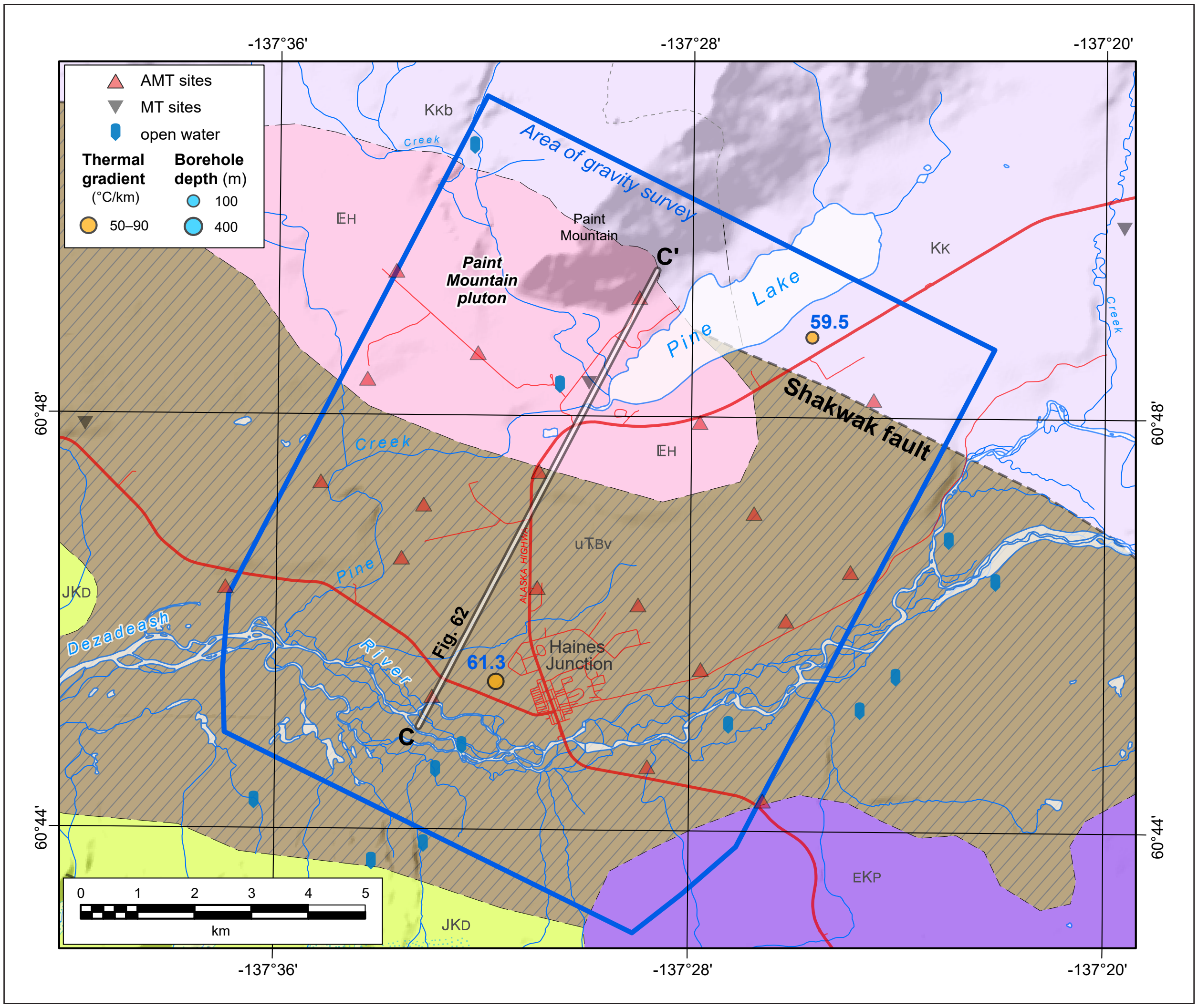

__Figure 60.__ Bedrock geology near the Village of Haines Junction (Dakwǎkǎda; after Yukon Geological Survey, 2022). The locations of magnetotelluric (MT) and audiomagnetotellurics (AMT) sites, thermal gradient boreholes, and areas of open water during winter are shown. The blue polygon indicates the area covered by the gravity survey shown in Figure 61. The location of the 3D resistivity section (C–C') shown in Figure 62 is also marked.

thick beneath the Dezadeash River near Haines Junction (Dakwǎkǎda) and that thermal waters of 39 to 74°C could be encountered near the bedrock interface at depths of 650 to 1225 m (Witter, 2024).

Jarvis River warm springs

Warm springs occur along the Jarvis River approximately 4 km south of Sulphur Lake and approximately 30 km northwest of Haines Junction (Dakwǎkǎda; Figs. 59, 63). The springs are within Category A Settlement Land of the Champagne and Aishihik First Nations and are accessed via a trail from the Alaska Highway (Yukon Highway 1). Six distinct springs have been identified, including two larger pools measuring 3 to 4 m in diameter (EBA Engineering Consultants Ltd., 2009e). The spring water temperature ranges from 8.6 to 17.9°C and produces gas bubbles. The Jarvis River warm springs occur along the fault juxtaposing the Bear Creek assemblage and the Kluane Schist (Figs. 59, 63). The fault coincides with a steep gradient in magnetic and electromagnetic data (EBA Engineering Consultants Ltd., 2010c, j, k). The warm springs emanate from the contact between Quaternary glaciolacustrine and till deposits

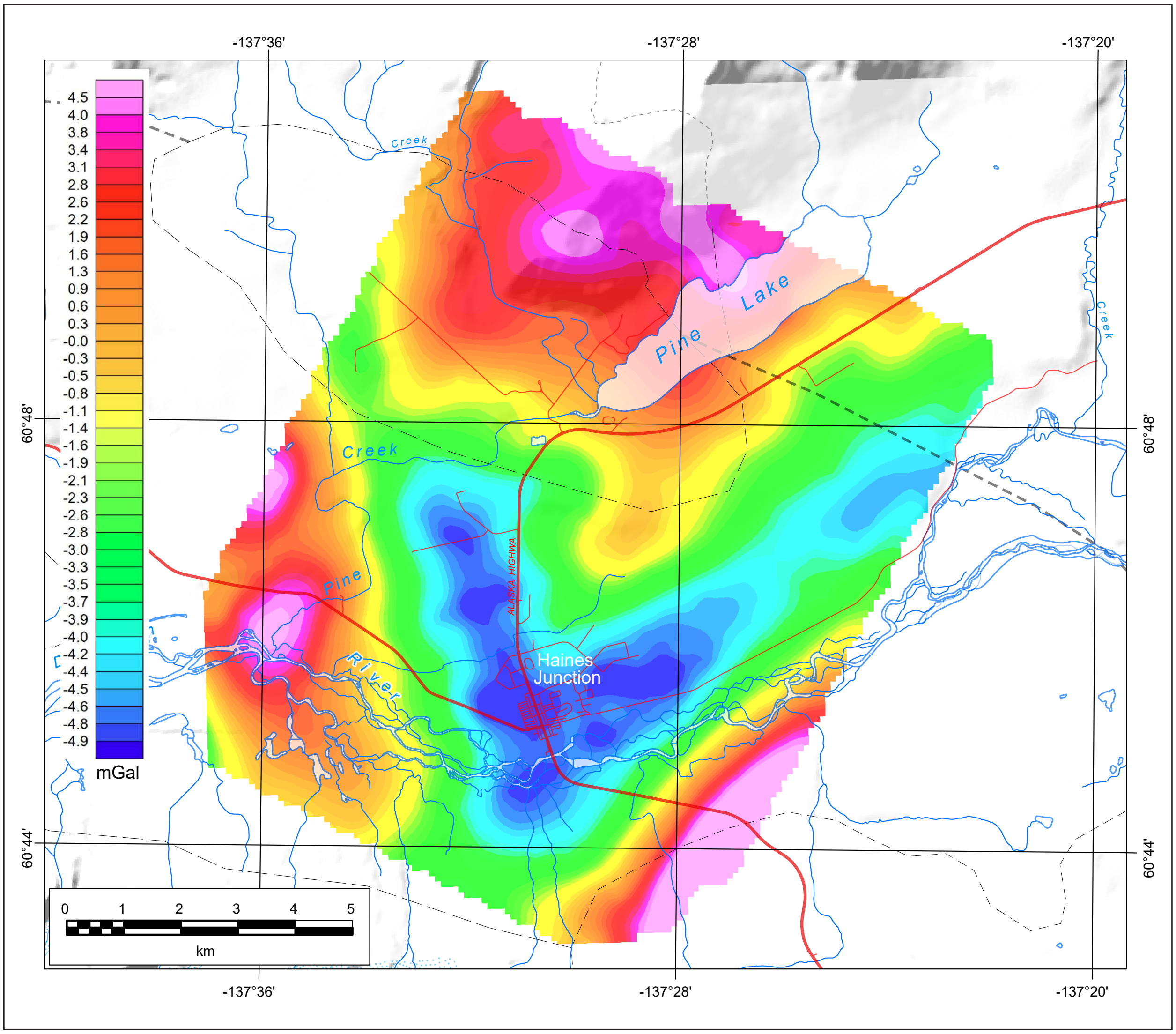

Figure 61. *Bouguer gravity anomaly map for a density of 2.67 g/cm*^{3} *with upward continued 2500 m trend removed (adapted from Witter, 2024).*

(EBA Engineering Consultants Ltd., 2009e). Test drilling at the Jarvis River site encountered a second, highly artesian aquifer (3 L/s) beneath the till at a depth of approximately 47 m (EBA Engineering Consultants Ltd., 2010d).

Water in the springs has a faint H_2S odour and is of sodium-bicarbonate and calcium-bicarbonate types with hardnesses of 66 to 95 mg/L, variable chloride concentrations (0.2–26.6 mg/L) and low fluoride (<0.5 mg/L; EBA Engineering Consultants Ltd., 2009c, h, 2010i, j). Analysis for gas composition indicated the presence of nitrogen and helium with low CO_2, low O_2 and trace CH_4 in one sample (EBA Engineering Consultants Ltd., 2009d).

Stable isotopes (^{2}H and ^{18}O) generally indicate meteoric sources and the ^{14}C concentration suggests a minimum radiocarbon date of 30 440 ± 220 years before present (EBA Engineering Consultants Ltd., 2010e). Analysis of helium and neon isotopes yielded a ^{3}He/^{4}He ratio of 0.5 Ra and Ne/He ratio of less than 0.3, suggesting mantle helium contributions and a long residence time for the groundwater (Table 2; EBA Engineering Consultants Ltd., 2010i). Geothermometer calculations for the Jarvis River warm springs indicated source temperatures of 73.0 to 110.5°C using the diluted silica geothermometer and 62.0 to 100.1°C with the alkali geothermometer (Table 2; EBA Engineering Consultants Ltd., 2009e, 2010e).

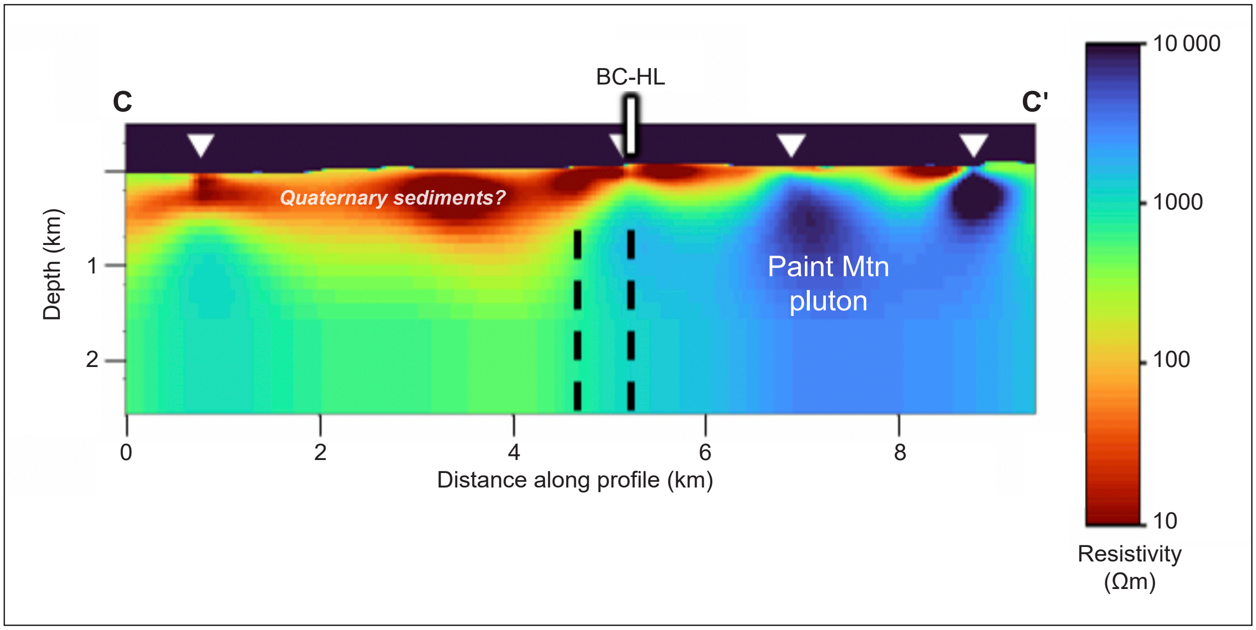

Figure 62. *Section through a 3D resistivity model based on broadband magnetotelluric data for the Haines Junction (Dakwăkăda) area (C. Hanneson, pers. comm., 2024). The location of the section is indicated on Figure 60. Note that depth is relative to the elevation at Haines Junction (Dakwăkăda; ~600 m above sea level). The strong resistivity in the northern part of the section (towards C') corresponds to the crystalline rocks of the Paint Mountain pluton (Hayden Lake suite). Strong near-surface conductivity likely reflects Quaternary sediment fill in the area. BC-HL indicates the approximate location of the contact between the Bear Creek assemblage (BC) and the Paint Mountain pluton (HL: Hayden Lake suite).*

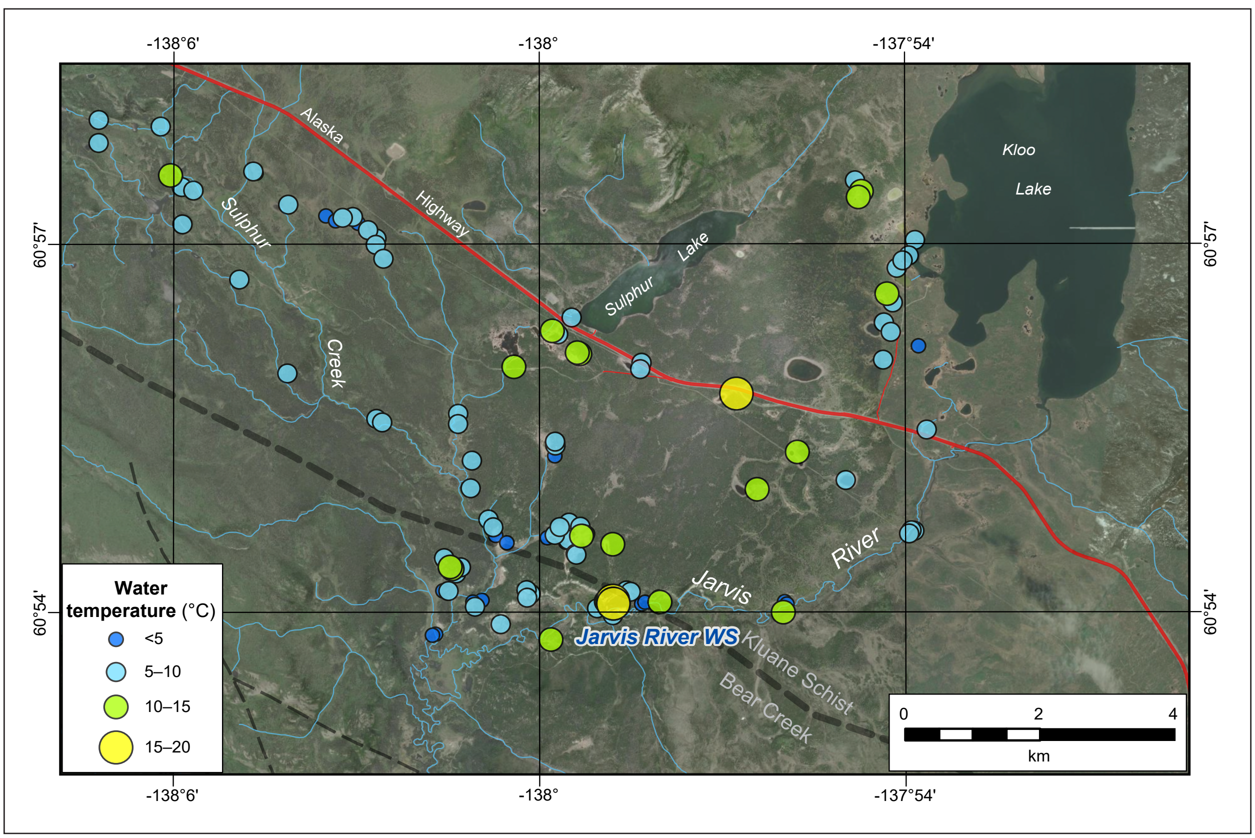

Figure 63. *Satellite imagery of the Jarvis River warm springs (WS) showing spring water temperatures measured at various locations near the Jarvis River (data from EBA Engineering Consultants Ltd., 2009e). Satellite image from ESRI World Imagery (ESRI, 2019).*

Burwash Landing area

The community of Burwash Landing, along the western shore of Kluane Lake (Łù'àn Mān̄), was subject to a range of geoscience studies aimed at evaluating the geothermal potential of the area (Figs. 58, 64). The community is approximately 4.5 km northeast of the Denali fault, characterized in this area by multiple strands that may indicate the presence of a releasing bend in the crustal-scale, dextral strike-slip fault (Bender and Haeussler, 2017; Witter, 2020). The CPD beneath Burwash Landing is approximately 14 km, suggesting a geothermal gradient of approximately 40°C/km (Fig. 5). A test borehole (KFN-L), drilled for Kluane First Nation in surficial sediments at Burwash Landing, encountered 15.9°C water at a depth of 387.4 m, indicating a geothermal gradient of approximately 41.3°C/km, which is consistent with the CPD estimate (EBA, A Tetra Tech Company, 2012a; Witter et al., 2018; Witter, 2020). To further evaluate the geothermal potential of the area, the YGS coordinated a multidisciplinary study centred on the Denali fault to assess its potential to host a shallow geothermal resource.

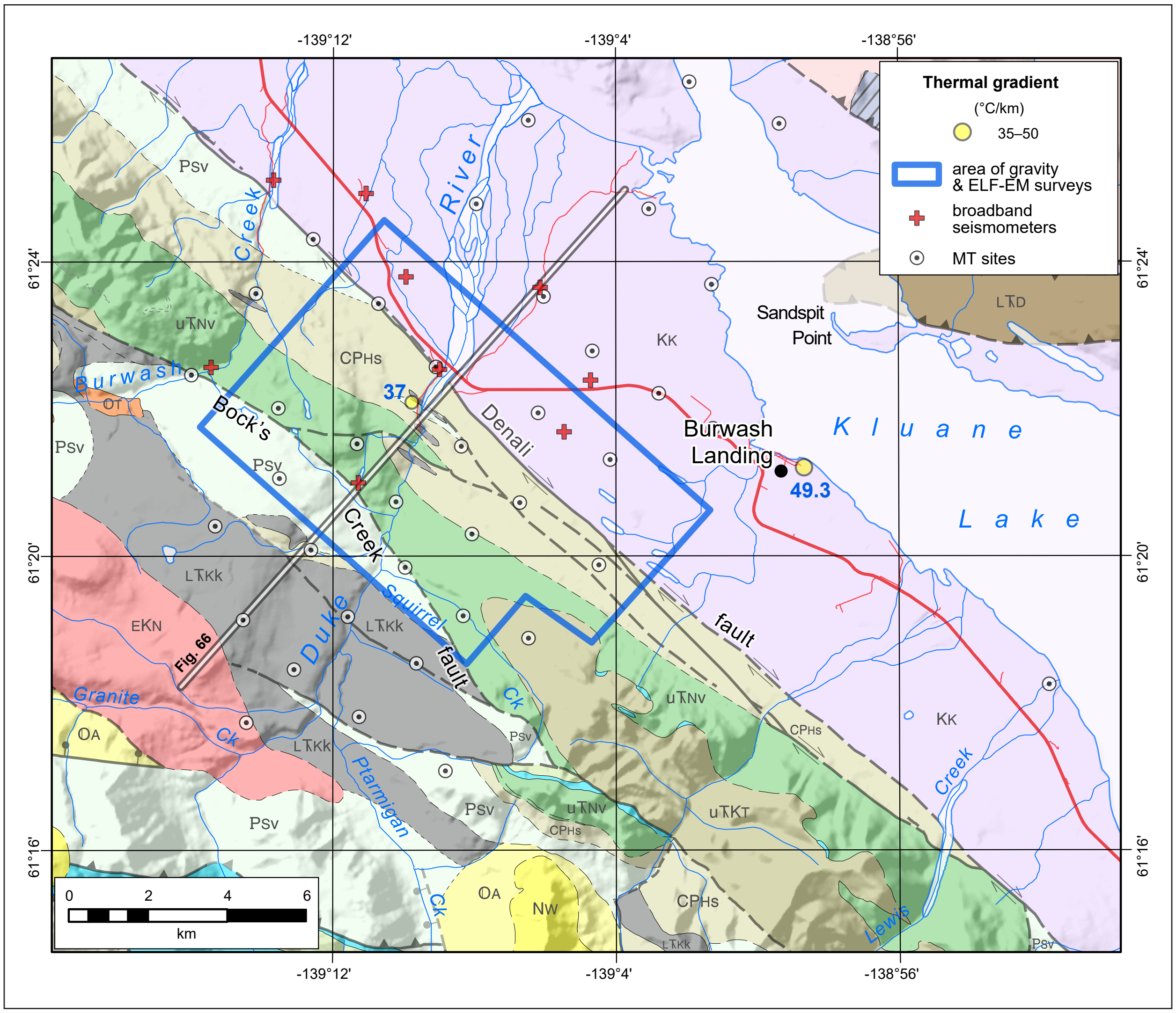

__Figure 64.__ Geology of the Burwash Landing area (Yukon Geological Survey, 2022). The area covered by gravity and extremely low frequency electromagnetic (ELF-EM) surveys (Fig. 65), magnetotelluric (MT) sites, and broadband seismometer locations are shown. The section line for the inversion profile shown in Figure 66 is also indicated.

The Denali fault juxtaposes upper Paleozoic to Triassic, low-grade metamorphic rocks of Wrangellia to the southwest (sedimentary and volcanic) against greenschist to amphibolite facies rocks of the Kluane Schist to the northeast (Fig. 64; Yukon Geological Survey, 2022). Wrangellia is intruded by Early Cretaceous (ca. 125–106 Ma) granodiorite and Oligocene (ca. 34–23 Ma) granite with low radiogenic heat potential (Fig. 6; Colpron, 2019) and is unconformably overlain by Oligocene clastic sedimentary rocks of the Amphitheatre Formation and bimodal volcanic rocks of the Neogene Wrangell lavas. Near Burwash Landing, the Denali fault occurs along the southwestern edge of the Shakwak Trench, which is filled with thick Quaternary deposits (Kennedy, 2013). Although few earthquakes have been documented along this segment of the fault (Biegel et al., 2023), air photo and lidar analyses show fault ruptures in Holocene sediments (Bender and Haeussler, 2017; Blais-Stevens et al., 2020; Finley et al., 2022).

Geological modelling across the Denali fault zone centred on Duke River (Shắr Ndü Chù) and integrated aeromagnetic data (Coyle and Oneschuk, 2015; Oneschuk et al., 2019) with ground gravity and ELF-EM data (Witter, 2020). A right-hand deflection near Duke River is evident in all geophysical data (Fig. 65), consistent with the interpretation of a releasing bend in the Denali fault zone in this region. Resistivity profiles of the ELF-EM data further highlighted near-surface (<1000 m) zones of strong conductivity that could indicate alteration and/or fluid pathways (Witter,

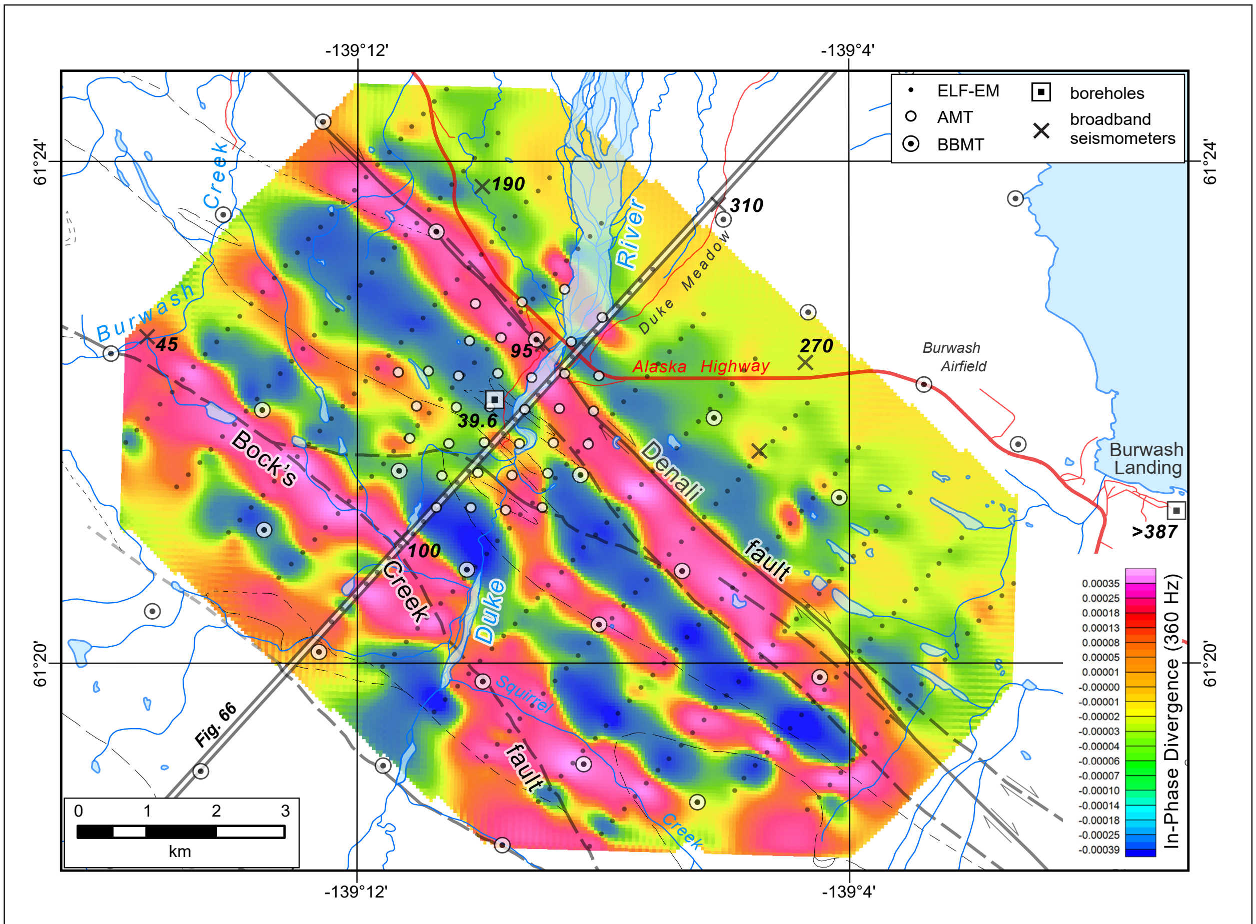

Figure 65. *Extremely low frequency electromagnetic (ELF-EM) survey for the Burwash Landing area (adapted from Witter, 2020). In-phase divergence at 360 Hz. The ELF-EM grid is shown with small grey dots; audiomagnetoteluric (AMT) sites are indicated by white circles; broadband magnetotelluric (BBMT) sites by white circles with black dot. Bold-italic numbers show bedrock depth estimates (in metres) derived from shear-wave velocity models created from broadband seismometer readings (Berumen-Borrego et al., 2024) and measured in the two boreholes.*

2020). Further investigation of the region involved deployment of AMT and BBMT instruments (Tschirhart et al., 2022b) and a range of passive seismic instruments (Figs. 64, 65). Joint 3D inversion of all electromagnetic data (ELF-EM, AMT and MT) extended the depth resolution of previous models and highlighted a series of strong conductors associated with mapped faults (C1–C3 in Fig. 66; Tschirhart et al., 2022a). Conductor C1 defines a tabular feature in the top approximately 1500 to 2000 m of the resistivity model that occurs mainly northeast of the Denali fault. This feature likely represents the presence of graphite in the Kluane Schist. Local extension of this conductive feature to near-surface southwest of the fault suggests remobilization of graphite along the fault zone (Tschirhart et al., 2022a). Conductor C2 occurs along the southwestern side of the Bock's Creek fault and extends deeper than C1, suggesting possible deep fluid migration along this fault. The modelling of shear-wave velocity from broadband horizontal-to-vertical spectral ratios provides estimates of the thickness of sediment cover in the area (~45–420 m) that are consistent with measured thickness from boreholes at Burwash Landing (>387 m) and near the Duke River (~40 m; Fig. 65; Berumen-Borrego et al., 2024).

Temperature gradient boreholes were drilled in the community of Burwash Landing (KFN-L, 387.4 m; EBA, A Tetra Tech Company, 2012a) and along the west side of the Duke River (~221 m; Figs. 64, 65; Appendix E). The KFN-L borehole was drilled entirely in Quaternary sediments of the Shakwak Trench and encountered permafrost to 48 m; a preliminary estimate of the geothermal gradient (based on three measurements) was 52°C/km (Tetra Tech EBA Inc., 2015b). A continuous temperature profile measured in 2022 yielded a more reliable geothermal gradient of 49.3°C/km (Fig. 67a). Ongoing analysis of the KFN-L borehole will determine the thermal conductivity of the Quaternary sediments and provide an estimate of heat flow at Burwash Landing (F. Chapman, pers. comm., 2023). The Duke River borehole was drilled to approximately 221 m by the YGS in the fall of 2022 (Appendix E). The borehole encountered bedrock at

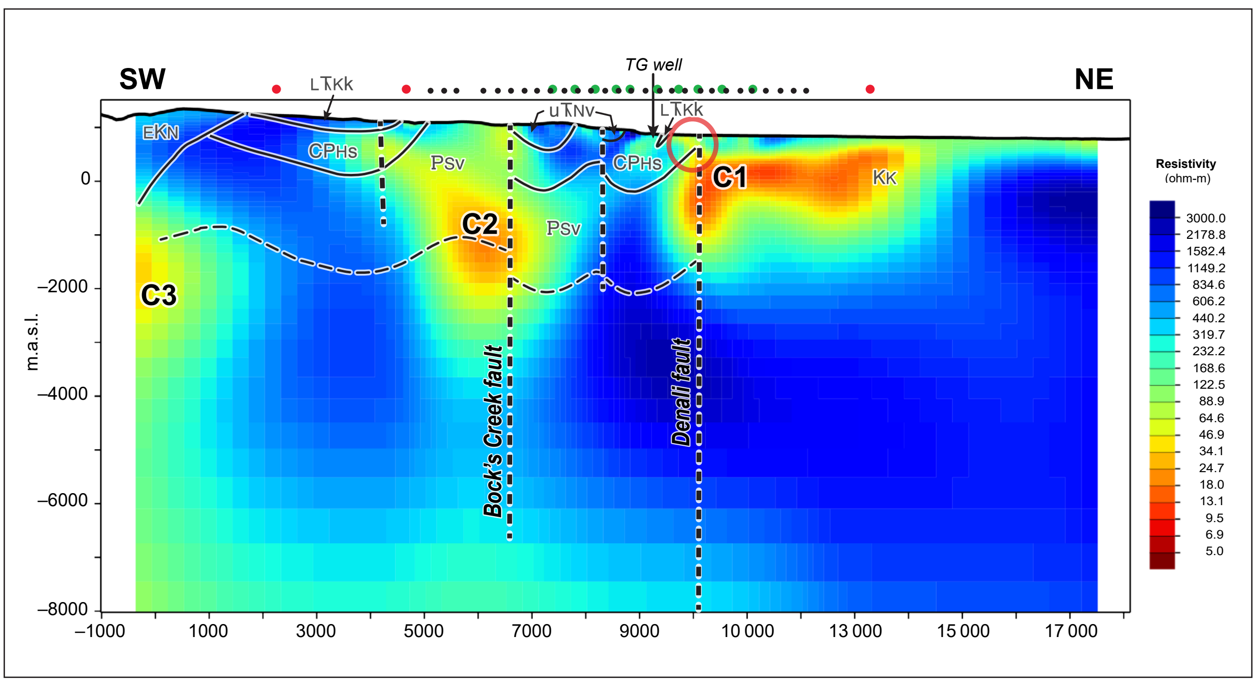

Figure 66. *Cross section through the preferred 3D resistivity model from the joint inversion of extremely low frequency electromagnetic (black dots at top of profile), audiomagnetotelluric (green dots) and broadband magnetotelluric (red dots) data (modified from Tschirhart et al., 2022a). C1–C3 are prominent conductors. The red circle highlights a thin conductor emanating from C1 and extending to the surface. A thermal gradient (TG) borehole located on the section is indicated. The location of the section is shown on Figures 64 and 65.*

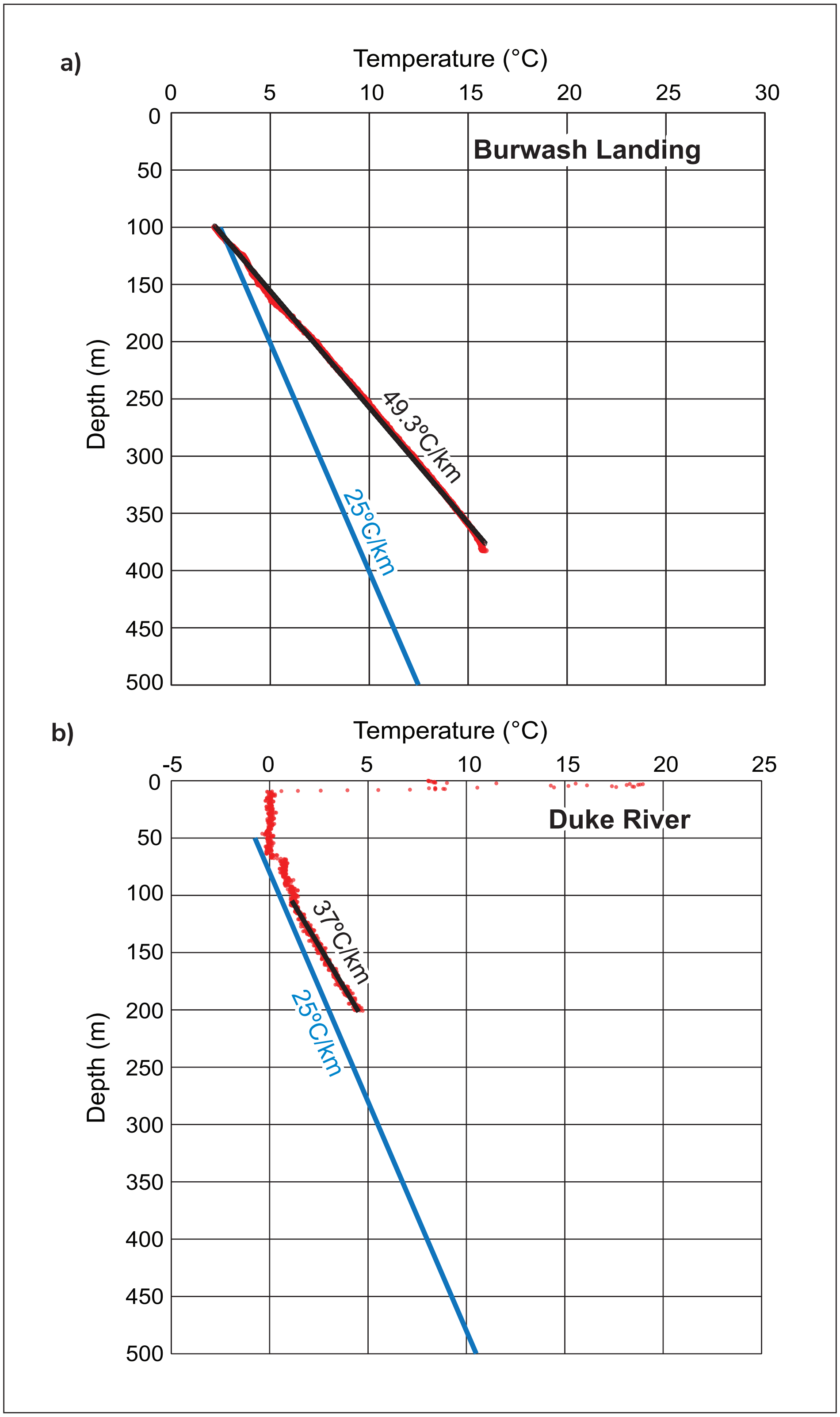

Figure 67. *Temperature profiles measured in the Burwash Landing area:* ***a)*** *Duke River borehole;* ***b)*** *KFN-L borehole at Burwash Landing. The blue line indicates the average geothermal gradient (25°C/km). The red curve shows the measured temperature profile, with the estimated geothermal gradient shown in black lines. Data in Appendix C.*

approximately 39.6 m and penetrated volcanic and volcaniclastic rocks of the Pennsylvanian Station Creek Formation (Wrangellia) to its completed depth. The borehole was instrumented with a fibre optic cable containing both distributed temperature (DTS) and distributed acoustic sensors (DAS). A DTS reading was collected approximately 6 months after borehole completion and yielded a continuous temperature profile between depths of approximately 100 and 200 m with a geothermal gradient of approximately 37°C/km (Fig. 67b). The drill report suggested that permafrost extends to a depth of 48.8 m (Appendix E). The measured temperature profile at the Duke River borehole site indicates a permafrost depth of approximately 65 m (Fig. 67b).

The KFN-L borehole is artesian, with a flow of 0.3 L/s. The groundwater in the KFN-L borehole has magnesium-sodium-calcium-bicarbonate–type chemistry and is hard, with a pH of 7.50 to 8.28 and electrical conductivity of 1060 µS/cm (EBA, A Tetra Tech Company, 2012a; Tetra Tech EBA Inc., 2015b). Dissolved gasses are present in the deep, confined aquifer. Silica geothermometer calculations for groundwater from the KFN-L borehole indicate source temperatures of 73 to 108°C (Table 2). Analysis of helium and neon isotopes yielded a $^{3}He/^{4}He$ ratio of 0.58 Ra and Ne/He ratio of 0.98, suggesting mantle helium contributions and a long residence time for the groundwater (Appendix B).

Summary and conclusions

The compilation of geothermal indicators and data summarized in this report, and available from the YGS website (https://data.geology.gov.yk.ca/Compilation/42; Yukon Geological Survey, 2024), supports some general observations about the geothermal potential in the Yukon and directions for future research.

Geothermal gradients

Temperature gradients were estimated for a total of 345 boreholes in the Yukon (Fig. 68). Of these, 186 (54%) have been assigned a moderate to high confidence rating (≥6; see Appendix A; Fig. 10) and temperature measurements taken at depths greater than 300 m were only available for 86 boreholes (25%). Temperature measurements collected from boreholes at depths of less than or equal to 300 m are likely to be influenced by past and present climate, or affected by advective heat transfer in shallow aquifers. The average estimated thermal gradient for those boreholes with moderate to high confidence is 29.9°C/km. Most temperature gradient estimates greater than 30°C/km have relatively low confidence rating (Fig. 68) and reliable estimates from deep boreholes remain sparse near Yukon communities (Figs. 7, 10).

The CPD map provides a first-order estimation of regional geothermal gradients and suggests that gradients of 40 to 60°C/km may exist in southern Yukon (Fig. 5). Data from temperature gradient boreholes drilled in southern Yukon locally support the estimates from CPD mapping. Boreholes drilled near Carmacks and Ross River have measured temperature gradients of 30 to 31°C/km (Figs. 35, 57) that are in general agreement with the estimated 29 to 32°C/km derived from CPD (18–20 km, Fig. 5). The approximately 450 m borehole drilled in granitoid rocks at the Carmacks Copper deposit has a lower gradient of 23°C/km, which may reflect low thermal conductivity of granodiorite at this location (Fig. 57). In the Burwash Landing area, CPDs of 13 to 14 km suggest geothermal gradients of 41 to 45°C/km (Fig. 5). The high-precision temperature profile measured in the KFN-L borehole at Burwash Landing indicates a gradient of 49°C/km, which is in good agreement with CPD estimates (Fig. 67). The CPD for the Whitehorse area (~15 km) suggests a geothermal gradient of 39°C/km (Fig. 5), but reliable temperature measurements from deep boreholes in the area indicate gradients of less than or equal to 25°C/km (Figs. 48, 52). Here as well, deep mineral exploration boreholes were drilled in granodiorite and diorite of the Whitehorse batholith that have low thermal conductivity and low radiogenic heat production.

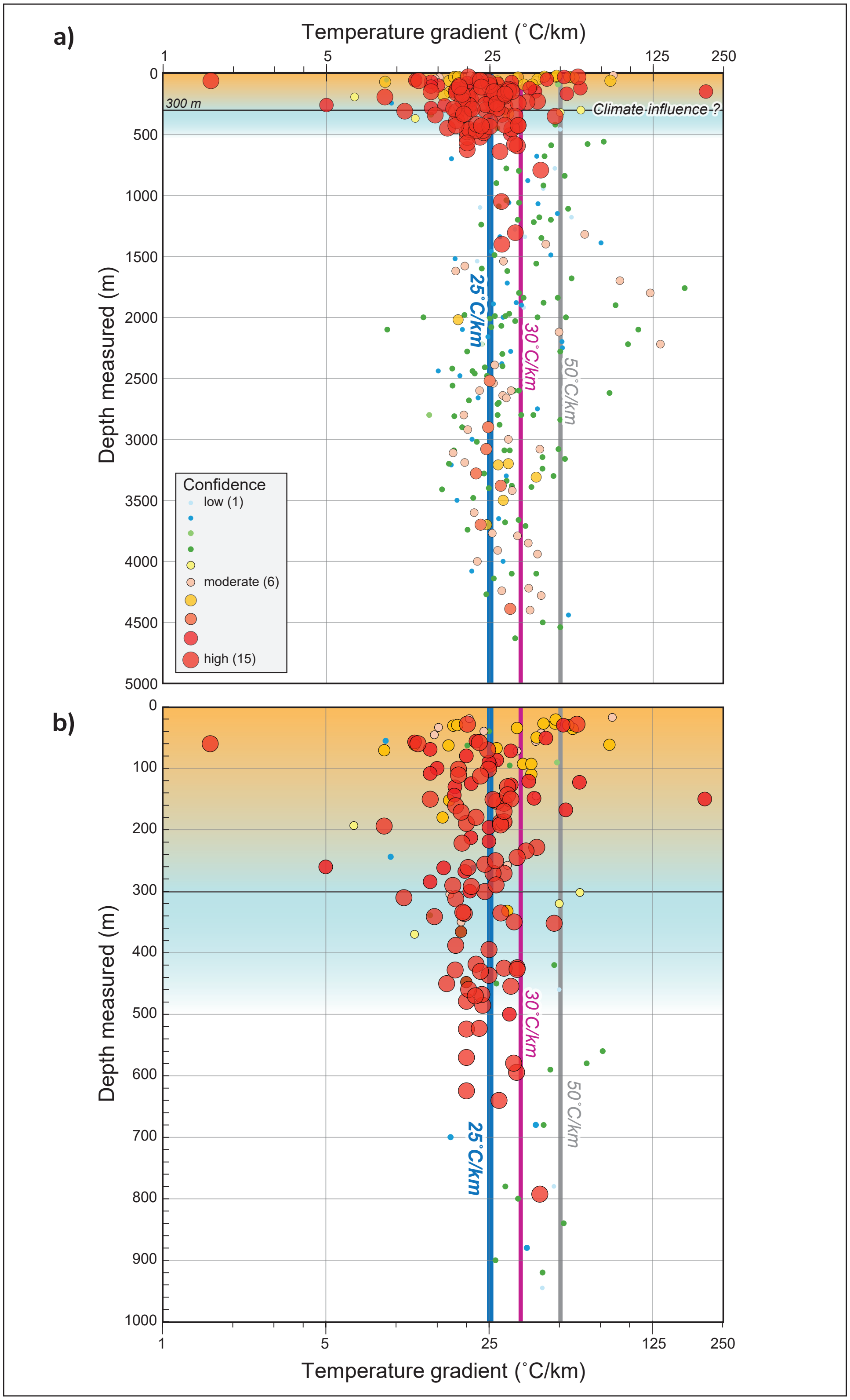

Figure 68. *Plots of the relationship between the thermal gradient (TG) and the maximum measurement depth for boreholes in the Yukon (data from Yukon Geological Survey, 2024):* ***a)*** *all TG boreholes (n = 345);* ***b)*** *TG boreholes <1000 m in depth (n = 166). Thermal gradient values are plotted on a logarithmic scale. Data points are coloured and ranked according to the confidence rating of the temperature gradient as defined in Appendix A. The shaded colour bands at the top of each plot indicate depths of potential climatic influence.*

Thermal springs

There are 21 known thermal springs in the Yukon with water temperatures ranging from 3 to 55°C (Table 2; excluding the Cantung springs, which are just east of the NWT border). Of these, seven are considered ‘hot’ springs with water temperature greater than or equal to 30°C. The hottest waters (>50°C) occur at the northern Larsen Creek and Pool Creek hot springs in Southeast Yukon, and at the McArthur hot spring along the Tintina Trench (Fig. 5). It is notable that five thermal springs (Mactung, McArthur, Partridge Creek, Crestview and Takhini) occur in proximity (≤3 km) to radiogenic granite with **A** greater than or equal to 4 μW/m^3. The waters from McArthur, Partridge Creek and Takhini hot springs contain elevated fluoride concentrations consistent with interaction of the groundwater with granitoids (the Mactung waters were not analyzed for fluoride).

Other thermal springs in the Whitehorse area may also appear to be related to radiogenic plutons. The Crestview, Stinky Lake, Versluce and Vista Mountain warm springs all occur within 4 km of Eocene plutons attributed to the same plutonic suite as the Flat Creek pluton near Takhini hot spring that yielded **A** values of 3.2 to 5.8 μW/m^3. Geochemical analyses from the Haeckel pluton near the Crestview, Stinky Lake and Versluce warm springs indicate elevated **A** values of 2.9 to 5.0 μW/m^3 (Fig. 50) that support this relationship. Water analyses from Vista Mountain yielded elevated fluoride concentrations supporting potential interaction with a granitoid; however, those of Crestview, Versluce and Stinky Lake warm springs showed low fluoride concentrations. Further geochemical analyses of granitoid plutons, particularly near Yukon communities, should be completed to further document this relationship.

Although they are farther (~10–25 km) from exposed plutons, the thermal springs in the Beaver River area of Southeast Yukon are also possibly associated with highly radiogenic syenite plutons (**A** = 5–7 μW/m^3; Figs. 6, 18). The thermal springs occur near a series of faults, including the Beaver River and Pool Creek faults, that could act as conduits for the flow of thermal waters heated by radiogenic plutons at depth.

Four Yukon thermal springs have no clear relationship to radiogenic plutons. The Caesar Lake and McPherson Lake thermal springs occur in proximity to large Cretaceous plutons (Fig. 17), but these generally have low **A** values (<3 μW/m^3); the Nash Creek springs are approximately 40 to 70 km from radiogenic plutons; and in Southwest Yukon, the Jarvis River warm spring is approximately 3 km from an Eocene diorite pluton with low **A** values (≤2 μW/m^3).

The local association of some Yukon thermal springs with radiogenic plutons raises the question of whether there might be more undiscovered thermal springs in the Yukon. The compilation of potential radiogenic heat production shows that some Yukon granitoids have strongly anomalous **A** values (Fig. 6; Colpron, 2019). Is there potential for discovery of additional springs in proximity to the highly radiogenic Seagull batholith near Swift River (Colpron et al., 2021), or plutons of the McQuesten and Tombstone suites near Mayo? Could warm waters discharge into lakes and streams, and not manifest as clear spring outlets?

Geothermometers

Source temperature estimates using the silica geothermometer show that very few thermal springs in the Yukon originated from geothermal reservoirs with temperatures sufficient for electricity generation (≥120°C; Table 2), although these data are likely underestimates of actual source temperatures. Relatively high source temperatures are only estimated at Takhini (maximum 136°C) and McArthur (maximum 164°C) hot springs. Both thermal springs are associated with radiogenic plutons. All other geothermometer calculations yielded lower source temperatures. Currently available data suggests limited opportunities for shallow (<2 km) geothermal reservoirs in the Yukon with sufficient heat for baseload power production using conventional technologies.

Helium isotopes

The helium isotopic composition of thermal waters was measured from nine thermal springs (EBA Engineering Consultants Ltd., 2010i) and two deep water boreholes in the Yukon (Table 2, Appendix B). All samples measured have $^3He/^4He$ ratios that are well above the crustal helium average of approximately 0.02 Ra, suggesting some component of mantle helium contribution to Yukon thermal waters (Fig. 69). The sparse Yukon dataset was compared to data on the well-studied Great Basin of the western United States, where average heat flow is similar to the Yukon (~75–100 mW/m^2; Lewis et al., 2003; DeAngelo et al., 2022). More than 50% of Yukon thermal springs have $^3He/^4He$ ratios greater than background levels in the Great Basin region (0.08–0.30 Ra), with values ranging from 0.50 to 2.50 Ra (Table 2, Fig. 69; Kennedy and van Soest, 2007; Siler and Kennedy, 2016). These elevated $^3He/^4He$ ratios suggest deep circulation, enhanced permeability, and high fluid-flow rates such that dilution of mantle helium by radiogenic ^4He in the crust is moderated. Elevated $^3He/^4He$ ratios in Yukon thermal waters may

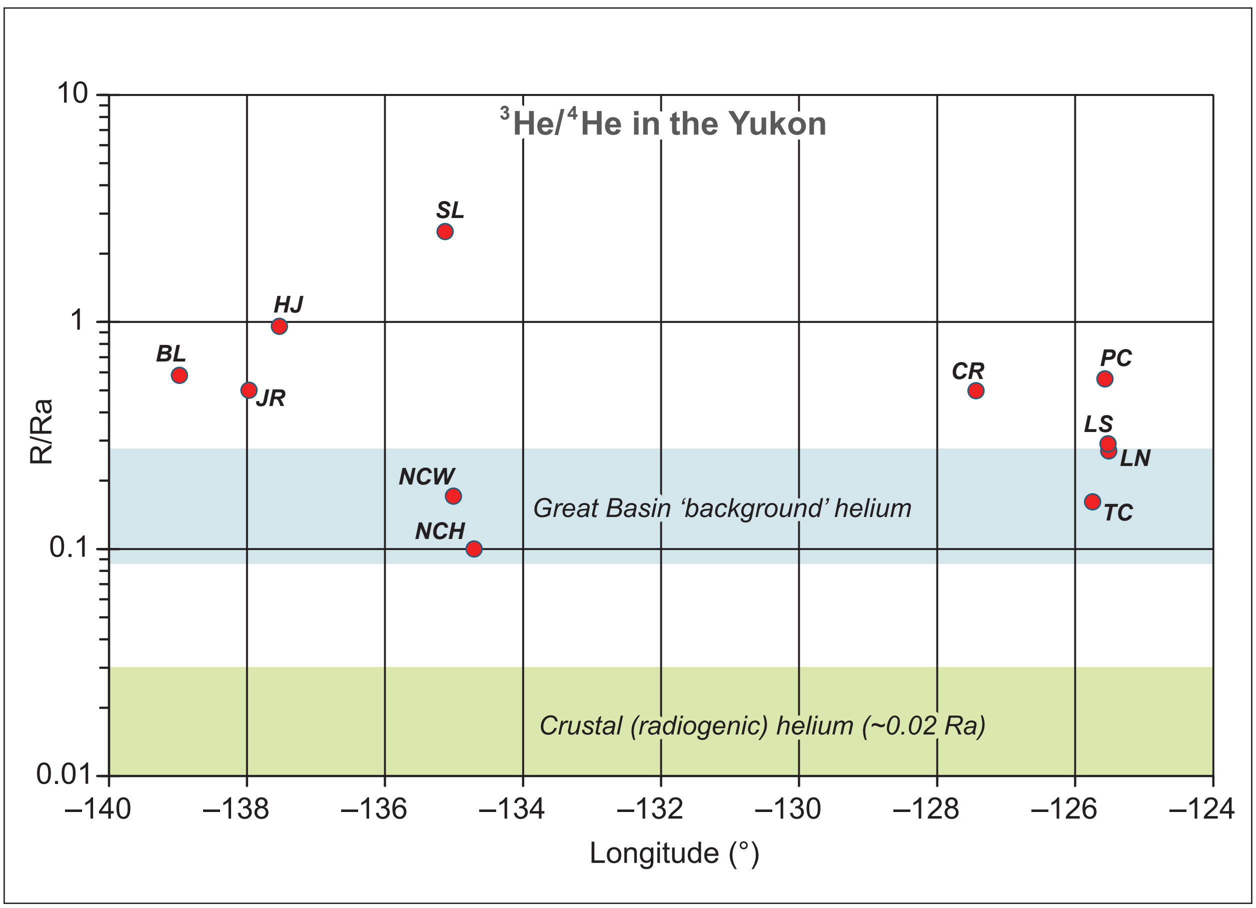

Figure 69. *Measured helium isotopic ratios of thermal springs in the Yukon. The $^3He/^4He$ ratio is plotted against the longitude of the thermal spring and compared to the background ratio for the Great Basin of the western United States (blue shading) and average crustal helium (green shading; after Kennedy and van Soest, 2007; Siler and Kennedy, 2016). Thermal springs: BL: Burwash Landing, CR: Coal River, HJ: Haines Junction, JR: Jarvis River, LN: northern Larsen Creek; LS: southern Larsen Creek, NCH: Nash Creek hot springs, NCW: Nash Creek warm spring, PC: Pool Creek, SL: Stinky Lake, TC: Thorpe Creek.*

indicate enhanced permeability along deep crustal faults in Southeast and Southwest Yukon. In Southeast Yukon, thermal springs occur in proximity to the Liard Line, a deep crustal structure that is inferred to be inherited from Neoproterozoic to lower Paleozoic development of the western Laurentian continental margin (Cecile et al., 1997; Lund, 2008; Hayward, 2015; Grasby et al., 2016). In Southwest Yukon, thermal waters with elevated $^3He/^4He$ ratios occur along the Shakwak Trench in proximity of the Denali fault (Fig. 4). The highest $^3He/^4He$ ratio was measured in the Stinky Lake spring in Whitehorse (2.50 Ra; Table 2, Fig. 69). It is notable that thermal springs in Whitehorse (Versluce, Stinky Lake, Crestview) all have elevated ^3H concentrations (5.9–11.3 TU) that may indicate some contribution of tritigenic ^3He (from decay of ^3H in atmosphere) to the elevated $^3He/^4He$ ratio measured at Stinky Lake. Geothermal systems in the Great Basin are all characterized by $^3He/^4He$ ratios that are above background (e.g., Kennedy and van Soest, 2007; Siler and Kennedy, 2016). Further analysis of groundwater for helium isotopes should be conducted to define the Yukon background $^3He/^4He$ ratio and refine potential geothermal targets.

Geological modelling

The development of 3D geological models that integrate geological mapping with a range of geophysical methods provides a powerful tool to identify potential areas of permeability and conductivity beneath Yukon communities. These models help define potential drill targets for future geothermal exploration. To date, 3D geological models have been constructed for the Tintina Trench near Ross River (Mira Geoscience, 2017) and Watson Lake (Witter, 2022), the Denali fault near Burwash Landing (Witter, 2020), and the villages of Teslin (Witter, 2023) and Haines Junction (Dakwǟkǟda; Witter, 2024). Geological models for Ross River, Watson Lake, Teslin and Burwash Landing helped refine fault mapping in the top few kilometres of the Earth's crust, where fracture-controlled permeability might allow the flow of deep geothermal fluids to surface. Combining the structural framework with deep conductors imaged by BBMT data provides further targets to be tested. The 3D geological models also provide depth-to-bedrock estimates that will be useful in refining hydrogeological modelling and identifying potential aquifers to be exploited by geo-exchange systems. The initial geological models will be improved as further data become available. For example, at the time of writing, passive seismic data had been collected for most study areas but had not been fully integrated into the 3D geological models.

Future research should aim to collect geophysical data to construct 3D geological models for most Yukon communities. At the time of writing (2024), geophysical data for a 3D geological model was being acquired in the Whitehorse area.

Regional geophysical studies

Between 2021 and 2023, the Geological Survey of Canada and the YGS collaborated to complete regional BBMT surveys across southern Yukon (Fig. 70). These surveys provide crustal-scale context for the detailed geophysical surveys of Yukon communities summarized in this report. Preliminary interpretations for parts of the new MT data are presented in Figures 49, 53 and 62 (C. Hanneson, pers. comm., 2024); however, much of the data are still awaiting interpretation. Similarly, a network of broadband seismometers was deployed across southern Yukon between 2021 and 2024 (Fig. 71) but data analysis had yet to begin at time of publication. These regional geophysical datasets will certainly provide new insights on crustal structures in southern Yukon and point to future geothermal exploration targets.

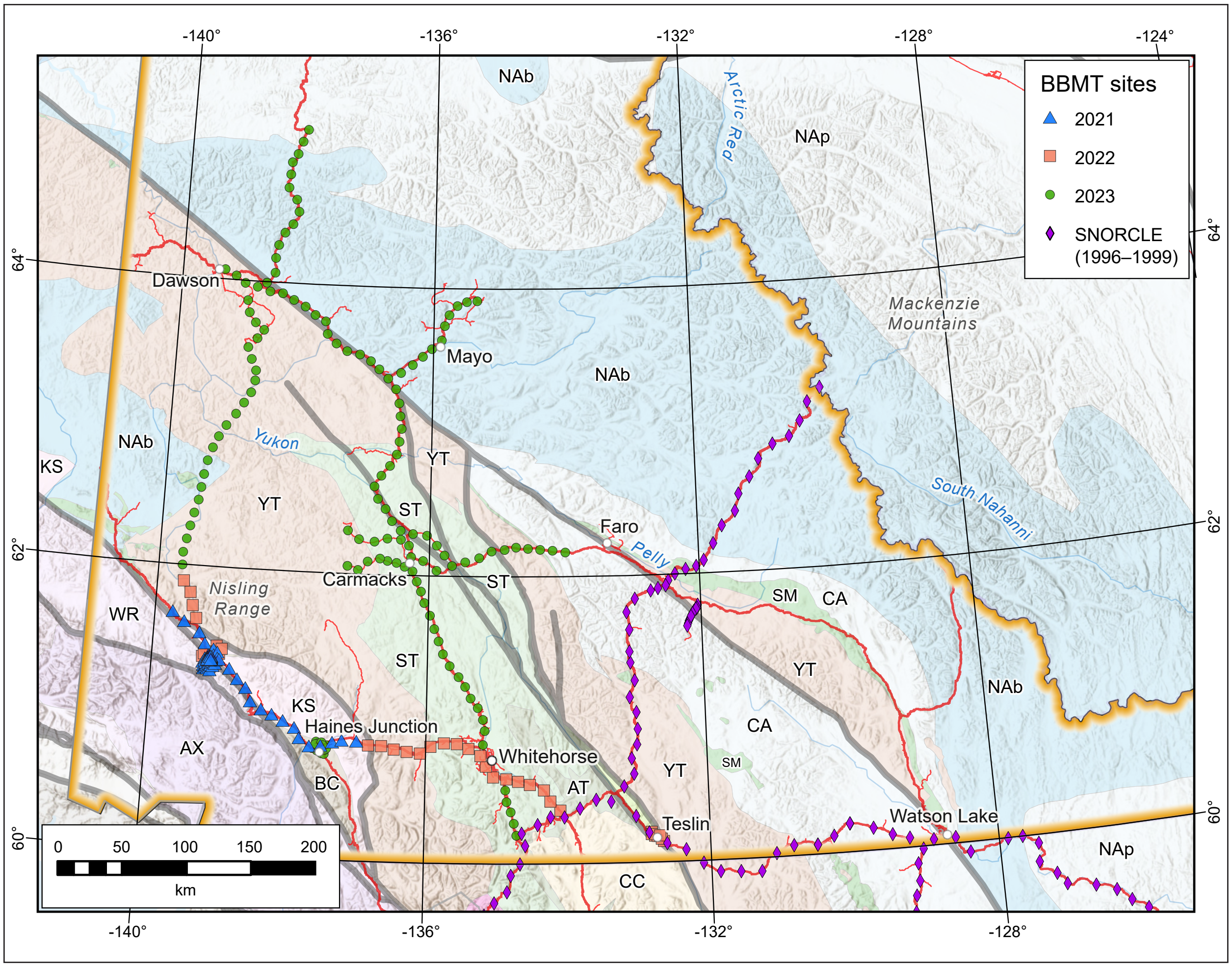

Figure 70. *Regional magnetotelluric (MT) surveys acquired by the Geological Survey of Canada (GSC) and Yukon Geological Survey (YGS) between 2021 and 2023. Previous MT data from the SNORCLE lithoprobe transect are also shown (Jones et al., 2005). BBMT: broadband magnetotelluric*

Geothermal opportunities in the Yukon

The available geothermal indicators suggest there are limited opportunities for locating geothermal reservoirs with sufficient temperature (≥120°C) to produce baseload electricity within approximately 2 km of the surface in the Yukon. Lower temperature (~80–120°C) geothermal reservoirs may exist and could be developed using a binary system; however, these systems usually have higher development costs and modest outputs compared to conventional systems. Other types of engineered geothermal systems (e.g., closed loop) may also be feasible but will require deep drilling to achieve adequate temperatures. It is not the purpose of this report to discuss the range of possible technologies for either power generation or direct-use applications; however, the existing data indicate that a range of direct-use geothermal applications may be feasible near Yukon communities. These could include shallow geo-exchange systems for specific buildings; heat sources for greenhouses, aquaculture and spas; and potentially district heating. The development of 3D geological models provides some constraints to explore these various possibilities beneath Yukon communities. Ultimately, the drilling of deep boreholes is required to provide direct evaluation of geothermal potential.

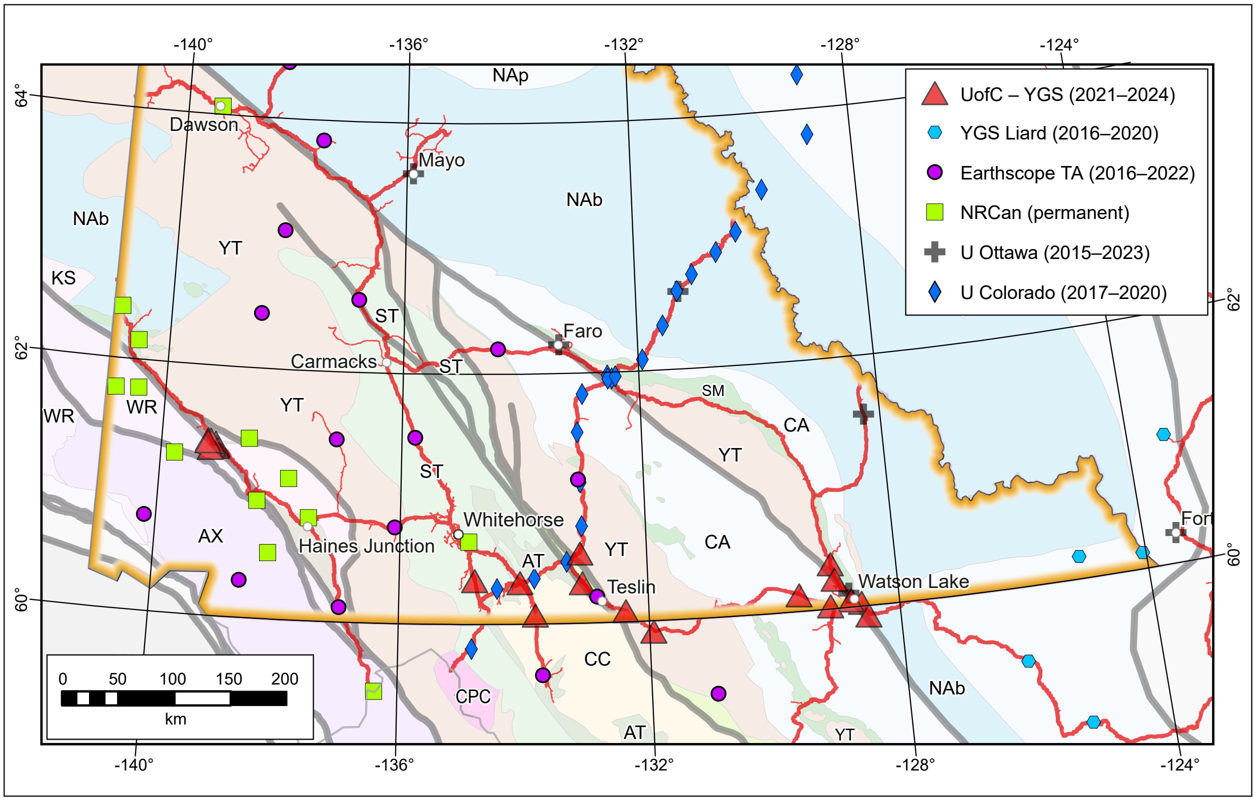

Figure 71. *Broadband seismometer networks in southern Yukon. Instruments installed by University of Calgary (UofC) and Yukon Geological Survey (YGS; red triangles) were specifically deployed to support the study of fault-controlled geothermal systems in southern Yukon.*

Acknowledgments

We thank the following organizations for giving permission to share previously unpublished reports that contribute to our growing understanding of the geothermal potential of the Yukon: Yukon Energy Corporation, the municipalities of Haines Junction (Dakwăkăda) and Mayo, the Kluane First Nation and Eclipse Nordic Hot Springs. The Yukon Geological Survey's geothermal research program benefited from collaboration and advice from several researchers including: Jasmin Raymond and Fiona Chapman (Institut national de la recherche scientifique, INRS); Steve Grasby, Jim Craven and Vicki Tschirhart (Geological Survey of Canada); Jeff Witter (Innovate Geothermal); Jan Dettmer, Hersh Gilbert and Jeremy Gosselin (University of Calgary); Theron Finley (University of Victoria); and Martyn Unsworth (University of Alberta). We acknowledge collaborations with Kluane First Nation, Liard First Nation, Champagne and Aishihik First Nations, Ta'an Kwäch'än Council, Kwanlin Dün First Nation and the Ross River Dena Council and their support of geothermal research on their Traditional Territories. Thanks to Aurora Geosciences and Quantec Geoscience for collecting geophysical data for this research. Thanks also to Eavor Yukon for providing access to the Carmacks borehole and core, and for sharing temperature data collected at Carmacks Copper, Casino and North Star. Kluane Drilling provided access to the North Star borehole and core in Whitehorse. This report benefitted from reviews by Carolyn Relf and Steve Grasby. Editorial comments by Leyla Weston (YGS) and Moretta Shuert (Purple Rock Inc.) have helped clarify the text.

References

Amante, C. and Eakins, B.W., 2009. ETOPO1 1 arc-minute global relief model: procedures, data sources and analysis. NOAA Technical Memorandum: National Geophysical Data Center, National Oceanic and Atmospheric Administration. https://doi.org/10.7289/V5C8276M

Amaru, M.L., 2007. Global travel time tomography with 3-D reference models. Geologica Ultraiectina, vol. 274, 174 p.

Aurora Geosciences, 2013. Partridge Creek ELF 3D inversion. Whitehorse, Yukon. https://data.geology.gov.yk.ca/Reference/96019

Bender, A.M. and Haeussler, P.J., 2017. Eastern Denali fault surface trace map, eastern Alaska and adjacent Canada, 1978-2008. U.S. Geological Survey data release. https://doi.org/10.5066/F7T151WC

Berumen-Borrego, F., Gilbert, H., Dettmer, J., Gosselin, J.M. and Shahsavari, P., 2024. Shearwave velocities from broadband HVSR measurements for geothermal resource assessment near Burwash Landing, Yukon. *In*: Yukon Exploration and Geology 2023, L.H. Weston and Purple Rock Inc. (eds.), Yukon Geological Survey, p. 1–15. https://ygsftp.gov.yk.ca/ApexUploads/Publications/96034/YEG2023_01.pdf

Biegel, K., Gosselin, J. and Dettmer, J., 2023. Preliminary double-difference relocation earthquake catalogue for southwestern Yukon centred along the Denali fault zone. *In*: Yukon Exploration and Geology 2022, K.E. MacFarlane (ed.), Yukon Geological Survey, p. 1–18 (plus digital appendices). https://ygsftp.gov.yk.ca/publications/yeg/yeg2022/papers/1_Biegel_etal.pdf

Blais-Stevens, A., Clague, J.J., Brahney, J., Lipovsky, P.S., Haeussler, P.J. and Menounos, B., 2020. Evidence for large Holocene earthquakes along the Denali fault in southwest Yukon, Canada. Environmental & Engineering Geoscience, vol. 26, p. 149–166. https://doi.org/10.2113/EEG-2263

Brandon, L.V., 1965. Groundwater hydrology and water supply in the District of Mackenzie, Yukon Territory, and adjoining parts of British Columbia. Geological Survey of Canada, Paper 64-39, 102 p. https://doi.org/10.4095/101002

Burgess, M.M., Judge, A.S. and Taylor, A.S., 1982. Yukon ground temperature data collection 1966 to August 1981. Earth Physics Branch, Open File 82-1, 138 p. https://doi.org/10.4095/8297

Canadian Geothermal Energy Association, 2016. The Yukon geothermal opportunities and applications report. Yukon Geological Survey, miscellaneous report, 376 p. https://data.geology.gov.yk.ca/Reference/95837

Caron, M.-E., Grasby, S.E. and Ryan, M.C., 2008. Spring water trace element geochemistry: a tool for resource assessment and reconnaissance mineral exploration. Applied Geochemistry, vol. 23, p. 3561–3578. https://doi.org/10.1016/j.apgeochem.2008.07.020

Cecile, M.P., Morrow, D.W. and Williams, G.K., 1997. Early Paleozoic (Cambrian to Early Devonian) tectonic framework, Canadian Cordillera. Bulletin of Canadian Petroleum Geology, vol. 45, p. 54–74.

Clague, J.J. and Rampton, V.N., 1982. Neoglacial Lake Alsek. Canadian Journal of Earth Sciences, vol. 19, p. 94–117. https://doi.org/10.1139/e82-008

Colpron, M., 2019. Potential radiogenic heat production from granitoid plutons in Yukon. Yukon Geological Survey, Open File 2019-16, 1 map and data. https://data.geology.gov.yk.ca/Reference/95816

Colpron, M. (compiler), 2022. Yukon bedrock geology map. Yukon Geological Survey, Open File 2022-1, scale 1:1 000 000. https://data.geology.gov.yk.ca/Reference/95934

Colpron, M., Hayward, N. and Crowley, J.L., 2021. Potential heat production from the Seagull and Teslin plutonic suites, southern Yukon: geochemistry, geochronology, rock physical properties, and 3D geophysical inversion of Bouguer gravity data. *In*: Yukon Exploration and Geology 2020, K.E. MacFarlane (ed.), Yukon Geological Survey, p. 47–72. https://data.geology.gov.yk.ca/Reference/95896

Colpron, M., Israel, S. and Friend, M., 2016a. Yukon plutonic suites. Yukon Geological Survey, Open File 2016-37, scale 1:750 000. http://ygsftp.gov.yk.ca/publications/openfile/2016/OF2016-37.pdf

Colpron, M., Israel, S., Murphy, D.C., Pigage, L.C. and Moynihan, D., 2016b. Yukon bedrock geology map. Yukon Geological Survey, Open File 2016-1, scale 1:1 000 000, map and legend. https://data.geology.gov.yk.ca/Reference/69477

Colpron, M. and Nelson, J.L., 2021. Northern Cordillera: Canada and Alaska. *In*: Encyclopedia of Geology, 2nd edition, S.A. Elias and D. Alderton (eds.), Elsevier, Reference Module in Earth Systems and Environmental Sciences, p. 93–106. https://doi.org/10.1016/B978-0-12-409548-9.12502-3

Cook, F.A., Clowes, R.M., Snyder, D.B., van der Velden, A.J., Hall, K.W., Erdmer, P. and Evenchick, C.A., 2004. Precambrian crust beneath the Mesozoic northern Canadian Cordillera discovered by lithoprobe seismic reflection profiling. Tectonics, vol. 23, p.TC2010, 28 p. https://doi.org/10.1029/2002TC001412

Coyle, M. and Oneschuk, D., 2015. Kluane Lake west aeromagnetic survey, residual total magnetic field, NTS 115-G/6 and parts of NTS 115-G/5 and 7. Yukon Geological Survey, Open File 2015-17; Geological Survey of Canada, Open File 7913, scale 1:50 000. https://data.geology.gov.yk.ca/Reference/69456

Crandall, J.T. and Sadlier-Brown, T.L., 1978. Data on geothermal areas, Cordilleran Yukon, Northwest Territories, and adjacent British Columbia, Canada. Earth Physics Branch, Open File 78-1, 80 p. https://doi.org/10.4095/8331

DeAngelo, J., Burns, E.R., Gentry, E., Batir, J.F., Lindsey, C.R. and Mordensky, S.P., 2022. Heat flow maps and supporting data for the Great Basin, USA. U.S. Geological Survey, data release. https://doi.org/10.5066/P9BZPVUC

DeAngelo, J., Burns, E.R., Gentry, E., Batir, J.F., Lindsey, C.R. and Mordensky, S.P., 2023. New maps of conductive heat flow in the Great Basin, USA: separating conductive and convective influences. 48th Workshop on Geothermal Reservoir Engineering: Stanford University, California, USA, 13 p.

Drooff, C. and Freymueller, J.T., 2023. New insights into the active tectonics of the Northern Canadian Cordillera from an enhanced earthquake catalog. Journal of Geophysical Research: Solid Earth, vol. 128, p. 19. https://doi.org/10.1029/2023JB026793

EBA, A Tetra Tech Company, 2011a. Preliminary geothermal assessment, Partridge Creek warm spring, north of Stewart Crossing, Yukon. Government of Yukon, Energy, Mines and Resources, Property File Collection, YEC report W23101159.116, 48 p. https://data.geology.gov.yk.ca/Reference/96012

EBA, A Tetra Tech Company, 2011b. Subsurface temperature data from borehole measurements in Yukon. Government of Yukon, Energy, Mines and Resources, Property File Collection, YEC report W23101159.114, 22 p. https://data.geology.gov.yk.ca/Reference/96013

EBA, A Tetra Tech Company, 2011c. Geology and hydrogeochemistry of the Stinky Lake warm spring, Whitehorse, Yukon. Government of Yukon, Energy, Mines and Resources, Property File Collection, YEC report W23101159.105, 30 p. https://data.geology.gov.yk.ca/Reference/96014

EBA, A Tetra Tech Company, 2011d. Geophysical survey at Stinky Lake, Whitehorse. Government of Yukon, Energy, Mines and Resources, Property File Collection, YEC report W23101159.106, 17 p. https://data.geology.gov.yk.ca/Reference/96015

EBA, A Tetra Tech Company, 2011e. Completion report for well field development, Na-Cho Nyäk Dun First Nation geothermal system, Mayo, Yukon. First Nation of Na-Cho Nyäk Dun, report W23101373.010.

EBA, A Tetra Tech Company, 2012a. Completion report for warm water well KFN-L, Burwash Landing, Yukon. Government of Yukon, Energy, Mines and Resources, Property File Collection, YG report W23101568, 136 p. https://data.geology.gov.yk.ca/Reference/95990

EBA, A Tetra Tech Company, 2012b. Geological mapping and geochemistry, Partridge Creek warm spring, north of Stewart Crossing, Yukon. Government of Yukon, Energy, Mines and Resources, Property File Collection, YEC report W23101159.117, 61 p. https://data.geology.gov.yk.ca/Reference/96017

EBA, A Tetra Tech Company, 2012c. Summary of result: geophysics survey of the Partridge Creek warm spring, Yukon. Government of Yukon, Energy, Mines and Resources, Property File Collection, YEC report W23101159.118, 13 p. https://data.geology.gov.yk.ca/Reference/96016

EBA, A Tetra Tech Company, 2012d. Preliminary geothermal assessment, Vista Mountain warm springs, north of Whitehorse, Yukon. Government of Yukon, Energy, Mines and Resources, Property File Collection, YEC report W23101579.004, 53 p. https://data.geology.gov.yk.ca/Reference/96018

EBA, A Tetra Tech Company, 2013a. Guidance document for development of cold and warm well system, Burwash Landing, Yukon. EBA File No. W23103077-01, 104 p. https://data.geology.gov.yk.ca/Reference/95991

EBA, A Tetra Tech Company, 2013b. Well no.5 gas sampling and analysis, Haines Junction, Yukon. Government of Yukon, Energy, Mines and Resources, Property File Collection, YG report W23103074-01, 15 p. https://data.geology.gov.yk.ca/Reference/96022

EBA Engineering Consultants Ltd., 2003. Resource assessment for heat potential study, Village of Haines Junction, Yukon. Lessoway Moir and Partners, Project no. 120049, 94 p. https://emrlibrary.gov.yk.ca/energy/resource_assessment_for_heat_potential_hj.pdf

EBA Engineering Consultants Ltd., 2007. Aquifer and wellhead protection plan - Kluane First Nation community wells Burwash Landing, YT. EBA File No. W23101003, 152 p. https://data.geology.gov.yk.ca/Reference/95989

EBA Engineering Consultants Ltd., 2008a. Detailed hydrogeological assessment Mactung project, Macmillan Pass, Yukon. Yukon Environmental and Socio-economic Assessment Board, report W23101021.023, 189 p. https://yesabregistry.ca/projects/c0e36ae3-e822-4904-a496-1d119cb5387a/documents

EBA Engineering Consultants Ltd., 2008b. Groundwater temperature, geothermometer and geothermal signature assessment, City of Whitehorse, Yukon. City of Whitehorse, report W23101137, 56 p.

EBA Engineering Consultants Ltd., 2009a. Yukon geothermal exploration program – open water survey. Government of Yukon, Energy, Mines and Resources, Property File Collection, YEC report W23101159.015, 24 p. https://data.geology.gov.yk.ca/Reference/95997

EBA Engineering Consultants Ltd., 2009b. Larsen Creek/Beaver River open water survey. Government of Yukon, Energy, Mines and Resources, Property File Collection, YEC report W23101159.029, 13 p. https://data.geology.gov.yk.ca/Reference/95996

EBA Engineering Consultants Ltd., 2009c. Discovery of artesian aquifer 30 km north of Haines Junction during the geothermal exploration drill program. Government of Yukon, Energy, Mines and Resources, Property File Collection, YEC report W23101159.023, 14 p. https://data.geology.gov.yk.ca/Reference/95992

EBA Engineering Consultants Ltd., 2009d. Gas sampling, Jarvis River warm springs, Yukon. Government of Yukon, Energy, Mines and Resources, Property File Collection, YEC report W23101159.018, 20 p. https://data.geology.gov.yk.ca/Reference/95993

EBA Engineering Consultants Ltd., 2009e. Ground-based geothermal reconnaissance program, multiple areas, Yukon. Government of Yukon, Energy, Mines and Resources, Property File Collection, YEC report W23101159.008, 120 p. https://data.geology.gov.yk.ca/Reference/95994

EBA Engineering Consultants Ltd., 2009f. Yukon geothermal project – results of thermal infrared imagery analysis. Government of Yukon, Energy, Mines and Resources, Property File Collection, YEC report W23101159.012, 61 p. https://data.geology.gov.yk.ca/Reference/95999

EBA Engineering Consultants Ltd., 2009g. Yukon geothermal project – results of satellite imagery analysis. Government of Yukon, Energy, Mines and Resources, Property File Collection, YEC report W23101159.011, 30 p. https://data.geology.gov.yk.ca/Reference/95998

EBA Engineering Consultants Ltd., 2009h. Integrated geothermal assessment Takhini Hot Springs, Yukon. Government of Yukon, Energy, Mines and Resources, Property File Collection, THS report W23101139, 119 p. https://data.geology.gov.yk.ca/Reference/96026

EBA Engineering Consultants Ltd., 2009i. Hydrogeochemistry and isotope signature of Stinky Lake and Versluce warm springs in Whitehorse, Yukon. Government of Yukon, Energy, Mines and Resources, Property File Collection, YEC report W23101159.014, 28 p. https://data.geology.gov.yk.ca/Reference/95995

EBA Engineering Consultants Ltd., 2010a. Ground-based geothermal reconnaissance - Larsen Creek/Beaver River area, southeast Yukon. Government of Yukon, Energy, Mines and Resources, Property File Collection, YEC report W23101159.029, 90 p. https://data.geology.gov.yk.ca/Reference/96011

EBA Engineering Consultants Ltd., 2010b. Exploration of geothermal potential at Jarvis River warm springs - 2009 electromagnetic geophysics survey program. Government of Yukon, Energy, Mines and Resources, Property File Collection, YEC report W23101159.017, 34 p. https://data.geology.gov.yk.ca/Reference/96006

EBA Engineering Consultants Ltd., 2010c. Exploration of geothermal potential at Jarvis River warm springs - 2009 detailed geology mapping program. Government of Yukon, Energy, Mines and Resources, Property File Collection, YEC report W23101159.019, 17 p. https://data.geology.gov.yk.ca/Reference/96000

EBA Engineering Consultants Ltd., 2010d. Exploration of geothermal potential at Jarvis River warm springs - 2009 diamond drill program. Government of Yukon, Energy, Mines and Resources, Property File Collection, YEC report W23101159.023, 11 p. https://data.geology.gov.yk.ca/Reference/96005

EBA Engineering Consultants Ltd., 2010e. Advanced geochemistry, Jarvis River warm springs and Shakwak Valley area, southwest Yukon. Government of Yukon, Energy, Mines and Resources, Property File Collection, YEC report W23101159.022, 67 p. https://data.geology.gov.yk.ca/Reference/96002

EBA Engineering Consultants Ltd., 2010f. 2009 Air photograph aquisition - Jarvis River area, Yukon. EBA File No. W23103077-01. 4 p. https://data.geology.gov.yk.ca/Reference/96007

EBA Engineering Consultants Ltd., 2010g. Ground-based geothermal reconnaissance, Nash Creek hot springs, Wernecke Mountains, central Yukon. Government of Yukon, Energy, Mines and Resources, Property File Collection, YEC report W23101159.016, 54 p. https://data.geology.gov.yk.ca/Reference/96001

EBA Engineering Consultants Ltd., 2010h. Desktop study - geothermal potential in the Swift River area, Yukon and British Columbia. EBA File No. W23101159.013, 13 p. https://data.geology.gov.yk.ca/Reference/96010

EBA Engineering Consultants Ltd., 2010i. Noble gas data from multiple warm and hot springs in southern and central Yukon. Government of Yukon, Energy, Mines and Resources, Property File Collection, YEC report W23101159.022, 18 p. https://data.geology.gov.yk.ca/Reference/96003

EBA Engineering Consultants Ltd., 2010j. Summary report - 2009 geothermal exploration program - multiple areas, Yukon. Government of Yukon, Energy, Mines and Resources, Property File Collection, YEC report W23101159.031, 35 p. https://data.geology.gov.yk.ca/Reference/96008

EBA Engineering Consultants Ltd., 2010k. Yukon geothermal study – structural interpretation of regional aeromagnetic mapping. Government of Yukon, Energy, Mines and Resources, Property File Collection, YEC report W23101159.021, 19 p. https://data.geology.gov.yk.ca/Reference/96004

EBA Engineering Consultants Ltd., 2010l. Exploration of geothermal potential at Volcano Mountain - 2009 geophysics survey program. Government of Yukon, Energy, Mines and Resources, Property File Collection, YEC report W23101159.020, 11 p. https://data.geology.gov.yk.ca/Reference/96009

ESRI, 2012. Topographic (basemap), ESRI World Imagery. https://services.arcgisonline.com/ArcGIS/rest/services/World_Imagery/MapServer [accessed March 10, 2024].

ESRI, 2014. Topographic (basemap), ESRI World Imagery. https://services.arcgisonline.com/ArcGIS/rest/services/World_Imagery/MapServer [accessed March 10, 2024]

ESRI, 2015. Topographic (basemap), ESRI World Imagery. https://services.arcgisonline.com/ArcGIS/rest/services/World_Imagery/MapServer [accessed March 10, 2024.

ESRI, 2019. Topographic (basemap), ESRI World Imagery. https://services.arcgisonline.com/ArcGIS/rest/services/World_Imagery/MapServer [accessed March 10, 2024].

ESRI, 2021. Topographic (basemap), ESRI World Imagery. https://services.arcgisonline.com/ArcGIS/rest/services/World_Imagery/MapServer [accessed March 10, 2024].

Estève, C., Audet, P., Schaeffer, A.J., Schutt, D., Aster, R.C. and Cubley, J., 2020a. The upper mantle structure of Northwestern Canada from teleseismic body wave tomography. Journal of Geophysical Research: Solid Earth, vol. 125, e2019JB018837, 18 p. https://doi.org/10.1029/2019JB018837

Estève, C., Audet, P., Schaeffer, A.J., Schutt, D.L., Aster, R.C. and Cubley, J.F., 2020b. Seismic evidence for craton chiseling and displacement of lithospheric mantle by the Tintina fault in the northern Canadian Cordillera. Geology, vol. 48, p. 1120–1125. https://doi.org/10.1130/G47688.1

Ferguson, G., Grasby, S.E. and Hindle, S.R., 2009. What do aqueous geothermometers really tell us? Geofluids, vol. 9, p. 39–48. https://doi.org/10.1111/j.1468-8123.2008.00237.x

Finley, T., Salomon, G., Stephen, R., Nissen, E., Cassidy, J. and Menounos, B., 2022. Preliminary results and structural interpretations from drone lidar surveys over the Eastern Denali fault, Yukon. In: Yukon Exploration and Geology 2021, K.E. MacFarlane (ed.), Yukon Geological Survey, p. 83–105. https://data.geology.gov.yk.ca/Reference/95940

Fournier, R.O., 1979. A revised equation for the Na/K geothermometer. Geothermal Resources Council Transactions, vol. 3, p. 221–224.

Fournier, R.O. and Truesdell, A.H., 1973. An emperical Na-K-Ca geothermometer for natural waters. Geochimica et Cosmochimica Acta, vol. 37, p. 1255–1275.

Fraser, T.A., Colpron, M. and Relf, C., 2019. Evaluating geothermal potential in Yukon through temperature gradient drilling. In: Yukon Exploration and Geology 2018, K.E. MacFarlane (ed.), Yukon Geological Survey, p. 75–90. https://data.geology.gov.yk.ca/Reference/81648

Friend, M. and Colpron, M., 2017. Potential radiogenic heat production from Cretaceous and younger granitoid plutons in southern Yukon. Yukon Geological Survey, Open File 2017-60, scale 1:1 000 000. https://data.geology.gov.yk.ca/Reference/79429

Gabrielse, H., 1985. Major dextral transcurrent displacements along the northern Rocky Mountain Trench and related lineaments in north-central British Columbia. Geological Society of America Bulletin, vol. 96, p. 1–14.

Gabrielse, H., Murphy, D.C. and Mortensen, J.K., 2006. Cretaceous and Cenozoic dextral orogen-parallel displacements, magmatism and paleogeography, north-central Canadian Cordillera. In: Paleogeography of the North American Cordillera: Evidence For and Against Large-Scale Displacements, J.W. Haggart, J.W.H. Monger and R.J. Enkin (eds.), Geological Association of Canada, Special Paper 46, p. 255–276.

Gartner Lee Limited, 2002. Haines Junction Well No. 5 completion report. Village of Haines Junction, Energy Mines and Resources, Property File Collection, report GLL 22-345, 66 p. https://data.geology.gov.yk.ca/Reference/96020

Gartner Lee Limited, 2003. Vanier School ground source heat pump project – hydrogeological assessment. Energy, Mines and Resouces, Energy Solution Center, report GLL 22-292, 49 p.

Geotech Ltd., 1984. Subsurface temperature data from wells north of sixty Yukon–Northwest Territories. Earth Physics Branch, Open File 84-28, 622 p. https://doi.org/10.4095/290116

Global Heat Flow Data Assessment Group, 2024. The global heat flow database: release 2024. GFZ Data Services. https://doi.org/10.5880/fidgeo.2024.014

Grasby, S.E., Ferguson, G., Brady, A., Sharp, C., Dunfield, P. and McMechan, M.E., 2016. Deep groundwater circulation and associated methane leakage in the northern Canadian Rocky Mountains. Applied Geochemistry, vol. 68, p. 10–18. https://doi.org/10.1016/j.apgeochem.2016.03.004

Grasby, S.E., Hutcheon, I. and Krouse, H.R., 2000. The influence of water-rock interaction on the chemistry of thermal springs in western Canada. Applied Geochemistry, vol. 15, p. 439–454.

Hasterok, D., Halpin, J., Hand, M., Collins, A., Kreemer, C., Gard, M.G. and Glorie, S., 2022. New maps of global geologic provinces and tectonic plates. Earth Science Reviews, vol. 231, paper 104069. https://doi.org/10.1016/j.earscirev.2022.104069

Hasterok, D. and Webb, J., 2017. On the radiogenic heat production of igneous rocks. Geoscience Frontiers, vol. 8, p. 919–940.

Hayward, N., 2015. Geophysical investigation and reconstruction of lithospheric structure and its control on geology, structure, and mineralization in the Cordillera of northern Canada and eastern Alaska. Tectonics, vol. 34, p. 2165–2189. https://doi.org/10.1002/2015TC003871

Hydrogeological Consultants Ltd., 2011. 1990 Warm water supply well (PW2), field program results, Yukon Territory. Village of Mayo, unpublished report 10-186.00, 36 p.

Hydrogeological Consultants Ltd., 2012. Recompletion of the 1975 Mayo warm water supply well (PW1) Yukon Territory. Village of Mayo, unpublished report 10-667.00, 23 p.

International Heat Flow Commission, 2016. Heat flow, North America, 1947–2010. International Heat Flow Commission. https://earthworks.stanford.edu/catalog/stanford-ph069rs7877

Jackson, L.E., Jr. and Huscroft, C.A., 2023. Eruptive history of the Fort Selkirk area, central Yukon. Canadian Journal of Earth Sciences, vol. 60, p. 1265–1282. http://dx.doi.org/10.1139/cjes-2022-0124

Jessop, A.M., Souther, J.G., Lewis, T.J. and Judge, A.S., 1984. Geothermal measurements in northern British Columbia and southern Yukon Territory. Canadian Journal of Earth Sciences, vol. 21, p. 599–608.

Jessop, A.M., Allen, V.S., Bentkowski, W., Burgess, M., Drury, M., Judge, A.A., Lewis, T., Majorowicz, J., Mareschal, J.C. and Taylor, A.E., 2005. The Canadian geothermal data compilation. Geological Survey of Canada, Open File 4887. https://doi.org/10.4095/220364

Jones, A.G., Ledo, J., Ferguson, I.J., Farquharson, C., Garcia, X., Grant, N., McNeice, G., Roberts, B., Spratt, J., Wennberg, G., Wolynek, L. and Wu, X., 2005. The electrical resistivity structure of Archean to Tertiary lithosphere along 3200 km of SNORCLE profiles, northwestern Canada. Canadian Journal of Earth Sciences, vol. 42, p. 1257–1275. https://doi.org/10.1139/E05-080

Kalkowski, T., Dziuba, F. and Robinson, J., 2015. Staking, soil sampling, prospecting and airborne geophysics report – Seagull tin project. Yukon Energy, Mines and Resources, Assessment Report 096722, 50 p.

Kennedy, B.M. and van Soest, M.C., 2007. Flow of mantle fluids through the ductile lower crust: Helium isotope trends. Science, vol. 318, p. 1433–1436. https://doi.org/10.1126/science.1147537

Kennedy, K.E., 2011. Surficial geology of the Village of Mayo (part of NTS 105M/12), Yukon. Yukon Geological Survey, Open File 2011-3, scale 1:20 000. https://data.geology.gov.yk.ca/Reference/50309

Kennedy, K.E., 2013. Surficial geology of Burwash Landing and Destruction Bay (parts of NTS 115G/2, 6 and 7), Yukon. Yukon Geological Survey, Open File 2013-14, scale 1:20 000. https://data.geology.gov.yk.ca/Reference/68062

KGS Group, 2016. Geothermal review and site inventory. Yukon Energy Corporation, 16-1404-01, 89 p. https://yukonenergy.ca/media/site_documents/Appendix_5.10_Geothermal_Review_and_Site_Inventory_(KGS_2016).pdf

Khan, A., Umar, R. and Kahn, H.H., 2015. Significance of silica in identifying the processes affecting groundwater chemistry in parts of Kali watershed, Central Ganga Plain, India. Applied Water Science, vol. 5, p. 65–72.

Langevin, H., Fraser, T.A. and Raymond, J., 2020. Assessment of the thermo-hydraulic properties of rock samples near Takhini Hot Springs and in the Tintina fault zone, Yukon. Yukon Geological Survey, Miscellaneous Report 19, 30 p. https://data.geology.gov.yk.ca/Reference/95840

Leonard, L.J., Mazzotti, S. and Hyndman, R.D., 2008. Deformation rates estimated from earthquakes in the northern Cordillera of Canada and eastern Alaska. Journal of Geophysical Research, vol. 113, paper B08406, 18 p. https://doi.org/10.1029/2007JB005456

Léveillée-Dallaire, X. and Raymond, J., 2024. Hydrothermal modelling of Takhini Hot Springs (NTS 105D/14). *In*: Yukon Exploration and Geology 2023, L.H. Weston and Purple Rock Inc. (eds.), Yukon Geological Survey, p. 77–96. https://data.geology.gov.yk.ca/Reference/96039

Lewis, T.J., Hyndman, R.D. and Flück, P., 2003. Heat flow, heat generation, and crustal temperatures in the northern Canadian Cordillera: thermal controls of tectonics. Journal of Geophysical Research, vol. 108, paper 2316, 18 p. https://doi.org/10.1029/2002JB002090

Li, C.-F., Lu, Y. and Wang, J., 2017. A global reference model of Curie-point depths based on EMAG2. Scientific Reports, vol. 7, paper 45129. https://doi.org/10.1038/srep45129

Lowey, G.W., 1998. A new estimate of the amount of displacement on the Denali fault system based on the occurrence of carbonate megaboulders in the Dezadeash Formation (Jura-Cretaceous), Yukon, and the Nutzotin Mountains sequence (Jura-Cretaceous), Alaska. Bulletin of Canadian Petroleum Geology, vol. 46, p. 379–386.

Lund, K., 2008. Geometry of the Neoproterozoic and Paleozoic rift margin of western Laurentia: implications for mineral deposit settings. Geosphere, vol. 4, p. 429–444.

Majorowicz, J.A. and Dietrich, J.R., 1989. Comparison of the geothermal and organic maturation gradients of the central and southwestern Beaufort – Mackenzie Basin, Yukon and Northwest Territories. In: Current Research, Part G, Geological Survey of Canada, Paper 89-1G, p. 63–67.

Majorowicz, J. and Grasby, S.E., 2014. Geothermal energy for Northern Canada: Is it economical? Natural Resources Research, vol. 23, p. 159–173. https://doi.org/10.1007/s11053-013-9199-3

Majorowicz, J.A. and Morrow, D.W., 1998. Subsurface temperature and heat flow. Geological Survey of Canada, Open File 3626, 29 p. https://doi.org/10.4095/209923

Miller, M.S. and Moresi, L., 2018. Mapping the Alaskan Moho. Seismological Research Letters, vol. 89, p. 2430–2436. https://doi.org/10.1785/0220180222

Mira Geoscience, 2017. Ross River geothermal exploration project: review of the 2014 work program. Yukon Geological Survey, Miscellaneous Report 18, 141 p. https://data.geology.gov.yk.ca/Reference/79427

MLM Ground-Water Engineering Ltd., 1986. Hydrogeological testing and assessment of a warm water well, Mayo, Yukon. Renewable Energy Branch, Energy, Mines and Resources, Canada, 28 p.

Oneschuk, D., Miles, W.F., Saltus, R.W. and Hayward, N., 2019. Alaska and Yukon magnetic compilation, residual total field. Geological Survey of Canada, Open File 7862, scale 1:1 125 000. http://gdr.agg.nrcan.gc.ca/gdrdap/dap/index-eng.php?db_project=10028

Pigage, L.C., 2009. Bedrock geology of NTS 95C/5 (Pool Creek) and NTS 95D/8 map sheets, southeast Yukon. Yukon Geological Survey, Bulletin 16, 150 p. https://data.geology.gov.yk.ca/Reference/43079

Pigage, L.C. and Mortensen, J.K., 2004. Superimposed Neoproterozoic and Early Tertiary alkaline magmatism in the LaBiche River area, southeast Yukon. Bulletin of Canadian Petroleum Geology, vol. 52, p. 325–342.

Pigage, L.C., Roots, C.F. and Abbott, J.G., 2015. Regional bedrock geology for Coal River map area (NTS 105D), southeast Yukon. Yukon Geological Survey, Bulletin 17, 155 p. https://data.geology.gov.yk.ca/Reference/69467

Rampton, V.N. and Paradis, S., 1982. Surficial geology and geomorphology, Pine Lake, Yukon Territory. Geological Survey of Canada, Preliminary Map 16-1981, scale 1:100 000.

Roddick, J.A., 1967. Tintina Trench. Journal of Geology, vol. 75, p. 23–33.

Russell, J.K., Edwards, B.R., Williams-Jones, G. and Hickson, C.J., 2023. Pleistocene to Holocene volcanism in the Canadian Cordillera. Canadian Journal of Earth Sciences, vol. 60, p. 1443–1466. http://dx.doi.org/10.1139/cjes-2023-0065

Rybach, L., 1981. Geothermal systems, conductive heat flow, geothermal anomalies. In: Geothermal Systems: Principles and Case Histories, L. Rybach and L.J.P. Muffler (eds.), John Wiley & Sons, p. 3–31.

Siler, D.L. and Kennedy, B.M., 2016. Regional crustal-scale structures as conduits for deep geothermal upflow. Geothermics, vol. 59, p. 27–37. http://dx.doi.org/10.1016/j.geothermics.2015.10.007

Slobodian, E.G., 2023. Magnetotelluric Investigations of the Tintina fault zone for geothermal exploration at Watson Lake, Yukon. Unpublished M.Sc. thesis. University of Alberta, 147 p.

Stanley Associates Engineering Ltd., 1980. Warm water well #2 Haines Junction, Yukon Territory. 36 p. https://data.geology.gov.yk.ca/Reference/96021

Terzer-Wassmuth, S., Araguas-Araguas, L., Copia, L. and Wassenaar, L.I., 2022. High spatial resolution prediction of tritium (3H) in contemporary global precipitation. Scientific Reports, vol. 12, 7 p. https://doi.org/10.1038/s41598-022-14227-5

Tetra Tech, 2017. Overarching Yukon source water supply protection study - summary report. Government of Yukon, Environment, report WTR.GWTR03022-04, 264 p. https://yukon.ca/sites/yukon.ca/files/env/env-overarching-yukon-source-water-supply-protection-study-summary-report.pdf

Tetra Tech Canada Inc., 2018. Summary of water temperatore and groundwater level results at Tagish Community Centre test wells, Tagish, Yukon. EBA File No. ENW.WENW03104-01, 8 p. https://data.geology.gov.yk.ca/Reference/96025

Tetra Tech EBA Inc., 2015a. Geoexchange feasibility, Burwash Landing, Yukon. Kluane First Nation, Property File Collection, report ENVH2O03086-01, 65 p. https://data.geology.gov.yk.ca/Reference/95988

Tetra Tech EBA Inc., 2015b. 2015 Hydrogeological assessment program, Burwash Landing, Yukon. Yukon Government, Community Services, Property File Collection, report ENVH2O03136-02, 152 p. https://data.geology.gov.yk.ca/Reference/95987

Timmerman, S., Honda, M., Burnham, A.D., Amelin, Y., Woodland, S., Pearson, D.G., Jaques, A.L., Le Losq, C., Bennett, V.C., Bulanova, G.P., Smith, C.B., Harris, J.W. and Tohver, E., 2019. Primordial and recycled helium isotope signatures in the mantle transition zone. Science, vol. 365, 3 p. https://doi.org/10.1126/science.aax5293

Tschirhart, V., Colpron, M., Craven, J., Hormozzade Galati, F., Enkin, R.J. and Grasby, S.E., 2022a. Geothermal exploration in the Burwash Landing region, Canada, using three-dimensional inversion of passive electromagnetic data. Remote Sensing, vol. 14, issue 23, paper 5963. https://doi.org/10.3390/rs14235963

Tschirhart, V., Craven, J., Colpron, M. and Quantec Geoscience Ltd., 2022b. Audiomagnetotelluric and broadband magnetotelluric data for geothermal exploration in the Burwash Landing area. Yukon Geological Survey, Open File 2022-7. https://data.geology.gov.yk.ca/Reference/95963

van Everdingen, R.O., 1973a. Analytical results for samples from Takhini Hot Springs, Yukon Territory. Inland Waters Directorate, 18 p.

van Everdingen, R.O., 1973b. Report on investigation of MacArthur Hot Springs, Yukon Territory. Inland Waters Directorate, 8 p.

Verma, S.P. and Santoyo, E., 1995. New improved equations for Na/K and SiO_2 geothermometers by error propagation. International Geothermal Association, Proceedings of the World Geothermal Congress, vol. 2, p. 963–968.

Verma, S.P. and Santoyo, E., 1997. New improved equations for Na/K, Na/Li and SiO_2 geothermometers by outlier detection and rejection. Journal of Volcanology and Geothermal Research, vol. 79, p. 9–23.

Waldien, T.S., Roeske, S.M. and Benowitz, J.A., 2021. Tectonic underplating and dismemberment of the Maclaren-Kluane Schist records Late Cretaceous terrane accretion polarity and ~480 km of post-52 Ma dextral displacement on the Denali fault. Tectonics, vol. 40, issue 10, paper e2020TC006677. https://doi.org/10.1029/2020TC006677

Witter, J.B., 2020. Early-stage exploration for geothermal energy resources along the Denali fault near Duke River, Yukon. Yukon Geological Survey, Open File 2020-3, 62 p. https://data.geology.gov.yk.ca/Reference/95836

Witter, J.B., 2022. Analysis of geoscience data for geothermal exploration along the Tintina fault near Watson Lake, Yukon. Yukon Geological Survey, Open File 2022-8, 50 p. https://data.geology.gov.yk.ca/Reference/95965

Witter, J.B., 2023. Analysis of geoscience data for geothermal exploration along the Teslin fault near Teslin, Yukon. Yukon Geological Survey, Open File 2023-3, 48 p. https://data.geology.gov.yk.ca/Reference/95984

Witter, J.B., 2024. Analysis of geoscience data for geothermal exploration in the Dakwäkäda (Haines Junction) area, Yukon. Yukon Geological Survey, Open File 2024-3, 42 p. https://data.geology.gov.yk.ca/Reference/96052

Witter, J. and Miller, C., 2017. Curie point depth mapping in Yukon. Yukon Geological Survey, Open File 2017-3, 37 p. https://data.geology.gov.yk.ca/Reference/79428

Witter, J.B., Miller, C.A., Friend, M. and Colpron, M., 2018. Curie point depths and heat production in Yukon, Canada. 43rd Workshop on Geothermal Reservoir Engineering: Stanford University, California, USA, 11 p.

Woodsworth, G., 2009. Hotsprings of Western Canada, A Complete Guide (2nd edition). Gordon Soules Book Publishers Ltd., Vancouver, BC, 328 p.

Yukon Geological Survey, 2020. A digital atlas of terranes for the northern Cordillera. Yukon Geological Survey, http://data.geology.gov.yk.ca/Compilation/2 [accessed November 30, 2023].

Yukon Geological Survey, 2022. Yukon digital bedrock geology. Yukon Geological Survey, http://datatest.geology.gov.yk.ca/Compilation/3, [accessed February 5, 2024].

Yukon Geological Survey, 2023a. Yukon lithogeochemistry data set. Yukon Geological Survey, http://data.geology.gov.yk.ca/Compilation/35 [accessed November 7, 2023].

Yukon Geological Survey, 2023b. Yukon geochronology – a database of Yukon isotopic age determinations. Yukon Geological Survey, http://data.geology.gov.yk.ca/Compilation/22 [accessed December 21, 2023].

Yukon Geological Survey, 2024. Yukon geothermal dataset. Yukon Geological Survey, https://data.geology.gov.yk.ca/Compilation/42 [accessed April 12, 2024].

Appendix A – Metadata for geothermal data compilations

Background

The geothermal compilation contains data sets related to geothermal potential in the Yukon. The data included in this dataset are derived from a variety of sources including historical subsurface thermal data compilations. The compilation includes: 1) boreholes from which temperature data was collected in the Yukon and near the border in the Northwest Territories; 2) thermal springs, including water chemistry and temperature, in the Yukon and in bordering areas of British Columbia, Northwest Territories and Alaska; 3) radiogenic heat production values calculated from lithogeochemical analyses compiled by the Yukon Geological Survey (https://data.geology.gov.yk.ca/Compilation/35; Yukon Geological Survey, 2023a); 4) location of open water observed in winter; and 5) the Curie point depth map of the Yukon, calculated using global data of Li et al. (2017).

Scope

The intended audience for this document is the members of the public interested in geothermal potential in the Yukon.

Data overview

Below are the published geothermal datasets:

1. Boreholes
2. Thermal springs
3. Radiogenic heat production
4. Winter open-water survey
5. Curie point depths

Layer attributes

Boreholes	
The borehole layer represents the compilation of available data from various boreholes throughout the Yukon and near the Yukon border. This data set includes oil and gas exploration wells, mineral exploration boreholes, water supply wells, and environmental monitoring wells.	
NAME	Common or published name or identifier of the feature. Some features have different names in various publications.
LATITUDE_DD	Feature location latitude in GCS_WGS_1984.
LONGITUDE_DD	Feature location longitude in GCS_WGS_1984.
ELEVATION	Ground elevation at feature in metres above mean sea level (m asl).
LOC_SOURCE	Feature locations are derived from a variety of sources including published coordinates and published location descriptions. Where possible, locations have been verified using digital imagery from Google Earth and/or ArcMap Earth applications.
LOCATION	Refers to the community, mine, or other major infrastructure reference nearest to the feature.
PURPOSE	Purpose of the borehole or well – i.e., oil exploration, mineral exploration, water supply, environmental monitoring, etc.
STATUS	Status of boreholes and wells (i.e., in use, decommissioned, abandoned) are recorded where known.
SCREEN_INT	Screened or open interval for water wells in metres below ground surface (m bgs).
STATIC_WL	Static water level in metres below ground surface (m bgs).
CAPACITY	Well rated production capacity in litres/second (L/s).
DISCHARGE	Artesian flowing well discharge rate in litres/second (L/s).
TEMP_WATER	Water temperature from a production well measured in degrees Celsius.
DRILL_DEPTH	Maximum drilled depth of the borehole in metres below ground surface (m bgs) is the depth to which a borehole was advanced.
BROCK_DEPTH	Depth to the top of bedrock in metres below the ground surface (m bgs).
TEMP_MIN	Minimum measure temperature of a feature in degrees Celsius. Note: this does not necessarily correspond to the measured thermal gradient interval, as spikes and lows in temperature are not necessarily included in a thermal gradient calculation.
TEMP_MAX	Maximum measured temperature of a feature in degrees Celsius. Note: this does not necessarily correspond to the measured thermal gradient interval, as spikes and lows in temperature are not necessarily included in a thermal gradient calculation.
INT_TOP	Top of the measured thermal gradient interval in metres below ground surface (m bgs).
INT_BOTTOM	Bottom of the measured thermal gradient interval in metres below ground surface (m bgs).
INT_THERM	Interval over which the thermal gradient is calculated in metres.

BOTTOM_UNK	Drilled depth or well bottom is unknown.
THERM_GRAD	Thermal gradient measured in degrees Celsius per kilometre below ground surface (°C/km).
TG_CONFIDENCE	TG_Confidence is a rating of data quality confidence based on the number of temperature measurements collected and whether the bore was allowed to thermally equilibrate between drilling and data collection. Further details on the confidence rating method are discussed below.
TG_METHOD	Method of thermal measurement collection: BHT = Bottom hole temperature, collected at the bottom of a borehole after drilling. The logs in this data set are collected both directly after drilling and over the course of several months or years. SLT = Single log temperature, collected in a single log run and can be collected directly after drilling and over the course of several months and years. Single thermistor probe is lowered down the hole and allowed to equilibrate at each measured depth to collect a single measurement from that interval. DST = Drill stem test, conducted while drilling. Because these tests are done during drilling, temperature measurements will not be accurate as the well is not allowed to equilibrate. A multi thermistor probe has several nodes and is lowered down the hole, allowed to equilibrate to collect temperature measurements from multiple depths. Multi-thermistor logs can be collected directly after drilling or after well equilibration as long as the hole is open. Continuous = temperature profile collected: 1) using a high-resolution probe taking continuous temperature and pressure readings as it is lowered in the borehole; or 2) measured using a distributed temperature sensor (DTS) fibre optic cable installed in the borehole.
TG_CORRECTION	Statistical correction applied to thermal gradient for paleoclimate or topographic factors.
TG_DATE	Date refers to the date(s) on which temperature measurements or logs were collected (YYYY-MM-DD).
TG_LOG_NUM	Log numbers refer to the log identifier number for a given thermal gradient measurement in the reference file.
THERM_COND	Thermal conductivity is a measure of the thermal conductivity of the subsurface material (soil or rock) in a borehole expressed in milliwatts per metre-Kelvin (mW/mK).
HEAT_FLOW	Heat flow is a measure of how much energy is transferred through a given material (soil or rock) measured in milliwatts per metre squared (mW/m2).
HF_CORRECTION	Statistical correction applied to heat flow calculation for paleoclimate or borehole location topography.
GT_SILICA	Silica geothermometer results from measured silica or silicon concentration in water expressed in degrees Celsius. Silica geothermometer calculations used the following formula based on the updated Fournier method developed by Verma and Santoyo (1995). This method is applicable for temperatures ranging from 20°C to 210°C. $T°C = -44.119 + 0.24469 \times [SiO_2] + 79.305 \log_{10}[SiO_2]$

GT_ALKALI	Alkaline geothermometer results from measured sodium, potassium and calcium concentration expressed in degrees Celsius. Alkaline geothermometer calculations were completed using the Fournier and Truesdell (1973) formula because calcium is the dominant cation in the water chemistry where the alkali geothermometer was calculated. The formula used is below: $$T°C = \frac{1647}{\log\left(\frac{Na}{K}\right) + \beta \log\left(\sqrt{\left(\frac{Ca}{Na}\right)} + 2.06\right) + 2.47} - 273.15$$
PH	Measured potential of hydrogen in water either from laboratory testing or field measurement.
CONDUCTIVITY	Electrical conductivity measured in water expressed in micro-Siemens per centimetre (μS/cm).
HARDNESS	Water hardness expressed in mg/L.
CA_MG_L	Calcium concentration measured in water expressed in mg/L.
MG_MG_L	Magnesium concentration measured in water expressed in mg/L.
NA_MG_L	Sodium concentration measured in water expressed in mg/L.
K_MG_L	Potassium concentration measured in water expressed in mg/L.
HCO3_MG_L	Bicarbonate concentration measured in water expressed in mg/L.
SO4_MG_L	Sulphate concentration measured in water expressed in mg/L.
CO3_MG_L	Carbonate concentration measured in water expressed in mg/L.
SIO2_MG_L	Chloride concentration measured in water expressed in mg/L.
CL_MG_L	Fluoride concentration measured in water expressed in mg/L.
F_MG_L	Silica concentration either directly measured or calculated from dissolved or total silicon measured in water expressed in mg/L.
E_ISO_18O	Environmental isotopes measured in water expressed in parts per thousand for oxygen-18.
E_ISO_2H	Environmental isotopes measured in water expressed in parts per thousand for deuterium (hydrogen-2).
RAD_ISO_3H	Radio isotopes measured in water expressed as concentration of tritium (hydrogen-3) in tritium units (TU).
GAS_NOBLE	Noble gasses detected in water – refer to reference for values.
GAS_DISS	Dissolved gasses expressed in mg/K for carbon dioxide and μg/L for hydrogen sulphide.
GAS_EMITTED	Gasses emitted or off-gassed from thermal water expressed in Mole %.
REFERENCE	Reference the data was compiled from.
REF_LINK	Link to relevant reference material provided where available.
COMMENTS	Comments on feature characteristics, background data variability, and other observations.
PUBLIC	Permission given to share publicly (Yes/No).

Thermal springs	
The thermal springs layer represents a compilation of available data from thermal springs throughout the Yukon and near the Yukon border.	
NAME	Common or published name or identifier of the thermal water feature. Some features have different names in various publications. Spring names are followed by an abbreviated designation as either a hot or warm spring. The threshold for warm vs. hot is defined in this compilation as 30°C. HS = Hot spring (30°C or greater water temperature) WS = Warm Spring (10 °C to 30 °C water temperature)
LATITUDE_DD	Feature location latitude in GCS_WGS_1984.
LONGITUDE_DD	Feature location longitude in GCS_WGS_1984.
LOC_SOURCE	Feature locations are derived from a variety of sources including published coordinates and published location descriptions. Where possible, locations have been verified using digital imagery from Google Earth and/or ArcMap Earth applications.
WATER_TEMP	Spring water temperature measured in degrees Celsius. Highest measured temperatures are presented here, additional data are included in some reference reports.
DISCHARGE	Spring discharge rate measured or estimated in litres/second (L/s).
GT_SILICA	Silica geothermometer results from measured silica or silicon concentration in water expressed in degrees Celsius. Silica geothermometer calculations used the following formula based on the updated Fournier method developed by Verma and Santoyo (1995). This method is applicable for temperatures ranging from 20 °C to 210 °C. $T°C = -44.119 + 0.24469 \times [SiO_2] + 79.305 \log_{10}[SiO_2]$
GT_ALKALI	Alkalinity geothermometer results from measured sodium, potassium and calcium concentration expressed in degrees Celsius. Alkaline geothermometer calculations were completed using the Fournier and Truesdell (1973) formula because calcium is the dominant cation in the water chemistry where the alkali geothermometer was calculated. The formula used is below: $T°C = \frac{1647}{\log\left(\frac{Na}{K}\right) + \beta \log\left(\sqrt{\left(\frac{Ca}{Na}\right)} + 2.06\right) + 2.47} - 273.15$
PH	Measured potential of hydrogen in water either from laboratory testing or field measurement.
CONDUCTIVITY	Electrical conductivity measured in water expressed in micro-Siemens per centimetre (µS/cm).
HARDNESS	Water hardness expressed in mg/L.
CA_MG_L	Calcium concentration measured in water expressed in mg/L.

MG_MG_L	Magnesium concentration measured in water expressed in mg/L.
NA_MG_L	Sodium concentration measured in water expressed in mg/L.
K_MG_L	Potassium concentration measured in water expressed in mg/L.
HCO3_MG_L	Bicarbonate concentration measured in water expressed in mg/L.
SO4_MG_L	Sulphate concentration measured in water expressed in mg/L.
CO3_MG_L	Carbonate concentration measured in water expressed in mg/L.
CL_MG_L	Chloride concentration measured in water expressed in mg/L.
F_MG_L	Fluoride concentration measured in water expressed in mg/L.
SIO2_MG_L	Silica concentration either directly measured or calculated from dissolved or total silicon measured in water expressed in mg/L.
E_ISO_18O	Environmental isotopes measured in water expressed in parts per thousand for oxygen-18.
E_ISO_2H	Environmental isotopes measured in water expressed in parts per thousand for deuterium (hydrogen-2).
RAD_ISO_3H	Radio isotopes measured in water expressed as concentration of tritium (hydrogen-3) in tritium units (TU).
RAD_ISO_14C	Radiocarbon (carbon-14) expressed in percent modern carbon.
GAS_NOBLE	Noble gasses detected in water – refer to reference for values.
GAS_DISS	Dissolved gasses expressed in mg/K for carbon dioxide and µg/L for hydrogen sulphide.
GAS_EMITTED	Gasses emitted or off-gassed from thermal water expressed in Mole %.
REFERENCE	Reference the data was compiled from.
REF_LINK	Link to relevant reference material provided where available.
COMMENTS	Comments on feature characteristics, background data variability, and other observations.
PUBLIC	Permission given to share publicly (Yes/No).

Radiogenic heat production	
This dataset presents results for calculations of the potential for granitoid plutons to produce radiogenic heat. The calculations are performed using U, Th and K concentrations from whole rock geochemical data compiled from various sources in the Yukon Geological Survey lithogeochemical compilation (https://data.geology.gov.yk.ca/Compilation/35). Plutons with anomalously high potential for radiogenic heat production (>2.8 μW/m^3) may help target exploration for geothermal resources.	
SAMPLE_NUM	Sample number.
AGE	Age of pluton/sample.
P_SUITE	Plutonic suite.
BATH_PLUT	Name of the batholith or pluton the sample is derived from.
DESC	Description of sample.
LATITUDE_DD	Feature location latitude in GCS_WGS_1984.
LONGITUDE_DD	Feature location longitude in GCS_WGS_1984.
LOC_ACC	Presumed accuracy of coordinates.
COMP	Composition of sample (e.g., felsic, intermediate, mafic).
ρ_kg_m^3	Density of sample (in kg/m^3).
K_2O	Potassium oxide (%).
cTh	Concentration of thorium (ppm).
cU	Concentration of uranium (ppm).
cK	Concentration of potassium (%).
A_μW_m^3	Potential radiogenic heat production (μW/m^3).

Open water layer	
The open water layer represents the compilation of later winter open water observations including regionally focused helicopter-based open water surveys from historical exploration work and various open water observations throughout the Yukon.	
Name	Name of open water site in original publication or field ID of observation recorded in winter 2023.
Latitude	Feature location latitude in GCS_WGS_1984.
Longitude	Feature location longitude in GCS_WGS_1984.
Loc_Source	Source of data for the open-water data point (e.g., in-flight GPS uncorrected for location error, in-flight GSP corrected for location error, anecdotal description, field GPS waypoint).
Location	Regional feature where open water was observed – e.g., Shakwak Trench, Beaver River/Larsen Creek thermal area, Whitehorse area.
Priority	Priority rating for open-water sites was assigned based on the likelihood that a given open-water observation occurred due to warm groundwater ingress considering water motion and magnitude of open areas.
WB_Type	Type of water body observed to be open.
Vege_Cov	Description of vegetation cover near a given open-water location.
Vege_Type	Type of vegetation cover observed in open-water area.
Date	Date of open-water observation (YYYY-MM-DD).
Description	Description of open-water observations includes notes on appearance, size, and duration/persistence of open-water site.
Reference	Reference the data was compiled from.
Public	Permission given to share publicly (Yes/No).

Curie point depth mapping

The Curie point is the temperature at which certain materials lose their permanent magnetic properties. For magnetite, the most common magnetic mineral, the Curie temperature is 580 °C. Therefore, the Curie point depth (CPD) is the depth at which a temperature of approximately 580 °C is encountered in the Earth's crust. The calculation of Curie point is done using regional aeromagnetic survey data (e.g., Witter and Miller, 2017; Witter et al., 2018).

The CPD map for the Yukon was generated using data from Li et al. (2017). This map shows the depth to the 580 °C isotherm and can be used as a proxy for estimation of the geothermal gradient. Shallower CPD may be indicative of higher heat flow and geothermal gradient, and could be used as a regional targeting tool for geothermal exploration.

Thermal gradient data confidence rating

This thermal gradient data confidence rating is based on the number of data points in a given thermal gradient record, and the period between drilling completion and thermal data collection where reported.

In the table below, higher confidence ratings have a higher rating number. A rating of 15 represents a data set where the gradient is based on continuous or near-continuous data with a clear thermal recovery period of one or more months; whereas a rating of 1 represents a thermal gradient based on a single downhole temperature measurement extrapolated to surface with no clear thermal equilibration period reported. Boreholes where no thermal gradient has been recorded have been assigned a thermal gradient confidence rating of zero (0).

Drill stem tests (DST), which involve formation fluid extraction in a given section, and Horner-corrected bottom-hole temperature (BHT) measurements from existing compilations are considered to sample thermally recovered formation temperatures with moderate confidence.

Number of temperature measurements	≥ 5	5	10	15
	4	4	8	12
	3	3	6	9
	2	2	4	6
	1	1	2	3
	0	1	2	3
		No thermal equilibration period	DST or Horner-corrected BHT	Thermally equilibrated

Confidence rating descriptions

0 – No thermal data exists.

1 – Thermal gradient based on a single BHT extrapolated to surface; measured directly after drilling or no thermal equilibration period reported.

2 – Thermal gradient based on a single downhole measurement with a thermal equilibration correction or thermal equilibration period of less than one month; or gradient based on 2–5 measurements with no thermal equilibration period.

3 – Thermal gradient based on 6–10 measurements with no thermal equilibration period reported; or thermal gradient based on one data point with high confidence thermal equilibration period.

4 – Thermal gradient based on 2–5 measurements with a thermal equilibration correction or thermal equilibration less than one month; or thermal gradient based on 11–15 temperature measurements with no reported thermal equilibration period.

5 – Thermal gradient based on more than 15 measurements with no thermal equilibration period.

6 – Thermal gradient based on 6–10 temperature measurements with a thermal equilibration correction; or thermal gradient based on 2–5 measurements with a thermal equilibration period.

8 – Thermal gradient based on 11–15 temperature measurements with a thermal equilibration correction.

9 – Thermal gradient based on 6–10 temperature measurements with a thermal equilibration period.

10 – Thermal gradient based on more than 15 temperature measurements with a thermal equilibration correction.

12 – Thermal gradient based on 11–15 temperature measurements with a thermal equilibration period.

15 – Thermal gradient based on more than 15 temperature measurements with a thermal equilibration period.

References

Fournier, R.O. and Truesdell, A.H., 1973. An empirical Na-K-Ca geothermometer for natural waters. Geochimica et Cosmochimica Acta, vol. 37, p. 1255–1275.

Li, C.-F., Lu, Y. and Wang, J., 2017. A global reference model of Curie-point depths based on EMAG2. Scientific Reports, vol. 7, paper 45129. https://doi.org/10.1038/srep45129

Verma, S.P. and Santoyo, E., 1997. New improved equations for Na/K, Na/Li and SiO_2 geothermometers by outlier detection and rejection. Journal of Volcanology and Geothermal Research, vol. 79, p. 9–23.

Witter, J. and Miller, C., 2017. Curie point depth mapping in Yukon. Yukon Geological Survey, Open File 2017-3, 37 p. https://data.geology.gov.yk.ca/Reference/79428

Witter, J.B., Miller, C.A., Friend, M. and Colpron, M., 2018. Curie point depths and heat production in Yukon, Canada. 43rd Workshop on Geothermal Reservoir Engineering, Stanford University, California, USA, 11 p.

Yukon Geological Survey, 2023a. Yukon lithogeochemistry data set. Yukon Geological Survey, http://data.geology.gov.yk.ca/Compilation/35 [accessed November 7, 2023].

Appendix B – Groundwater noble isotope data collected by the Yukon Geological Survey [digital only]

Appendix C – Temperature profile data collected by the Yukon Geological Survey (2017–2023) [digital only]

Appendix D – Carmacks EY22-01 drill log

Drilled by Kluane Drilling (tricone by Midnight Sun Drilling), November 2022
Latitude: 62.132904; Longitude: -136.369110; Elev. 482m

E.O.H length: 707.1 m
Logged by: J. van Randen (November 2022); M. Colpron (March 2023)

Main Lithology			Interpreted formational name	Description
From (m)	To (m)	Rock name		
0	128.1	CASING		no core recovered - Midnight Sun Drilling triconed down through overburden to bedrock
128.1	156.5	SANDSTONE	TANTALUS	grey somewhat speckled (<1mm sized)granular sandstone with local wisps of organic rich material especially at start of the recovered drill core. Mostly homogeneous, fine to medium-grained sandstone; swaley, wispy cross laminations in sections. Sandstone – angular grains of chert, quartz, feldspar. first chert pebbles @153.92m.
156.5	157.6	CHERT PEBBLE CONGLOMERATE	TANTALUS	heterolithic rounded clast supported conglomerate with coal lumps and fragments up to 5cm wide
157.6	158.1	COAL	TANTALUS	dull black fine grained coal; broken lower contact
158.1	158.5	CHERT PEBBLE CONGLOMERATE	TANTALUS	matrix poor conglomerate; most clasts are <1cm and subrounded
158.5	160.2	SANDSTONE	TANTALUS	gritty sandstone between layers of coal and fine to medium sized conglomerate beds. Shale chips in sandstone.
160.2	161.9	CHERT PEBBLE CONGLOMERATE	TANTALUS	conglomerate with clasts up to 2cm across
161.9	163.0	ORGANIC RICH MUDSTONE	TANTALUS	organic rich layers gradationally into sandstone
163.0	170.7	SANDSTONE	TANTALUS	clean sandstone
170.7	174.0	ORGANIC RICH MUDSTONE	TANTALUS	organic rich layers gradationally into coal seams
174.0	176.0	ORGANIC RICH MUDSTONE	TANTALUS	mixed interval of dominantly organic rich mudstones with coal as <1m beds and grittier sandstones
176.0	177.0	COAL	TANTALUS	mixed interval of dominantly organic rich mudstones with coal as <1m beds
177.0	179.0	ORGANIC RICH MUDSTONE	TANTALUS	mixed interval of dominantly organic rich mudstones with coal as <1m beds and grittier sandstones
179.0	180.0	COAL	TANTALUS	mixed interval of dominantly organic rich mudstones with coal as <1m beds
180.0	184.0	ORGANIC RICH MUDSTONE	TANTALUS	mixed interval of dominantly organic rich mudstones with coal as <1m beds and grittier sandstones
184.0	189.9	ORGANIC RICH MUDSTONE	TANTALUS	organic layers gradually decrease downhole into sandstone unit below
189.9	215.1	SANDSTONE	TANTALUS	clean sandstone with minor coarser conglomeratic interbeds generally less than 20cm wide; gradational contact to conglomerate section below. REDUCE PQ to HTW core size at 205.74m block in box 36.
215.1	217.9	CHERT PEBBLE CONGLOMERATE	TANTALUS	conglomerate with clasts up to 2cm across
217.9	223.2	SANDSTONE	TANTALUS	sandstone with wisps and fragments of organic rich material
223.2	224.4	COAL	TANTALUS	coal
224.4	246.4	SANDSTONE	TANTALUS	grey sandstone with local organic rich fine grained mudstone layers but no coal in this section

Main Lithology			Interpreted formational name	Description
From (m)	To (m)	Rock name		
246.4	247.0	COAL	TANTALUS	good coal bed
247.0	261.0	ORGANIC RICH MUDSTONE	TANTALUS	mixed interval of dominantly organic rich mudstone with local well developed coal seams with common slickensides and minor brecciation at coal contacts
261.0	264.9	SANDSTONE	TANTALUS	clean sandstone interval with minor open space cavities
264.9	270.3	ORGANIC RICH MUDSTONE	TANTALUS	dark grey to black very organic rich mudstone with coal sections
270.3	270.95	COAL	TANTALUS	broken black coal
270.95	321.56	ORGANIC RICH MUDSTONE	TANTALUS	dark grey to black very organic rich mudstone with coal sections
321.56	322.7	DACITE	EOCENE DIKE?	sharp contact into pale cream coloured hypabyssal dacite dike. Very distinct unit with shard angular darker shards in a very fine grained leucocratic matrix. Clay altered.
322.7	328.4	SANDSTONE	TANTALUS	equigranular sandstone with local organic wisps giving bedding at 40-50 degrees to core axis
328.4	336.4	DACITE	EOCENE DIKE?	same as above unit with highly deformed lower contact then sharp 30 degrees tca. Convoluted dike margin; chilled margin.
336.4	342.0	SANDSTONE	TANTALUS	clean immature equigranular sandstone
342.0	346.25	DACITE	EOCENE DIKE?	as above. No reaction to HCl - ?clay along fractures
346.25	382.0	SANDSTONE	TANTALUS	dominantly medium to coarse sandstone with local coarser conglomerate beds and isolated fragments of chert and shale trains; local <10cm wide dark grey to black organic rich mudstone layers especially near 362m; soft sediment deformation features observed in this section
382.0	382.3	CHERT PEBBLE CONGLOMERATE	TANTALUS	gradational contact from sandstone into chert pebble conglomerate with relatively smaller rounded clasts
382.3	384.75	SANDSTONE	TANGLEFOOT	dominantly sandstone. Sandstone seems more quartz-rich; shale and/or Hbl grains instead of chert? Transition into Tanglefoot??
384.75	385.2	CHERT PEBBLE CONGLOMERATE	TANGLEFOOT	distinctly coarser pebble conglomerate with clasts up to 3cm of black shale
385.2	392.0	SANDSTONE	TANGLEFOOT	dominantly medium to coarse sandstone with local coarser conglomerate beds and isolated “trains” composed of chert and shale fragments; soft sediment deformation features observed
392.0	395.5	DACITE	EOCENE DIKE?	dacite unit as described above with low angle convoluted contacts; local organic rich layers
395.5	420.1	SANDSTONE	TANGLEFOOT	large section of dominantly clean sandstone and by ~416m sandstone becomes darker with 3-5mm shale chips which are dark grey soft and angular; bedding low angle 20 degree tca at 417m; no reaction to HCl
420.1	421.7	DACITE	EOCENE DIKE?	light grey dacite with sharp lower contact 45 degree tca; local 5cm by 1cm elongate voids filled with cloudy white to pale pink chalcedony (....agates known in this area around Carmacks)
421.7	424.9	DIORITE	EOCENE DIKE?	distinctive more equigranular, fine-grained diorite unit; transitions in the coarser-grained, more mafic Hbl diorite below... Common unfoliated aggregates of biotite and lesser hornblende in this section; feldspar phenocrysts.
424.9	443.0	DIORITE	EOCENE DIKE?	more mafic biotite and hornblende rich diorite, non foliated, with 1-2mm mafics in a dark matrix. Local white silica filled circular amygdules crosscut by hair width late fracture fills; becomes finer grained downhole with a gradational contact to dacite below. irregular curvilinear ??zenoliths or igneous clasts up to 2cm of paler material observed within this unit giving it a blotchy overall look...This is the thickest sill/dike in this hole; looks like a blow-out with mafic core, gradational into more differentiated margins. Another possibility is that these dikes are related to Late Cretaceous Carmacks volcanism (ca. 70 Ma)?? Mafic part of the dike becomes more pitted before transitioning back to more inetermediate/felsic compositions. Strongly magnetic!

Main Lithology			Interpreted formational name	Description
From (m)	To (m)	Rock name		
443.0	444.5	DACITE	EOCENE DIKE?	light grey dacite as seen further up hole with highly convolute lower contact approximately 50 degree tca
444.5	448.7	ORGANIC RICH MUDSTONE	TANGLEFOOT	mottled dark grey very fine grained mudstone/sandstone to siltstone with darker grey organic rich layers
448.7	451.5	DACITE	EOCENE DIKE?	light grey Dacite as seen uphole with very complex contact with interpenetration between the intrusive and sedimentary host. Two distinct pulses of felsic magmatism in this section (~450.04m)
451.5	454.2	ORGANIC RICH MUDSTONE	TANGLEFOOT	contact mixed zone of black banded mudstone with interbedded sandstone; bedding at low angle tca
454.2	468.3	SANDSTONE	TANGLEFOOT	dominantly sandstone with low angle black siltstone layers with common very black polished slickensides; at 464.9m local brittle micro offsets and siltstone shale fragments. Rip-up clasts in sandstone.
468.3	468.3	SANDSTONE	TANGLEFOOT	section of grey speckled sandstone with local minor larger shale and chert larger clasts
468.3	486.45	DACITE	EOCENE DIKE?	wedges of Dacite unit as seen uphole with upper contact 45 degrees tca
486.45	487.2	SANDSTONE	TANGLEFOOT	section of grey speckled sandstone with local minor larger shale and chert larger clasts
487.2	488.2	DACITE	EOCENE DIKE?	sandstone host with rafts and blocks of Dacite volcaniclastic rock with deformed lower contact at low angle to core axis
488.2	493.9	SANDSTONE	TANGLEFOOT	section of grey speckled sandstone with local minor larger shale and chert larger clasts
493.9	500.9	ORGANIC RICH MUDSTONE	TANGLEFOOT	Dark grey organic rich zone locally porous and containing slickensides on fractures; interbedded siltstone and sandstone with late overprint of white wisps and fracture fills but no reaction to HCl; unit grades into coal downhole
500.9	501.4	DACITE	EOCENE DIKE?	Dacite volcaniclastic unit as above with sharp upper contact and highly complex interpenetrative lower contact (similar texture to YGS M. Colpron peperite) - soft sediment deformational contact
501.4	502.7	COAL	TANGLEFOOT	crumbly dull very black coal with shiny fracture surfaces often with well developed slickensides; see photo
502.7	503.2	DACITE	EOCENE DIKE?	very convoluted contacts to Dacite volcaniclastic unit
				FAULT?
503.2	504.3	ORGANIC RICH MUDSTONE	TANTALUS	dull black fine grained mudstone to siltstone with 80cm light grey grainy sandstone interbed?
504.3	510.3	COAL	TANTALUS	black coal with shiny slickensides fracture surfaces at low angle tca and locally broken subparallel to core axis
510.3	536.5	ORGANIC RICH MUDSTONE	TANTALUS	black fine grained shaley mudstone with high organic contact and 20cm coal seam between 520.4-520.6m; common low angle fractures
536.5	560.5	CHERT PEBBLE CONGLOMERATE	TANTALUS	“large section of very coarse grained heterolithic clast supported chert pebble conglomerate; classic Tantalus formation as is observed at Tantalus Butte at the southeast end of the Yukon River Bridge in nearby Carmacks. First occurrence of the coarse conglomerate with local pale green chert subrounded clasts locally up 3cm across. Sharp upper contact to mudstone above 50deg tca. ---Between 536.5-538.3m is mostly sandstone with bands of coarse chert pebble conglomerate - see photo bx 143. ---local graphitic slips and coal/organic rich seams at low angle to core axis. ---structure between 545.7-547.8m is coal seam with slickensides subparallel tca, see photo --between 553.9-557.8m fault of broken chert pebble conglomerate with fractures subparallel to core axis ---sharp lower contact of coarse chert pebble conglomerate 10 degrees to core axis”

Main Lithology			Interpreted formational name	Description
From (m)	To (m)	Rock name		
560.5	567.5	SANDSTONE	TANTALUS	fine grained sandstone with minor interbeds of medium sized chert pebble conglomerate as observed in sandstone units uphole; bedding less than 25 degrees to core axis
567.5	577.3	CHERT PEBBLE CONGLOMERATE	TANTALUS	"mixed interval of dominantly very coarse grained ""Tantalus type section"" chert pebble conglomerate with interbeds of sandstone with minor shaley angular fragments and fracture coatings with lesser mudstone beds . ----Coarse 3cm clasts size conglomerate bed between 574.6-577.3m is fining upwards with upper contact 35 and lower contact 20 degrees to core axis. "
577.3	606.85	SANDSTONE	TANTALUS	"dominantly sandstone with two up to 20cm long very coarse chert pebble conglomerate interbeds and common medium grained (less coarse) chert pebble conglomerate intervals. bedding 30deg at ~580.8m ---minor 10cm faulted broken section at 588.3m --592.1-596.2m and 604.0-605.0m subintervals of sandstone which are slightly darker coloured with common wisps and fracture coatings of organic rich material with low angle faulted organic rich layers having sharp lower contact 20 degree to core axis with local slickensides"
606.85	608.1	CHERT PEBBLE CONGLOMERATE	TANTALUS	coarse to medium grained chert pebble conglomerate with sharp lower contact 10 degrees to core axis
608.1	610.9	SANDSTONE	TANTALUS	speckled sandstone as seen throughout hole so far
610.9	614.0	CHERT PEBBLE CONGLOMERATE	TANTALUS	medium to coarse chert pebble conglomerate bed with sharp lower contact 50 degrees tca
614.0	629.8	ORGANIC RICH MUDSTONE	TANTALUS	dark grey organic rich mudstone with minor sandstone interbeds and local poorly developed coal beds. Grades into coal by 629.8m
629.8	632.1	COAL	TANTALUS	dull black broken coal in organic rich mudstone; convolute low angle contacts
632.1	642.1	ORGANIC RICH MUDSTONE	TANGLEFOOT	dark grey fine grained organic rich mudstone with mottled brecciated stressed appearance in contact with the Dacite at the bottom of this section
642.1	658.1	DACITE	EOCENE DIKE?	light tan Dacite interval with sharp and dominantly highly complex contacts into mudstone...see photos Wedge shaped 25cm intersection of Dacite at start with sharp upper contact 20 degrees tca then a short interval of mudstone to 642.7m and back into large section of Dacite. Dacite has a white ragged fracture fill/overprint - non calcareous as no reaction to HCl and has grainier sections of possible sandstone intermixed with the dike??
658.1	677.7	SANDSTONE	TANGLEFOOT	light grey fine to medium grained speckled sandstone as seen throughout hole with local organic rich layers and fracture fill (especially between 644.5-665.7m).
677.7	681.9	QUARTZ PEBBLE CONGLOMERATE	TANGLEFOOT	"Highly unusual mixed section of dark grey matrix supported quartz pebble conglomerate with 60% matrix and rounded clasts and coal seams/fracture coatings and rubbly sandstone. Stylolitic like suture at 679.1m See photos --broken and sheared at ~681.7 25 degrees to core axis and graphitic slickensides at 681.2m going 55 degrees tca More likely Tanglefoot Fm conglomerate. Does not look anything like the chert pebble conglomerates observed anywhere else in the hole - this zone looks highly strained and sheared with common dark grey organic rich layers and local slickensides observed."
681.9	707.1	SANDSTONE	TANGLEFOOT	"large sandstone section which is lighter in colour and much more monotonous in character than the sandstones up hole (could be the Tanglefoot formation that is known to have more qtz and feldspar and less chert fragments than the Tantalus sandstone in YGS Open file 2015-23 and YGS M. Colpron concurs with this interpretation but would like to investigate in detail with thin sections and more time spent detailed logging this core.) ----End of Hole 707.1m Box 195"

Appendix E – Duke River borehole: Phase 1 completion report

Prepared by Sarah Sternbergh; Edited by Maurice Colpron

Introduction

A 221 m deep borehole was drilled near the Duke River, Yukon, approximately 9 km west of Burwash Landing (Fig. E1), between October 26th and November 24th, 2022, to evaluate the geothermal potential of the area. The drill site is located on Kluane First Nation Category A Settlement land, within the Denali fault zone, near an apparent releasing bend indicated by mapping and geophysical surveys (Figs. 64, 65; Witter, 2020). The site is accessed from an existing trail along the Duke River and is located in an area of historical disturbance approximately 1.4 km south of the Alaska Highway. The borehole was designed for drilling in two phases: Phase 1 using a mud rotary drill and Phase 2 using a diamond drill for core recovery. This report provides a summary of materials and drilling conditions encountered in Phase 1 drilling at the Duke River geothermal borehole site. The borehole was cased and instrumented for scientific monitoring and left ready for eventual re-entry and Phase 2 drilling.

Site description and preparation

The drill site is located in a previously disturbed area. It is sparsely treed with black spruce and covered with mossy ground cover. Poor drainage causes ponding water between the mossy hummocks. The site is underlain by unconsolidated glacial till and glaciofluvial sediments and slopes gently to the southeast toward the Duke River.

Clearing for drilling consisted of removing only the trees, taller shrubs and some hummocky moss. Organic material was windrowed at the edges of the site for future replacement during reclamation. The mossy ground cover was left in place to preserve permafrost and natural site

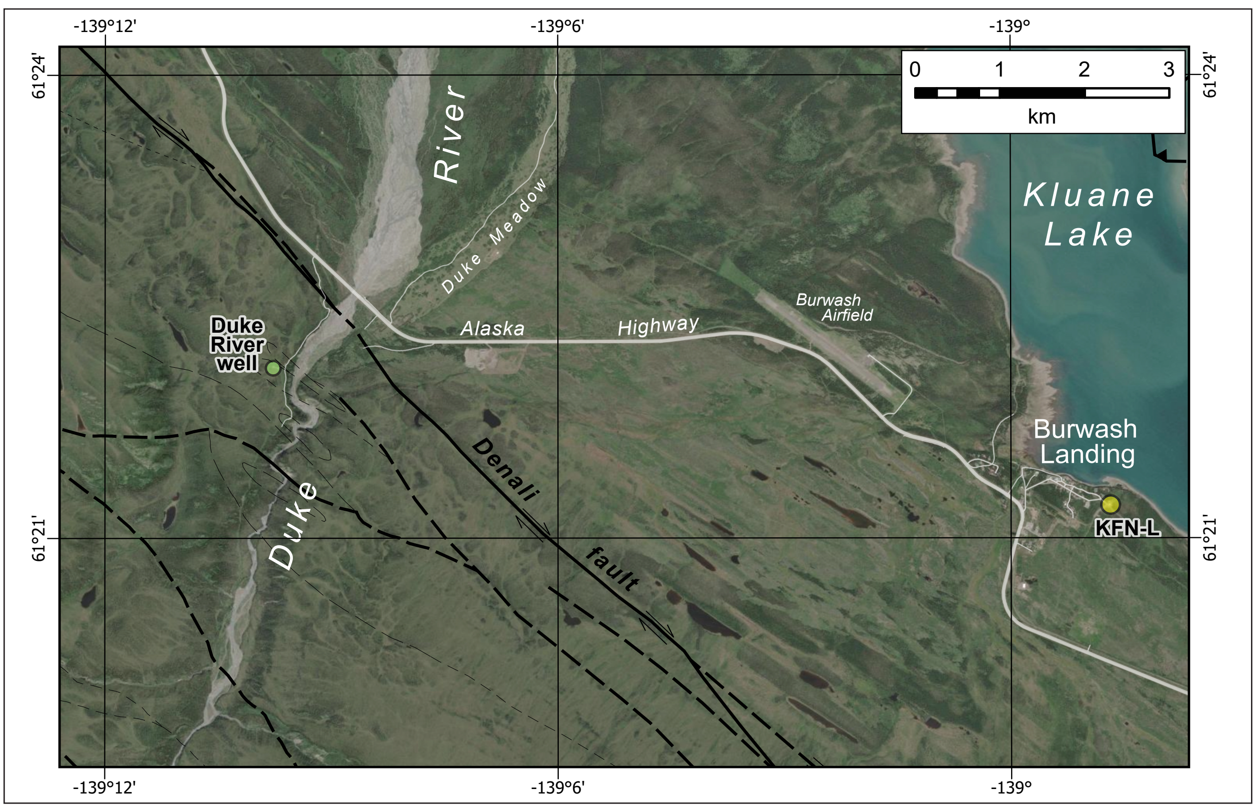

Figure E1. *Location of the Duke River geothermal borehole near Burwash Landing.*

drainage. A drilling pad and access road consisting of pit run gravels was built overlying mossy organics near the northern edge of the site. To facilitate access to the site, the existing trail along the Duke River was brushed, widened, and locally infilled for approximately 1.4 km from the Alaska Highway.

Methodology

The borehole was drilled using a mud rotary system with a shale shaker and internal mud tanks to remove cuttings, store mud, and recirculate the drilling fluid downhole (Figs. E2a, b). Mud rotary drilling was used to prevent any uncontrolled artesian flow from the borehole. Drilling mud was comprised of a mix of water and additives including bentonite, barite, and drilling polymers to manage the viscosity and density of the drilling fluid. The mud rotary drill used a tricone bit that cuts or crushes material, which is then entrained in the mud and pumped out of the hole to pass through the shale shaker. This drilling method makes detailed logging of lithology, structures, and exact depths difficult, if not impossible.

Drill cuttings were monitored as they were removed from the drill mud on the shale shaker screens and samples were collected at 4.5 m intervals throughout the drilling process. Samples collected included grab samples stored in plastic bags and subsamples collected in chip trays to create a visual log of the borehole material (Fig. E2c).

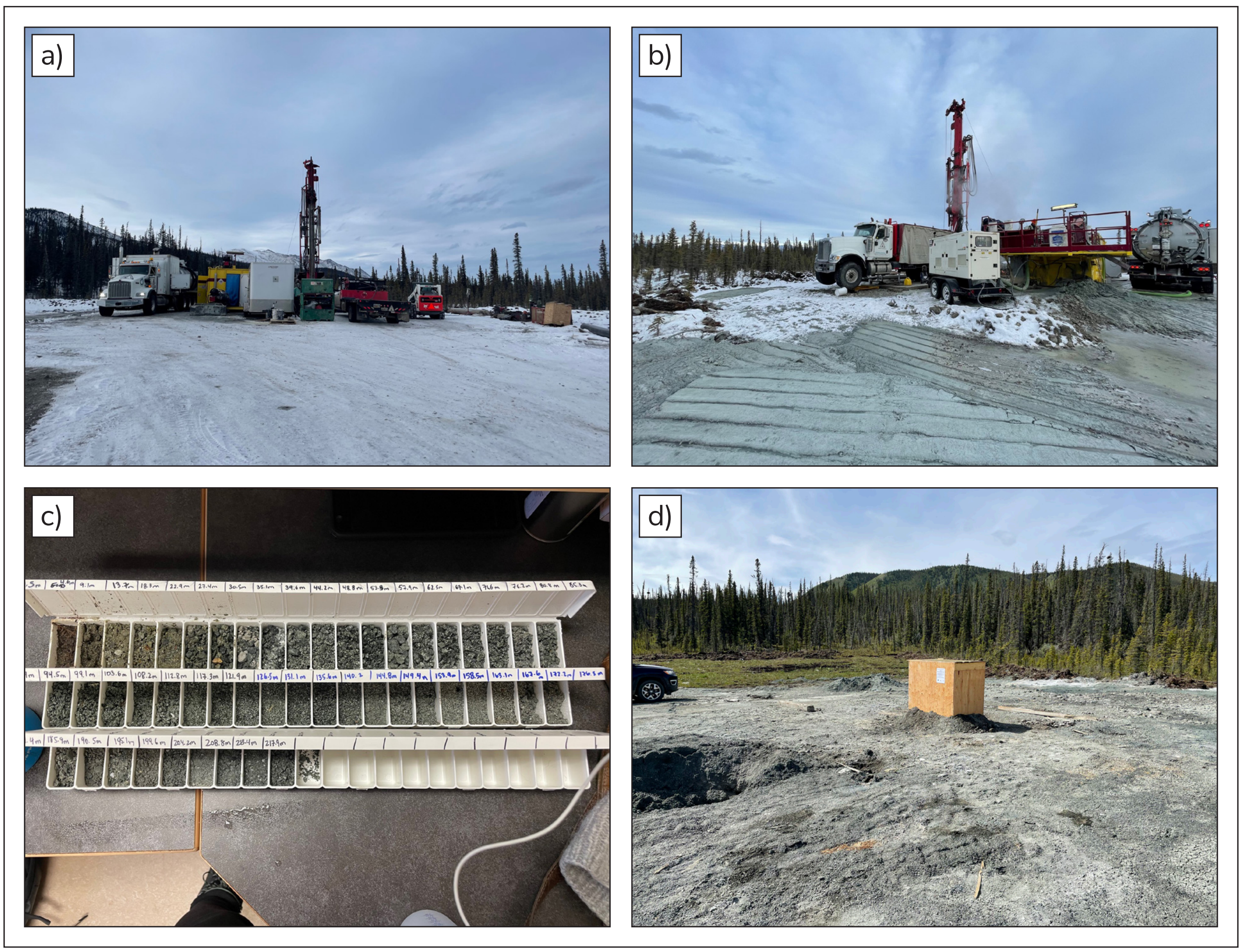

***Figure E2. a)** Drill setup at the Duke River geothermal borehole site (November, 2022). **b)** Drilling shaker unit, drill cuttings and water truck during drilling operation. **c)** Trays with rock chip samples recovered from the Duke River geothermal borehole. **d)** Plywood shed covering the wellhead at the Duke River geothermal borehole site.*

Borehole construction

The construction details for the borehole are shown in Figure E3. The installation consists of two telescoping sections of casing cemented into place and equipped with a fibre optic cable mounted and cemented outside the casing to a depth of 214.3 m. The surface casing has an inner diameter of 305 mm and is cemented in place at a depth of 26.5 m, with the bottom of the casing in frozen sediment. The second casing has an inner diameter of 203 mm with a cement casing shoe installed at a depth of 219.5 m (Fig. E3). The borehole is topped with a welded cap to prevent any ingress while it is dormant between drilling phases. The fibre optic cable was constructed by Silixa LLC with two single mode (distributed acoustic sensor [DAS]) and two multi-mode (distributed temperature sensor [DTS]) fibres within an armoured steel tube attached to a downhole termination assembly. The installation is intended to be used as a semi-permanent monitoring site for ground temperature and seismic studies. After drilling completion, the wellhead was covered by a small plywood shed to protect the surface casing and secure the site (Fig. E2d).

Drilling results

Figure E4 is a detailed log of lithology, drilling conditions, and groundwater observations. The drill intersected frozen surficial sediments down to 39.6 m and various volcanic and volcaniclastic rocks assigned to the Station Creek Formation to its completion depth of 221 m. Drilling conditions changed at approximately 48.8 m; this is inferred to mark the depth of the permafrost. Lithology was determined from drill cuttings taken from the shale shaker screen and qualitative observations of drilling mud, penetration rate, and ‘roughness’ of drilling. Drill cuttings ranged in size from clay-sized fines to rock fragments up to approximately 10 mm (Fig. E2c). Cuttings were washed to remove silt and clay fractions. The drill behaviour, including drilling roughness resulting from inconsistent pressure on the drill bit and increases or decreases in drill advance rate, can indicate the presence of boulders, cobbles or bedrock fractures. Evidence of fractures in drill cuttings include clay gouge; alteration minerals on fracture surfaces, such as iron oxidation due to groundwater circulation; and slickensides on rock chips. Additional indirect evidence of fractures includes ingress of water diluting drilling mud, reducing both mud weight and viscosity.

Overburden at the site extends to a depth of 39.6 m depth and consists of a thin veneer of organic soil over fluvial gravels and glacial till. The glacial till comprises silt with variable amounts of gravel, cobble and boulders. The lithology of the cobble and boulders are a mix of regional bedrock lithologies. The Station Creek Formation units observed in drill cuttings include andesite, volcaniclastic sandstone, crystal-lithic tuff with large epidote crystals, and fine-grained grey-green tuff at the bottom of the hole. Logging of the bedrock is from pebble- to sand-sized fragments, and the differentiation between crystal-lithic tuff and volcaniclastic sandstone is based on the occurrence of rounded grains in the sandstone.

The drilling encountered evidence of extensive bedrock fracturing at several depths in the borehole. An extensive zone of bedrock fracturing was encountered between 57.9 and 62.5 m, where chip samples contain pale grey-green clay gouge and slickensides. Drilling was faster and easier in this zone. Disseminated pyrite is present in the rocks above and below this fractured zone. Another significant zone of bedrock fracturing was interpreted between 143.3 and 158.5 m deep (Fig. E4). In this interval, extensive groundwater influx was indicated by dilution of the drilling mud and easier drilling conditions. Other, smaller intervals of bedrock fracturing are suggested by presence of slickensides, calcite mineralization and rough drilling conditions.

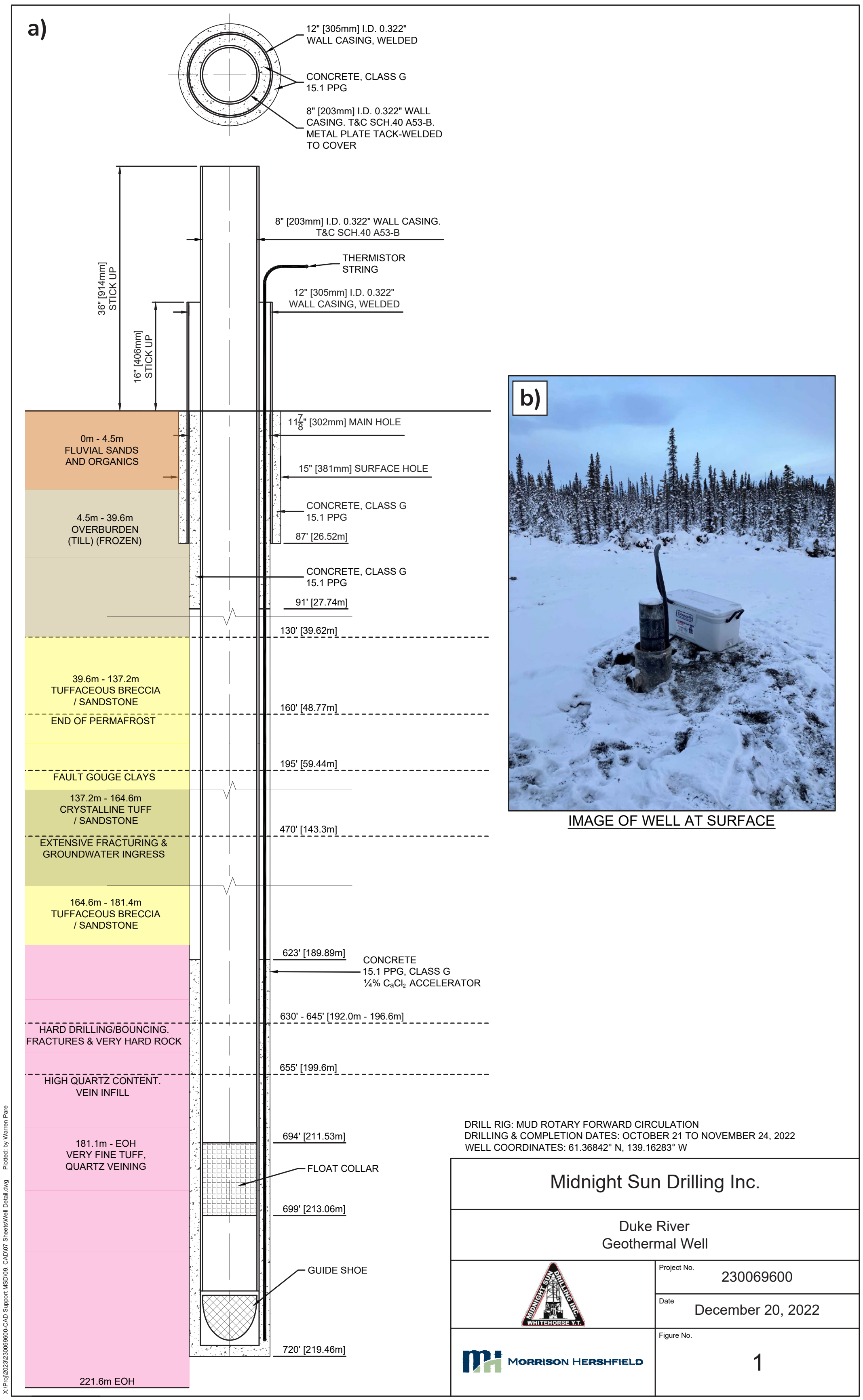

***Figure E3. a)** Construction diagram for the Duke River geothermal borehole; **b)** Image of the borehole at the surface.*

Duke River geothermal borehole

Borehole ID: DRG-22 | Driller: Midnight Sun Drilling Ltd. | Latitude: 61.36842

October 26 to November 24, 2022 | Drilling Method: Mud Rotary | Longitude: −139.16283

Interval (m)		Material Type	Material Description	Drilling Notes	Sample Depth (m)
Top	Bottom				
0	3	ORGANICS AND FILL	ORGANICS, sandy, trace gravel. Gravels are subrounded, smooth. Organics are mix of organic silt and fibrous plant matter.	Hard drilling (frozen)	G01 @1.5
3	4.5	FLUVIAL	Sand, trace/occasional organics. Sand is well sorted, dark green, medium grained.	Hard drilling (frozen)	G02 @4.5
4.5	39.6	TILL	TILL - SILT with variable amounts of gravel, cobbles, boulders and sand. Gravels are angular, rough, mixed lithology	Hard drilling (frozen)	G03 @9.1 G04 @13.7 G05 @18.3 G06 @22.9 G07 @27.4 G08 @30.5 G09 @35.1 G10 @39.6
			@4.5–5.5 - Cobbles	Very hard, rough drilling	
			@5.5–10.7 - GRAVEL, sandy, silty. Gravels >80% granitic, some greenstone and ultramafic.	Hard drilling (frozen)	
			@10.7–12.2 - Cobbles	Very hard, rough drilling	
			@12.2–17.4 - GRAVEL, sandy, silty. Gravels are granodiorite, greenstone, ultramafic.	Hard drilling (frozen)	
			@17.4–18.3 - Cobbles	Very hard, rough drilling	
			@18.3–39.6 - SILT, gravelly, sandy, cobbly. Dark grey-black. Rock is mixed greenstone and granodiorite	Hard drilling (frozen)	
39.6	80.8	STATION CREEK ANDESITE	Andesite, medium to course grained, dark grey- green with disseminated pyrite grains.	Hard drilling	G11 @44.2 G12 @48.8 G13 @53.3 G14 @57.9 G15 @62.5 G16 @67.1 G17 @71.6 G18 @76.2 G19 @80.8
			@48.4 - End permafrost	Drilling becomes less hard	
			@48.8 - Disseminated fine pyrite grains	Less hard drilling	
			@57.9 to 62.5 - Fault gouge clay and slickenlined fragments in samples	Easy drilling through this zone	
			@62.5, 67.1, 71.6, 76.2 - Disseminated fine pyrite grains		
80.8	137.2	STATION CREEK SANDSTONE	Sandstone with fragments of amygdaloidal basalt (with epidote infill), epidote fragments/sand particles mixed with pyroxene, quartz	Hard drilling (harder rock)	G20 @85.3 G21 @89.9 G22 @94.5 G23 @99.1 G24 @103.6 G25 @108.2 G26 @109.7 G27 @112.8 G28 @117.3 G29 @121.9 G30 @126.5 G31 @131.1 G32 @135.6
			@85.3 - Disseminated fine pyrite grains ~5%, slickenlines and chlorite alteration on fracture surfaces		
			@135.6 - Epidote fragments ~1cm across, chalcopyrite and bornite in samples		
137.2	164.6	STATION CREEK TUFF	Crystal-lithic tuff. Poorly welded. Basalt fragments are present, but smaller. Crystals are medium grained.	Easier drilling	G33 @140.2 G34 @144.8 G35 @149.9 G36 @153.9 G37 @158.5 G38 @163.1
			@143.3–158.5 - Extensive fracturing and groundwater ingress in this section. Drill mud diluted by groundwater ingress.		
164.6	181.4	STATION CREEK SANDSTONE	Sandstone, larger chip size, epidote fragments are larger	Increased drilling rate	G39 @167.6 G40 @172.2 G41 @176.8 G42 @181.4
181.4	221	STATION CREEK TUFF	Very fine grained tuff, light grey, welded/silicified. Calcite infill in fractures/veins	Increased drilling rate and chip size due to bit change	G43 @185.9 G44 @190.5 G45 @195.1 G46 @199.6 G47 @204.2 G48 @208.8 G49 @213.4 G50 @217.9
			@192.0–196.6 - Fractured hard rock	Hard drilling, bouncing	
			@195.1 - Increase in calcite infill material	Easier drilling	
			@199.6 - High calcite infill content		
			@217.9 - Change to blueish grey colour	Very hard, rough drilling	

Figure E4. *Drilling log for the Duke River geothermal borehole.*

References

Witter, J.B., 2020. Early-stage exploration for geothermal energy resources along the Denali fault near Duke River, Yukon. Yukon Geological Survey, Open File 2020-3, 62 p. https://data.geology.gov.yk.ca/Reference/95836